Loughborough University

This item was submitted to Loughborough's Research Repository by the author.
Items in Figshare are protected by copyright, with all rights reserved, unless otherwise indicated.

# Strategic feedback control of pharmaceutical crystallization systems

PLEASE CITE THE PUBLISHED VERSION

PUBLISHER

© Ali Nauman Saleemi

LICENCE

CC BY-NC-ND 4.0

REPOSITORY RECORD

Saleemi, Ali N.. 2011. “Strategic Feedback Control of Pharmaceutical Crystallization Systems”. figshare.
https://hdl.handle.net/2134/8530.

Loughborough University

This item was submitted to Loughborough's Institutional Repository (https://dspace.lboro.ac.uk/) by the author and is made available under the following Creative Commons Licence conditions.

creative commons

COMMONS DEED

**Attribution-NonCommercial-NoDerivs 2.5**

**You are free:**

- to copy, distribute, display, and perform the work

**Under the following conditions:**




**Attribution**. You must attribute the work in the manner specified by the author or licensor.



**Noncommercial**. You may not use this work for commercial purposes.



**No Derivative Works**. You may not alter, transform, or build upon this work.

- For any reuse or distribution, you must make clear to others the license terms of this work.
- Any of these conditions can be waived if you get permission from the copyright holder.

**Your fair use and other rights are in no way affected by the above.**

This is a human-readable summary of the Legal Code (the full license).

Disclaimer

For the full text of this licence, please go to:
http://creativecommons.org/licenses/by-nc-nd/2.5/



# STRATEGIC FEEDBACK CONTROL OF PHARMACEUTICAL CRYSTALLIZATION SYSTEMS

**by**

**ALI NAUMAN SALEEMI**

**A Doctoral Thesis submitted in partial fulfilment of the requirements for the award of the degree of Doctor of Philosophy in Chemical Engineering**

**© by Ali Nauman Saleemi (2011)**

# Abstract

Crystallization is a widely used purification and separation technique in the pharmaceutical industry. More than 90 % of the active pharmaceutical ingredients are produced in the crystalline form. The quality of the crystalline product greatly affects the downstream processing and bioavailability of the drug. The Food and Drug Administration (FDA) initiated in 2004 the use and implementation of process analytical technology (PAT) in the pharmaceutical development and production and encourages the pharmaceutical industry to adopt quality by design (QBD) approaches. The prime objective of this initiative has been to optimize the drug development and manufacturing process by reducing cost, improving product quality and reducing the number of failed batches. The work presented in this thesis focuses on expanding the use of two PAT tools, namely attenuated total reflection ultra violet/visible spectroscopy (ATR-UV/Vis spectroscopy) and focused beam reflectance measurement (FBRM). ATR-UV/Vis spectroscopy and FRBM are mostly used for process monitoring. The aim here was to develop sophisticated control approaches using these *in situ* tools for enhancing the product quality. Chemometrics is an integral part of PAT, and can provide valuable information about the system. This tool has also been used in this study for calibration model development and monitoring the cooling and anti-solvent crystallization processes for single and muticomponent crystallisations.

The development of an accurate and robust calibration model is necessary for qualitative and quantitative analysis of a system using spectroscopy. A systematic methodology was therefore presented for the selection of a suitable calibration model for ATR-UV/Vis spectroscopy. The developed model was then used as part of supersaturation control approach (SSC). SSC uses information from ATR-UV/Vis spectroscopy in a feedback control loop to keep the system at desired supersaturation. The developed approach resulted in the production of crystals of uniform size and can represent the bases for a model-free direct design approach for crystallization systems.

A novel automated direct nucleation control approach (ADNC) based on FBRM was also evaluated. For most crystallisation systems significant variations exist in the metastable zone width (MSZW) due to changing operating conditions, scale and impurity profile. These variations can significantly deteriorate the quality of the final product. The ADNC approach,

which is a model-free approach, was able to detect all these dynamic changes and consistently produced high quality product. The performance of this control approach was tested against traditionally used linear and programmed cooling profiles and it was shown that ADNC approach always gave better results in terms of crystal size and crystal size distribution (CSD). A combined ADNC and SSC approach was also presented which was based on the concept of internal seed generation. This approach also outperformed the crystallisation processes controlled using linear and natural cooling profiles. A thorough evaluation of the ADNC approach was then carried out under different conditions including accidental seeding and external seed addition. During all these tests and evaluations ADNC yielded high quality products, demonstrating its robustness and efficiency. A 100 L pilot plant crystallizer was used to test the applicability of the ADNC approach as a simple, efficient and robust scale-up tool. The results obtained showed that ADNC approach performed equally well on pilot scale generating crystals with larger size and less agglomeration. The approach was also compared with natural and linear cooling profiles on the 100 L scale. The product obtained from ADNC was superior (larger crystals, with narrower CSD and less fines) compared to crystals resulted from the open loop control approaches.

Often compounds exist in mixtures especially after the synthesis stage during the drug development process. Separation and monitoring of the compounds is therefore necessary as a high degree of purity is required in the pharmaceutical industry. A complex nonlinear model capable of simultaneously monitoring the concentration of two isomers during cooling and anti-solvent crystallization was developed. The model was based on the absorbance values provided by the *in situ* ATR-UV/Vis spectroscopy while two FBRM probes were used for monitoring the solid phase. A novel interconnected setup of two and three crystallizers was developed for the separation of the two and three positional isomers (ortho, meta and para) of amino benzoic acid, using seeded cooling crystallization. It was shown that seeded cooling crystallization can be used to obtain products of high purity from a mixture using the innovative crystallizer setup. The products obtained showed no signs of cross contamination, this demonstrated the successful implementation of this approach for the separation of the compounds, when present together in a mixture and offers a cost effective alternative to more expensive high performance liquid chromatography.

# Acknowledgements

First of all I would like to thank Almighty Allah for all His blessings, secondly I would like to thank my family for all their support during this process.

I am greatly indebted to my supervisors Professor Zoltan Nagy and Professor Chris Rielly for their continuous support and guidance throughout my PhD. Especially, I am grateful to Professor Nagy for giving me the opportunity to do PhD. He was always available for guidance and discussions and his late night emails (1 am – 4 am) were really helpful in finishing the thesis and in submission of conference abstracts. I hope that I will be able to learn more from him in the future.

Next I would like to thank my roommates in S158, Dr. Bahareh (a.k.a The Presenter), Dr. Fahd (a.k.a Mr. Bubble), Hakim, Latifah (a.k.a Mrs. Bread), Dr. Mathew (a.k.a Mr. Bacteria), Redah (a.k.a Cheeni). All the pizza parties and their company, support and help made the whole task a lot easier.

I am also thankful to members of crystallization systems engineering research group (past and present) along with all my friends in the chemical engineering department and in Loughborough University.

The PhD would not have completed without the support of technical staff. All the help from technical staff including Dave, Graham, Jim, Kim, Monika, Sean and Tony and the workshop "boys" Mark and Steve is greatly appreciated, Dr. David Ross from materials engineering department for his help in microscopy

I would also like to thank Dr. Gerry Steele from AstraZeneca for his cooperation and support in carrying out some of the experiments and providing data for the experiments that were carried out at AstraZeneca Charnwood site pilot plant. Financial support from EPSRC grant no. EP/E022294/1 is also acknowledged.

I wish best of luck to all the people who were involved at some point during my PhD in their future endeavours.

*Dedicated to my late father for all the inspiration and support*

# Contents

Abstract ..... i

Acknowledgements ..... iii

Contents ..... v

List of Figures ..... ix

List of Tables ..... xvii

Abbreviations ..... xviii

Chapter 1 Introduction ..... 1

1.1 Background ..... 1

1.2 Research Aims and Objectives ..... 4

1.3 Research Methodology ..... 5

1.4 Research Contribution ..... 6

1.5 Structure of the Thesis ..... 8

Chapter 2 Literature Review ..... 10

2.1 Solubility and Supersaturation ..... 10

2.2 Nucleation ..... 13

2.3 Polymorphism ..... 18

2.4 Crystal Size Distribution ..... 20

2.5 Control of Crystallization Processes ..... 21

2.5.1 Cooling Crystallization ..... 21

2.5.2 Anti-solvent Crystallization ..... 23

2.5.3 Combined cooling and anti-solvent crystallization ..... 24

2.6 Model-based Approaches ..... 25

2.7 Model-free (direct design) Approaches ..... 26

2.8 Process Analytical Technology and Chemometrics ..... 28
2.9 ATR-UV/Vis Spectroscopy ..... 30
2.10 ATR-Fourier Transform Infrared Spectroscopy (ATR-FTIR) ..... 34
2.11 Near Infrared Spectroscopy (NIR) ..... 35
2.12 Raman Spectroscopy ..... 35
2.13 Focused Beam Reflectance Measurement (FBRM) ..... 37
2.14 Chemometrics ..... 42
2.15 Calibration Model Development Techniques ..... 44
2.15.1 Univariate Calibration ..... 45
2.15.2 Multivariate Calibration ..... 47
2.15.3 Principal Component Analysis (PCA) and Principal Component Regression (PCR) ..... 48
2.15.4 Partial Least Squares Regression ..... 51
2.15.5 Artificial Neural Networks ..... 53
2.15.6 Pre-Processing Techniques ..... 55
2.15.7 Design of Experiments ..... 57
2.16 Summary ..... 59
Chapter 3 Calibration Model Development for ATR-UV/Vis Spectroscopy for Crystallization Monitoring ..... 61
3.1 Introduction ..... 61
3.2 Experimental Setup and Methodology ..... 61
3.3 Results and Discussion ..... 64
3.3.1 Performance analysis of Calibration Models ..... 70
3.3.2 *In situ* and real-time monitoring of crystallization using ATR-UV/Vis spectroscopy ..... 80
3.4 Conclusions ..... 82

Chapter 4 Comparative Investigation of Supersaturation and Direct Nucleation Control of Crystal Size Distributions using ATR-UV/Vis Spectroscopy and FBRM ..... 84

4.1 Introduction ..... 84

4.2 Methodology ..... 86

4.2.1 Supersaturation Control Approach for Cooling Batch Crystallisation ..... 86

4.2.2 Automated Direct Nucleation Control Approach (ADNC) ..... 88

4.3 Experimental Procedures ..... 92

4.3.1 Materials and Instrumentation ..... 92

4.3.2 Calibration Model Development ..... 92

4.4 Results and Discussion ..... 94

4.4.1 Unseeded Linear Cooling Crystallization Experiments ..... 94

4.4.2 Seeded Crystallisation Experiments using Linear Cooling or Supersaturation Control ..... 96

4.4.3 Direct Nucleation Control Experiments ..... 102

4.4.4 Combined ADNC and SSC Approach ..... 111

4.5 Conclusions ..... 115

Chapter 5 Assessment of Direct Nucleation Control Approach for Different Process Conditions during Cooling Crystallization ..... 117

5.1 Introduction ..... 117

5.2 Results and Discussion ..... 117

5.2.1 Seeded Direct Nucleation Control Experiments ..... 118

5.2.2 Evaluation of Direct Nucleation Control in Case of Accidental Seeding ..... 123

5.3 Conclusions ..... 129

Chapter 6 Assessment of the Automated Direct Nucleation Control Approach as a Scale up Tool ..... 131

6.1 Introduction ..... 131

6.2 Experimental Procedure ..... 133
6.2.1 Materials and Instrumentation ..... 133
6.3 Results and Discussion ..... 135
6.3.1 Scale-up Experiments Using the OABA in Water System ..... 135
6.3.2 Industrial Scale-up Experiments Using the Paracetamol in IPA System ..... 143
6.4 Conclusions ..... 146
Chapter 7 Separation and Monitoring of the crystallization of mixtures of Aminobenzoic Acid Isomers using ATR UV/Vis and FBRM ..... 147
7.1 Introduction ..... 147
7.2 Experimental Section ..... 149
7.2.1 Materials and Equipment ..... 149
7.3 Calibration Model Development ..... 150
7.3.1 Design of Experiments ..... 150
7.3.2 Monitoring and Calibration Model Development ..... 150
7.4 Separation of the two Isomers ..... 160
7.5 Separation of the three Isomers ..... 165
7.6 Conclusions ..... 169
Chapter 8 Conclusions and Future Work ..... 170
8.1 Conclusions ..... 170
8.2 Future Work ..... 172
References ..... 174
Appendix A ..... 186
Appendix B ..... 189

# List of Figures

Figure 1.1 Drug development stages ..... 1

Figure 1.2 Breakup of drug development costs ..... 3

Figure 2.1 Phase diagram for crystallization process ..... 12

Figure 2.2 Changes in Gibbs free energy (adapted from Myerson, 2000) ..... 16

Figure 2.3 Variation in MSZW based on nucleation types (adapted from Mersmann, 2001)..... 17

Figure 2.4 Phase diagram showing enantiotropic and monotropic polymorphic systems..... 19

Figure 2.5 Different Cooling Profiles ..... 22

Figure 2.6 Schematic representation of first principle approach (adapted from Nagy *et al*., 2008) ..... 26

Figure 2.7 Schematic representation of direct design approach (adapted from Nagy *et al*., 2008) ..... 27

Figure 2.8 Classification of different tools used under PAT ..... 28

Figure 2.9 Classification of different process tools based on market share ..... 30

Figure 2.10 Electronic energy levels and possible electron transitions (adapted from Pavia *et al.*, 2009) ..... 31

Figure 2.11 Working of ATR probe ..... 33

Figure 2.12 Chord length measurement by FBRM..... 37

Figure 2.13 Benefits of using PAT and chemometrics ..... 42

Figure 2.14 Classification of calibration model development methods (adapted from Bakeev, 2010) ..... 44

Figure 2.15 Structure of a neuron ..... 54

Figure 2.16 Structure of a feed forward network..... 54

Figure 2.17 Central composite design for three factors at two levels..... 59

Figure 3.1 Schematic representation (a) and picture (b) of the experimental setup used for calibration model development and crystallisation monitoring ..... 62

Figure 3.2 Spectrum of paracetamol in IPA at constant temperature and concentration, lower half of the figure shows the first derivative of the absorbance with respect to wavelength ..... 64

Figure 3.3 Variation of absorbance values at different wavelengths and time during a typical crystallisation experiment. ..... 66

Figure 3.4 Absorbance at 252 nm, total counts/s and temperature profile for a typical calibration experiment ..... 66

Figure 3.5 Concentrations used in the calibration model development ..... 69

Figure 3.6 Variation of 1st derivative at 266 nm with respect to temperature at different concentrations, except for the validation experiment ..... 69

Figure 3.7 1st derivative at 266 nm versus different concentrations at 30°C ..... 70

Figure 3.8 Actual and predicted concentration using uni-variate model ..... 71

Figure 3.9 Actual and predicted concentrations using multivariate model with temperature term ..... 72

Figure 3.10 Actual versus predicted concentration values for multivariate model with 3 absorbances ..... 73

Figure 3.11 PCM spectra in IPA at different temperatures (10 °C – 60 °C) ..... 73

Figure 3.12 Covariance between different wavelengths ..... 74

Figure 3.13 Regression coefficients for 8 factor PCR ..... 76

Figure 3.14 Regression coefficients for 8 factor PLSR ..... 76

Figure 3.15 Actual and predicted concentrations using 8 factor PCR ..... 77

Figure 3.16 Actual and predicted concentrations using 8 factor PLSR ..... 77

Figure 3.17 Actual and predicted concentrations, nonlinear method using 1st derivative ..... 78

Figure 3.18 Total counts/s, temperature and absorbance profiles for slurry experiment ..... 80

Figure 3.19 Comparison of model predicted solubility and literature values ..... 80

Figure 3.20 Performance analysis of nonlinear calibration model ..... 81

Figure 3.21 Total counts/s, concentration and absorbance profiles for experiment shown in Figure 3.20 ..... 82

Figure 4.1 Block diagram for the supersaturation control approach for batch cooling crystallisation processes ..... 88

Figure 4.2 Phase diagram showing a typical operating curve during supersaturation control ..... 88

Figure 4.3 Block diagram for the Direct Nucleation Control approach for batch cooling crystallisation ..... 90

Figure 4.4 Phase diagram indicating a typical operating profile in the case of direct nucleation control approach ..... 90

Figure 4.5 Schematic representation of the working principle of the automated direct nucleation control (ADNC) approach ..... 92

Figure 4.6 Concentration and temperature points covered in the phase diagram ..... 93

Figure 4.7 1st derivative at 266 nm for various concentrations at different temperatures ..... 93

Figure 4.8 Predicted concentrations plot against gravimetrically determined concentrations ..... 94

Figure 4.9 Unseeded cooling crystallization experiments with slow and fast cooling rates. Slow run was selected for comparison with other approaches; ADNC target counts were also selected based on slow run ..... 95

Figure 4.10 SWMCL plots (a) slow cooling crystallization experiment (b) fast cooling crystallization experiment ..... 96

Figure 4.11 Seeded crystallisation experiment with 5 % seed and linear cooling ..... 97

Figure 4.12 Programmed cooling experiment with 5 % seed ..... 98

Figure 4.13 Comparison of CSD for programmed and linear cooling profiles ..... 98

Figure 4.14 SSC1 experiment with 5 % seed and 0.010 g/g as supersaturation setpoint ..... 98

Figure 4.15 SSC2 experiment with 5 % seed and 0.012 g/g as supersaturation setpoint ..... 99

Figure 4.16 SSC3 experiment with 10 % seed and 0.010 g/g as supersaturation setpoint ..... 99

Figure 4.17 Supersaturation profile for SSC1 experiment ..... 99

Figure 4.18 SWMCL plots for seeded experiments (a) linear seeded crystallization (b) SSC1 (c) SSC2 (d) SSC3. The inset for linear seeded run shows high levels of noise in SWMCL when the solids are completely dissolved, hence only the SWMCL after nucleation is used for analysis. 101

Figure 4.19 Comparison of CSDs (at the end of the batches) for seeded cooling crystallization experiments. The CSD of the seed crystals used in all cases is also shown. ..... 102

Figure 4.20 ADNC1 with 8000 target counts and ±1000 limits ..... 102

Figure 4.21 ADNC2 with 8000 target counts and ±100 limits ..... 103

Figure 4.22 ADNC3 with 4000 target counts and ±1000 limits ..... 103

Figure 4.23 ADNC4 with 4000 target counts and ±100 limits ..... 103

Figure 4.24 Phase diagrams for direct nucleation control (ADNC) experiments (a) ADNC1 (b) ADNC2 (c) ADNC3 (d) ADNC4 ..... 105

Figure 4.25 Evolution of fine and course particles for ADNC experiments (a) ADNC1 (b) ADNC2 (c) ADNC3 (d) ADNC4 ..... 106

Figure 4.26 Evolution of CSD during ADNC1. The time shown is in minutes. ..... 106

Figure 4.27 SWMCL for ADNC experiments (a) ADNC1 (b) ADNC2 (c) ADNC3 (4) ADNC4 ..... 108

Figure 4.28 CSD (at the end of the batches) comparison of ADNC experiments with SSC3, the setpoints for each ADNC run are shown in the bracket. ..... 108

Figure 4.29 Microscopic images of selected experiments for comparison (a) unseeded linear cooling experiment (b) seeded linear cooling experiment (c) SSC3 run (d) ADNC4 ..... 109

Figure 4.30 ADNC5, heating/cooling rate 0.2 °C/min ..... 110

Figure 4.31 ADNC6, heating/cooling rate 0.4 °C/min ..... 110

Figure 4.32 Phase diagrams for (a) ADNC5 (b) ADNC6..... 111

Figure 4.33 ADNC-SSC1, target counts were 6000, supersaturation setpoint was 0.010 g/g .... 112

Figure 4.34 ADNC-SSC2, target counts were 14000, supersaturation setpoint = 0.005 g/g ..... 113

Figure 4.35 Phase diagrams for (a) ADNC-SSC1 (b) ADNC-SSC2 ..... 113

Figure 4.36 Supersaturation profile for ADNC-SSC1 experiment, SS setpoint was 0.01 g/g .... 114

Figure 4.37 CSD distributions for ADNC-SSC1 and ADNC-SSC2 experiments at the end of the batches ..... 115

Figure 4.38 Microscopic images of (a) ADNC-SSC1 (b) ADNC-SSC2 ..... 115

Figure 5.1 (a) Total counts/s, concentration and temperature for S-ADNC1 (b) Phase diagram for S-ADNC1 ..... 119

Figure 5.2 Evolution of fine and coarse particles for S-ADNC1 ..... 120

Figure 5.3 (a) Total counts/s, concentration and temperature profile for S-ADNC2 (b) Phase diagram for S-ADNC2 ..... 121

Figure 5.4 (a) Evolution of fine and coarse particles for S-ADNC2 (b) Variation in CSD for S-ADNC2 ..... 122

Figure 5.5 (a) Total counts/s, concentration and temperature profile for AS-ADNC1 (b) Phase diagram for AS-ADNC1 ..... 123

Figure 5.6 (a) Evolution of fine and coarse particles for AS-ADNC1 (b) Variation in CSD for AS-ADNC1, 472-482 min CSD prior to seed addition, 491-502 min CSD immediately after seed addition, 556-566 min CSD after the correction, end of the experiment ..... 125

Figure 5.7 (a) Total counts/s, concentration and temperature profile for AS-ADNC2 (b) Phase diagram for AS-ADNC2 ..... 126

Figure 5.8 (a) Evolution of fine and coarse particles for AS-ADNC2. (b) Variation in CSD for AS-ADNC2, 500-510 min CSD prior to seed addition, 539-549 min CSD immediately after seed addition, 579-589 min CSD after the correction, end of the experiment ..... 127

Figure 5.9 Comparison of CSD (at the end of the batches) of all the experiments ..... 128

Figure 5.10 SWMCL for (a) ADNC4 (b) S-ADNC1 (c) S-ADNC2 (d) AS-ADNC1 (e) AS-ADNC2 ..... 128

Figure 5.11 Micrographs of the products (a) ADNC4 (b) AS-ADNC1 (c) AS-ADNC2 (d) S-ADNC1 (e) S-ADNC2 ..... 129

Figure 6.1 Pilot plant crystallizer, 100 L capacity ..... 134

Figure 6.2 Schematic representation of the rig used, dimensions shown are in cm ..... 134

Figure 6.3 Total counts/s and temperature profile for OABA/water laboratory scale experiment ..... 135

Figure 6.4 Evolution of coarse particles for the laboratory scale OABA/water run using ADNC ..... 136

Figure 6.5 Micrograph of OABA crystals (form 2) obtained by ADNC at laboratory scale (1 L) ..... 137

Figure 6.6 Process and jacket temperature profiles for the linear cooling experiment at pilot plant scale ..... 137

Figure 6.7 Process and jacket temperature profiles for natural cooling experiment at pilot plant scale ..... 138

Figure 6.8 Total counts/s and process temperature profile for linear cooling experiment at pilot plant scale ..... 138

Figure 6.9 Total counts/s and process temperature profile for natural cooling run ..... 139

Figure 6.10 Total counts/s and temperature profile for ADNC run ..... 139

Figure 6.11 Micrographs of crystals (a) linear cooling (b) natural cooling (c) ADNC approach 140

Figure 6.12 DSC thermogram of OABA sample obtained at laboratory scale. Same results were obtained for samples from pilot scale experiments using the natural and linear cooling profiles. ..... 141

Figure 6.13 DSC thermogram of OABA sample obtained at pilot plant using the ADNC approach ..... 142

Figure 6.14 Total counts/s, concentration and temperature profile for PCM/IPA run in the industrial pilot plant crystallizer ..... 144

Figure 6.15 Operating curve in the phase diagram during the ADNC of the industrial crystallisation reactor. The difference between the primary and secondary MSZW can be clearly seen. ..... 145

Figure 6.16 Evolution of the SWMCL for the PCM/IPA run at the industrial scale crystallizer using the ADNC approach ..... 145

Figure 6.17 CSD for PCM/IPA experiment at the end of the batch ..... 145

Figure 7.1 Separately recorded spectra of OABA, PABA and MABA in IPA, all concentrations were 0.01 g/g. ..... 151

Figure 7.2 Spectrum of OABA, PABA and MABA when present together. The spectrum was recorded with 100 % IPA, concentrations of OABA and PABA were 0.219 g/g. ..... 151

Figure 7.3 Absorbance, total counts/s and temperature profiles for a calibration experiment ..... 152

Figure 7.4 Variation in absorbance at 339nm at constant temperature ..... 153

Figure 7.5 Absorbance values at 30 °C. Concentrations of OABA and PABA were 0.145 g/g. ..... 154

Figure 7.6 Variation in peak OABA absorbance at 339 nm with temperature and total counts/s ..... 154

Figure 7.7 Variation in peak PABA absorbance at 293 nm with temperature and total counts/s 155

Figure 7.8 Predicted concentration of OABA by the PCR model ..... 155

Figure 7.9 Predicted concentration of OABA by the ANN model ..... 156

Figure 7.10 Predicted concentration of PABA by the PCR model ..... 156

Figure 7.11 Predicted concentration of PABA by the ANN model ..... 156

Figure 7.12 Variation in total counts and absorbance at 339 nm for OABA ..... 158

Figure 7.13 Variation in total counts and absorbance at 293 nm for PABA ..... 158

Figure 7.14 Structure of PC-ANN model used with 8 inputs and 2 outputs ..... 159

Figure 7.15 Predicted dissolved mass of OABA ..... 159

Figure 7.16 Predicted dissolved mass of PABA ..... 160

Figure 7.17 Experimental setup used for the separation of the two isomers ..... 161

Figure 7.18 Absorbance and total counts profile for vessel 1 (OABA) ..... 162

Figure 7.19 Absorbance and total counts profile for vessel 2 (PABA) ..... 162

Figure 7.20 DSC thermogram of OABA (a) seeds (b) recovered product from the 2 isomers separation experiment. Heating rate was 15 °C/min. ..... 163

Figure 7.21 DSC thermogram of PABA (a) seeds (b) recovered product from the 2 isomers separation experiment. Heating rate was 15 °C/min. ..... 163

Figure 7.22 Microscopic images of OABA (a) seed (b) recovered product from the 2 isomers separation experiment ..... 164

Figure 7.23 Microscopic images of PABA (a) seed (b) recovered product from the 2 isomers separation experiment ..... 164

Figure 7.24 Experimental setup used for the separation of the three isomers ..... 165

Figure 7.25 Absorbance and total counts profile for vessel 1 (OABA) ..... 166

Figure 7.26 Absorbance and total counts profile for vessel 3 (PABA) ..... 166

Figure 7.27 DSC thermogram of OABA (a) seed (b) recovered product from the 3 isomers separation experiment. Heating rate was 15 °C/min. ..... 167

Figure 7.28 DSC thermogram of PABA (a) seed (b) recovered product from the 3 isomers separation experiment. Heating rate was 15 °C/min. ..... 167

Figure 7.29 DSC thermogram of MABA (a) seed (b) recovered product from the 3 isomers separation experiment. Heating rate was 15 °C/min. ..... 168

Figure 7.30 Microscopic image of recovered products from the 3 isomers separation experiment (a) OABA (b) PABA ..... 168

# List of Tables

Table 2.1 Different mechanisms of secondary nucleation ..... 17

Table 2.2 Effect of CSD on downstream processing ..... 20

Table 2.3 Refractive indices of different ATR materials ..... 34

Table 2.4 Various applications of FBRM ..... 40

Table 2.5 Summary of various offline and inline techniques used in crystallization ..... 41

Table 3.1 Summary of the calibration experiments ..... 65

Table 3.2 Root Mean Square Error of Prediction values for different models used ..... 79

Table 4.1 Summary of the experimental conditions for all experiments ..... 95

Table 5.1 Summary of the experimental conditions ..... 118

Table 7.1 Concentrations of OABA and PABA used at several IPA/water ratios for model building ..... 152

# Abbreviations

| | |
|---|---|
| ABA | Aminobenzoic acids |
| ADNC | Automated direct nucleation control |
| ANN | Artificial neural networks |
| API | Active pharmaceutical ingredient |
| ATR | Attenuated total reflection |
| BCG | Boston Consulting Group |
| BVI | Bulk video imaging |
| CLD | Chord length distribution |
| CryPRINS | Crystallization process informatics system |
| CSD | Crystal size distribution |
| CWMCL | Cubic weighted mean chord length |
| DOE | Design of experiments |
| DSC | Differential scanning calorimetry |
| FBRM | Focused beam reflectance measurement |
| FDA | Food and drug administration |
| FT-IR | Fourier transform infra-red |
| HSM | Hot stage microscopy |
| ICH | International Conference on Harmonization |
| IPA | Iso propyl alcohol |
| LWMCL | Length weighted mean chord length |
| MABA | Meta aminobenzoic acid |
| MSZ | Metastable zone |
| MSZW | Metastable zone width |
| NIR | Near infra-red |
| NMR | Nuclear magnetic resonance |
| OABA | Ortho aminobenzoic acid |
| PABA | Para aminobenzoic acid |
| PAT | Process analytical technology |
| PCA | Principal component analysis |
| PCM | Paracetamol |
| PCR | Principal component regression |
| PC-ANN | Principal component artificial neural networks |
| PLSR | Partial least squares regression |
| PVM | Particle vision and measurement |
| QBD | Quality by design |
| QBT | Quality by testing |
| RMSEP | Root mean squared error of prediction |
| SDI | Strategic Directions International |
| SNV | Standard normal variate |
| SSC | Supersaturation control |
| SWCLD | Square weighted chord length distribution |
| SWMCL | Square weighted mean chord length |
| UV/Vis | Ultra violet visible |
| XRD | X-ray diffraction |
| XRPD | X-ray powder diffraction |

# Chapter 1 Introduction

## 1.1 Background

Drug development is a long, expensive and cumbersome process (DiMasi *et al.*, 2003). Unlike other industries, which have made major changes in their research and development (R&D) processes, the situation in the pharmaceutical industry has not changed significantly since the 1960's (Kaitin, 2010). The traditionally followed research path is sluggish, low in efficiency, perilous and very costly (Kaitin, 2010). The drug development process is spanned over several stages, these are shown in Figure 1.1.

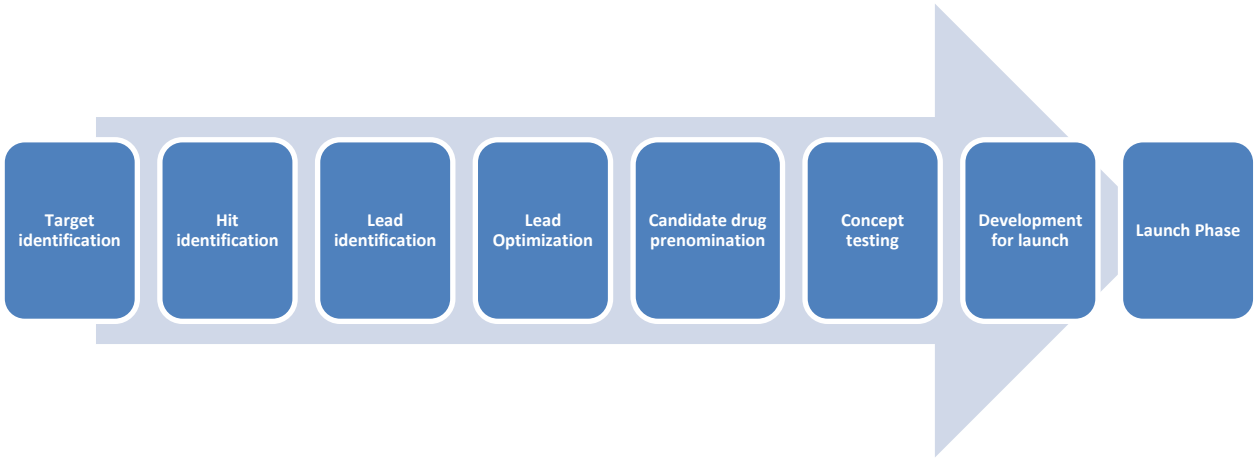



**Figure 1.1 Drug development stages**

According to Hinz, (2005) it takes 10-15 years on average to bring a drug to the market. The timeline varies depending on the therapeutic area (Kaitin, 2010). The pharmaceutical industry is now under pressure to reduce the historically accepted greater than 10 years development time. This has resulted in a shorter time available for route designing and scale-up (Federsel, 2008), motivated by the economic impact related to patent expiry, which can result in massive profit decline for the pharmaceutical industry (Keyhani *et al.*, 2006). Typical examples are the drugs enalapril, fluoxetine and ranitidine, for which the profit decreased by 61 %, 51 % and 69 %, respectively, after their patent expired (Boersma *et al.*, 2005). The issue was highlighted by Kaitin (2010), who reported the sales of the top 36 blockbuster drugs (drugs with annual sales of

$1billion dollars or more) will amount to $112 billion, but after the patent expiry these figures will drop dramatically. It is worth noting that the average R&D cost is only matched by 3 out of 10 products in terms of revenue (Grabowski *et al.*, 2002). Furthermore, companies now have to justify and show the superiority of their product in terms of therapeutic efficiency and cost.

The cost of drug development has increased considerably in the last 30 years (Rawlins, 2004). According to DiMasi *et al.* (2003) the average cost for a new drug is $802 million, increasing at 7.4 % per year. Boston Consulting Group (BCG) (E. Ref 1) estimated this to be $880 million. Adams and Brantner (2010) have calculated this to be in excess of $1 billion, depending on the therapeutic category. DiMassi and Grabowski (2007) stated that $1.24 billion would be required for launching a new biopharmaceutical product, while $1.32 billion will be required for a conventional drug including the cost of failures. Such high costs have resulted in R&D spending in excess of $50 billion only in USA in 2008 (Kaitin, 2010). The main factor responsible for the high drug costs is that a very small proportion of candidate drugs make it to the market. Out of 5000-10000 compounds that are selected in the drug discovery phase only 250 make it to the preclinical phase, 5 enter the clinical trials and only 1 gets approved by FDA. These failures result in increased development times and cost.

A breakup of the R&D expenses has been given by BCG (2001), and is shown in Figure 1.2. These figures reveal that substantial amount of money is invested during each phase of drug development. Reduction of time and minimization of failures during each of these phases can result in significant savings both in time and cost but also can help in extending the revenue generating period in the patent life of the product, and can bring new drugs to the market earlier. Pharmaceutical companies are under increasingly high pressure to decrease development time.

The main purpose of the PAT initiative by FDA, introduced in 2004, was to improve the understanding and control of the processes during process R&D and the routine manufacturing of pharmaceutical products. A better understanding and control can lead to improved product quality, lower number of failed batches, less variability and consequently reduction in drug development and manufacturing cost and time. Although PAT is used at different processing stages, its most significant application is during crystallization, as 90 % of the active

pharmaceutical ingredients (API) exist in crystalline form. Downstream processes such as filtration, drying and tableting along with bioavailability are significantly affected by the quality of the crystalline product (Chung *et al.*, 2000; Wibowo *et al.*, 2001; Mullin, 2001).

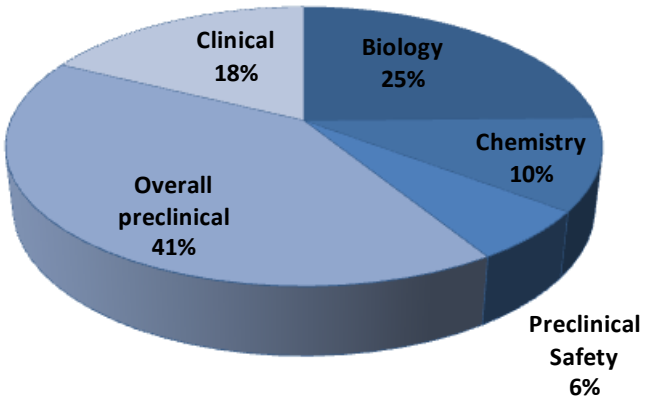



**Figure 1.2 Breakup of drug development costs**

CSD, polymorphism, purity and crystal habit are some of the most important properties of crystalline products. Although crystallization is an old unit operation, still it is not well understood and obtaining products with required properties, and the consistent scale up of the process poses a significant challenge to the industry. With the availability of PAT, FDA encourages the industries to adapt QBD approaches rather than the traditional quality-by- testing (QBT). QBD ensures that quality is built into the product during processing by continuous monitoring and control. Using the available set of PAT tools any unwanted events that may occur during the processing can be detected and appropriate actions taken swiftly. This results in minimization of failures and improved quality, which then affect the overall economics and efficiency of the system (Bakeev, 2010).

The QBD concept considers the application of PAT tools for the entire drug development process from the evaluation of raw materials until the final product rolls out of the plant. For example *in situ* near infrared (NIR) spectroscopy is frequently used for rapid screening and testing of the raw materials (Fevotte *et al*., 2004), ATR fourier transform infrared (FTIR) (Fevotte, 2002) and ATR-UV/Vis spectroscopy can be used at the synthesis stage (Thurston *et al*., 2004) or during the separation by crystallization for detection of any impurities and application of supersaturation control for improved quality. Similarly focused beam reflectance measurement (FBRM) can be

used to determine metastable zone width (MSZW) along with monitoring changes in CSD (Barrett and Glennon, 2002). Additionally, feedback control approaches based on the use of FBRM can be applied to enhance CSD. Raman spectroscopy can be employed for determination and characterization of polymorphic forms and hydrates (Hausman *et al*., 2005). All these tools give real time information and therefore their application is often more accurate and less time consuming than the traditional offline techniques. PAT has also enabled the development and use of more sophisticated control approaches (both first principles and direct design techniques) which is a major shift from trial and error or open loop control methodologies (Fujiwara *et al*., 2005).

Some of the challenges faced by the pharmaceutical industry have been discussed in the previous section. PAT can play a crucial role to overcome some of the problems faced during drug development and manufacturing and therefore is the way forward. It is crucial to fully exploit the benefits, uses and applications of all the PAT tools available, at laboratory, pilot and industrial scales. Only a handful of studies are available that deal with the application of FBRM as a process controlling tool, there is no research available that shows the use of ATR-UV/Vis spectroscopy in a feedback control approach and only a few publications deal with its application in the crystallization process. Also the literature that deals with the application of these approaches on pilot and industrial scale is scarce. The main aim of the work undertaken is therefore to expand the utility and application of these techniques both on laboratory and pilot scale as monitoring and control tools.

## 1.2 Research Aims and Objectives

The main aims and objectives of the work undertaken are as follows:

i. To investigate the capability of ATR-UV/Vis spectroscopy for the qualitative monitoring and control of pharmaceutical crystallization processes.
ii. To evaluate novel automated model-free control approaches for batch crystallization processes based on the use of ATR-UV/Vis spectroscopy and FBRM devices.

iii. To investigate the performance of the developed model-free control approaches for various pharmaceutical crystallization systems at different scales.

iv. To compare the proposed automated direct nucleation control (ADNC) approach with other control approaches, such as open-loop control, linear cooling and supersaturation control.

v. To investigate the use of the model-free control approaches as a means of rapid scale-up methodology.

vi. To develop complex non-linear calibration procedures, which enable the simultaneous monitoring of several compounds in multi-component pharmaceutical crystallization.

vii. To prepare novel crystallization systems for the separation of mixtures of compounds.

## 1.3 Research Methodology

The PAT tools used in the current work for process monitoring and control were ATR-UV/Vis spectroscopy and FBRM. ATR-UV/Vis spectroscopy gives absorbance data which can be used to determine the concentration(s) of compound(s) in a solution. This spectroscopic technique can provide both qualitative and quantitative information about the system. Concentration of a solution can be determined by using ATR-UV/Vis spectroscopy data by developing a calibration model. ATR-UV/Vis spectroscopy was used in the development of a control approach used in this research. FBRM was used for monitoring of the solid phase. The laser back-scattering tool measures chord lengths and can be used to obtain qualitative information about different crystallization related phenomena such as nucleation, dissolution, growth and agglomeration of particles. FBRM was used for the development of one of the feedback control strategies presented in the current work. Single and multi component cooling and anti-solvent crystallization processes were the main focus in this work especially cooling crystallization, because of its wide application in the industry. For scale up study cooling experiments were carried out at 1 L laboratory and 100 L pilot plant scale.

Several different chemometrics aspects were used in the work, these include: calibration model development and assessment using principal component regression (PCR), partial least squares

regression (PLSR), artificial neural networks (ANN), principal component-artificial neural network (PC-ANN). Design of experiments (DOE) was also used to perform experiments in a systematic and optimal way for calibration model development.

## 1.4 Research Contribution

A summary of the major contributions of the work is as follows:

- A systematic calibration model development approach for concentration determination in crystallization using ATR-UV/Vis spectroscopy is presented. A simple non linear model using derivative at a single wavelength will be developed. The developed model should be able to predict the concentration with high accuracy. Solubility data obtained using this model will be compared with the literature data to confirm its predictive ability.

- A model-free crystallization control approach will be developed based on the real-time and *in situ* use of ATR-UV/Vis spectroscopy coupled with a non-linear calibration model. The approach should be able to follow a particular operating trajectory in the crystallization phase diagram, using the supersaturation feedback control concept. This will enable the production of uniform crystals, and can be used as a fast direct design approach for crystallization systems. The work will provide the first experimental demonstration of the ATR-UV/Vis spectroscopy for feedback supersaturation control.

- A comprehensive analyses of a new ADNC model-free approach is provided. The ADNC approach adaptively drives the crystallization process in the phase diagram using a sequence of controlled nucleation and dissolution events so that a desired number of particle counts obtained from the FBRM probe is maintained. Detailed guidelines for the practical implementation of the ADNC will be provided. The performance of the approach to produce large uniform crystals will be demonstrated for cooling crystallization of paracetamol (PCM) and iso-propyl alcohol (IPA) system.

- Innovative internal seeding methodology is proposed based on the combined use of ADNC and SSC. The proposed ADNC-SSC approach will combine the information obtained from FBRM and ATR-UV/Vis spectroscopy for controlling crystallization process. It will be demonstrated that the *in situ* seed generation approach based on the combined ADNC approach outperforms the traditionally used linear and programmed cooling based operations using externally generated seed, yielding uni-modal distribution and larger mean crystal size.

- A fast and robust scale-up methodology is proposed based on the use of the ADNC approach. The ability of the ADNC approach to adapt the operating profile to the changing conditions due to scale-up will be demonstrated for the model pharmaceutical compound ortho-aminobenzoic acid (OABA) in water. The control approach will be implemented on 100 L and 1 L scales and it will be shown that the ADNC based scale-up method outperforms common approaches used in the industry, which simply implements linear and natural cooling trajectories on both scales.

- A new non-linear calibration model capable of simultaneously measuring concentrations of a mixture of OABA and para aminobenozic acid (PABA) for both cooling and anti-solvent crystallizations will be developed using PC-ANN approach. This will be based on absorbance spectra measurements obtained by ATR-UV/Vis spectroscopy.

- A novel setup comprising of two and three interconnected crystallizers will be developed and used for the simultaneous separation of two and three positional isomers of amino benzoic acid when present together in the solution. The simultaneous combined use of ATR-UV/Vis spectroscopy and FBRM probes will be demonstrated for the first time for the monitoring of multi-component crystallization in interconnected vessels. ATR-UV/Vis spectroscopy and FBRM will be used for monitoring of liquid and solid phases respectively. The proposed approach will employ seeded cooling crystallization and sintered disk filters for the separation.

## 1.5 Structure of the Thesis

The thesis comprises of seven chapters which are presented in the following order:

- Chapter 1 introduces the economic aspects of the drug development process and the benefits of using PAT for optimizing the product quality and process costs are highlighted.

- Chapter 2 reviews the relevant literature and concepts of crystallization processes are discussed, such as solubility, supersaturation, polymorphism and crystallization kinetics etc. Several PAT tools and their applications for monitoring and control of crystallization processes are discussed.

- Chapter 3 presents a systematic methodology for calibration model development, this includes analysis of data for linearity/non-linearity, selection of a suitable calibration model, analysis of various calibration model development techniques and validation. A detailed analysis of the selected calibration model is also provided.

- Chapter 4 introduces the ADNC, SSC, ADNC-SSC approaches. The working principle, advantages, disadvantages and comparison of several control policies used for paracetamol/IPA system are presented. The novel internal seeding approach based on the ADNC-SSC is introduced.

- Chapter 5 analyzes the robustness of the ADNC approach when the system is subjected to disturbances common in industrial operation such as accidental seeding. The results of a detailed comparison between seeded and unseeded ADNC operations are also presented in this chapter.

- Chapter 6 proposes the novel feedback control based scale-up methodology, using ADNC. The previously described ADNC approach is extended here and applied on a 100 L pilot plant scale. Ortho aminobenzoic acid (OABA) and water is used as the model

system. The application of the DNC as a scale up approach is discussed here by analyzing the results obtained on 100 L and 1 L scales.

- Chapter 7 is divided in two sections. In the first part the development of a calibration model for the monitoring of a complex multi-component system using ATR-UV/Vis spectroscopy is discussed. Several chemometric approaches such as principal PCR, ANN and PC-ANN were used and tested for their concentration prediction ability. A systematic experimental design approach was used to significantly decrease the number of experiments required to develop the complex non-linear calibration model. The second part of the chapter proposes an innovative setup based on interconnected crystallizers, for the separation of aminobenzoic acid (ABA) isomers. The Separation of two and three isomers when present together in the solution is carried out using two and three interconnected crystallizers via seeded cooling crystallization and the process is monitored using ATR-UV/Vis spectroscopy and two FBRM probes.

- Chapter 8 concludes the work presented and recommendations for future work are discussed.

# Chapter 2 Literature Review

## 2.1 Solubility and Supersaturation

Solubility is the amount of a substance that can be dissolved in a solvent at a given temperature. Knowing the solubility curve in a given solvent (or solvent system) is required prior to the commencement of any crystallization process. Several important properties of the crystalline product i.e. polymorphic form, shape of crystals and yield are dependent on solubility and supersaturation (Karunanithi *et al.*, 2007; Modarresi *et al.*, 2008). Furthermore, the selection of the type of crystallization process e.g. cooling or anti-solvent crystallization is also dictated by the solubility of the compound in selected solvents. It is worth noting that for a given solute in a given solvent, the solubility curve is a function of temperature; however, impurities can affect the solubility. Often the solvent is selected during the early drug development phases i.e. during target and hit identification followed by hit refinement and lead refinement stages (Bleicher *et al.*, 2003; Myerson, 2002). This therefore requires process engineers to be in contact with synthetic chemists for appropriate selection of the solvent for subsequent crystallization of the drug compound.

The usage of high throughput screening has resulted in large number of poorly soluble drug compounds, posing a major challenge to the formulation scientists for oral delivery of these drugs (Leuner and Dressman, 2000). Although water is still one of the most widely used solvents because of its availability at lower cost and non-toxicity (Mullin, 2003) it has been reported that the number of drug candidate compounds with low aqueous solubility is increasing (Blagden *et al.*, 2007). A number of different strategies have been reported to improve the solubility of the compounds. These include: increasing surface area of the particles by micronisation (Chaumeil *et al.*, 1998), usage of co-solvents, solubility enhancement by using salt forms, micellar solutions and cyclodextrin complexes (Rajewski and Stella, 1996). However, the effectiveness of these methods is limited e.g. the use micellar systems are dependent on properties of therapeutic molecules and limited range of pharmaceutical excipients (Blagden *et al.*, 2007). Micronisation

improves the dissolution profile of the drugs, but the equilibrium solubility still remains unchanged (Müller, 2001).

In the crystal engineering framework, tailoring size and habit of crystals can be used to to enhance the solubility, dissolution profile and bioavailability of drugs with poor solubilities. For example, during the growth of the crystals, the mechanism shifts from screw dislocation to surface nucleation and ultimately to growth in the presence of certain solvents on additive molecules. These changes in growth mainly arise from change in solubility caused by additive molecules and solvents. Change in crystal habit has been observed to change the *in vitro* dissolution rate. For example, the dissolution of rod shaped dipyridamole crystals is quicker compared to rectangular needle shaped crystals (Adhiyaman and Basu, 2006). Other factors that contribute to solubility and dissolution rates include polymorphic form, crystalline versus amorphous form of drugs and co crystals. A review of how these factors influence solubility is provided by Blagden *et al.* (2006). Co-crystals is particularly an area of growing interest in terms of solubility enhancement and improvement of other physiochemical properties of the drugs, the advantages of using them are discussed in detail by Good and Rodriguez-Hornedo (2009).

A variety of techniques are available for solubility measurements, these are classified as isothermal and non-isothermal methods. In the isothermal method solvent is kept at desired temperatures for 4-24 hours with excess of solids, and then a clear sample is taken and analyzed. The main purpose of using longer time is to make sure that thermal equilibrium has been reached and the dissolution rate is closer to the saturation point. Isothermal methods are considered more accurate compared to that of non-isothermal methods (Mohan *et al.*, 2002). Mohan *et al.* (2002) also demonstrated the use of differential scanning calorimetry (DSC) for solubility measurement. The results were close to typically employed techniques, except for the compounds having little change in the solubility with temperature. With advancement in PAT inline methods e.g. ATR-FTIR can be used for determination of solubility (Barrett *et al.*, 2005; Dunuwila *et al*., 1994).

As mentioned before the selection of solvent and behaviour of solute plays a crucial role during crystallization. Often the experimental data is not available for new molecules. In these cases model based calculations are used to predict the solubility and selection of solvents. Computer

aided molecular design (CAMD) is used for solvent selection and design (Harper and Gani, 2000). CAMD uses properties estimated by different available models, such as Universal Functional Activity Coefficient (UNIFAC) (Fredenslund *et al.*, 1977), connectivity indices (CI model) (Gonzalez *et al.*, 2007), combined UNIFAC/CI models, Non-random Two-Liquid segment activity coefficient model (NRTL-SAC) (Chen and Crafts, 2006) and others. A review on the use and limitations of these models is provided by Modarresi *et al.* (2008).

The main driving force in crystallization is the difference in chemical potential between the solution and the solid phase. This is typically expressed in terms of the supersaturation, which is the difference between the solution concentration and the saturation concentration. Supersaturation can be created by several methods such as cooling, evaporation, and/or addition of anti-solvent, including changing the pH by addition of acid or base (Fujiwara *et al.*, 2005).

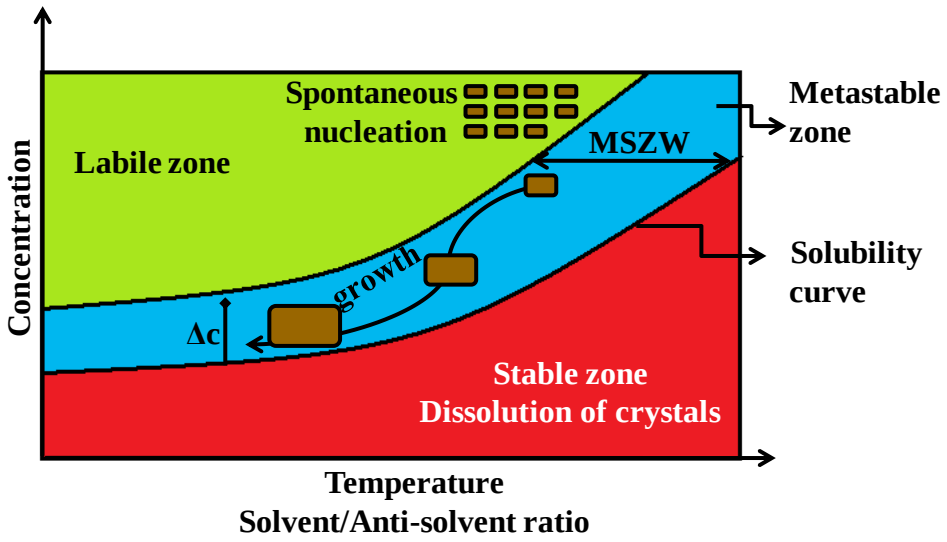



**Figure 2.1 Phase diagram for crystallization process**

A typical phase diagram for a crystallization process is shown in Figure 2.1. Absolute supersaturation, $S$, here can be defined as the difference between the concentration of the solution, $c$, and the solubility concentration, $c_s$, at a particular temperature:

$$S = \Delta c = c - c_s \tag{2.1}$$

The relative supersaturation is another way to express supersaturation and is described as:

$$\sigma_s = \frac{c - c_s}{c_s} \tag{2.2}$$

As shown in Figure 2.1 the area below the solubility curve is the undersaturated region where crystals cannot exist in equilibrium, while the area between the solubility curve and labile region is called metastable zone (MSZ). In this area crystal growth takes place without significant spontaneous nucleation. The labile zone is the metastable region where spontaneous nucleation dominates. Presence of foreign particles and crystals can significantly affect the metastable zone width (MSZW), a clear metastable limit is therefore difficult to define because of its dependence on various factors. Factors affecting the MSZW and subsequently the crystalline product will be discussed in the following sections. As mentioned previously several methods are available for generation of supersaturation. The degree of supersaturation dictates the nucleation, crystal growth and finally the CSD. A better control and management of supersaturation generation methods can be used to optimize the supersaturation level in the system and hence the crystals with desired properties can be obtained.

## 2.2 Nucleation

Nucleation can be termed as the first step towards the formation of a solid phase (Jones, 2003). Nucleation is often the decisive step in the crystallization process and is of practical importance in pharmaceutical systems. Nucleation phenomena are equally important in the control of crystal properties and in the selective crystallization of a particular polymorph (Rodriguez-Hornedo and Murphy, 1999).

With reference to the phase diagram in Figure 2.1, when the supersaturation level exceeds a certain limit i.e. beyond labile zone spontaneous nucleation will take place. A supersaturated solution exists in unstable state, nucleation is therefore an attempt to reach a stable state by the solution. The mechanism of nucleation is still not very well understood. The classical nucleation theory is briefly described next.

Nuclei are formed by combination of embryos a few nanometres in size. These nuclei upon reaching a critical size grow to form crystals. The rate of nucleus formation is given by the following expression:

$$B_o = A\exp\left(-\frac{\Delta G_{cr}}{kT}\right) \tag{2.3}$$

where $B_o$ is the rate of nucleus formation, $A$ is the pre-exponential factor having a value at the order of magnitude of $10^{30}$ nuclei/cm$^3$ sec$^{-1}$, $k$ is the Boltzman constant $1.3805\times10^{-23} JK^{-1}$, $T$ is the temperature and $\Delta G_{cr}$ is the change in free energy for a nuclei of critical size. The free energy change for an aggregate undergoing a phase transition $\Delta G$ is given by:

$$\Delta G = \Delta G_s + \Delta G_v = 4\pi r^2\gamma + \frac{4\pi r^3 \Delta G_v}{3} \tag{2.4}$$

where $\Delta G_s$ is the surface free energy change associated with the formation of the aggregate (a positive quantity), $\Delta G_v$ is the volume free energy change associated with the phase transition (a negative quantity) and $\gamma$ is the interfacial tension, and $r$ is the radius of the aggregate . The right-hand terms of equation (2.4) are of opposite sign and depend differently on $r$ (radius), so the free energy of formation $\Delta G$, passes through a maximum (see Figure 2.2). This maximum value $\Delta G_{cr,}$ corresponds to the critical nucleus, $r_c$ . The critical size is given by:

$$r_c = \frac{-2\gamma}{\Delta G_v} \tag{2.5}$$

The critical size therefore represents the minimum size of a stable nucleus. Particles smaller than $r_c$ will dissolve, or evaporate if the particle is a liquid in a supersaturated vapour, because only in this way can the particle achieve a reduction in its free energy. Similarly particles larger than $r_c$ will continue to grow. $\Delta G_{cr}$ is given by the following equation:

$$\Delta G_{cr} = \frac{4}{3}\pi\gamma r_c^2 \tag{2.6}$$

From the Gibbs-Thompson equation:

$$\ln S = \frac{2\gamma\nu}{kTr} \tag{2.7}$$

where $\nu$ is the molecular volume and $S$ is the supersaturation ratio, $S = \frac{C}{C_s}$. From equation (2.6):

$$\Delta G_{cr} = \frac{16}{3}\frac{\pi\gamma^3\nu^2}{(kT\ln S^2)} \tag{2.8}$$

And from equations 2.7 and 2.5:

$$B_o = A\exp\left(-\frac{16}{3}\frac{\pi\gamma^3\nu^2}{k^3T^3(\ln S^2)}\right) \tag{2.9}$$

From equation (2.9) we can see that the nucleation rate is dependent upon supersaturation, temperature and interfacial tension.

Although classical nucleation theory is widely accepted, discrepancies exist between experimental results and theoretically predicted mechanisms suggesting that the nucleation process is more complex than explained in the classical theory. A two step model has been proposed, it was originally considered for protein crystallization, but its application for small organic molecules suggest that this model can explain majority of the crystallization processes from solutions. According to this model solute molecules initially combine to form a cluster of sufficient size, the cluster is then reorganized in an ordered structure and finally the formation of crystals takes place. A detailed description and comparison of classical nucleation theory and the two step model is given by Erdemir *et al*. (2009) and Vekilov (2010).

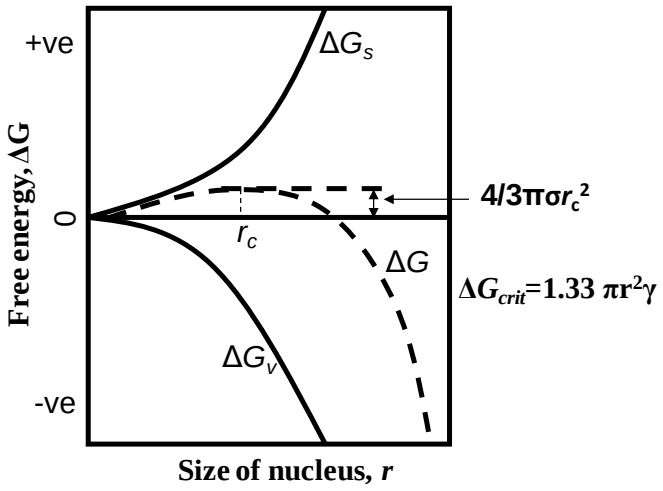



**Figure 2.2 Changes in Gibbs free energy (adapted from Myerson, 2000)**

Nucleation can be primary or secondary depending on whether supersaturated solution is free of crystalline surfaces or contain crystals, respectively (Seader and Henley, 2006). Primary nucleation can be divided into two types, namely homogeneous nucleation and heterogeneous nucleation. Homogeneous nucleation rarely occurs in large volumes since solutions contain random impurities that may induce nucleation. The heterogeneous nucleation of a solution can take place by seeding from embryos retained in cavities, e.g. in foreign bodies or the walls of the retaining vessels, under conditions in which the embryos would normally be unstable on a flat surface. Heterogeneous nucleation processes are of fundamental and of practical importance in pharmaceutical systems since unintentionally or intentionally added surfaces or interfaces may induces nucleation. The reactivity of crystals surfaces as heterogeneous nuclei has significant effects on the crystallization of the desired compound and in the control of conversions between these modifications, since the free energy required for the formation of two-dimensional nuclei is lowered by the presence of an appropriate substrate (Rodriguez-Hornedo and Murphy, 1999).

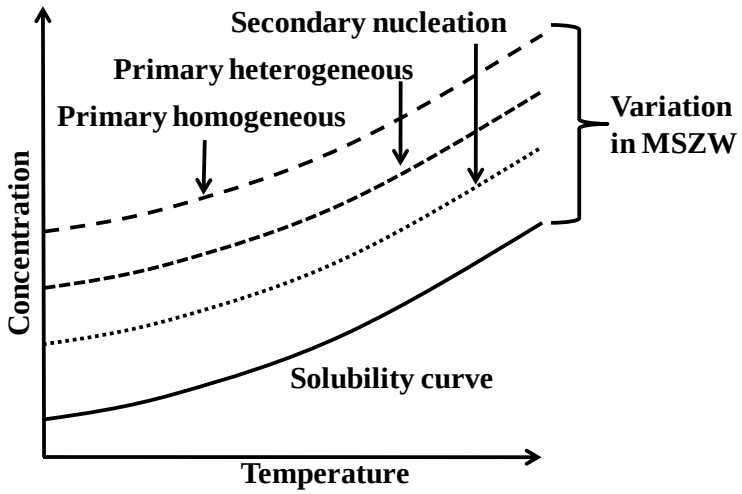



**Figure 2.3 Variation in MSZW based on nucleation types (adapted from Mersmann, 2001)**

The presence the foreign bodies such as dust in pharmaceutical plant can induce nucleation at degrees of supercooling lower than those required for spontaneous nucleation. The MSZW based on each of these nucleation mechanisms appears at different points in the phase diagram as shown in Figure 2.3. These variations in the MSZW can have profound effects on the outcome of the crystallization process and will be discussed in the following sections. Nucleation in industrial crystallizer occurs mainly by secondary nucleation caused by the presence of existing crystals in the supersaturated solution. Secondary nucleation can occur by mechanisms mentioned in Table 2.1 (Tavare, 1995):

**Table 2.1 Different mechanisms of secondary nucleation**

| No. | Type | Cause |
|---|---|---|
| **1** | Initial breeding | Dust on dry seeds |
| **2** | Needle breeding | Breakage of dendritic growth on parent crystals |
| **3** | Polycrystalline breeding | Breakage of agglomerates |
| **4** | Shear nucleation | Fluid shear on growing crystal face |
| **5** | Contact nucleation | Collision breeding: crystal-crystal, crystal-impeller, crystal-vessel internals |

Contact nucleation is the most common type of secondary nucleation and since it can occur at the low values of supersaturation that are typically encountered in industrial applications.

## 2.3 Polymorphism

The ability of a molecule to exist in more than one crystalline forms is termed as polymorphism. The difference in crystalline structure can arise from different arrangement or conformation of the molecules in the crystal lattice (Brittain, 2009). It is convenient here to mention some other attributes of crystal structures arising from the formation of solvates, hydrates or an amorphous form of a compound. In solvates, the crystals contain solvent in certain amounts, when the solvent used is water, the term hydrate is used. In amorphous solid molecules are arranged in a disorderly manner as compared to ordered arrangement of molecules in a crystal. Generally, the most stable polymorphic form is used in the drug development, however, there are a few exceptions; e.g. if the stable polymorph has a lower solubility and the desired dosage form cannot be achieved a more soluble metastable form can be selected. A metastable form can also be used to achieve faster dissolution (Singhal and Curatolo, 2004).

During drug development a thorough knowledge of polymorphs and their formation and stability conditions is crucial. Polymorphs can have different physical and chemical properties e.g. different solubility, this in turn can affect the bioavailability of the drug in the human body. Downstream processes such as filtration, drying, milling and tableting are also affected by different polymorphs as they have different habits, packing and mechanical properties etc. Polymorphs can have significant commercial and economic impact. The classical example is the discovery of a new polymorphic form in the drug ritonavir which caused a disruption in the production (Bauer *et al.*, 2001). On the other hand a pharmaceutical company manufacturing Zantac successfully defended another polymorph for the same drug and fended off the competition after the patent had expired (Brittain, 2009). Polymorphs and their properties take center stage in generic drug production and abbreviated new drug applications, where bioequivalence of the product must be proved prior to its approval for production (Raw *et al.*, 2004).

The polymorphs of a particular compound can be either enantiotropically or monotropically related to each other, these two phenomenon are shown in Figure 2.4. In enantiotropic system a particular polymorph is stable below a certain temperature, while the other is metastable, it

should be noted that transformations in enantiotropic systems are reversible. Both kinetic and thermodynamic factors determine the interconversion rates of different polymorphs. In terms of nucleation of a polymorphic form, Ostwald's rule of stages states that the metastable form will nucleate first and will subsequently convert to the most stable form (Ostwald, 1897). In monotropic systems there is no crossover of the solubility curves and therefore only one form is stable, while the other forms are metastable. Enantiotropic systems require a careful selection of processing conditions under which a particular polymorph can be obtained, in contrast obtaining a stable polymorph is monotropic systems is generally easier (Mangin *et al.*, 2009).

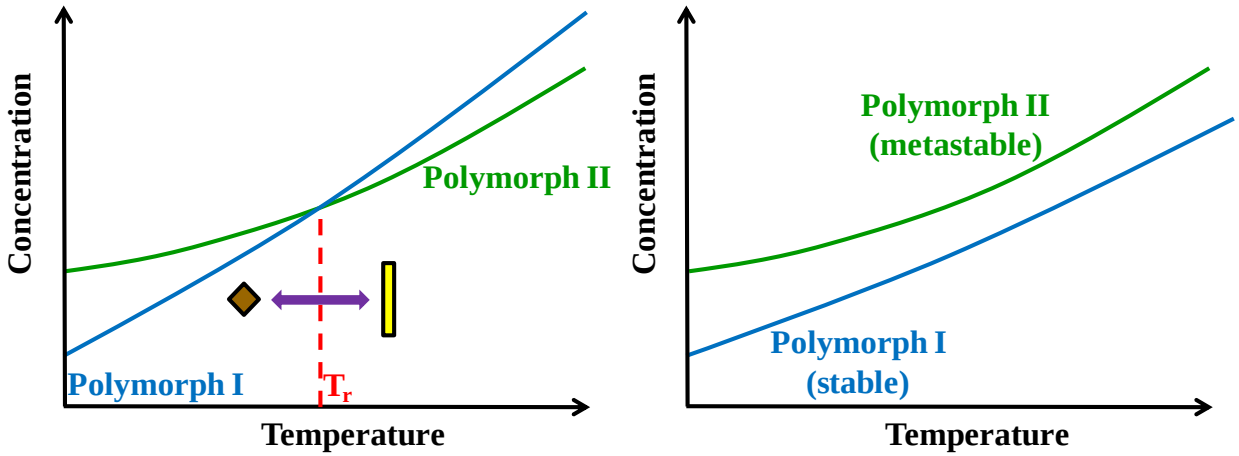



**Figure 2.4 Phase diagram showing enantiotropic and monotropic polymorphic systems**

Factors that can lead to the formation of a particular polymorph during crystallization include temperature, supersaturation, solvent, heating/cooling rates and hydrodynamics. When a change occurs in the polymorphic form in the presence of a solvent, this is termed as a solvent mediated transformation. Seeding can be used as a way to produce the desired polymorph as long as the crystals do not undergo a solvent mediated transformation. This requires knowledge of the MSZW and temperature dependency of the stability of different polymorphic forms. Characterization and screening of polymorphs, solvates, hydrates and amorphous forms is carried out by using various techniques, including, x-ray diffraction, powder x-ray diffraction, raman spectroscopy (Hu *et al*., 2005; Hausman *et al*., 2005), DSC, microscopy and others.

## 2.4 Crystal Size Distribution

During drug production several steps are involved after crystallization before the final product is obtained. The performance of all these processes therefore strongly depends on the quality of the crystalline product. Poor CSD can be characterized by the presence of excessive fines, a very broad or narrow distribution and unacceptable average crystal size. Table 2.2 summarises the effects of the CSD on different downstream processes (Wibowo *et al*., 2001). The presence of fines can result in longer filtration times and can also clog the filtration medium. Similarly smaller average size can extend the washing and drying duration. Solvent inclusion is another problem which can be caused by the presence of excessive fines, and can affect the quality of the product. A suitable crystallization control approach therefore must be able to address these issues.

**Table 2.2 Effect of CSD on downstream processing**

| Downstream Processes | Too much fines | CSD too wide | CSD too narrow | Avg. size too small |
|---|---|---|---|---|
| **Filtration**<br>Higher solvent requirement, large filter area, clogging | **X** | **X** | | **X** |
| **Washing**<br>Higher solvent requirement, longer washing time | | **X** | | **X** |
| **Deliquoring**<br>Longer time or larger than what is available, high residual liquid in cake | **X** | **X** | **X** | **X** |
| **Drying**<br>Longer drying time and high energy consumption, dust | **X** | **X** | **X** | **X** |
| **Compaction**<br>Low agglomeration strength | | | **X** | |

## 2.5 Control of Crystallization Processes

Crystallization is predominantly used as a batch process in the pharmaceutical industry as very large quantities of active pharmaceutical ingredients (API) are seldom required. Furthermore same crystallizers are used for crystallization of different compounds. Since these compounds may require significantly different control recipes, batch operation offers the flexibility to implement different operating policies with relative ease. Therefore in the following section commonly used crystallization methods will be discussed along with their advantages and disadvantages, with main emphasis on batch processes.

### 2.5.1 Cooling Crystallization

Cooling is the most widely used method to generate supersaturation in crystallization processes, it can be used for both seeded and unseeded systems. Typically, cooling crystallization is employed for systems which show an increase in solubility as the temperature increases and are not prone to thermal degradation. Another advantage of this approach is that it is not limited by the volume of the vessel, which could potentially be a limiting factor for anti-solvent crystallization. Cooling crystallization is used both for external seed addition and *in situ* seed generation. It should be noted that seeding is a popular method for obtaining desired crystal size distribution and polymorphic forms. Depending on the requirements the seed amounts can be adjusted. The effect of the various seed amounts is summarized as follows (Tung *et al.*, 2009):

- A very small amount can be helpful in elimination of oiling out and crashing out of the solution.

- Less than 1% can give some control over nucleation, the system is prone to secondary nucleation events and bi-modal distribution in the final product can be expected.

- 5-10% of seeds can suppress secondary nucleation events and improve CSD.

- Large amounts of seed crystals are typically used in continuous or semi batch operations, to increase production yield.

Seeded cooling crystallization is also termed as controlled crystallization as the presence of seeds prevents the system from going into the labile zone. Several cooling profiles have been purposed for obtaining product with desired qualities, some of these are:

### *Natural cooling*

In natural cooling (Figure 2.5) the system is cooled rapidly in the beginning resulting in high amounts of supersaturation causing significant nucleation event(s) (Jones and Mullin, 1974). The crystalline product obtained consists of large amounts of fines often leading to bi-modal distribution. Other issues with the product may include dendritic growth and occlusions of solvent or impunities in the crystals (Mullin, 2001).

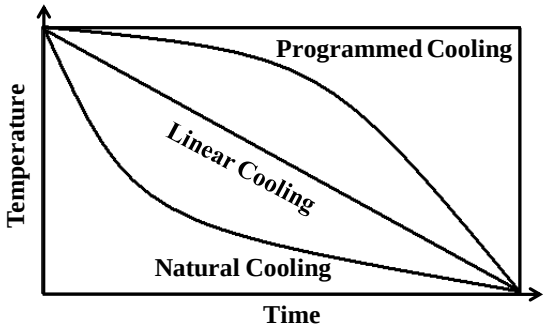



**Figure 2.5 Different Cooling Profiles**

### *Linear Cooling*

In linear cooling a constant cooling rate is adopted, as shown in Figure 2.5, this profile eliminates the higher supersaturation levels generated in the case of natural cooling and can lead to improved CSD (Jones, 1974). The main attraction for using linear cooling profile is that it can be implemented easily especially on larger scale. However, it does require the existence of suitable temperature control systems, as opposed to the natural cooling operation, which can be achieved without temperature control

***Programmed Cooling***

The aim of programmed cooling profile is to ensure that the supersaturation always matches the available crystal surface area on which the crystal mass forms. This means that initially when the surface area of the crystals existing in the solution is small, the rate of supersaturation production has to be slow and therefore low cooling rates are used to prevent nucleation. If the initially generated large amount of supersaturation can be controlled, then an improved CSD can be obtained. This can be achieved by introduction of seeds in the system and then maintaining the operating curve within the metastable zone (Mullin, 2003). A simple correlation for determining an approximation of the optimal cooling curve is given by Mullin (2003) as follows:

$$T_t = T_o - \left(T_o - T_f\right)\left(\frac{t}{\tau}\right)^3 \tag{2.10}$$

where $T_o$, $T_f$ and $T_t$ are the temperatures at the beginning, end and at any time $t$ during the process, and $\tau$ is the overall batch time.

## 2.5.2 Anti-solvent Crystallization

Anti-solvent crystallization is another way of attaining supersaturation. Anti-solvent processes have been widely used to crystallize pharmaceuticals, because the technique eliminates the use of thermal energy that may degrade the biological activity of actual pharmaceutical ingredients (Guo *et al*., 2005). In anti-solvent crystallization, supersaturation is created by mixing a third component with the saturated solution, to reduce the solubility of the solute. It normally takes place at or near ambient temperatures and is effective in crystallization of thermally degradable substances (Yu *et al.* 2006 a; b), further the compounds which show little change in their solubility at different temperatures are also crystallized by addition of appropriate anti-solvent.

Anti-solvent crystallization is usually performed in a semi-batch manner, whereby anti-solvent is pumped into the crystallizer at a constant or varying flow rates. It has been found that a

predetermined time-varying flow rate can yield a better particle size distribution (PSD) by matching the generation rate of supersaturation with the growing crystal (Mullin, 2001). The derivation of such a flow-rate profile requires prior knowledge of the exact crystallization kinetics, which is difficult and time consuming to obtain for industrial conditions. Furthermore, operating conditions such as seed size distribution, seeding timing, impurity content, mixing and starting solute concentration often change from batch to batch and are difficult to be tracked precisely, which will render the predetermined profile not optimal anymore.

The composition of solvents (and also anti-solvents) is known to influence the crystallization behaviour of polymorphs. For example, the relative nucleation, growth rates and transformation rates of the polymorphs of L-histidine are known to be influenced by the composition of the solvent (i.e. mixture of water and ethanol) (Kitamura and Sugimoto, 2003).

### 2.5.3 Combined cooling and anti-solvent crystallization

Nagy *et al.*, (2008) have compared the combined cooling and anti-solvent crystallization technique using lovastatin as the model system. Optimal profiles for cooling, anti-solvent and combined system for both seeded and non-seeded systems were implemented, and compared crystal quality. The results obtained showed that a combination of both cooling and anti-solvent crystallization gave better results, producing more uniform crystal size distribution with larger mean size as compared to the individual approaches. Lindenberg *et al.* (2009) showed that the combined approach gave superior results for acetylsalicylic acid compared to the conventional approaches.

Combined cooling and anti-solvent crystallization processes are often used in the pharmaceutical industries. For example anti solvent can be added at the beginning of the batch to induce nucleation, or at the end to increase yield. However optimal design of the simultaneous cooling and anti-solvent addition policies require more sophisticated model based design approaches.

The heuristic choice of temperature or anti-solvent addition profiles based on the conditions described in the previous sections is the most common approach applied in the pharmaceutical industries because of ease of implementation. There is a growing interest now to switch to more sophisticated control methodologies to consistently obtain products of desired quality. These methodologies can be classified as model-based and model-free (direct design) approaches and will be described in the next section.

## 2.6 Model-based Approaches

Model based approaches for crystallization have gained popularity in the last decade. One of the main reasons has been to shift the research paradigm from an art towards a better understood scientific process. Other factors include availability of *in situ* sensors for measuring concentration and CSD such as ATR-FTIR, FBRM etc. The model-based approaches for controlling and optimizing a crystallization process, typically consider a certain property of the CSD, such as mean crystal size, as coefficient of variation. Material and energy balance equations are then used to obtain the best operating conditions that optimize the selected property. (Fujiwara *et al.*, 2005; Aamir *et al.*, 2010, Braatz and Hasebe, 2002; Ma *et al.*, 2002; Nagy and Braatz, 2004; Shi *et al.*, 2006, Braatz, 2002). For the material balance, population balance equations are used, in which nucleation and growth kinetics are included along with certain assumptions to simplify the model development. Generally, agglomeration or dendritic growth are neglected and change in shape is considered. Furthermore lumped models are preferred over distributed parameter models because of simplicity and computational efficiency. Since crystallization is inherently non-linear process therefore non-linear control approaches are used with dynamic optimization methods.

Continuous efforts have been made to develop more efficient models e.g. two dimensional growth was included in the model for potassium dihydrogen phosphate system by Ma *et al.* (2002), agglomeration which frequently occurs in crystallization was included by Costa *et al.* (2005). Sarkar *et al.* (2006) used multi-objective optimization for obtaining narrow CSD, Worlitschek and Mazzotti (2004) developed a model for paracetamol/ethanol system that

included thermodynamics, crystal growth and secondary nucleation for obtaining desired monomodal CSD. Aamir *et al.* (2010) demonstrated how the prediction capability of a model can be affected by certain parameters for potassium dichromate and water system. In their work the predicted CSD matched with the measured CSD when crystalline seeds were used, however the model was unable to predict accurately the shape of experimental CSD when very fine particles were used as seeds. The use of fine particles caused significant agglomeration and different growth dispersion rates. These phenomena were not included in the model causing the significant deviations between predicted and measured CSDs. This demonstrates that for accurate and prediction all the relevant parameters must be included in the model. The accuracy of the model can greatly facilitate the control of a crystallization process to obtain a CSD with desired properties. Schematic working of the model based approach is shown in Figure 2.6.

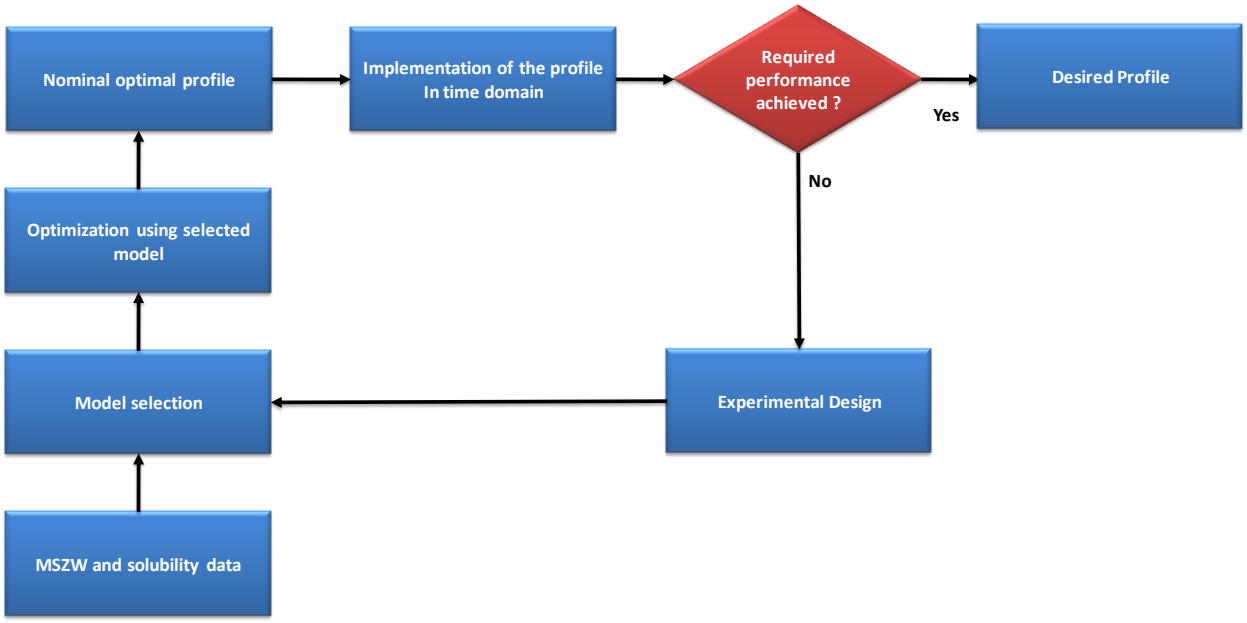



**Figure 2.6 Schematic representation of first principle approach (adapted from Nagy *et al.*, 2008)**

## 2.7 Model-free (direct design) Approaches

One of the main objectives in crystallization is to obtain crystals of desired size distribution. For this generally the operating curve is kept within the metastable limit. Any crystallization process operating very close to the metastable limit has a higher tendency for secondary nucleation

resulting in undesired CSD, on the other hand any operating curve very close to the solubility curve will avoid secondary nucleation, but will lead to slow growth and longer batch times, which can yield economic losses. The selection of an operating curve is mostly done by trial and error, trying to find a suitable compromise between these two effects, this approach is not only time consuming but can lead to batch to batch variability and poor control of the process.

The use of PAT has enabled the development and implementation of much more efficient and robust control approaches. These control strategies, which are termed as model-free or direct design, use feedback control based on information from *in situ* sensors (Zhou *et al*., 2007). The system typically follows an adjustable supersaturation setpoint within the metastable zone. Unlike the model-based approach where a certain objective function is optimized, the main aim in this methodology is to avoid secondary nucleation and maximize crystal growth. A significant advantage of these approaches is that no information about process kinetics is required. This is a major advantage of this approach as multiple phenomena take place during crystallization, for which the parameters estimation and modelling can be very difficult.

The direct design approach is sometimes termed as concentration control or supersaturation control. Supersaturation is not directly measured and therefore is determined through concentration measurements using spectroscopic tools such as ATR-FTIR, ATR-UV/Vis spectroscopy, and from the known solubility data for the system. A schematic representation of the direct design approach is shown in Figure 2.7.

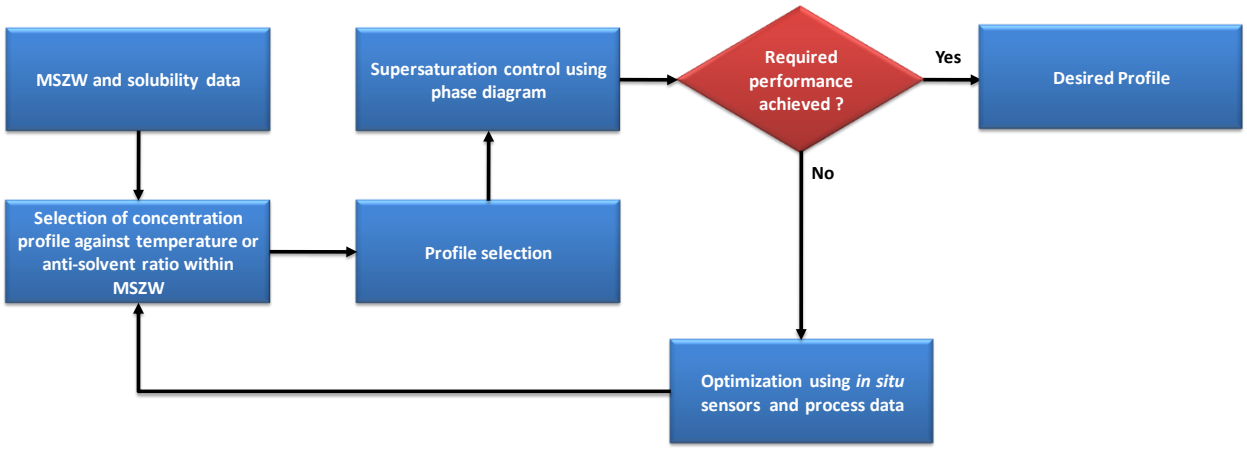



**Figure 2.7 Schematic representation of direct design approach (adapted from Nagy *et al*., 2008)**

The direct design approach has been successfully used for enhancing the crystalline product quality in many applications. Zhou *et al.* (2006) used this approach based on ATR-FTIR for anti-solvent crystallization of a proprietary pharmaceutical compound. They demonstrated that the approach provides rapid determination of an optimal recipe for suppressing secondary nucleation and enhancing crystal growth. Liotta and Sabesan (2004) reported significant improvement in crystal size when supersaturation control was applied for cooling crystallization of a drug compound. Kee *et al.* (2009) showed how the direct design approach can be used for production of the α-form of L-glutamic acid, by using ATR-FTIR based supersaturation control.

## 2.8 Process Analytical Technology and Chemometrics

Process analytical technology (PAT) has gained popularity and momentum in the pharmaceutical industry in the past five to ten years. The main reasons that led to this was the initiative by the FDA which promoted to use modern sensor technologies and monitoring and control concepts to achieve reduction in process time and cost, decrease variability, improve product quality and minimize batch failures (Yu *et al.*, 2004). This guidance was initially launched by the FDA in 2004 and was further emphasized by the International Conference on Harmonization (ICH) (E. Ref 2) in 2008. The later commented on PAT as an "opportunity to develop more flexible regulatory approaches". PAT comprises of the tools shown in Figure 2.8.

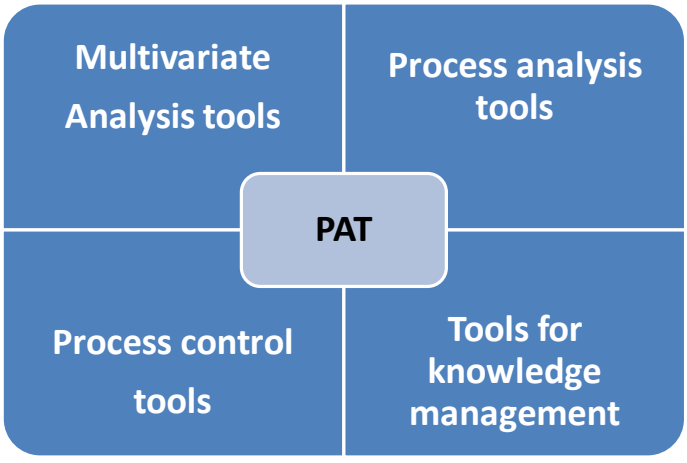



**Figure 2.8 Classification of different tools used under PAT**

The main benefit of PAT is the ability to monitor and control the system in real time resulting in a better overall control and improved product quality. The quality control in this case is in-process, which was previously carried out in the laboratory on the final product.

In view of the use of PAT, the concept and practice of QBD was introduced by ICH (ICH Q8, 2005), the generally accepted definition of QBD is that, "quality should not be tested into a product, it should be by design". This practice is a shift from the conventional QBT approach in the pharmaceutical industry. PAT is the most feasible way for the application of QBD concepts and can be considered as integral part of each other. For QBD, a design space with multiple variables is initially outlined encompassing raw materials and the process leading to a required product quality. This offers flexibility of applying changes to the manufacturing process within the design space if required by regulatory procedures. The protocol developed based on this design space and regulations becomes part of the marketing plan for the product being developed. The design space is initially developed on the laboratory scale and later applied on the pilot and industrial scale, whilst controlling the process in the same boundaries. This is often referred to as QBD Control Strategy. The role of PAT in the context of QBD is clear as the defined variables are mostly controlled and monitored by PAT approaches. Design of experiments and development of control strategies further enhances the effectiveness of QBD approach (Yu *et al*., 2004).

PAT provides valuable information about different processes at various stages of the drug development. This includes measurement of solubility and MSZW, supersaturation and concentration measurement, monitoring and formation of polymorphic forms, hydrates, solvates, and CSD monitoring and enhancement, as well as crystallization process scale up. A division of PAT tools based on their market share (E. Ref 3- Strategic Directions International (SDI)) along with other instrumentation is shown in Figure 2.9.

These statistics show that the field of PAT is dominated by spectroscopy followed by electrochemistry tools (e.g. pH measurement etc). According to market research (E. Ref 3) PAT used in pharmaceutical industry was worth nearly $150 million in 2005, this has grown to nearly

$195 million in 2010 and it is expected to be nearly $279 million worth in 2015 with an expected growth rate of 7.4% , (E. Ref 4 - Business Cooperation Company (BCC)).

Note that a significant part of the market share is attributed to the dedicated software systems, indicating that the successful application of PAT requires both hardware and suitable software tools.

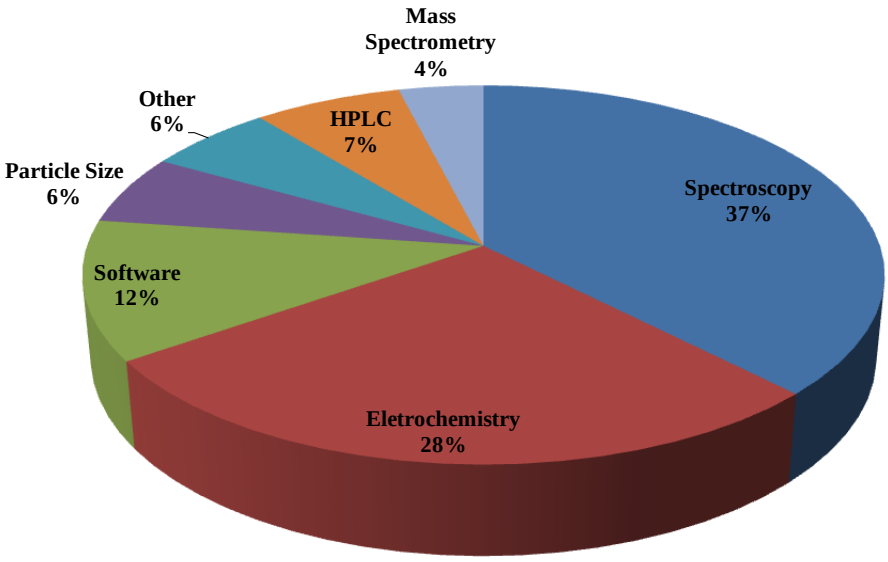



**Figure 2.9 Classification of different process tools based on market share**

In the following section working, advantages and disadvantages of the most common PAT tools will be presented.

## 2.9 ATR-UV/Vis Spectroscopy

UV/Vis spectroscopy for *in situ* analysis is a relatively new technique. Its more conventional applications were limited to colour and concentration measurements through filter photometers. The availability of UV resistant optical fibres, cheap diode array detectors and chemometrics has facilitated its inline/online applications in many fields. The application of UV/Vis spectroscopy

is limited as most of the compounds or functional groups are transparent in the UV/Vis spectroscopy range i.e. 190 nm to 800 nm (Bakeev, 2010).

The absorbance of energy in the UV/Vis region of the electromagnetic spectrum causes transitions between electronic energy levels. This energy causes the electrons to shift from an occupied orbital to an unoccupied orbital of higher potential energy. The shifting of electrons normally takes place from highest occupied molecular orbital (HOMO) to lowest unoccupied molecular orbital (LUMO). The arrangement of these energy levels is shown in Figure 2.10.

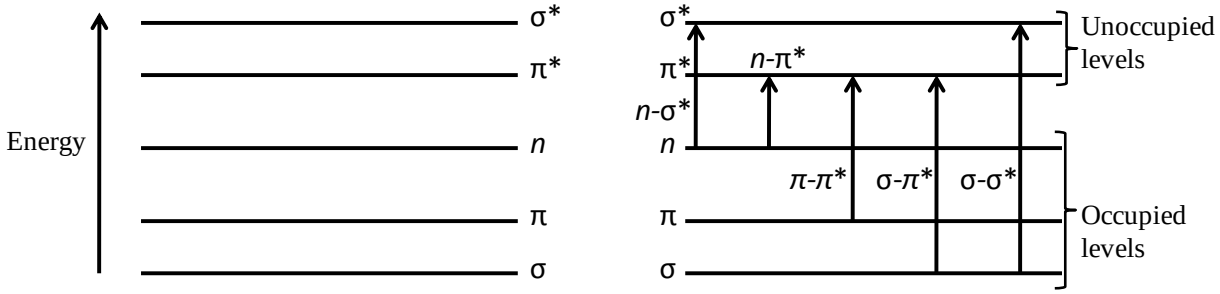



**Figure 2.10 Electronic energy levels and possible electron transitions (adapted from Pavia *et al.*, 2009)**

As shown in Figure 2.10 σ orbitals have the lowest energy, π orbitals are at higher energy level and *n* orbitals are at even higher energy levels. The anti-bonding orbitals π* and σ* have the highest energy and the amount of energy involved in *n* to π* transfer is less than for the π to π* transfer (Pavia *et al*., 2009).

Although the shifting of electrons play a vital role in the creation of a UV/Vis spectrum, the presence of chromophores and conjugation is very important. In a bond, the nuclei that hold the electrons together influences the wavelengths at which the light is absorbed, as the former affects the excited and ground states for electrons. Such groups of atoms are called chromophores. Normally σ to σ* transitions are observed in the case of alkanes. Sulphur compounds undergo *n* to π* transitions. Alkenes and alkynes show π to π* transitions, while carbonyl compounds mostly undergo *n* to π* changes. The presence of conjugation and hence delocalization of electrons brings the energy levels in chromophores closer to each other and therefore less energy is required to cause an electronic shift. The radiation is thus absorbed at longer wavelengths. This

delocalization effect can be observed in case of phenolphthalein, which changes its colour in an alkaline medium. The alkaline form (magenta in colour) shows a peak at 553 nm, the peak at this longer wavelength is the result of extended delocalization covering the whole molecule.

Absorbance is correlated with the concentration of a compound according to the Beer-Lambert's Law:

$$A = log\left(\frac{I_o}{I}\right) = \epsilon cl \tag{2.11}$$

where $A$ is the absorbance, $I_o$ is the incident light intensity, $I$ is intensity of light leaving, $c$ is the molar concentration of the solute, $l$ is the path length (cm) and $\epsilon$ is the molar absorptivity.

Based on this law absorbance is linearly dependent on concentration, provided that molar absorptivity and path length remain constant. However, absorbance also depends on the temperature. The presence of more than one absorbing species, interaction between solute and solvent can also cause deviations from this law.

The instrumentation used for UV/Vis can be classified into the following four types (Cazes, 2005):

- Scanning instruments
- Diode-array instruments
- Photometers
- Fibre-optic diode array and CCD instruments

The former two are more suitable for offline measurements, whereas the latter two are suitable for online/*in situ* analysis.

Photodiode array (PDA) spectrometers coupled with fibre optics are the best option for online or in-situ measurements. Sample interface is provided by an ATR probe. The advent of the non-

solarising fibre optics has made it possible to have the spectrometer away from the process, and the light is carried through the fibre optics. The working of the ATR probe is described next.

The ATR probe is based on the difference in refractive indices of the ATR crystal and that of the solution. An evanescent wave propagates (Figure 2.11) through the optically rare medium (solution) when it comes in contact with an optically dense medium (the crystal). Inside the crystal the light goes through internal reflection. The penetration depth of this evanescent wave is only a few microns, as a result of this the signal obtained has minimum disruption from the particles or the bubbles present in the solution. The penetration depth can be calculated from the following equation:

$$d_p = \frac{\lambda}{2\pi n_1 \left[sin^2\theta - \left(\frac{n_2}{n_1}\right)^2\right]^{1/2}} \qquad (2.12)$$

where $d_p$ is the penetration depth, $\lambda$ is the wavelength (nm), $\theta$ is the angle of incidence of the propagating wave, $n_1$ is the refractive index of the ATR crystal, and $n_2$ is the refractive index of the solution.

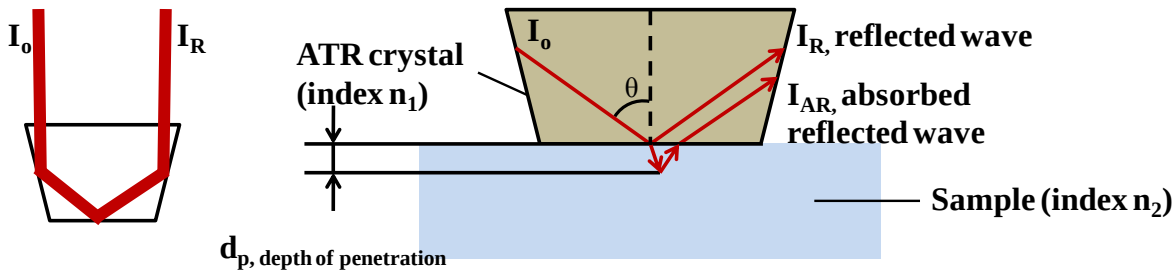



**Figure 2.11 Working of ATR probe**

The path length mentioned in Beer Lambert's law, $l$, is a function of the penetration depth ($d_p$) and the number of reflections ($z$) in the ATR crystal, $l = zd_p$ (Billot *et al.*, 2010). The number of internal reflections can affect the absorbance significantly. It was shown that an ATR crystal with 3 internal reflections resulted in absorbance values greater by a factor of 4.48 compared to the crystal with one reflection (E. Ref 5). Refractive indices of commonly used materials for ATR crystal are shown in Table 2.3:

Whilst ATR probes are commonly used in conjunction with FTIR spectroscopy, very few studies are available that demonstrate the use of ATR-UV/Vis spectroscopy in crystallization. Anderson *et al.*, (2001) for the first time reported the use of ATR-UV/Vis spectroscopy for monitoring the crystallization of sulfathiazole. Thompson *et al.*, (2005) used ATR-UV/Vis spectroscopy for *in situ* concentration measurements of a drug candidate and developed calibration model using partial least squares regression (PLSR). Recently Abu Bakar *et al.*, (2009) used ATR-UV/Vis spectroscopy for monitoring the seeded cooling crystallization of sulfathiazole. They developed a simple non-linear calibration model, which included a single absorbance, temperature and temperature-absorbance interaction term. Billot *et al.*, (2010) gave an overview of this technique using several compounds.

**Table 2.3 Refractive indices of different ATR materials**

| Material | Refractive index at 20°C |
|---|---|
| Sapphire | 1.65-1.73 |
| Silicon | 3.4-3.5 |
| Germanium | 3.9-4.1 |
| Zinc Selenide | 2.3-2.5 |
| Zinc Sulphide | 2.0-2.3 |
| AMTIR ($Ge_{33}As_{12}Se_{55}$) | 2.5-2.6 |
| Diamond | 2.4 |

## 2.10 ATR-Fourier Transform Infrared Spectroscopy (ATR-FTIR)

ATR- Fourier transform infrared spectroscopy (FTIR) is a form of vibrational spectroscopy and perhaps one of the most widely used techniques in pharmaceutical crystallization (Togkalidou *et al.*, 2001; 2002) . The IR region covers the spectral range from 4000 $cm^{-1}$ to 400 $cm^{-1}$ (2.5 µm to 25 µm) and is bounded by near infrared and far infrared regions. An IR spectrum is usually expressed as transmittance versus the wavenumber. A major advantage of using IR is the structure determination of the molecules as the spectrum generated is a fingerprint of a particular

molecule. The IR energy corresponds to the energy related to bond vibrations e.g. bond stretching, bending etc. The frequencies at which IR energy is absorbed is a characteristic of a molecule, this fact can be used to identify a compound and hence the term fingerprint is used. IR absorptivities occur in CH, OH and NH groups, either of these exist in any organic molecule and therefore IR is extensively used in pharmaceutical crystallization.

The availability of IR spectrometers with ATR probe have enabled real time monitoring and control of crystallization, some of the applications include determination of metastable zone width, concentration measurement (Wang and Berglund, 2000), supersaturation control, detection of impurities etc. These applications are listed in Appendix A.

## 2.11 Near Infrared Spectroscopy (NIR)

Near infrared (NIR) spectroscopy is another form of vibrational spectroscopy along with Raman and IR. NIR covers the 4000 $cm^{-1}$ to 12500 $cm^{-1}$ range in the electromagnetic spectrum. NIR detects overtones and combinations arising from X-H bond vibrations. The intensity of the NIR bands is weaker than the corresponding fundamental bands, as a result of this no sample dilution is required. Another advantage of this approach is that it allows the measurement of thick samples. The penetration depth of NIR beam is up to a few millimeters, this is particularly helpful in analysis of bigger sample volumes such as raw materials etc. Applications of NIR are listed in Appendix A.

## 2.12 Raman Spectroscopy

Raman spectroscopy belongs to the vibrational spectroscopy family along with IR and NIR. The approximate spectral range of Raman spectroscopy is between 50-4000 $cm^{-1}$. When monochromatic light is incident on a material, the majority of the light or photons undergo Rayleigh scattering, i.e. there is no change in the energy or frequency of photons. A very small quantity of photons (0.0001%) however, undergoes Stokes and anti-Stokes scattering. When the

energy of the photon is absorbed by the molecule, it is termed as Stokes scattering resulting in red-shifted scattered light. An electron in the ground state is excited and lifted to a higher vibrational energy level. In case of anti-Stokes scattering, molecules give energy to the photon, resulting in blue shifted light, with a shorter wavelength and higher energy. An electron in the ground state is lifted to a higher level through a virtual state and ends up at a low vibration energy level. Raman spectrum is due to a change in the polarizability of the molecule. The qualitative aspect of Raman spectroscopy lies in the fact that change in the wavelength of scattered light is dependent upon the vibrational energy levels of the molecules. This fact is used to identify the state and nature of bonds present in a molecule.

Both IR and Raman are based on the vibrational energy levels of a molecule. The difference between the two is that IR measures the loss of intensity of light between incident, absorbed and scattered light, while Raman instruments measure the amount of photons emitted as a function of their wavelength. Most of the pharmaceutical compounds show clear and well resolved bands, Raman spectroscopy is therefore a very powerful tool for qualitative and quantitative analysis and can be used at different stages during the drug production.

In a multiphase mixture of solids and liquids many properties can be monitored and controlled through Raman spectroscopy. Since Raman spectroscopy is based on vibrational energy changes, it can distinguish almost all the crystal forms. This property is extremely useful for characterizing different forms of a pharmaceutical compounds, such as polymorphic forms, hydrates and solvates.

Raman spectroscopy is a nondestructive technique and requires very small amounts of sample, especially for pharmaceutical compounds, which are prepared in small amounts during the early stages of development. It does not require special sample preparation, which is another advantage, since some compounds can undergo changes during sample preparation, required for using other techniques (Vergote *et al*., 2004).

## 2.13 Focused Beam Reflectance Measurement (FBRM)

FBRM is an extensively used *in situ* technique that gives information about nucleation, dissolution, metastable zone width, polymorphic transformation, growth and size distribution in particulate systems in real time (Barthe and Rousseu, 2006, Doki *et al.*, 2004, Barrett and Glennon, 2002; Barthe *et al.*, 2008; Sheikhzadeh *et al.*, 2008a; Sheikhzadeh *et al.*, 2008b; Howard *et al.*, 2009; Abu Bakar *et al.*, 2009).

The probe is directly inserted in a crystallizer and provides *in situ* information about the system. A laser is used to scan a certain region. The beam is highly focused and is projected through the sapphire window of the probe. This beam rotates at a speed of 2-6 m/s (Pons *et al*, 2006) and scans the particles on which it is being focused. The beam after hitting the particles is back scattered and received by an optical receiver. The focused beam crosses the particles on a straight line between any two points on the edge of the particle as shown in Figure 2.12. Based on the rotating speed of the laser ($v_s$) and back scattering time ($\Delta t$) , the chord length distribution (CLD) for the particles is obtained using the following equation.

$$\text{chord length} = v_s \Delta t \tag{2.13}$$

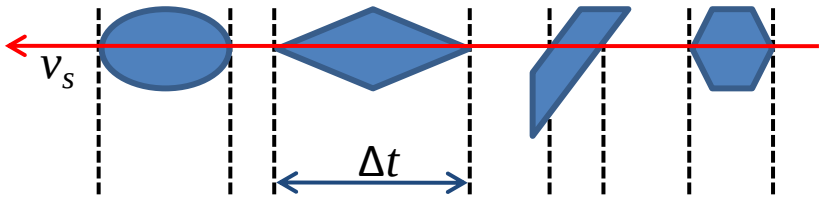



**Figure 2.12 Chord length measurement by FBRM**

The chord length distribution (CLD) measured by the FBRM can be related to different phenomena, such as nucleation, growth, agglomeration and attrition (Yu *et al.*, 2007). The CLD obtained from FBRM is grouped in 90 channels from 0.8 – 1000 µm. The readings obtained from FBRM can be displayed in a variety of formats from simple total number of counts per second to square weighted or cubic weighted distributions.

Three of the most important statistics used by FBRM are the cubic weighted (CWMCL), square weighted (SWMCL) and length weighted (LWMCL) mean chord lengths:

$$\text{Cubic Weighted Mean Chord Length} = \text{CWMCL} = \frac{\sum_{i=1}^{k} n_i M_i^4}{\sum_{i=1}^{k} n_i M_i^3} \tag{2.14}$$

$$\text{Square Weighted Mean Chord Length} = \text{SWMCL} = \frac{\sum_{i=1}^{k} n_i M_i^3}{\sum_{i=1}^{k} n_i M_i^2} \tag{2.15}$$

$$\text{Length Weighted Mean Chord Length} = \text{LWMCL} = \frac{\sum_{i=1}^{k} n_i M_i^2}{\sum_{i=1}^{k} n_i M_i^1} \tag{2.16}$$

where $n_i$, is the counts in an individual measurement channel, and $M_i$, is the midpoint of an individual channel.

FBRM can be used for measurement of solubility, nucleation detection and MSZW determination (Barett *et al.*, 2002), controlling CSD (Doki *et al.*, 2004), monitoring of crystal growth and nucleation (Barrett *et al.*, 2005) and detection of agglomeration in crystals (Loan *et al.*, 2002). FBRM does not require any sampling or isolation of samples and thus prevents any changes in crystal size or distribution because of breakage or agglomeration (Kougoulos *et al.*, 2005; Barrett *et al.*, 2005), FBRM also enables the use of a robust crystallization process control approach without any prior knowledge of the kinetics of a particular system (Woo *et al.*, 2009; Abu Baker *et al*., 2009).

The conversion of chord length distribution (CLD) to CSD is difficult due to the large number of variables involved (Braatz, 2002), especially for dense crystal slurries (Monnier *et al.*, 1996; Monnier *et al.*,1997). Numerous studies have been carried out in an attempt to carry out this conversion (Worlitschek *et al.*, 2005; Li and Wilkinson, 2005; Tadayyon and Rohani, 1998; Ruf *et al.*, 2000). The main limitation in these approaches, is that they require an assumption about a fixed particle shape, which in most cases is assumed to be spherical unlike the shape of most crystals, therefore it is critical to use the right geometry of the crystals as shown by Ruf *et al.*, (2000).

FBRM can oversize small particles less than 150 µm (Law *et al.*, 1997) undersize particles greater than 300 µm and over size particles greater than 500 µm (Heath *et al.*, 2002). Deposition of particles on the FBRM probe window can also give false readings.

FBRM has mostly been used as a monitoring tool along with other *in situ* tools. Very limited research is available in which FBRM has been used to control the process. The control studies along with application of FBRM are outlined in Table 2.4. Appendix A contains a more extensive review of FBRM applications for various purposes.

**Table 2.4 Various applications of FBRM**

| Process Control | | | |
|---|---|---|---|
| **Reference** | **System Investigated** | **Application Area** | **Other Tools used in the study** |
| Doki *et al.,* (2004) | Cooling crystallization of glycine in water | Production of stable polymorph size and monitoring | ATR-FTIR |
| Chew *et al*., 2007(b) | Cooling crystallization of glycine in water | Improving CSD by applying feedback control using FBRM | ATR-FTIR |
| Abu Baker *et al*., 2009 | Cooling and anti-solvent crystallization of glycine, ethanol as anti-solvent | Improving CSD by applying feedback control using FBRM | |
| Woo *et al*., 2009 | Cooling crystallization of paracetamol in water | Combination of concentration control with FBRM | ATR-FTIR |
| Hojjati *et al.*, 2006 | Anti-solvent crystallization of paracetamol in IPA with water as anti-solvent | Enhancement of CSD | ATR-FTIR |
| Chew *et al*., 2007(a) | Cooling crystallization of glycine in water | Improving CSD by applying feedback control using FBRM | |
| Hermanto *et al*., 2010 | Anti-solvent crystallization of glycine in water with ethanol as anti-solvent | Applied feedback control using FBRM for better CSD | |

The *in situ* techniques mentioned so far provide information about the liquid and solid phase. However, these tools are often accompanied by various offline analysis techniques for a thorough assessment and characterization of crystalline product (Howard *et al*., 2009). Some of the techniques used and their applications are summarized in Table 2.5.

**Table 2.5 Summary of various offline and inline techniques used in crystallization**

| Technique | Description and Application |
|---|---|
| Optical microscopy | Size analysis, characterization of polymorphic forms based on different shapes and colour. |
| Hot stage microscopy | The technique can reveal any changes that may appear in crystals because of thermal events e.g. conversion of polymorphic form. |
| Scanning electron microscopy | Provides images of crystals, can be used to detect any defects in the crystals |
| Differential Scanning Calorimetry (DSC) | Very commonly used technique especially for polymorphic characterization and determination of polymorphic transformation temperatures. A melting or crystallization event appears as peaks on curve. Solvate and hydrate detection can also be carried out. |
| Thermogravimetry | Characterization of solvates and hydrates is carried out by using this method. |
| X-ray diffraction (XRD) | Determines crystal structure and useful in characterization of polymorphic forms. |
| Nuclear magnetic resonance (NMR) | A complex technique used for determining structure of compounds. |

Some of the other useful techniques which are used for monitoring crystallization processes are briefly described as follows:

Particle vision and measurement (PVM), gives real time information about changes in crystal shape and morphology, and often used as a complementary technique alongside FBRM and spectroscopic tools. Bulk video imaging (BVI) is a cheap but useful alternative to PVM, combined with image analysis it can provide useful information about crystallization such as MSZW, solubility etc. Turbidimetry is another monitoring tool, it measures the changes in optical properties of the solution and can be used for detection of nucleation or dissolution during crystallization processes.

## 2.14 Chemometrics

PAT is fast becoming an integral part of the drug development process. Many *in situ* sensors are used at various drug development stages. These sensors produce large amounts of data and quite often several sensors are used simultaneously, which increases the process related data manifolds. In order to extract maximum information from these data, multivariate statistical data analysis and mathematical tools are used. These tools are termed "Chemometrics" (Yu *et al.*, 2004). Chemometrics combined with PAT provides useful information about the system, Figure 2.13. The information provided can be used for modelling, monitoring and controlling the process, which helps in obtaining products of required quality, which may include a particular size distribution, manufacturing of a particular polymorphic form or others etc.

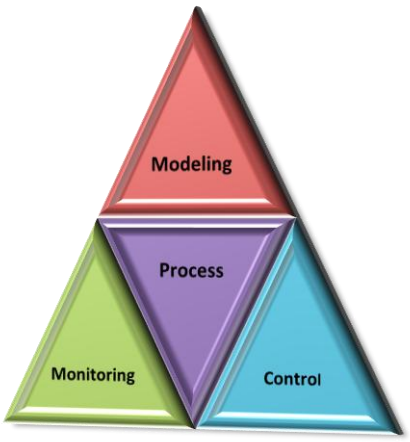



**Figure 2.13 Benefits of using PAT and chemometrics**

Some of the key features of chemometrics are as follows (Geldai, 2003):

- Experimental design
- Acquisition and enhancement of data
- Feature selection and extraction
- Pattern recognition
- Calibration and regression analysis

Spectroscopy is widely used in crystallization in conjunction with chemometrics for monitoring and controlling of this separation process. Aaltonen *et al.* (2003) did rapid screening of sulfathiazole polymorphs using NIR spectroscopy and PCA. Falcon and Berglund (2004) showed that PCA was very helpful in monitoring of the anti-solvent crystallization of progesterone using *in situ* Raman spectroscopy. Caillet *et al.* (2006) used Raman spectroscopy for monitoring the phase transition of citric acid in water from anhydrous to monohydrate form, PLSR was used for development of the calibration models. The robustness of the equipment was checked after 20 months based on the calibration model and no drift was observed. Starbuck *et al.*, (2002) used PCA and Raman spectroscopy for process optimization and polymorphic characterization of a complex pharmaceutical system. Pollanen *et al.* (2005), characterized different polymorphic forms of sulfathiazole using diffuse reflectance Fourier transform–infra-red (DRIFT) spectroscopy, while ATR-FTIR was used for concentration measurements. Multi-variate statistical process control (MSPC) and PCA were used for quality evaluation of crystals from DRIFT spectra. The results obtained from DRIFT spectra and X-ray powder diffraction (XRPD) was subjected to PLS analysis. These analyses confirmed the quantification made by XRPD and provided a complimentary method for polymorph characterization. Chen *et al.* (2009) proposed an extended loading space standardization method for monitoring the concentration of monosodium glutamate and L-glutamic acid during cooling crystallization using ATR-FTIR. A comparison was made between PLS based model and shown that the proposed technique can handle nonlinear data much better than PLS model. A simpler but non linear calibration model was used with ATR-UV/Vis spectroscopy for monitoring and concentration measurement in sulfathiazole crystallization (Abu Bakar *et al.*, 2009). Aamir *et al.* (2010) used a similar model for concentration determination of potassium dichromate by ATR-UV/Vis spectroscopy during cooling crystallization. Thurston *et al.* (2003) used ATR-UV/Vis spectroscopy for reaction monitoring of phenylhydrazine and benzophenone along with crystallization. PCA plots were used to monitor the different stages of the reaction and interpretation of spectral data. Borissova *et al*. (2009) used ATR-FTIR for determining concentration of L-glutamic acid using advanced chemometric techniques. In the following section some of the commonly used chemometric techniques will be discussed.

## 2.15 Calibration Model Development Techniques

Calibration refers to the development of a relationship between a set of variables such as spectra to some property(s) of interest e.g. concentration. Several methods are available for development of calibration models; the simplest one is a uni-variate method in which the concentration of a single compound is measured using a single variable e.g. absorbance at a particular wavelength. Multivariate methods are used when a number of variables are used to predict the concentration(s). In the following section all these methods will be briefly discussed along with their advantages and disadvantages.

Assuming that a linear relationship exists between spectral measurements (variables from here onwards will refer to spectral measurements) and concentration (independent variable or parameter of interest), there are two ways to predict concentration $c$ from the spectral measurements $x$ by least squares. The first method assumes absorbance as a function of concentration, this method is closer to the Beer-Lambert's law and therefore called as direct method. The second method assumes concentration as a function of absorbance and called as the inverse method. This method is preferred because the objective is to predict concentration from the data not the vice versa. Multivariate methods such as PCR and PLSR, all are based on the inverse method. A classification of calibration development methods is shown in Figure 2.14. The discussion in this case will be limited to inverse methods and ANN.

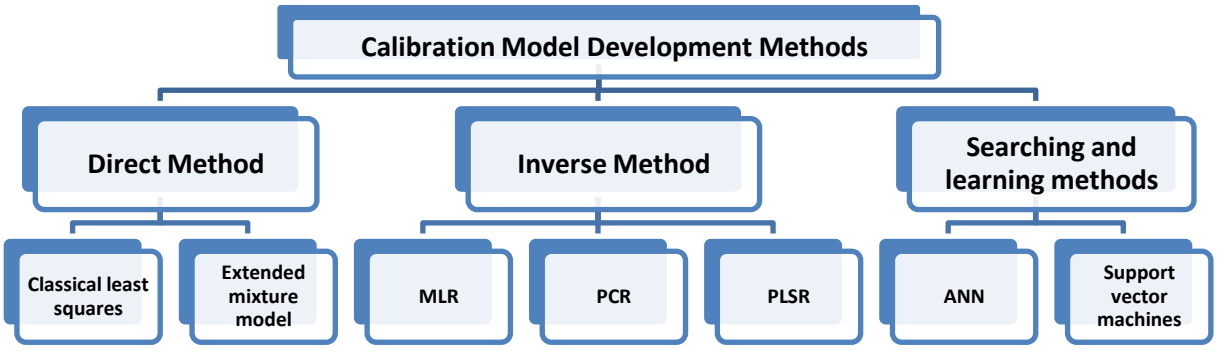



**Figure 2.14 Classification of calibration model development methods (adapted from Bakeev, 2010)**

### 2.15.1 Univariate Calibration

Univariate calibration model is developed using only one response variable, e.g. in the case of concentration determination using a spectroscopic tool the employment of absorbance at a single wavelength. In univariate calibration it is assumed that no interferences are present that might affect the response variable, furthermore this is normally carried out at a constant temperature. The general form of the model in mathematical terms can be represented as (Bakeev, 2010; Gamperline, 2006; Brereton, 2003);

$$c_i = b_o + b_1 x_i + e_i \tag{2.17}$$

where $c_i$ are the concentration values in experiments $i$, $(i = 1, \dots, n)$ with $n$ being the number of experiments), corresponding to the absorbance (or derivative) $x_i$. If the experimental data are pre-processed (e.g. via mean centring), the intercept (free) term ($b_0$) can be neglected from the calibration equation:

$$c_i = b_1 x_i + e_i \tag{2.18}$$

In vector notation the above equation can be represented as:

$$\mathbf{c} = \mathbf{x} b_1 + \mathbf{e} \tag{2.19}$$

Here $\mathbf{c}$ is the concentration vector, $\mathbf{c} = [c_1, \dots, c_n]^{\mathrm{T}}$, $\mathbf{x}$ is response vector, $\mathbf{x} = [x_1, \dots, x_n]^{\mathrm{T}}$ e.g. absorbance, $b_1$ is the regression coefficient and $\mathbf{e}$ is the error vector, $\mathbf{e} = [e_1, \dots, e_n]^{\mathrm{T}}$. The intercept can be added by adding a column of ones in the $\mathbf{x}$ and consequently an additional regression coefficient:

$$\mathbf{X} = \begin{bmatrix} 1 & x_1 \\ \vdots & \vdots \\ 1 & x_n \end{bmatrix} \tag{2.20}$$

In this case the coefficient vectors will contain both the intercept and the slope terms $\mathbf{b} = b = [b_o \quad b_1]^{\mathrm{T}}$. Least squares regression can be used to estimate the regression coefficients from known **c** and **x** values as:

$$b_1 = (\mathbf{x}^{\mathrm{T}}\mathbf{x})^{-1}\mathbf{x}^{\mathrm{T}}\mathbf{c} \tag{2.21}$$

If a non-zero intercept is used, equation (2.21) can be written as:

$$\mathbf{b} = (\mathbf{X}^{\mathrm{T}}\mathbf{X})^{-1}\mathbf{X}^{\mathrm{T}}\mathbf{c} \tag{2.22}$$

Here $b_1$ and **b** represents the estimated values of the regression coefficients (a single scalar in the first case and a vector with two elements in the second case), and can be used to predict the concentration as:

$$\mathbf{c_{pred}} = \mathbf{x_{meas}} b_1 \tag{2.23}$$

or considering the intercept term, the prediction can be carried out as:

$$\mathbf{c_{pred}} = \mathbf{X_{meas}}\mathbf{b} \tag{2.24}$$

The subscript "meas" is used to denote the vectors of measured absorbances for the samples with unknown concentrations.

### 2.15.2 Multivariate Calibration

In multivariate calibration, as the name suggests, more than one response variables are involved. This is particularly helpful if the variability in the independent variable can be explained in a better way by using multiple variables (Bakeev, 2010; Gamperline, 2006; Brereton, 2003). The linear regression equation then takes the following form:

$$\mathbf{c} = \mathbf{Xb} + \mathbf{e} \tag{2.25}$$

where $\mathbf{X}$ is an $n \times m$ matrix of multiple variables such that each row corresponds to a complete spectra recorded at $m$ wavelengths. A column of ones can be introduced to account for the intercept term; in this case $\mathbf{X}$ will have $n \times (m + 1)$ dimensions. The vector $\mathbf{b}$ ($\mathbf{b} = [b_0, b_1, \dots, b_m]$) has all the regression coefficients, each corresponding to a specific variable present in the $\mathbf{X}$ matrix. The equation used for determining the coefficients is same as that of (2.22), and the prediction can be performed with equation (2.24). Note that the concentration matrix $\mathbf{C}$ can also be multivariate, e.g. the concentration of several species in the solution can be predicted simultaneously. In this case $\mathbf{C}$ is an $n \times s$ matrix, with $s$ being the number of species for which the concentration is determined from the calibration model.

A necessary condition for this calibration model is that the number of samples ($n$) must be greater than the measured variables ($m$) otherwise the matrix inversion in equation (2.22) will not be possible. A possible disadvantage of this approach comes from the existence of multicollinearity in the data. Multicollinearity refers to the fact that some of the variables can be expressed as linear functions of some of the other variables. The presence of such properties in the data can lead to an unstable model with poor prediction capability.

Some of the techniques that can overcome these issues will be discussed in the next section.

### 2.15.3 Principal Component Analysis (PCA) and Principal Component Regression (PCR)

Generally a large amount of data is produced from PAT tools, in particular from spectroscopic measurements, which e.g. produce the absorbance values in a large number of wavelengths for each concentration. Sometimes part of the data generated is not required or irrelevant and thus can be made redundant. Removal of such data improves efficiency of the models developed, e.g. by eliminating collinearity. PCA is one of the most widely used techniques for data compression and dimensionality reduction (Bakeev, 2010; Gamperline, 2006; Brereton, 2003; Adams, 2004). Principal components are the linear combinations of the original variables. Geometrically these components give a new coordinate axes by rotating the original axes. PCA is used to simplify the data structure and still account for the as much of the total variation in the original data set as possible. PCA reveals the internal structure of the data in a way that lett explains the variance in the data.

Mathematically PCA represents an orthogonal linear transformation that maps the data into a new coordinate system such that the greatest variance by any projection of the data will be in the first coordinate (called the first principal component), the second greatest variance in the model in the second coordinate and so on. The directions of the new coordinate system are determined by the eigenvectors of the data correlation (variance-covariance) matrix, whereas the eigen values correspond to the principal components. To explain the PCA we consider the data matrix $\mathbf{X}$ with dimensions $n \times m$, corresponding to the absorbances measured at different wavelengths in $n$ samples.

The first step in performing the PCA is to pre-process the data to obtain normalized data matrix $\widetilde{\mathbf{X}}$, with zero empirical mean and unit variance, using the scaling parameter vectors $\bar{\mathbf{x}} = [\bar{x}_1, \dots, \bar{x}_m]^{\mathrm{T}}$ and $\boldsymbol{\sigma} = [\sigma_1, \dots, \sigma_m]^{\mathrm{T}}$ as the empirical (sample) mean and variance vectors of the process variables in the data matrix, respectively. The elements of the normalized data matrix $\widetilde{\mathbf{X}}$ are defined as:

$$\tilde{x}_{ij} = \frac{x_{ij} - \bar{x}_j}{\sigma_j} \text{ for } i = 1, \dots, n \text{ and } j = 1, \dots, m \tag{2.26}$$

The normalized data matrix can be represented as:

$$\widetilde{\mathbf{X}} = \mathbf{T}\mathbf{P}^{\mathrm{T}} + \mathbf{E}_{\mathrm{x}} \tag{2.27}$$

where **T** is the $n \times q$ latent (or score) matrix and **P** is the $m \times q$ principal components matrix (loadings), with $q$ being the number of principal components retained in the model **P**. The residual matrix $\mathbf{E}_{\mathrm{x}}$ represents the error since only $q \ll m$ principal components are selected. **P** can be obtained from the normalized data correlation matrix, defined as:

$$\mathbf{V} = \frac{1}{n-1}\widetilde{\mathbf{X}}\widetilde{\mathbf{X}}^{\mathrm{T}} \tag{2.28}$$

Applying singular value decomposition (SVD) to **V**:

$$\mathbf{V} = \mathbf{U}\mathbf{S}\mathbf{U}^{\mathrm{T}} \tag{2.29}$$

**P** can be obtained by selecting the first $q$ columns of **U**. This factorization produces a diagonal matrix $\mathbf{S} = diag(\lambda_1, \lambda_2, \dots, \lambda_m)$ where $\lambda_i$ are the eigenvalues of **V** sorted in decreasing order $(\lambda_1 > \lambda_2 >, \dots, > \lambda_m)$, and the corresponding columns in **U** are the eigenvectors $\mathbf{p}_i$ and are the so called principal components.

For the data reduction $\mathbf{P_q} = [\mathbf{p_1}, \mathbf{p_2}, \dots, \mathbf{p_q}]$ and $\mathbf{S}_q = diag(\lambda_1, \lambda_2, \dots, \lambda_q)$ are selected, and every normalized sample vector $\tilde{\mathbf{x}}(\mathrm{k})$ with dimensions $1 \times m$ is projected in the principal component space generated by $\mathbf{P_q}$, obtaining the principal score vector of reduced dimension $q \times 1$.

$$\mathbf{t}(\mathrm{k}) = \tilde{\mathbf{x}}(\mathrm{k})\mathbf{P_q} \tag{2.30}$$

The selection of the number of principal components $q$ used for the data reduction can be done by calculating the cumulative percent variance(CPV).

$$\mathrm{CPV}\ (q) = \frac{\sum_{i=1}^{q} \lambda_i}{trace\ (\mathbf{V})} 100 \tag{2.31}$$

The (CPV) is a measure of the percent variance captured by the first $q$ principal components. Generally $q \ll m$ accounts for a significant part of the variations in the data.

After applying the data reduction a calibration model can be developed by using multi-linear regression to the principal score vector called principal component regression, PCR. This approach significantly reduces the number of model parameters to be determined. After the selection of principal components, the regression coefficients can be determined as:

$$\mathbf{c} = \mathbf{tb} + \mathbf{e} \tag{2.32}$$

and the regression coefficients are

$$\mathbf{b} = (\mathbf{t}^{\mathrm{T}}\mathbf{t})^{-1}\mathbf{t}^{\mathrm{T}}\mathbf{c} \tag{2.33}$$

The prediction step is then carried out as follows:

1. Take new measurement $\mathbf{X_{meas}}$
2. Calculate normalized measurement matrix $\widetilde{\mathbf{X}}_{\mathbf{meas}}$ using $\bar{\mathbf{x}}$ and $\boldsymbol{\sigma}$
3. Project the measurement data in the reduced space determined by the PCA

$$\mathbf{t_{meas}} = \widetilde{\mathbf{X}}_{\mathbf{meas}}\mathbf{P} \tag{2.34}$$

4. Calculate predicted concentration

$$\mathbf{c_{pred}} = \mathbf{t_{meas}}\mathbf{b} \tag{2.35}$$

The root mean square error of prediction (RMSEP) can be used to check the predictive capability of the model as:

$$\text{RMSEP} = \sqrt{\frac{\sum_{i=1}^{n}(c_i - \hat{c}_i)^2}{n}} \tag{2.36}$$

### 2.15.4 Partial Least Squares Regression

Partial least squares regression (PLSR) is another popular calibration model building technique similar to PCR. The main difference between PCR and PLSR comes from the way the data is compressed. In PCR regression is applied only to those variables that account for variance in **X** data, in case of PLSR variance present in both **X** and **c** are considered during model building. The

compressed variables obtained from PLSR are different from the ones obtained through PCR and are termed as latent variables (Bakeev, 2010; Gamperline, 2006; Brereton, 2003);

According to this approach both the inputs and (matrix of predictors e.g. absorbances) and the responses (e.g. concentrations) are represented as:

$$\widetilde{\mathbf{X}} = \mathbf{T_1}\mathbf{P}^{\mathrm{T}} + \mathbf{E_x} \tag{2.37}$$

$$\tilde{\mathbf{c}} = \mathbf{T_2}\mathbf{q}^{\mathbf{T}} + \mathbf{e_c} \tag{2.38}$$

where $\widetilde{\mathbf{X}}$ has the dimensions $n \times m$, $\tilde{\mathbf{c}}$ has $n \times 1$ dimensions $\mathbf{P}$ (latent variables) $m \times q$ and $\mathbf{q}$ $1 \times q$ are the loading matrices and $\mathbf{E_x}$ $n \times m$ and $\mathbf{e}_{\boldsymbol{c}}$ $n \times 1$ are the error matrix and error vector respectively, $\mathbf{T_1}$ and $\mathbf{T_2}$ are the score matrices for $\widetilde{\mathbf{X}}$ and $\tilde{\mathbf{c}}$ respectively, both having dimensions $n \times q$ where $q \ll m$ . PLSR using eigen value decomposition is described as follows:

The scores for $\mathbf{T_1}$ matrix are calculated as:

$$\mathbf{t_1} = \widetilde{\mathbf{X}}\mathbf{w} \tag{2.39}$$

where $\mathbf{w}$ is the eigenvector corresponding to the first eigenvalue of $\widetilde{\mathbf{X}}^{\mathrm{T}}\tilde{\mathbf{c}}\tilde{\mathbf{c}}^{\mathrm{T}}\widetilde{\mathbf{X}}$. The first score for $\mathbf{T_2}$ is calculated as:

$$\mathbf{t_2} = \tilde{\mathbf{c}}\mathbf{g} \tag{2.40}$$

where $\mathbf{g}$ is the eigen vector corresponding to the first eigenvalue of $\tilde{\mathbf{c}}^{\mathrm{T}}\widetilde{\mathbf{X}}\widetilde{\mathbf{X}}^{\mathrm{T}}\tilde{\mathbf{c}}$. Once these vectors are calculated as they are subtracted from the original values of $\widetilde{\mathbf{X}}$ and $\tilde{\mathbf{c}}$ as:

$$\widetilde{\mathbf{X}}_{\mathbf{1}} = \widetilde{\mathbf{X}} - \mathbf{t_1}\mathbf{t_1^{\mathrm{T}}}\widetilde{\mathbf{X}} \tag{2.41}$$

$$\tilde{\mathbf{c}}_{\mathbf{1}} = \tilde{\mathbf{c}} - \mathbf{t_2}\mathbf{t_2^{\mathrm{T}}}\tilde{\mathbf{c}} \tag{2.42}$$

The above process is then repeated to extract the second factor and so on and so forth.

The latent variables can then be calculated as:

$$\mathbf{p}_1^{\mathrm{T}} = \left(\mathbf{t}_1^{\mathrm{T}}\mathbf{t}_1\right)^{-1}\mathbf{t}_1^{\mathrm{T}}\widetilde{\mathbf{X}} = \mathbf{t}_1^{\mathrm{T}}\widetilde{\mathbf{X}} = \mathbf{w}_1^{\mathrm{T}}\widetilde{\mathbf{X}}^{\mathrm{T}}\mathbf{X} \tag{2.43}$$

The final regression coefficients are given by:

$$\mathbf{b} = \mathbf{W}(\mathbf{P}^{\mathrm{T}}\mathbf{W})^{-1}\mathbf{g}^{\mathrm{T}} \tag{2.44}$$

The prediction steps are similar as described for PCR. The performance of PLSR is quite similar to that of PCR, the former can sometime over fit the data. Although it is more complex than PCR as it uses information simultaneously from dependent and independent variables, some authors claim that PLSR can give reasonable solutions for low precision data.

### 2.15.5 Artificial Neural Networks

Artificial neural networks (ANN) can be used in chemometrics for modeling nonlinear data (Massart, 1997). This technique is different from the previously mentioned techniques for several reasons:

- The ANN model structure is explained by a map or architecture unlike the other methods where a simple equation is used.
- ANN uses searching algorithm for finding out model variables instead of regression.
- ANN can easily deal with non-linear data by using non-linear transfer functions.

ANNs are composed simple elements, called neurons, operating in parallel. These neurons are an abstraction of the biological neuron and are interconnected (Agatonovic and Beresford, 2000).

The structure of a neuron is shown in Figure 2.15. A neuron can have a number of inputs but only one output, the input(s) are passed onto the neuron where they are weighted and summed; after this a transfer function $f$ is applied. A bias term $\boldsymbol{b}$ may also added before the transfer function is applied. Each input is multiplied by its associated weight. The sum of this product is the argument of the transfer function. The connection between the neurons and their associated weights control the propagation of signal. The associated weights also determine the strength of the connection between the neurons.

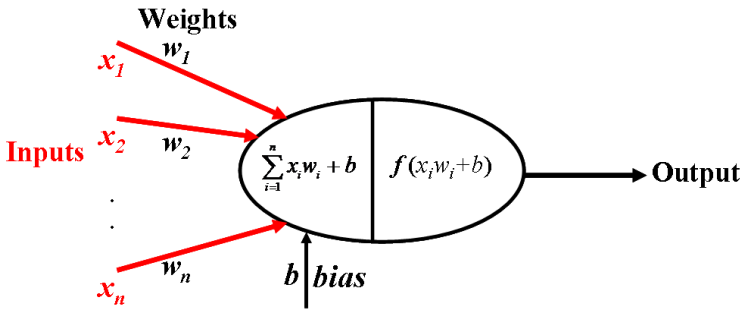



**Figure 2.15 Structure of a neuron**

The neurons can be arranged to form layers which in turn can form a network. The typical structure of a multi-layer feed forward network, is shown in Figure 2.16.

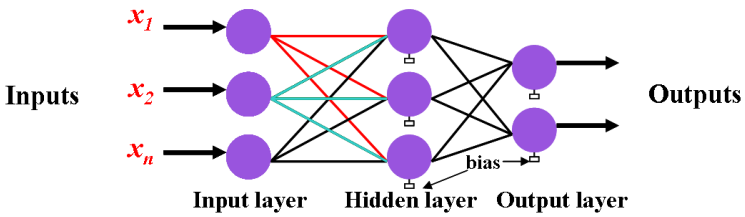



**Figure 2.16 Structure of a feed forward network**

The network architecture gives information about the number of layers in the network, number of neurons in each layer and the way the layers are connected. The network shown has an input layer, a hidden layer and an output layer. A network can have more than one more hidden layers. The outputs from the neurons of a layer serve as inputs for the neurons of the next layer.

The ANN has the advantage of handling nonlinear data (Bourquin *et al*., 1997), however, at the same time, ANN are very prone to over-fit the data, since the number of parameters in the ANN model quickly increases with its complexity. Longer computational times are sometimes required to develop the required model. The models developed through ANN are more difficult to interpret compared to the models obtained through PCR and PLSR.

To reduce the dimensions of the ANN and decrease computational time quite often PCA is applied to the data prior to model development using ANN. The combination of these two methods is termed as PC-ANN and has been reported to give better results and reduced computational times (Dou *et al*., 2007; Dou *et al*., 2006; Zhou *et al*., 2007)

### 2.15.6 Pre-Processing Techniques

Large amounts of data are produced during spectroscopic measurements, part of this data sometimes is irrelevant because of various reasons such as base line drift, multiplicative effects etc. In order to build a robust calibration model it is recommended to remove this part of data by using several pre processing techniques (Bakeev, 2010). In the following section some of the commonly used techniques will be discussed:

***Mean Centring***

Mean centring is frequently used as a pre processing technique. In this method an average data vector or spectrum is calculated by calculating a vector of $m$ averages by calculating the average of the $n$ absorbances in each column, this mean is then subtracted from each vector in the data. Mathematically this can be described as:

$$x_{ij}^{+} = x_{ij} - \frac{\sum_{i=1}^{n} x_{ij}}{n} \text{ for } i = 1, \dots, n \text{ and } j = 1, \dots, m \tag{2.45}$$

where $x_{ij}^{+}$ is the mean centred absorbance at $ith$ sample and $jth$ wavelength. A mean centred matrix can be transformed into the original matrix by simply adding the mean values. A potential benefit of mean centring is the removal of any absolute values from the spectral data.

***Baseline Correction***

Baseline correction is another technique similar to mean centring for removing baseline drifting in spectroscopic instruments. Baseline can sometime appear in the instruments with a particular trend such as gradually going up or down slope. The spectral intensity at wavelength(s) where no activity is observed i.e. no change in the intensity, the average values for this particular region can be calculated and subtracted from each spectrum. Sometimes a polynomial function can be used if the background signal is curved.

***Standard Normal Variate Transformation***

Standard normal variate (SNV) transformation is useful if variable path lengths are encountered (e.g. in reflectance spectroscopy), such differences give rise to multiplicative variations in the spectral data. Other sources may include variations in the samples such as particle size or thickness or even variations in spectrometer optics. These variations can disturb the quantitative information aspect of the data such as concentration of samples.

In transformation each spectrum is treated by subtracting its mean and normalizing it by dividing with the standard deviation. These parameters come from the individual variables that constitute a spectrum, as described by equation (2.26) in PCA section.

***Derivative Spectroscopy***

Derivative spectroscopy is another useful pre-processing and filtering technique. The derivative of a continuous function removes any baseline shift as the derivative of a constant is zero. The other benefits include enhancement of spectral features in case of overlapping spectra. Savitzk-Golay filters are frequently used for smoothing and derivative calculations (Brereton, 2003).

These filters are applied by using the adjustable parameters which include size of the window, derivative order and polynomial order.

A predefined set of coefficients is available corresponding to the afore-mentioned parameters. The application of the filter is performed by sequential multiplication of a set of absorbances by these coefficients in a moving window manner. In this way the derivative of each point is calculated. First order derivative normally removes the baseline offset, while second order derivative removes both the baseline offset and difference in baseline slopes due to drift in the spectral data. Use of high window size is recommended for noisy data, however, this may come at a cost of loss in spectral resolution.

### 2.15.7 Design of Experiments

Design of experiments (DOE) plays a very crucial role in development of calibration models using PAT tools. The main aim of DOE is to extract and collect as much as information possible through experiments with minimum experimental and financial effort (Bakeev, 2010; Gamperline, 2006; Brereton, 2003).

The data used for calibration model development should cover the expected range of instrument response with respect to the independent variables in real time operation e.g. absorbance data covering a specific temperature and concentration(s) range. It should also include any other factors that might affect the instrument response. A strong emphasis is placed on defining the working boundary of the model within which the model would be used. If a nonlinear system is encountered the data used for model development must be able to provide enough information for a model that can describe these effects. A part from development of calibration models, DOE can also be used to analyze the effect of a particular design variable on the response.

After setting the objectives, all those variables that can affect the instrument response must be identified. In the case of crystallization, temperature, pH, solvent/anti-solvent ratio, composition of various species (if more than one compounds are present) should be carefully considered.

Once the variables have been identified the next step is to select the number of levels. In calibration model development the objective can be to predict concentration of multiple compounds at various temperatures and solvent/anti-solvent ratios. In this case the limits for each of these variables must be defined and based on that suitable levels must be chosen, so that the application of model in real time situation can yield the desired output as accurately as possible under different conditions. Calibration models such as ANN and PCR can be very efficient, if the data generated covers all the linear and non linear relationships between the independent variables and instrument response.

Factorial design is the simplest DOE method, based on this method experiments have to be performed for all the variables at selected levels. For example for a 2 level design with 3 factors i.e. variables $2^3 = 8$ experiments have to be performed. The 2 levels here correspond to the minimum and maximum limit of a particular variable, similarly 3 levels will correspond to minimum, middle and maximum limits. The factorial design approach is suitable in cases where a smaller number of variables and levels are investigated, however, any increase in the number of levels and variables can exponentially increase the number of experiments required, practically making it impossible to use this technique e.g. 5 variables at 3 levels would require 243 experiments which is extremely difficult and impractical to carry out.

In order to overcome this issue several other DOE methods were developed, such as Box-Behnken, Face-Centered Cube, Central Composite Design (CCD) and others (Brereton, 2003). These methods differ in the way they characterize the interaction between different variables along with the number of experiments recommended. CCD is briefly described here. Figure 2.17 shows the design for a three variable two level design. The full factorial 2 level design is changed by adding axial or star points, while some of the replicate measurements are also carried out.

The number of experiments required can be calculated using the following equation:

$$N = 2^{\mathrm{f}} + 2\mathrm{f} + \mathrm{f_c} \tag{2.46}$$

Here $N$ represents the number of experiments, f is the number of levels and $f_c$ the number of centre points. The main advantage of CCD is that they consider non linear relationship between variables, this property is particular helpful in model development for non linear and systems. An application of CCD for non linear model development will be discussed in chapter 7.

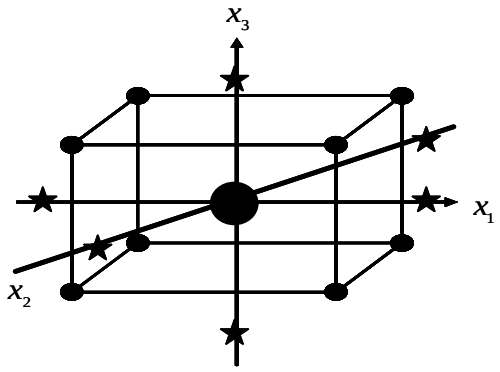



**Figure 2.17 Central composite design for three factors at two levels**

## 2.16 Summary

Crystallization is a complex and nonlinear process, the outcome of which is governed by the solubility, nucleation, growth and MSZW. A better control and monitoring of these mechanisms by various PAT tools can help in enhancing the quality of the crystalline product. More and more sophisticated control approaches using these *in situ* tools are gaining popularity as they consistently provide products with desired properties. Chemometrics combined with PAT provides qualitative and quantitative information about the system and can help in designing and implementation of model-free control approaches.

The literature shows the advantages of using these new control approaches. For example supersaturation control based on ATR-FTIR spectroscopy provided a better control of the crystallization process. Similarly control studies using FBRM show that the product quality is improved compared to the traditionally used linear or natural cooling profiles. It has been identified that only a handful of monitoring studies are available that deal with the application of ATR-UV/Vis spectroscopy in pharmaceutical crystallization. Unlike other spectroscopic tools for

which detailed methodologies are available for calibration model development, not much information is available for calibration model development for this technique. In case of FBRM, very few applications are available that show its use as a control tool.

The literature review highlights the importance of PAT and chemometrics for process monitoring and control. It also shows the underutilization of ATR-UV/Vis spectroscopy and FBRM for process control. The aim of the thesis is therefore to expand the application and use of these two tools both on laboratory and pilot plant scale for process monitoring and control. Two control approaches, namely, supersaturation control using ATR-UV/Vis spectroscopy and automated direct nucleation control approach using FBRM were developed and implemented.

# Chapter 3 Calibration Model Development for ATR-UV/Vis Spectroscopy for Crystallization Monitoring

## 3.1 Introduction

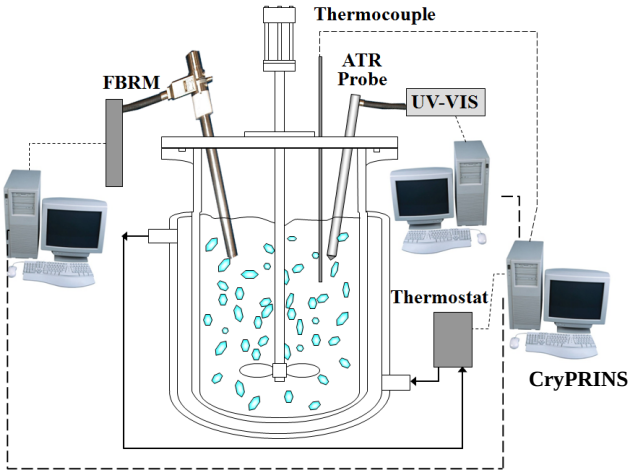
The use of PAT tools has become an integral part of drug development and manufacturing processes. These *in situ* tools as discussed before provide useful information but at the same time generate large amounts of data. Sophisticated mathematical and statistical tools are therefore required to analyze and extract meaningful information from the data. Chemometrics can be employed for this purpose. The general scope of chemometrics has been discussed in the previous chapter. The main purpose of this chapter is to demonstrate that ATR-UV/Vis spectroscopy can be used for quantitative crystallization monitoring and to introduce a calibration model development methodology for this monitoring tool. Several different calibration methods will be evaluated for their prediction ability.

## 3.2 Experimental Setup and Methodology

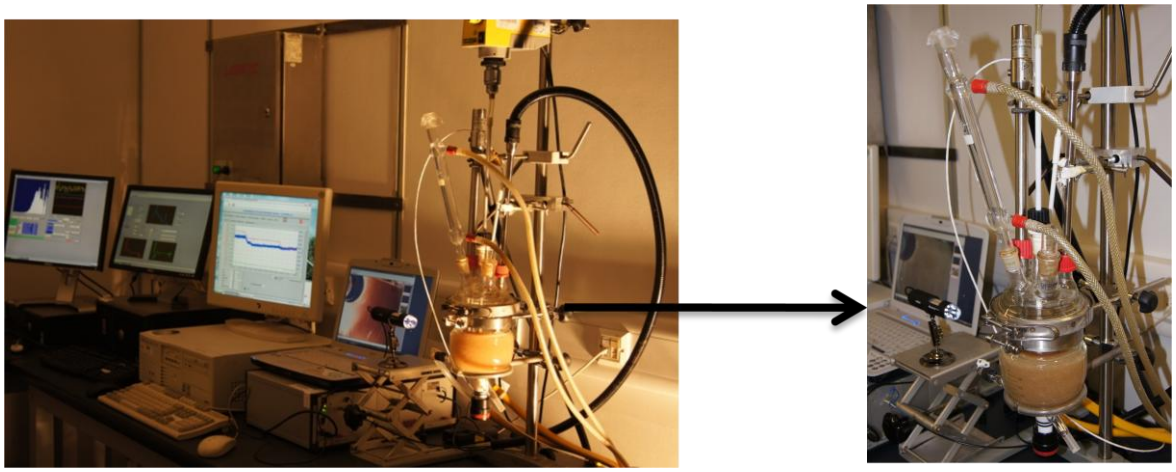
The experiments were carried out in a 500 mL jacketed glass vessel fitted with an overhead PTFE coated 4-pitched blade turbine and thermocouple. The temperature was controlled by a thermo fluid circulator bath (Huber Variostat CC-415 VPC). An FBRM probe (model D600, Lasentec) was used to measure chord length distributions. FBRM data collection and monitoring was carried out by the FBRM control interface software (version 6.7). FBRM was used during the experiments as a monitoring tool of the solid phase and provides useful information about dissolution and nucleation events. The UV/Vis spectra of the solution were measured using a Hellma 661.822 ATR probe connected to a Carl Zeiss MCS621 UV/Vis spectrometer. Software written in LabVIEW (National Instruments) using libraries provided by Carl Zeiss was used for spectra collection. The FBRM, UV/Vis and temperature data were recorded every 10 seconds. The data collected by computers connected to FBRM and UV/Vis were sent to a third computer, running the Crystallization Process Informatics System (CryPRINS) software (in-house developed software) written in LabVIEW. This software is capable of receiving and sending data

through an RS232 interface, by file sharing, or using an OPC (OLE - Object Linking and Embedding - for Process Control) server. The software enables the simultaneous monitoring of the data from various PAT tools and the implementation of the required temperature profiles in an automated way.

The experiments were carried out using paracetamol (4-acetaminophenol, 98% purity, purchased from Aldrich), analytical grade 2-propanol (isopropanol, IPA). A schematic representation and picture of the equipment are shown in Figure 3.1 (a) and (b).




**(a)**



**(b)**

**Figure 3.1 Schematic representation (a) and picture (b) of the experimental setup used for calibration model development and crystallisation monitoring**

The development of the calibration model followed the following generic steps:

1) Determination of solubility for the desired system. This can be done using literature data or experimental solubility determination procedures (e.g. gravimetric analysis).
2) Identification of the operating envelope or design space (e.g. determination of concentration and temperature ranges). In this step the number of data sets within the range (levels) must also be determined. The operating envelope should include both undersaturated and supersaturated regions. Note that the temperatures ranges change with concentration hence the selection of these ranges can be done based on the metastable zone width of the process. Often before or during the calibration experiments a metastable zone determination is performed, for the more precise identification of the operating envelope.
3) Calibration experiments that cover the design space are performed based on the process limits selected.
4) Analysis of the raw data for outlier detection and nonlinearity check. At this stage plotting absorbances versus temperature at constant concentrations and absorbances versus concentration data at constant temperature can help in the selection of the calibration model structure. Whether preprocessing is needed or whether absorbance or derivative data should be used can also be decided at this stage.
5) Model structure identification. In this step the form of the calibration equation is chosen. A decision whether a nonlinear or linear model structure will be used is made based on the analysis of the data in the previous step.
6) Model identification. The parameters of the model are determined using appropriate model identification methods
7) Model validation.

For the current study paracetamol in IPA was selected as the model system as it is a widely used compound and relevant solubility data are easily available, and the aforementioned steps of the calibration model development were followed.

## 3.3 Results and Discussion

Absorbance measurements from the ATR-UV/Vis spectroscopy spectrometer were used to develop a calibration model. Spectra were measured in the range of 242-400 nm. An example of an absorbance spectrum and the corresponding first derivatives are shown in Figure 3.2.

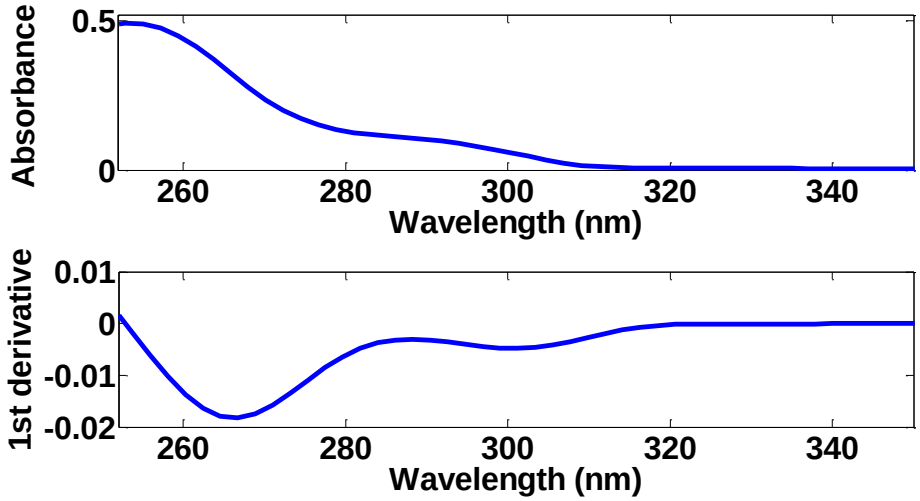



**Figure 3.2 Spectrum of paracetamol in IPA at constant temperature and concentration, lower half of the figure shows the first derivative of the absorbance with respect to wavelength**

For the calibration model development, experiments were conducted at 8 different concentrations. In each experiment the data was recorded at several temperatures to ensure that absorbance data are available for both supersaturated and undersaturated regions. For validation of the developed models, an additional validation experiment was carried out. A summary of the concentrations used for model development and validation is given in Table 3.1.

The general practice is to measure the concentration in "mass/volume" units, in accordance with Beer-Lambert's law. In crystallization monitoring, the volume based measurement has the drawback that the actual total volume is based on the volume of the solid and the solvent used, which can both change during the crystallization process. As crystallization progresses, both the concentration in the liquid phase and the volume of the solid phase change, causing variations in the total volume, which can lead to errors in the concentration prediction. The use of "mass of solute/mass of solvent" units eliminates this problem and therefore is recommended for

crystallization monitoring. The concentrations used in this work are expressed in "grams of solute/grams of solvent" and from here onwards will be denoted as "g/g".

**Table 3.1 Summary of the calibration experiments**

| Training Data Concentration (g/g) | Saturation Temperature (approximate values in °C) |
|---|---|
| 0.2109 | 58 |
| 0.205 | 55 |
| 0.187 | 49 |
| 0.172 | 43 |
| 0.1505 | 34 |
| 0.135 | 30 |
| 0.1 | 18 |
| 0.093 | 13 |
| **Validation Data** | |
| **Concentration (g/g)** | |
| 0.18 | |

A typical experiment carried out at a concentration of 0.18 g/g is shown in Figure 3.3. Spectral data was recorded at several different temperatures to obtain a comprehensive set of data. The temperature effect on all absorbances, dissolution and nucleation events are shown in Figure 3.3. The evolution of the absorbance at 252 nm is shown in Figure 3.4. The temperature steps helped in analyzing the reproducibility and repeatability of the absorbance data at the same temperatures but at different times. This experimental procedure with the decreasing and increasing temperature steps is important to identify baseline shift, drift or hysteresis in the signal. No significant drift was observed in this case even when the instrument was used for fairly long time continuously. The sensitivity of the ATR-UV/Vis spectroscopy for the nucleation and dissolution events can be observed. Both these events are clearly identified from the absorbance plot as the concentration keeps increasing because of the continuous dissolution of the solids as the temperature was increased, this dissolution was also highlighted by decrease in FBRM counts/s. The absorbance increased until the solids were completely dissolved. The decrease in absorbance after that dissolution shows the temperature effect on absorbance. Absorbance increases as the temperature is decreased and decreases vice versa. These variations indicate the importance of including a correction of the temperature effect in the calibration models and will be discussed later. The nucleation event is also detected by ATR-UV/Vis spectroscopy by a sharp decrease in

absorbance at the time of nucleation. An increase in the FBRM counts/s approximately at the same time also shows the nucleation event.

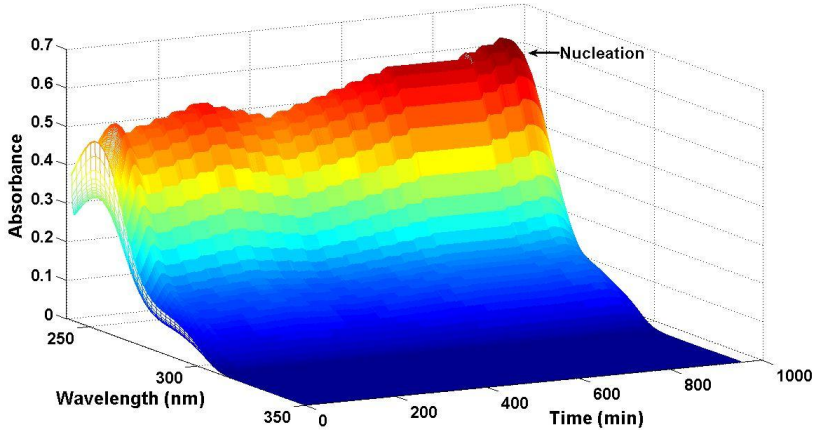



**Figure 3.3 Variation of absorbance values at different wavelengths and time during a typical crystallisation experiment.**

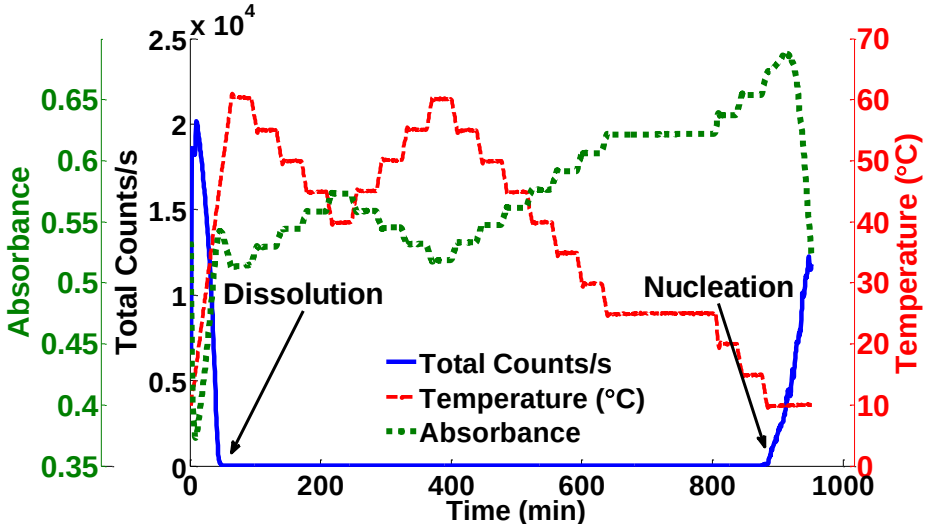



**Figure 3.4 Absorbance at 252 nm, total counts/s and temperature profile for a typical calibration experiment**

Prior to calibration, a decision must be made on (1) the form of the calibration model and (2) the method used to determined the coefficients in the model. If a linear relationship exists between the concentration and spectral data then multivariate methods such as MLR, PCR and PLSR can be used. Since crystallization processes are often conducted under large ranges of concentrations which generally includes high concentrations, nonlinearities between the absorbance and concentration are often encountered. If nonlinearities are present in the data then linear methods

may not be used, and approaches that can take these nonlinearities into account may need to be considered. The nonlinearities can be classified in to following types:

1) The nonlinearity in variables e.g. in the spectral data between two absorbance values as a result of wavelength shift or interaction between absorbance and temperature.
2) Nonlinearity between concentration and absorbance at a certain wavelength; such nonlinearities are called univariate nonlinearities.
3) Total nonlinear relationship between absorbance and all variables, such as concentration, temperature, solvent composition and others.

Two main approaches can be used to incorporate potential nonlinearities in the calibration model development. The first approach is to use a nonlinear regression method with nonlinear relationships e.g. ANN. This method is capable of modelling any nonlinear relationship as mentioned above, however leads to a complex calibration model structure with a large number of parameters. Special care has to be taken during the development to avoid over-parameterization which can significantly reduce the prediction ability of the ANN model. An alternative approach is to model nonlinearity (first two types of nonlinearities) by introducing higher order terms, e.g. quadratic, interaction (between variables) and in some cases even cubic terms. These additional variables along with the original variables can be used for prediction by application of multivariate linear regression (Berglund and Wold, 1997). An example of such model is shown in equation (3.1). The model has nonlinear variable terms, however the coefficients can be determined by a typical linear regression methods.

$$c = b_o + b_1 x + b_2 T + b_3 xT + b_4 x^2 \tag{3.1}$$

where $c$ is the concentration, $T$ is the temperature, $x$ can be the absorbance or the derivative of the absorbance at a particular wavelength and $b_i, i = 0, \ldots, 4$ are the model parameters to be determined during the calibration procedure. During model building it is recommended to determine the magnitude of nonlinearity and if possible its source. If a minor nonlinearity exists then linear models can still be reliably used.

Preprocessing is an essential part of calibration model building. The data used in the models were mean centered and the 1st derivative of spectral data (with respect to wavelengths) was also used for the calibration model development. The 11 point derivative was calculated using the Savitzky-Golay algorithm (Brereton, 2003). The derivative of the absorbance retains the essential information in the spectral data, while at the same time eliminates any drift that may have been present. It is important to note that the application of the derivative increases noise in the signal hence it is important to use smooth absorbance spectra. This was achieved by collecting in all experiments 100 spectra with a sampling rate of 10-20 ms, and averaging the values before applying the derivative calculation. Additionally the approach used for the derivative includes a filtering methodology (Savitzky-Golay method), which was built in the LabVIEW interface of the ATR-UV/Vis spectrometer. In case of the PCR and PLSR calibration methods, PCA is applied to the data which can also remove baseline effects therefore absorbance data treated with PCA was used as input for the PCR and PLSR models instead of the derivative. For the subsequent simpler but nonlinear calibration models the derivative of the absorbance at 266 nm was used, since at this wavelength it shows high sensitivity to change in concentrations. Using a derivative or absorbance in the low sensitivity region, makes the calibration model more prone to be affected by noise in the data.

First the range of concentration was selected to cover the operating range during the crystallization process both in terms of concentration and temperature. Figure 3.5 shows how the measurement points covered the operating region in the phase diagram. Measurements were taken for each concentration at different temperature steps, both in the under-saturated and supersaturated regions.

In order to investigate the presence of nonlinearity between the variables used, the 1st derivative of the absorbance was plotted against temperature at constant concentrations (see Figure 3.6), and against concentration at constant temperature (see Figure 3.7). These plots help in understanding whether the variation in absorbance (or derivative of absorbance) is linear or nonlinear for different concentrations and at different temperatures. These plots show that a linear relationship exists between absorbance and temperature at individual concentrations. On the other hand a change in slopes can also be observed, showing that an interaction between

temperature and absorbance exists. This observation suggests the addition of an interaction term (between the absorbance and temperature) in the calibration model be required.

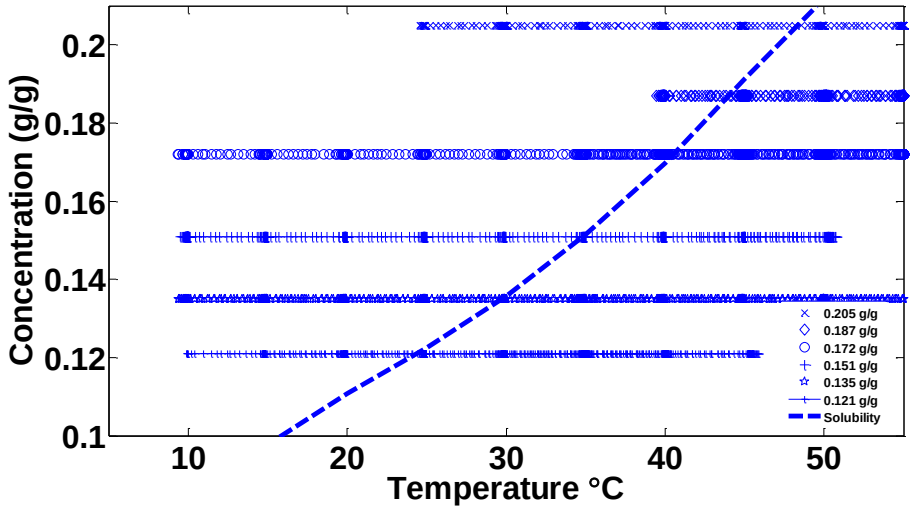



**Figure 3.5 Concentrations used in the calibration model development**

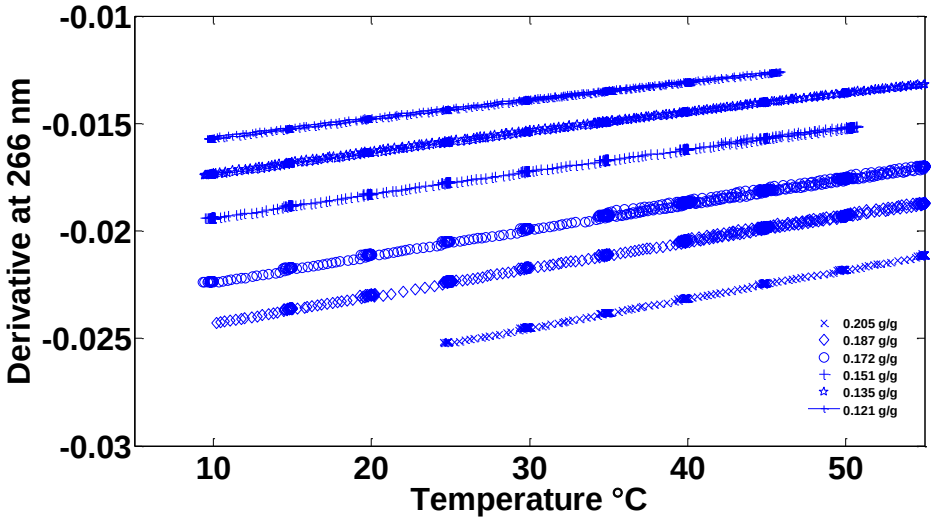



**Figure 3.6 Variation of 1st derivative at 266 nm with respect to temperature at different concentrations, except for the validation experiment**

Similarly the behaviour of absorbance derivatives against concentration was also investigated at constant temperatures (a sample plot at 30 °C is shown in Figure 3.7), and no nonlinearities were observed. The same analysis carried out at several temperatures showed the same results, therefore eliminating the need to add a quadratic term in the nonlinear model.

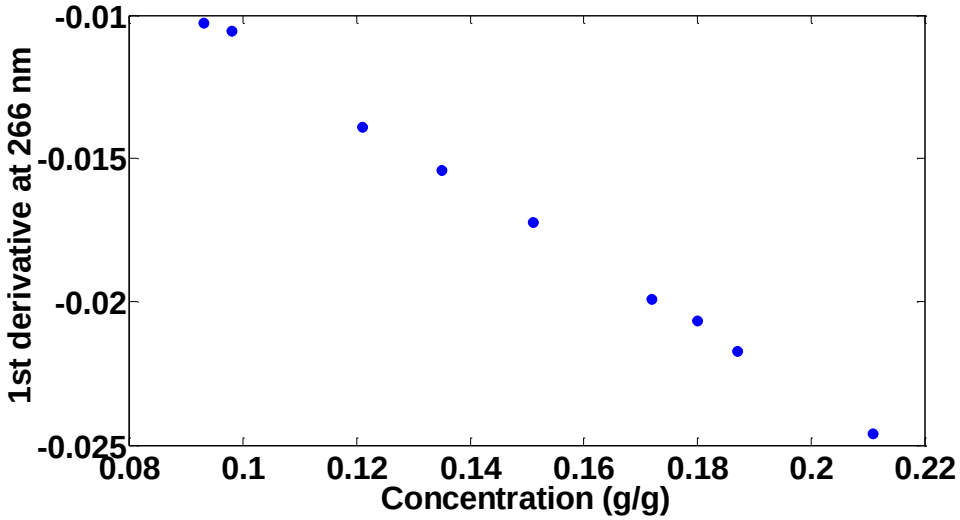



**Figure 3.7 1st derivative at 266 nm versus different concentrations at 30°C**

From these analyses it can be concluded that only a slight moderate nonlinearity exists in the data hence linear calibration methods may provide acceptable performance. Therefore different linear and nonlinear models will be discussed and compared for their predictive capabilities in the next section.

### 3.3.1 Performance analysis of Calibration Models

When developing a calibration model it is always preferred to have the simplest possible model which can give satisfactory results. By intuition, uni-variate model involving just wavelength is the first choice. In the previous section temperature dependency of absorbance was demonstrated and the need for adding an interaction term. To illustrate this further quantitatively, results using a simple uni-variate method are presented. Absorbance at 252nm was used in the model in the development of the following calibration model:

$$c = b_0 + b_1 x \tag{3.2}$$

where $c$ is the concentration in g/g and $x$ is the absorbance. The residuals (which are the difference between the actual and the predicted values) were used to test the predictive capability of the model. The spread and high absolute values of the residuals indicate poor performance of

the model. A plot of the predicted versus actual concentration and corresponding residuals is shown in Figure 3.8 These results indicate that this simple model did not perform well and hence is not suitable for crystallisation monitoring. These results clearly indicate that uni-variate models should only be used if the system's absorbance is only dependent on the concentration of a single species without any interference from other compounds and temperature.

Next a multivariate model was considered with temperature as the added term built in the model, using the following calibration equation:

$$c = b_0 + b_1 x + b_2 T \tag{3.3}$$

The results are shown in Figure 3.9.

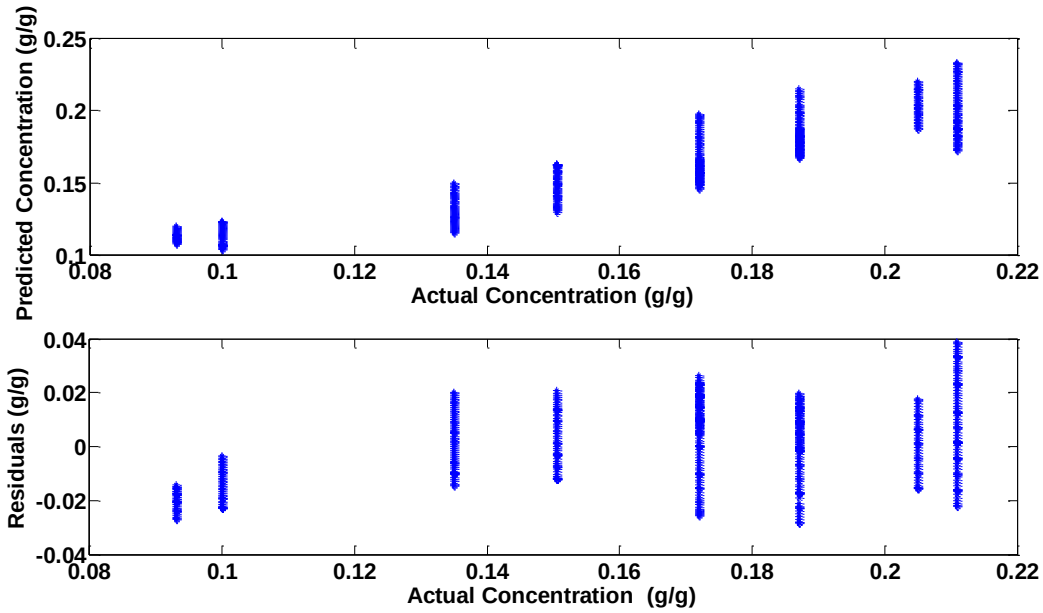



**Figure 3.8 Actual and predicted concentration using uni-variate model**

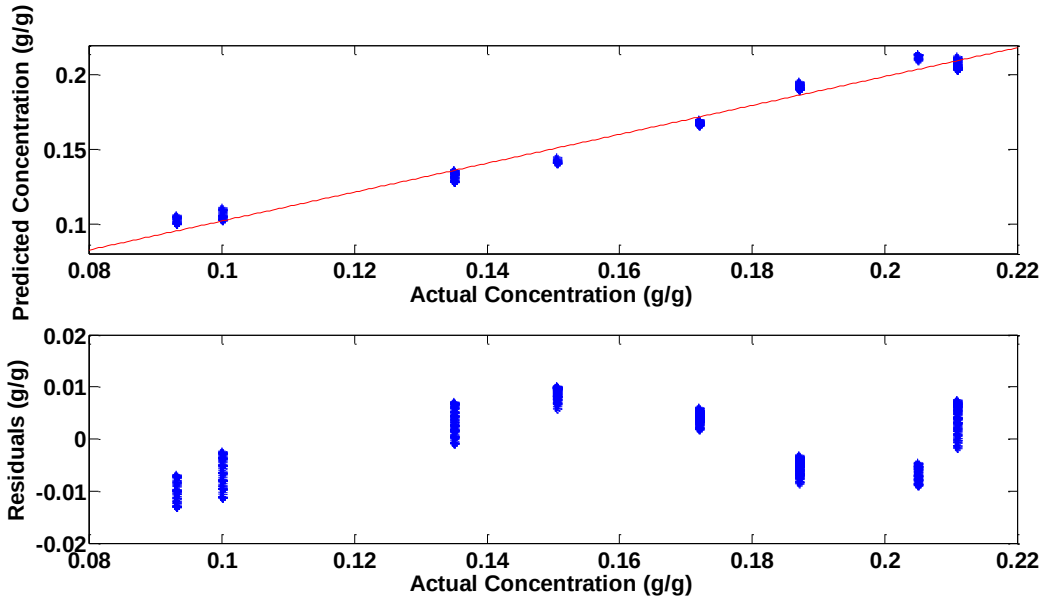



**Figure 3.9 Actual and predicted concentrations using multivariate model with temperature term**

The results show an improvement in the prediction performance of the model. The much less spread of the data indicates that the addition of the temperature term has improved the prediction performance of the model.

To further increase the prediction performance of the model the effect of adding additional absorbance terms in the model was evaluated. A calibration model of the form:

$$c = b_0 + \sum_{i=1}^{N_x} b_i x_i + b_{N_x+1} T \qquad (3.4)$$

was used, with $N_x$ being the number of absorbances used in the model. The prediction results when three absorbances ($N_x = 3$) were used (at wavelengths 242 nm, 252 nm and 280 nm) are shown in Figure 3.10. It was expected that the addition of multiple absorbances would improve the model prediction, however, this was not the case; in fact the performance of this model was lower than the previously developed model. To investigate the reason behind this result, the data were checked for multicollinearity. It was mentioned in the previous chapter (section 2.15.2) that the presence of multicollinearity in the data can give rise to unstable models with poor predictive ability.

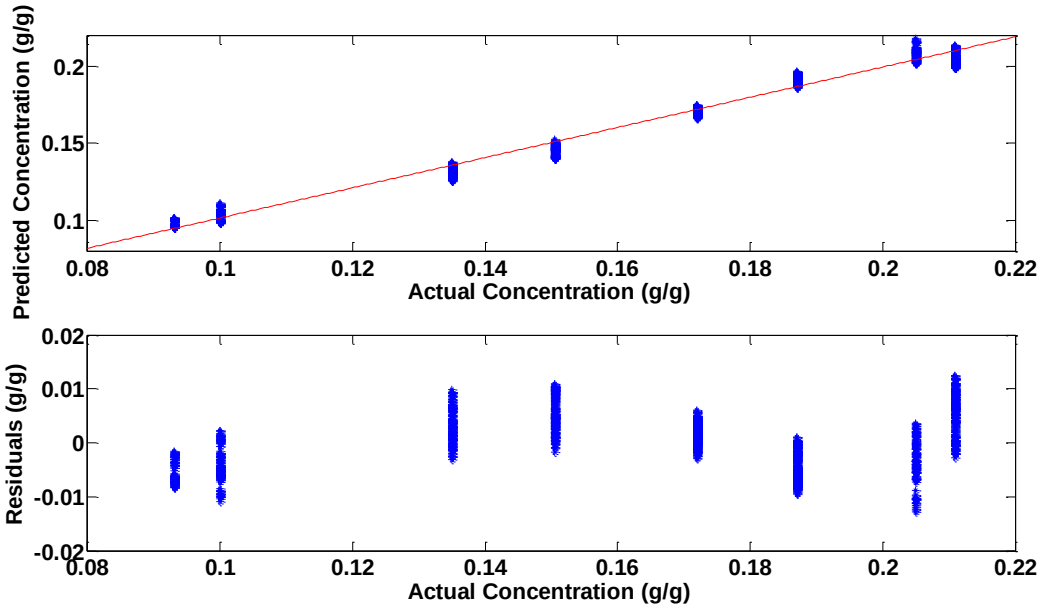



**Figure 3.10 Actual versus predicted concentration values for multivariate model with 3 absorbances**

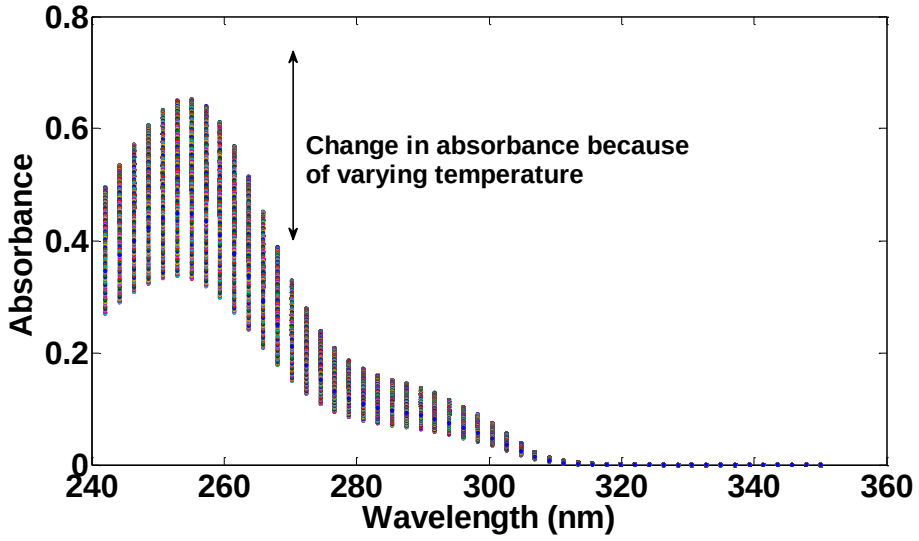



**Figure 3.11 PCM spectra in IPA at different temperatures (10 °C – 60 °C)**

PCM spectra at constant concentration and varying temperatures are shown in Figure 3.11. The absorbance pattern at different wavelengths indicates that the majority of the absorbances increase or decrease in a similar fashion. This implies that absorbances can be expressed as linear functions of each other. This linearity can be regarded as the cause of multicollinearity. A covariance matrix for the spectral data can be developed for detection of this property. The covariance values between four selected absorbances in correlation to the rest of the spectrum are

shown in Figure 3.12. The wavelengths were selected at different points in the spectrum for the collinearity check. The absorbances which are closer to the peak values behave in a similar way, the wavelengths further away from 280 nm and close to 310 nm vary in a different way, however, at these wavelengths the sensitivity reduces and more noise is involved, using these wavelengths for calibration model development is therefore not recommended. The absorbances in the range of 240-290 nm are highly correlated and show the highest covariance. Compared to the absorbances at wavelengths higher than 300 nm, the covariances with the lower wavelengths quickly decrease (for the larger wavelength which is in this range the covariance increase as expected), indicating decreased collinearity between absorbances in the 240-300 nm range and above. However, due to their low sensitivity, absorbances above 290 nm are not suitable for calibration model development. These results demonstrate the strong multicollinearity between the absorbances at different wavelength, and suggest that models with a single absorbance anywhere in the range of 240-290 may perform similarly. These results also indicate that if absorbances at multiple wavelengths are to be used, multivariate methods such as PCR and PLSR should be employed to avoid the strong multicollinearity in the data.

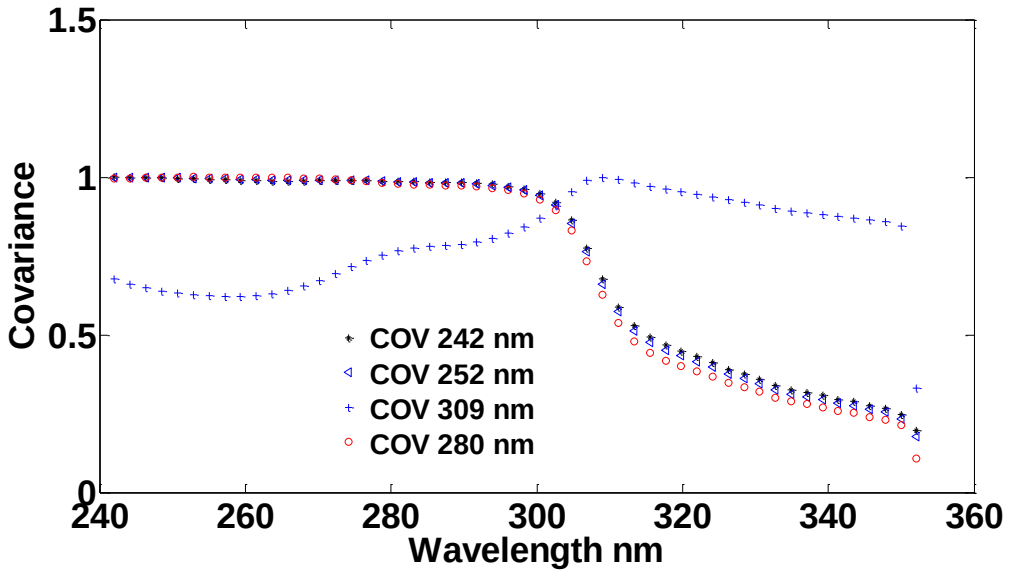



**Figure 3.12 Covariance between different wavelengths**

The results of using the PCR and PLSR calibration methods are presented next.

Both PCR and PLSR determine a calibration model similar in form to equation 3.2, but the variables $x_i$ are no longer directly the absorbance (or derivative) values, instead they represent linear combinations of the absorbances (derivatives) at all wavelength in the range considered. These linear combinations are determined by the PCR and PLSR methods to eliminate the collinearity between the variables $x$, and their actual structure will depend by the method employed. In this case all absorbances within a range of wavelength are automatically considered but the number of calibration model coefficients is significantly reduced since those are determined for only a small number of $N_x$ linear combinations between the absorbances.

The major benefit of these approaches is that the selection of wavelengths is carried out by the method itself based on the contribution of each wavelength (or factor) as a result, wavelengths that show little sensitivity towards changes in concentration or temperature would not be considered critical by the model. The representation of the data in the new geometric coordinates results in variables that are independent (perpendicular to each other) of each other but linear combinations of the original variables. This property solves the collinearity issue and a reduced number of variables can be used for model development.

It is always desirable to have an accurate model therefore the number of factors capturing more than 90 % of the variance can be selected and used for model development. It should be mentioned that including too many factors may give rise to unstable solutions as noise would be included in the model. Another important issue is the selection of the model development technique. In the literature it has been mentioned that both techniques essentially give similar results and no appreciable difference exists between the two (Naes *et al*., 2002). The results here showed that 8 factor PCR and PLSR gave the best results and by selecting the same number of factors for both techniques a direct comparison could be performed.

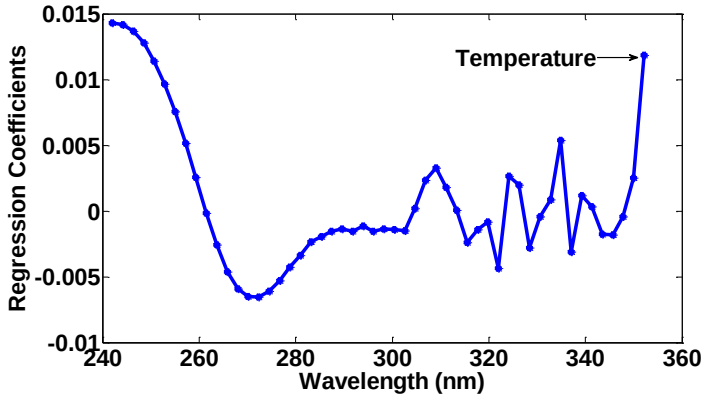



**Figure 3.13 Regression coefficients for 8 factor PCR**

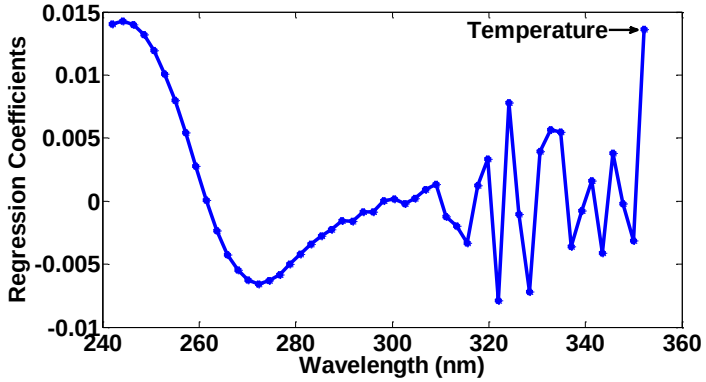



**Figure 3.14 Regression coefficients for 8 factor PLSR**

The regression coefficients generated by PCR and PLSR are shown in Figure 3.13 and Figure 3.14, respectively. The trends in both these plots are similar indicating that both PCR and PLSR give similar regression coefficients. The coefficients corresponding to the absorbances above 310 nm appear as random variables with zero mean, which also suggest that those absorbance values have very low (close to zero) sensitivities hence should not be taken into account for the calibration model. This is in correlation with the results in Figure 3.11 where very little change in absorbance values is seen for these wavelengths. A high value for regression coefficient for temperature can be seen here, indicating that both models recognized the contribution of temperature towards the spectra.

The prediction results from both models are shown in Figure 3.15 and Figure 3.16, respectively. Compared to the multivariate models shown in Figure 3.9 and Figure 3.10, both these models gave significantly better results. Smaller values were obtained for both models and predicted

values were much closer to the actual values than the previous multivariate models. The improved results by these techniques show that the models capable of dealing with multicollinearity perform better than the simple multivariate models.

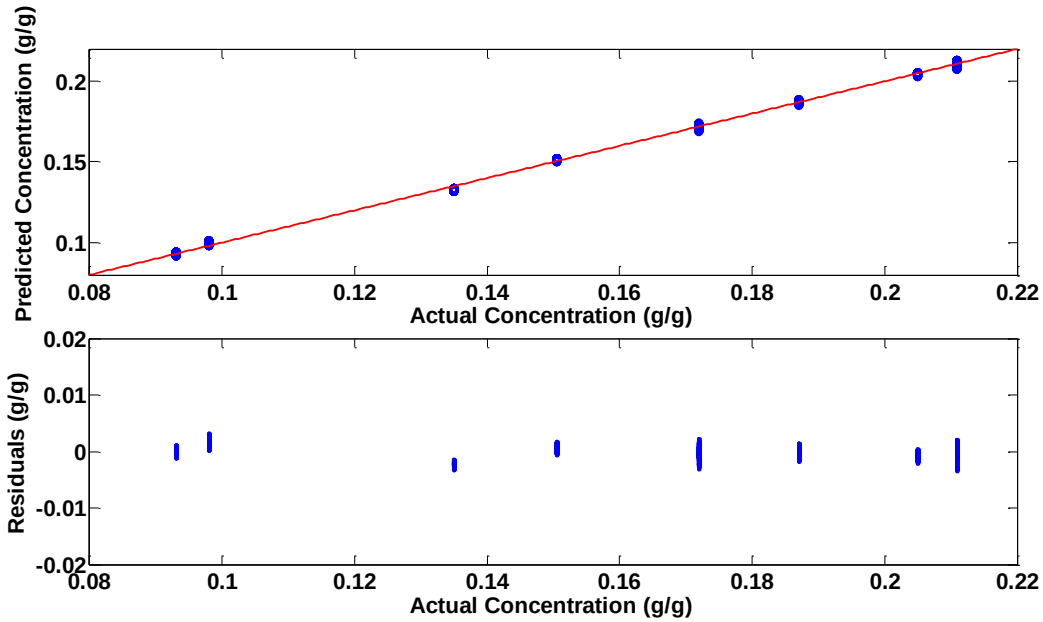



**Figure 3.15 Actual and predicted concentrations using 8 factor PCR**

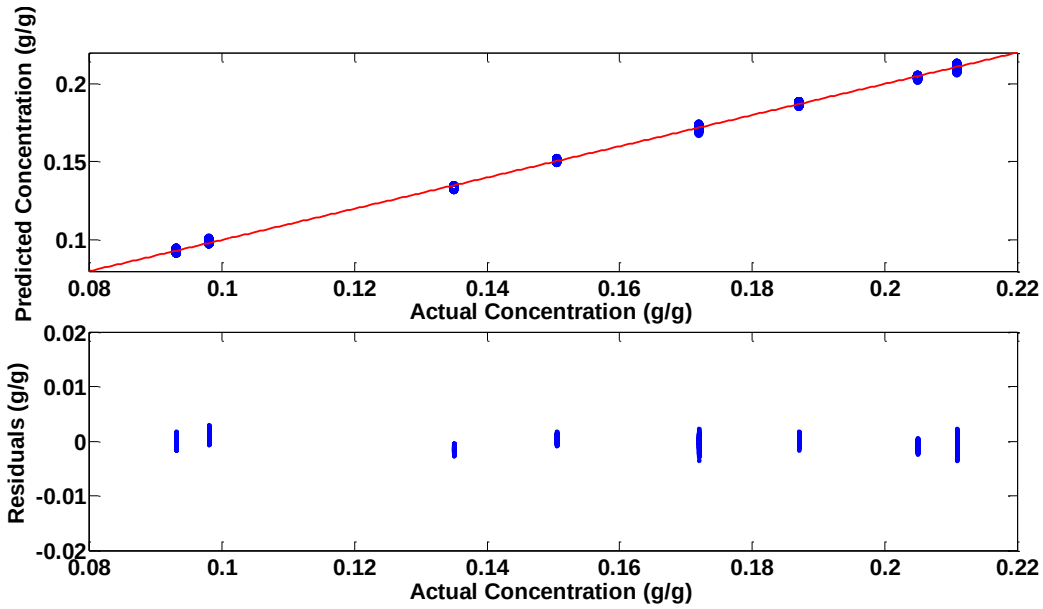



**Figure 3.16 Actual and predicted concentrations using 8 factor PLSR**

The preliminary analysis of the calibration data identified a moderate level of nonlinearity in the data. It was therefore decided to also develop a model using nonlinear terms. This method offers flexibility of using different types of equations containing any nonlinear terms, including polynomial, exponential or various interaction terms. The model evaluated has the similar form as the nonlinear equation (3.1), and consists of the linear terms for the temperature and derivative of the absorbance at wavelength 266 nm, and a nonlinear term expressed as a product between the absorbance derivative and temperature to incorporate the nonlinear effect in the data. The equation used therefore has the form:

$$c = b_o + b_1 x + b_2 T + b_3 xT \tag{3.5}$$

where $x$ represents the derivative of the absorbace at 266 nm. The coefficients of the model were determined using a standard nonlinear least square optimisation approach implemented in the MATLAB function "fmincon". The results are shown in Figure 3.17 and are very similar to PCR and PLSR results, but are better than the results obtained with the simple bivariate calibration model with no interaction term.

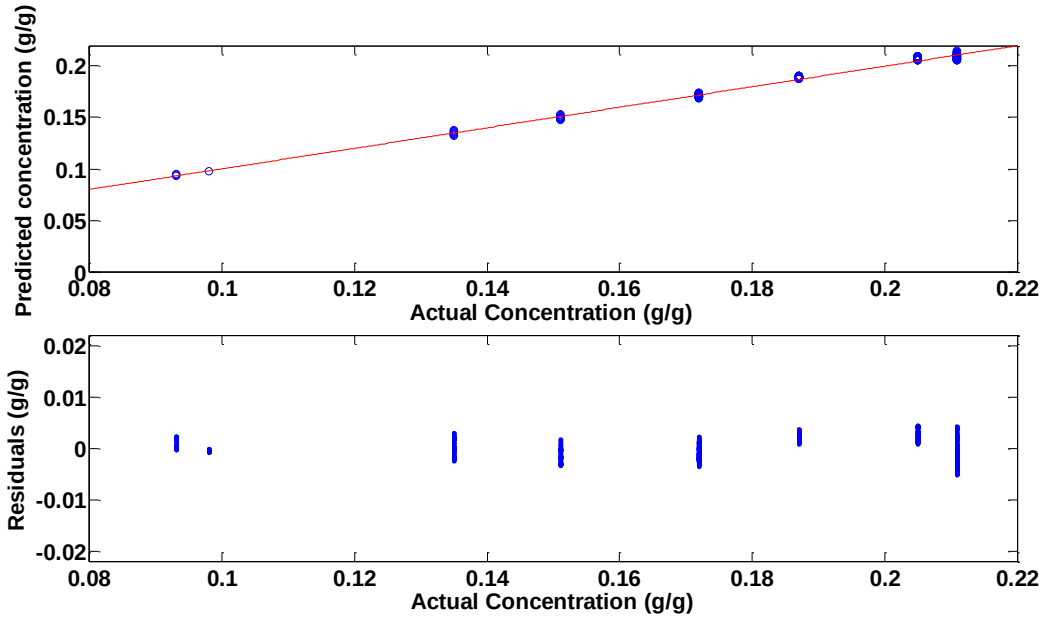



**Figure 3.17 Actual and predicted concentrations, nonlinear method using 1st derivative**

A major benefit of using a single wavelength nonlinear calibration model with derivative is that there is no issue of multicollinearity as only one spectral variable is used. Secondly this is computationally much more efficient and extremely easy to implement for real time monitoring, especially on the industrial scale, where programming complex calibration equations with a large number of parameters that result from PCR and PLSR into the DCS is often difficult. The linear and the moderately nonlinear methods both gave similar performances, however PCR and PLSR required more components to give a similar prediction to the nonlinear model. According to Naes *et al*. (2004) PCR based linear models can give a stable solution by using a larger number of principal components for slightly nonlinear data, but a nonlinear model can give much better solutions using fewer variables. This has been observed in this case too, since by using only two variables and their interaction term (essentially three terms), the performance of the nonlinear model was similar to that of the 8 factor PCR and PLSR. The performance of the nonlinear, PCR and PLSR models was further evaluated by using the validation experiment. The RMSEP was used to quantify the prediction performances for all three models. The values obtained are shown in Table 3.2. The RMSEP values are similar for all three models, with the smallest prediction error corresponding to the nonlinear model.

**Table 3.2 Root Mean Square Error of Prediction values for different models used**

| | **PCR** | **PLSR** | **Nonlinear model** |
|---|---|---|---|
| **RMSEP** | 0.0035 | 0.0040 | 0.0034 |

In the light of the analyses presented in this section the nonlinear model was selected as a suitable calibration model to be used with ATR-UV/Vis spectroscopy, because of its simplicity and accuracy. To check the robustness of the model a number of tests were performed.

### 3.3.2 *In situ* and real-time monitoring of crystallization using ATR-UV/Vis spectroscopy

In the first case a slurry experiment was performed as shown in Figure 3.18. The main purpose was to obtain data that can be fed to the developed model and obtain solubility data points at the selected temperatures. A solution of PCM corresponding to saturation temperature of 45°C was prepared. The solution was then heated up in several steps, and the temperature was maintained for 1 hour at the selected temperatures to establish near thermal equilibrium conditions at the specified temperatures. This resulted in stepwise partial dissolution of the crystals present in the solution.

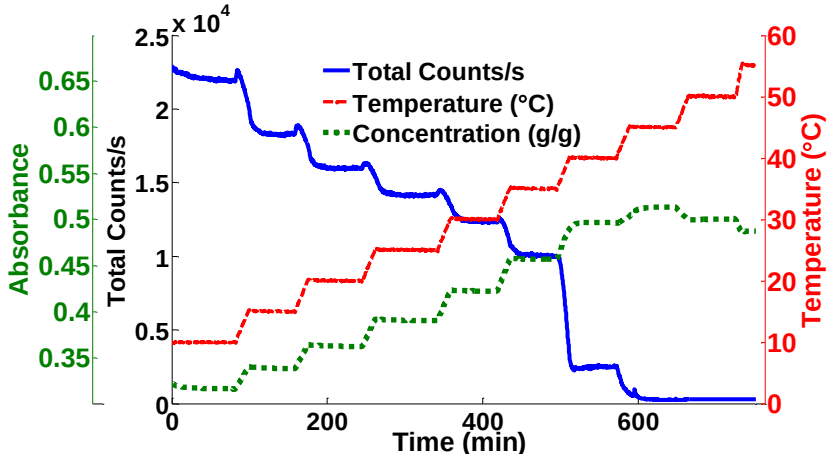



**Figure 3.18 Total counts/s, temperature and absorbance profiles for slurry experiment**

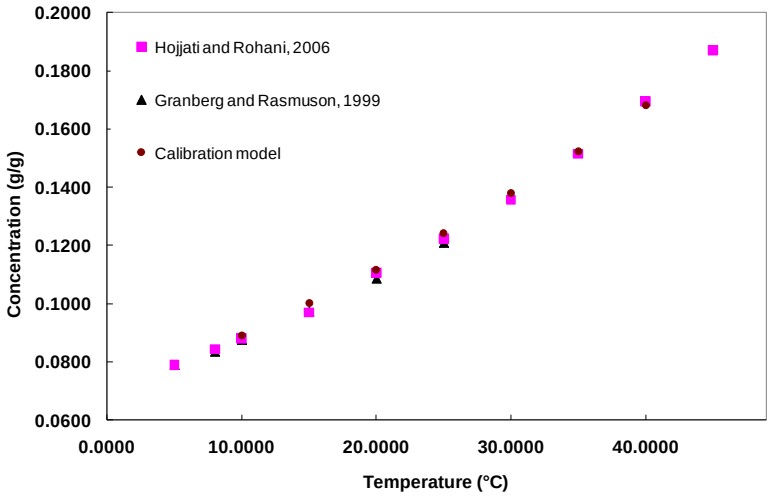



**Figure 3.19 Comparison of model predicted solubility and literature values**

The stable FBRM counts and constant UV/Vis absorbance values both indicate that an equilibrium between the solid and liquid phases was achieved, as no appreciable change in counts or absorbance was observed at the constant temperatures. The absorbance values collected in these equilibrated points should correspond to the solubility concentration of the compound at each temperature value.

The results obtained by the application of the model to the data obtained are shown in Figure 3.19. The results indicate that the solubility predicted by the model is in good agreement with the solubility data available in the literature and capable of measuring concentrations with high accuracy and precision.

The robustness of the model developed was further checked by monitoring the concentration of PCM in real time during a more complicated crystallisation experiment. The result of monitoring the crystallisation process using ATR-UV/Vis spectroscopy coupled with the simple nonlinear calibration model is shown in the phase diagram in Figure 3.20 and, by plotting the operating curve during the experiment. The solubility curve (obtained from the literature) is also plotted here as a reference point.

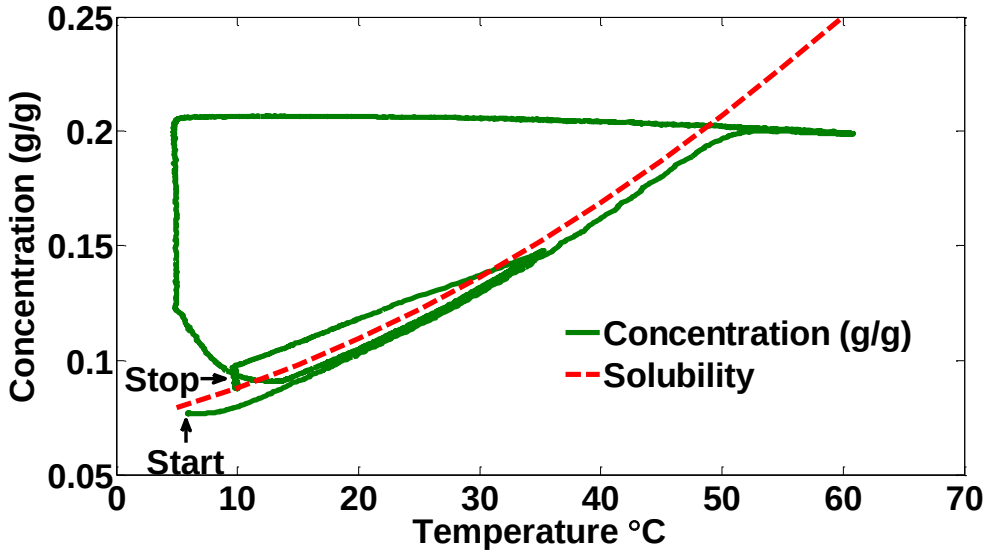



**Figure 3.20 Performance analysis of nonlinear calibration model**

During the heating up phase the concentration of the solution was increasing and as expected stayed just below the solubility curve as complete thermal equilibrium could not be achieved

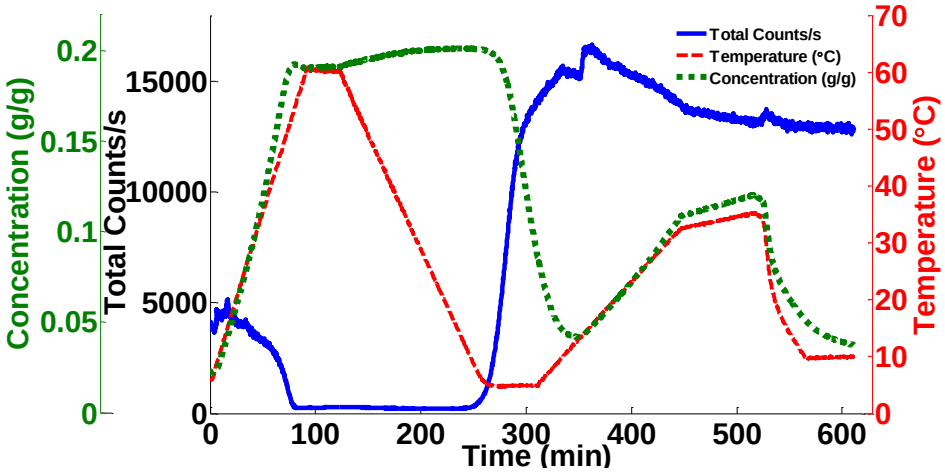



**Figure 3.21 Total counts/s, concentration and absorbance profiles for experiment shown in Figure 3.20**

because of the continuous increase in the temperature. The concentration (as predicted by the model) closely followed the solubility curve until complete dissolution took place. The concentration profile remained flat after dissolution as the temperature increased and then decreased until nucleation took place. The flatness of the profile indicates that the model captured the temperature effect properly. The temperature of the solution was then increased until the nucleated crystals partially dissolved. The second heating curve followed very well the operating curve from the previous heating cycle, but stopped at a lower temperature since only partial dissolution of the nucleated solid was required. This indicates the repeatability and reproducibility of the model. After the second heating phase a slower cooling profile was applied and the supersaturation was kept at a much lower value to promote growth and avoid secondary nucleation. The results indicate that the model developed gave satisfactory results and was able to give accurate quantitative information about the system.

## 3.4 Conclusions

This chapter presented a methodology for calibration model development. The building of a robust and accurate model requires knowledge about the relationship that exists between the variables and the property of interest. A linear calibration model can be used if the relationship is linear, in case of nonlinearity the selection of the method depends on the type of nonlinearity. Several procedures are available to model nonlinear behaviour. The performance of different linear calibration methods was analysed and compared to a simple nonlinear model which

included linear absorbance (derivative) and temperature terms and a simple interaction terms (expressed as the product between the absorbance and temperature). The simple nonlinear model provided slightly better results than PCR and PLSR, however with significantly less model parameters. The robustness of the model developed was checked by determining solubility of PCM in IPA, and comparing the results with the literature data, obtaining very good agreement. The developed model satisfactorily captured the temperature effects and detected nucleation and dissolution events. The chapter provided a methodology description and experimental validation of the capability of ATR-UV/Vis spectroscopy with a relatively simple moderately nonlinear calibration model as an efficient tool for *in situ* and real-time crystallization monitoring and control.

# Chapter 4 Comparative Investigation of Supersaturation and Direct Nucleation Control of Crystal Size Distributions using ATR-UV/Vis Spectroscopy and FBRM

This chapter presents a thorough evaluation of different control policies used in cooling crystallization, namely: unseeded linear cooling, seeded linear cooling, supersaturation control, direct nucleation control and combined direct nucleation and supersaturation control. The sensitivity and robustness of supersaturation and direct nucleation control approaches are checked by varying different process parameters such as seed loading, heating and cooling rates for paracetamol crystallization in isopropyl alcohol. The supersaturation control approach uses concentration information provided by ATR-UV/Vis spectroscopy, while the direct nucleation control approach is based on FBRM.

## 4.1 Introduction

During crystallization obtaining a narrow and reproducible CSD is important to achieve efficient downstream processing and desired final product properties with reduced variability. The most widespread control approach applied for industrial scale cooling batch crystallisation systems is based on open loop temperature control strategies, in which the system follows a pre-set temperature profile. Typically a linear cooling profile is used because of its simplicity. However, this often results in a poor CSD (Chew *et al*., 2007). So-called programmed cooling profiles are another option in which the temperature is decreased slowly at the beginning and at a faster rate towards the end of the batch to promote growth (Mullin, 2001; Jones, 1974). These simple approaches ignore any disturbances, as they are unable to respond to changes that occur in the system. This may result in a broad bi-modal CSD and batch to batch variability. Therefore developing monitoring and control approaches which can detect and react to disturbances and adapt to changing operating conditions can result in a significant improvement of the crystallisation process and product quality.

One of the most widespread methods for monitoring concentration during the crystallisation process is ATR-FTIR spectroscopy. ATR-UV/Vis spectroscopy, however can also be used as a cheaper alternative with more robust and faster calibration procedures. The main limitation of the ATR-UV/Vis spectroscopy is its applicability only to compounds with chromophoric groups (which absorb in the UV/Vis range). This is however fulfilled by the large proportion of pharmaceutical compounds that are chromophoric, making ATR-UV/Vis spectroscopy an excellent candidate for monitoring pharmaceutical crystallisation processes. Despite its potential advantages there is very little literature available on the application of ATR-UV/Vis spectroscopy in pharmaceutical crystallization. Some of the earliest studies were carried out by Anderson *et al*. (2000) and Thompson *et al*. (2005), and recently ATR-UV/Vis spectroscopy has been used as a monitoring and concentration measuring tool in the crystallisation of pharmaceuticals and inorganic compounds (Abu Bakar *et al*., 2009; Aamir *et al*., 2010). This is the first time that a feedback control approach, SSC, based on ATR-UV/Vis spectroscopy will be applied in a pharmaceutical crystallization process.

The current work also proposes a novel combined ADNC and SSC approach using ATR-UV/Vis spectroscopy and FBRM, based on the sequential application of the ADNC and SSC approaches with automatic switching between the two. The approach is applied for automated *in situ* seed generation. A comparison study is carried out using various operating modes and control strategies, including unseeded and seeded operating modes, with linear cooling, SSC, ADNC and ADNC-SSC approaches. The aim is to identify the advantages and disadvantages of each control strategy in terms of its ability to produce a narrow and uniform CSD, whilst remaining insensitive to variations in process conditions.

In the current work paracetamol (PCM) in IPA is used as a model system. The high solubility of PCM in IPA, slow growth and significant variations in the MSZW for primary and secondary nucleation events make it a challenging system to test the robustness of the various control strategies to obtain a desired CSD.

## 4.2 Methodology

### 4.2.1 Supersaturation Control Approach for Cooling Batch Crystallisation

In the supersaturation control approach, the system follows an operating curve in the phase diagram which generally corresponds to constant supersaturation. The feedback control requires concentration measurement, which in this work is obtained using ATR-UV/Vis spectroscopy used in conjunction with a suitable calibration model. The supersaturation is computed using the concentration measurement and the solubility information for the compound in the particular system. The solubility curve can be represented as any (nonlinear) function of the temperature $C_{sol} = C_{sol}(T)$. This function can be expressed by the van't Hoff solubility equations; however often simple empirical polynomial expressions are used. The solubility curve in this study was represented by a second-order polynomial fitted to experimental data:

$$C_{sol}(T) = a_2 T^2 + a_1 T + a_o \tag{4.1}$$

In the current study the absolute supersaturation ($S$) has been used, which is the difference between the solution concentration ($C$) and the equilibrium concentration (solubility) at a particular temperature, given by:

$$S = C - C_{sol} \tag{4.2}$$

Introducing equation (4.1) into (4.2) and setting the supersaturation equal to the desired setpoint supersaturation ($S_{set}$), allows the calculation of the temperature ($T_{set}$) required to achieve the target supersaturation, by simply solving the following generic nonlinear equation:

$$T_{set} = \underset{T}{\arg}\ (C - C_{sol}\ (T) - S_{set} = 0) \tag{4.3}$$

When the polynomial equation (4.1) is used for the solubility term, this reduces to the solution of a simple polynomial equation. The resulting temperature $T_{set}$ is tested to be within the physical limits for the process and is used as the setpoint for the lower level temperature control system.

The concentration is computed from the derivative of the absorbance at a characteristic wavelength for the compound corrected for the effect of the temperature, using the calibration model of the following form:

$$C = b_o + b_1\, d + b_2 T + b_3 dT \tag{4.4}$$

where $C$ is the concentration in (g/g solvent) and, $b_o$, $b_1$, $b_2$ and $b_3$ are the regression coefficients, $d$ is the derivative absorbance at the selected wavelength and $T$ is the process temperature (see Experimental Procedures section).

In this case, the temperature profile is a function of the measured concentration and the supersaturation setpoint. SSC is implemented using feedback control and requires a chemometrics-based calibration model, but it does not need extensive experimentation to obtain kinetic model parameters, such as growth and nucleation rate constants. A block diagram for the SSC approach is shown in Figure 4.1, while its operation in the phase diagram is shown in Figure 4.2.

If a slow growing system is used or the solid density is low, a supersaturation setpoint closer to solubility curve should be selected and maintained throughout the process as shown in Figure 4.2. The seed addition point is also critical. If the system is seeded at a higher supersaturation there is a possibility of nucleation in the system therefore it is preferred to seed the system at lower supersaturations. Solubility data, in the form of equation (4.1), for the specific system to be used are input to the software. Once the seeds have been added, or generated *in situ*, SSC can be started. The setpoint is selected or can be adjusted depending on the number of particles, or growth characteristics of the system. Concentration is continuously measured and fed to the supersaturation controller, which then sends a signal for temperature manipulation based on the process conditions and obtained from equation (4.3). In this way a constant supersaturation may

be maintained throughout the batch time. In practice, maximum and minimum temperature limits should also be specified to define the process boundaries, reflecting the operating range of the cooling / heating system.

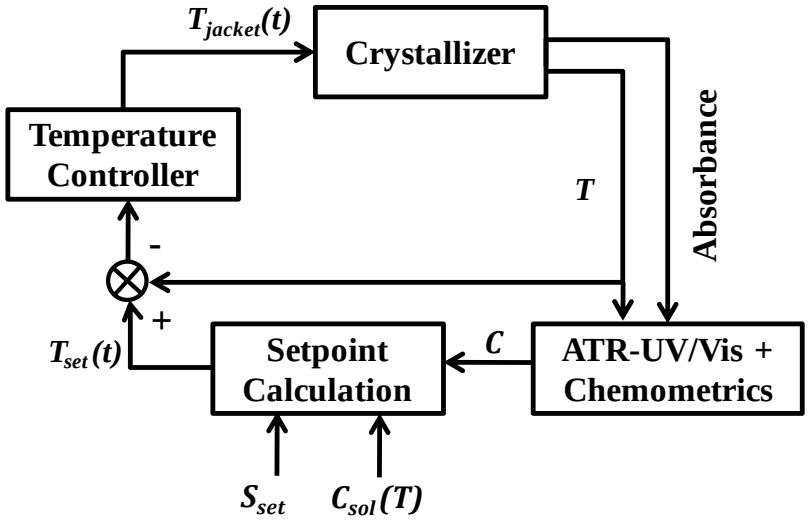



**Figure 4.1 Block diagram for the supersaturation control approach for batch cooling crystallisation processes**

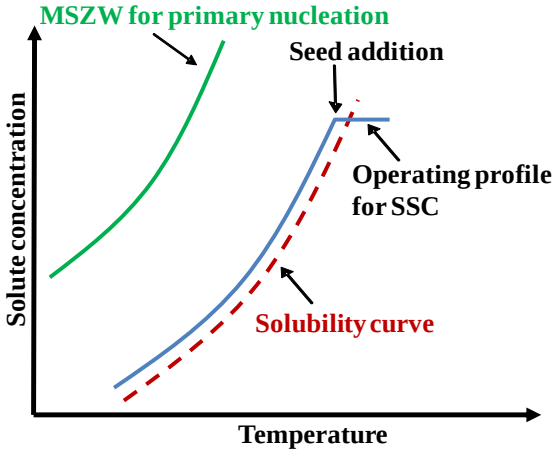



**Figure 4.2 Phase diagram showing a typical operating curve during supersaturation control**

### 4.2.2 Automated Direct Nucleation Control Approach (ADNC)

In the current work, a fully automated ADNC approach for controlling CSD is presented. This is a model-free feedback control approach, which makes use of FBRM to measure chord length

distributions, which can be related to the number and size of the particles present in the system. The chord lengths given by FBRM are grouped into 90 size bins from 0.8 – 1000 µm. From these raw data, weighted and un-weighted statistics may be calculated by the FBRM software; e.g., total counts/s is the number of chord length measurements for the whole size range. An increase in the total counts/s indicates nucleation or breakage in the system. The FBRM software also produces a SWMCL, which is sensitive towards the larger particles and can be used as a growth/agglomeration and average particle size indicator in the system (Abu Bakar *et al*., 2009).

The ADNC approach is based on the fact that a major source of variability in the CSD comes from primary and secondary nucleation events that occur in the system. *In situ* fines removal through heat addition can therefore help in improving the CSD by promoting the growth of bigger crystals and reducing the number of fines. This also eliminates the use of external heating loops in some crystallizer designs that are used for removing fines. A schematic block diagram for the ADNC approach is shown in Figure 4.3. The total counts/s measured by the FBRM are continuously sent to the nucleation controller, where they are compared against the target counts/s. The nucleation controller sends a signal to temperature controller which then varies the vessel jacket temperature accordingly. The operating profile is therefore based on the real time detection of nucleation and dissolution events in the process and does not follow a predetermined temperature profile.

A typical ADNC operating profile is shown in Figure 4.4. It is a well known fact that large variations exist in MSZW because of the presence of impurities and particles. If a control strategy based on keeping the operating curve within the meta-stable zone for primary nucleation does not detect changes in the MSZW this may result in secondary nucleation during the process, yielding a broad product CSD. The ADNC approach is based on feedback control based on the measurements related to variations in the number of particles in the system and hence is able to respond to any changes in the MSZW because of the presence of for example impurities, particles or crusting.

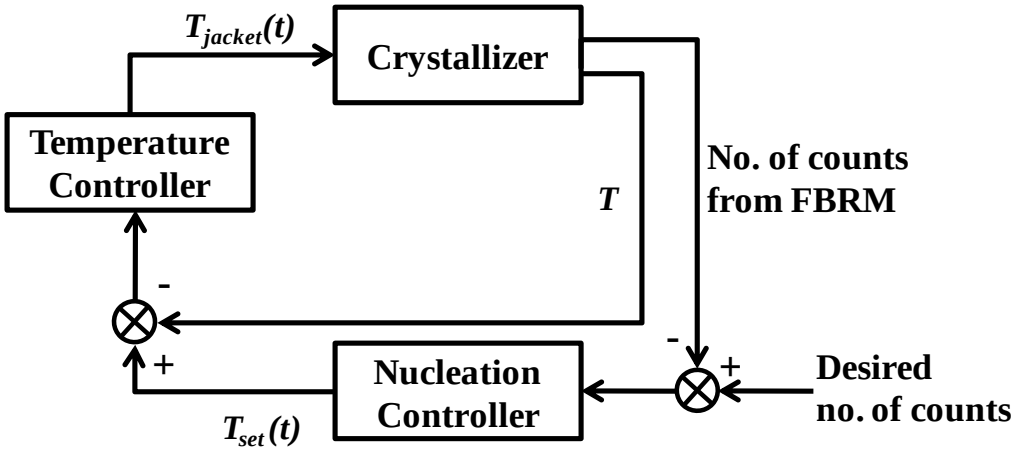



**Figure 4.3 Block diagram for the Direct Nucleation Control approach for batch cooling crystallisation**

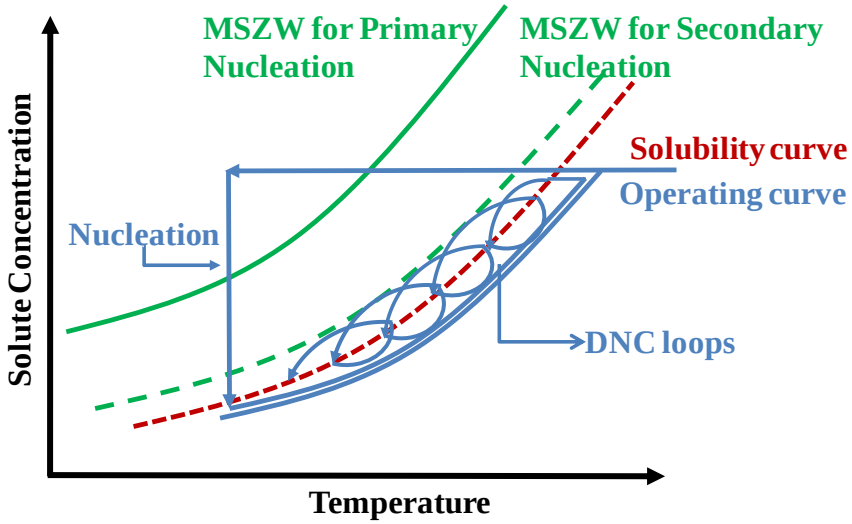



**Figure 4.4 Phase diagram indicating a typical operating profile in the case of direct nucleation control approach**

The continuous heating and cooling cycles remove fines and promote growth; in addition these cycles also help in preventing agglomeration and solvent inclusion in the crystals. Thus, in principle, ADNC can be used to obtain a narrow CSD of high purity products.

Figure 4.5 illustrates the feedback control approach for the ADNC approach used to maintain the total counts/s at its target value. In addition to the target setpoint, the method uses upper and

lower limits and proportional gains (i.e. $k_h$ and $k_c$) for the heating and cooling phases. When the counts/s fall between the lower and upper limits, proportional control is applied to the jacket temperature. When the counts/s fall outside these lower and upper limits then the heating and cooling is achieved following linear heating and cooling curves with predetermined slopes. The jacket temperature is set to the minimum and maximum values, whenever these limits are achieved. Thus, in Figure 4.5, initially the counts/s are below the lower limit and the temperature setpoint follows the predetermined fastest linear cooling profile. This should force nucleation, causing an increase in the counts/s. When the counts/s crosses the lower limit, the cooling rate is reduced. Typically, nucleation causes an overshoot and the counts/s exceed the target value; at that point the ADNC switches to heating rather than cooling and operates under proportional control. If the counts/s exceeds the upper limit, the heating rate is set to its maximum value. Fine particles are removed by dissolution and the counts/s returns towards its target value. Thus the controller requires specification of the setpoint or target number of counts/s, the upper limits for the heating and cooling rates, the minimum and maximum temperatures in the crystallizer and the adjustable $k_h$ and $k_c$ values.

From a clear solution, the ADNC process begins with cooling the system at a specified rate until the nucleation takes place and target counts are reached. During the process slow cooling (based on the $k_c$ value) starts once the counts have crossed the lower limit. Slow heating (based on $k_h$) will turn on if the number of counts is between the target counts and upper limit. Once the upper limit is crossed maximum heating mode will be switched on. The heating and cooling cycles will continue until the total counts have reached the target value.

The FBRM measurements are transmitted to the Crystallisation Process Informatics System (CryPRINS) software, in which the various crystallisation control approaches have been implemented. In the current work, ADNC using total counts/s as the target was implemented, but the software has the option of implementing ADNC using any other statistics.

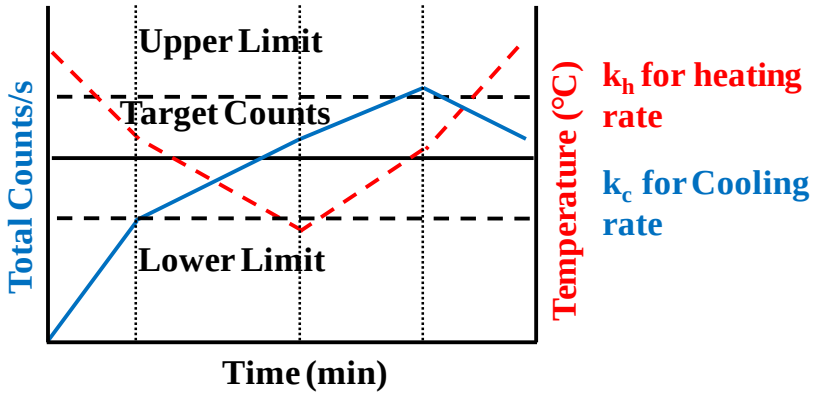



**Figure 4.5 Schematic representation of the working principle of the automated direct nucleation control (ADNC) approach**

## 4.3 Experimental Procedures

### 4.3.1 Materials and Instrumentation

The experiments were carried out using paracetamol (4-acetaminophenol, 98 % purity, purchased from Aldrich). The experimental setup described in chapter 2 was used here. ATR-UV/Vis spectroscopy was used for monitoring the liquid phase and implementation of SSC, while FBRM was used for monitoring phase and ADNC application.

### 4.3.2 Calibration Model Development

The details of calibration model development approach have been described in chapter 3. The same methodology was used here and the non-linear model was selected for determining the concentrations from ATR-UV/Vis spectroscopy data.

Spectra were recorded over a range of different concentrations and temperatures for undersaturated and supersaturated (single phase) solutions. A model using seven different concentrations (0.1106 to 0.1840 g/g) across a range of temperatures was built, using derivative spectra at 266 nm. The concentrations used are shown in a phase diagram in Figure 4.6.

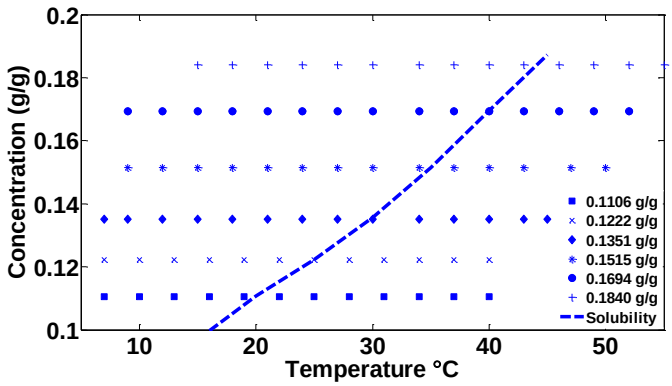



**Figure 4.6 Concentration and temperature points covered in the phase diagram**

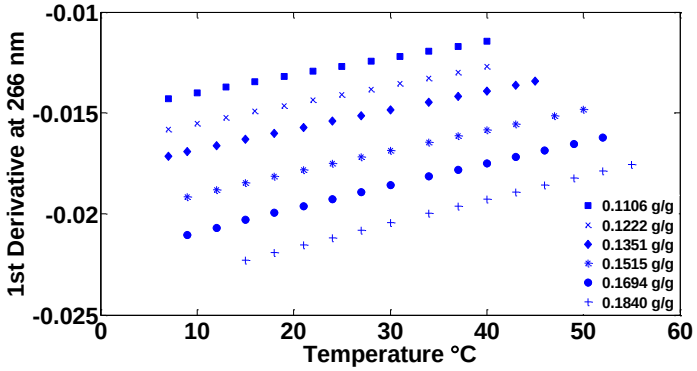



**Figure 4.7 1st derivative at 266 nm for various concentrations at different temperatures**

The nonlinear model as described in the previous chapter consisted of intercept term, derivative, temperature and interaction terms. The model parameters which were obtained from the calibration model were $b_o = -0.005$, $b_1 = -3.7889$, $b_2 = 0.0002$ and $b_3 = -0.0203$; the temperature was measured in °C and the first derivatives are in $nm^{-1}$. The root mean square error of prediction, calculated using this model was 0.0013 g/g, while maximum and minimum relative errors were 1.73 % and $-2.41$ %, respectively. In order to check the robustness of the model a separate calibration experiment was performed in which samples were withdrawn from the slurry in the vessel at different temperatures and checked by gravimetric analysis. The calibration model gave concentrations which were within $\pm 3$ % of the gravimetric analyses. The results obtained from gravimetric analysis were compared with the results obtained from the model and are shown in Figure 4.8.

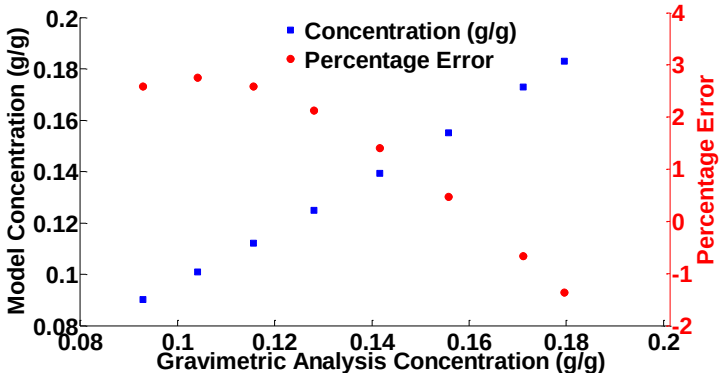



**Figure 4.8 Predicted concentrations plot against gravimetrically determined concentrations**

## 4.4 Results and Discussion

### 4.4.1 Unseeded Linear Cooling Crystallization Experiments

Table 4.1 summarizes the conditions for all the experiments carried out. Two unseeded linear cooling crystallization experiments were carried out to provide a base case and to check the maximum number of nuclei that could be generated by the system. A concentration of 0.206 g/g was used for both runs, with cooling rates of 0.5 °C/min and 0.05 °C/min. The results are shown in Figure 4.9.

For the fast cooling experiment the nucleation took place at a lower temperature, 5 °C and hence at a higher supersaturation, resulting in a greater number of total counts than for slow cooling. For the latter, as expected, nucleation took place at a higher temperature and a lower supersaturation, resulting in a smaller number of total counts. The SWMCL for both experiments is shown in Figure 4.10 (a) and (b).

**Table 4.1 Summary of the experimental conditions for all experiments**

| No. | Experiment | Heating /cooling rate (°C/min) | Amount of seeds (mass %) | SSC setpoint (g/g) | ADNC setpoint (Total counts/s) and bounds |
|---|---|---|---|---|---|
| 1 | Unseeded slow linear cooling | 0.05 | | | |
| 2 | Unseeded fast linear cooling | 0.5 | | | |
| 3 | Seeded linear cooling | | 5 | | |
| 4 | Programmed cooling | | 5 | | |
| 5 | SSC1 | | 5 | 0.010 | |
| 6 | SSC2 | | 5 | 0.012 | |
| 7 | SSC3 | | 10 | 0.010 | |
| 8 | ADNC1 | 0.2/0.4 | | | 8000 (±1000) |
| 9 | ADNC2 | 0.2/0.4 | | | 8000 (± 100) |
| 10 | ADNC3 | 0.2/0.4 | | | 4000 (±1000) |
| 11 | ADNC4 | 0.2/0.4 | | | 4000 (± 100) |
| 12 | ADNC5 | 0.2/0.2 | | | 4000 (± 100) |
| 13 | ADNC6 | 0.4/0.4 | | | 4000 (± 100) |
| 14 | ADNC-SSC1 | 0.2/0.4 | | 0.010 | 8000 (±1000) |
| 15 | ADNC-SSC2 | 0.2/0.4 | | 0.005 | 14000 (±1000) |

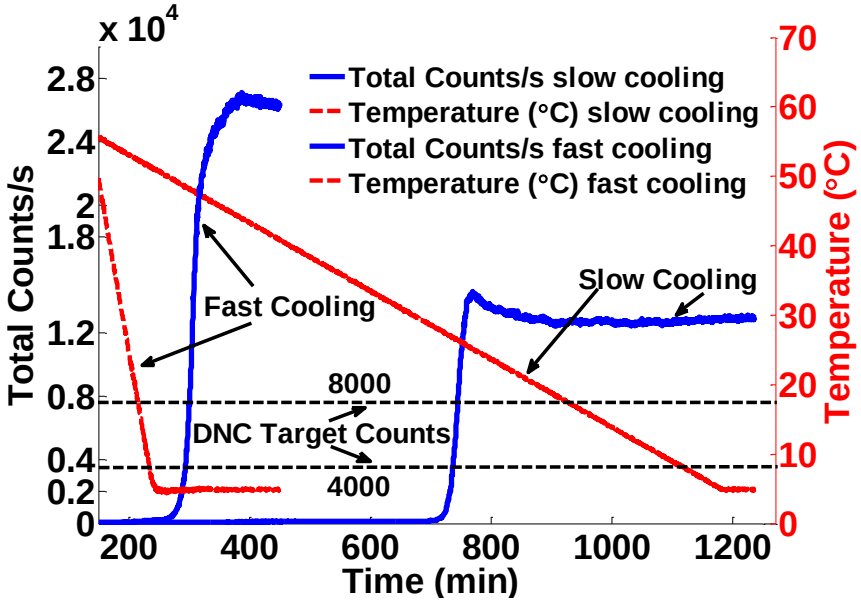



**Figure 4.9 Unseeded cooling crystallization experiments with slow and fast cooling rates. Slow run was selected for comparison with other approaches; ADNC target counts were also selected based on slow run**

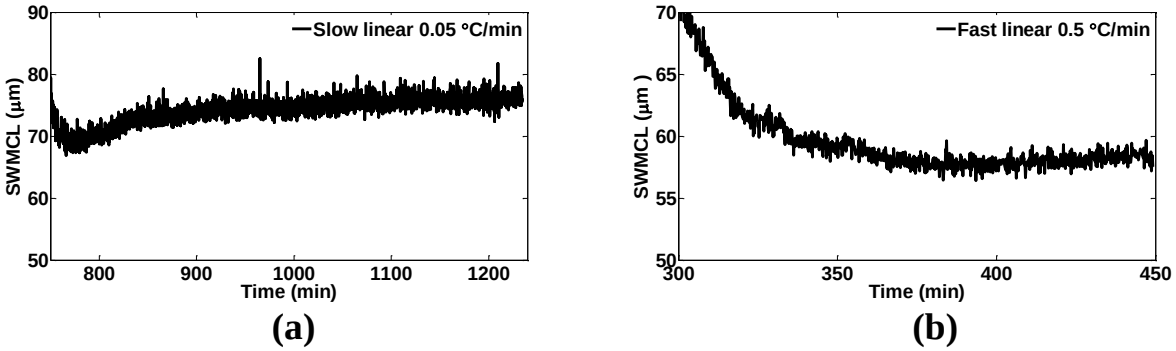



**Figure 4.10 SWMCL plots (a) slow cooling crystallization experiment (b) fast cooling crystallization experiment**

Clearly there is more growth during slow cooling experiment as fewer particles were generated. Based on these results, the unseeded slow cooling crystallization experiment was selected for comparison with other control strategies. For ADNC experiments target counts of 8000 and 4000, since they were well below the counts/s recorded for either of the unseeded cooling crystallization experiments.

### 4.4.2 Seeded Crystallisation Experiments using Linear Cooling or Supersaturation Control

The aim of the next stage of the study was to investigate the effect of different seed loadings and supersaturation setpoints on the final CSD using SSC. In all the experiments the saturation temperature was 50 °C (0.206 g/g) and seeds were added after cooling to 48 °C. Crystalline seeds in the size range of 125-185 µm obtained using sieve analysis were used in all these experiments, as they are less prone to agglomeration (Fujiwara *et al*., 2002). Three SSC experiments were carried out at with different seed loadings and supersaturation setpoints, details are given in Table 4.1.

Seeded crystallization experiments with linear and programmed cooling were also conducted for comparison (see Table 4.1). The duration of these experiments was based on SSC1 experiment, i.e. the time from seed addition till the process reached 5 °C (Figure 4.11). The programmed cooling profile (Figure 4.12) successfully suppressed nucleation until 350 minutes, contrary to

the linear cooling profile where a slow and steady increase in the counts was observed. In the case of the programmed cooling profile significant nucleation took place at about 25 °C. The system also nucleated during the linear cooling run but the magnitude was smaller than the former case. This is due to the fact that linear cooling generated a small but continuous nucleation during the entire process, and hence the supersaturation was kept at a lower value, whereas in the case of the programmed cooling the number of particles was constant until the onset of the sudden nucleation, which occurred at a higher supersaturation. The late nucleation event significantly affected the final CSD for programmed cooling profile, the size distribution in Figure 4.13 shows presence of higher number of fines. These results also indicate that the system is characterised by slow growth, which is not enough to use the increasing supersaturation as the cooling rate increases during the programmed cooling, leading to the significant secondary nucleation when the supersaturation exceeds a certain limit. Longer batch times would be needed to avoid secondary nucleation in this case. Based on this comparison, the linear cooling profile was selected for comparison with SSC and ADNC experiments.

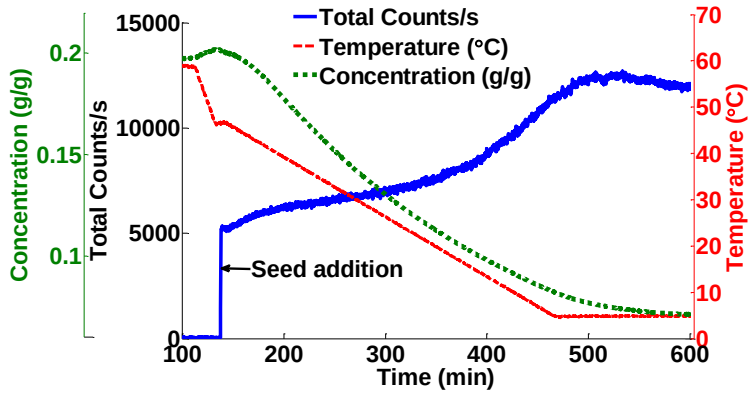



**Figure 4.11 Seeded crystallisation experiment with 5 % seed and linear cooling**

Total counts/s, temperature and concentration profiles for all SSC experiments are shown in Figure 4.14, Figure 4.15 and Figure 4.16. To demonstrate the control performance and show the ability of the system to keep the supersaturation at the desired level, a supersaturation plot for SSC1 is shown in Figure 4.17. The controller throughout the run managed to keep the supersaturation at the desired level; similar profiles were obtained for the other SSC runs, too.

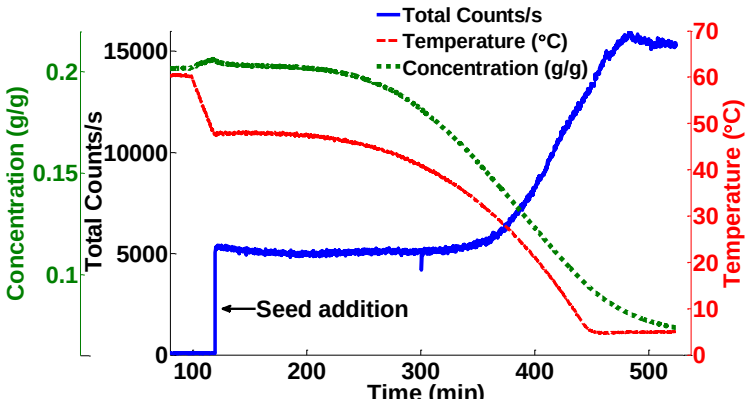



**Figure 4.12 Programmed cooling experiment with 5 % seed**

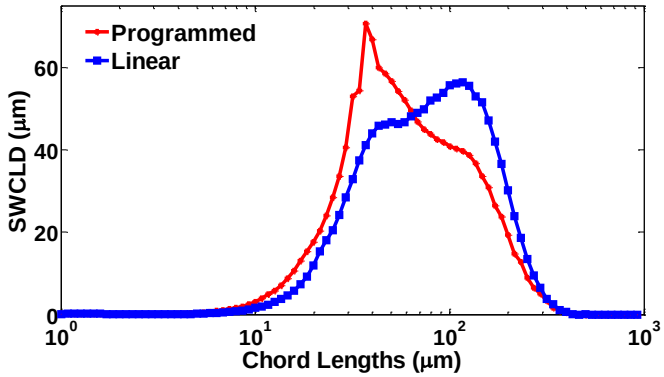



**Figure 4.13 Comparison of CSD for programmed and linear cooling profiles**

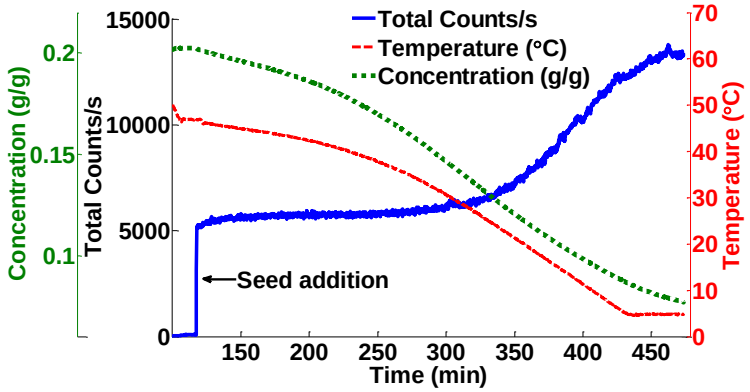



**Figure 4.14 SSC1 experiment with 5 % seed and 0.010 g/g as supersaturation setpoint**

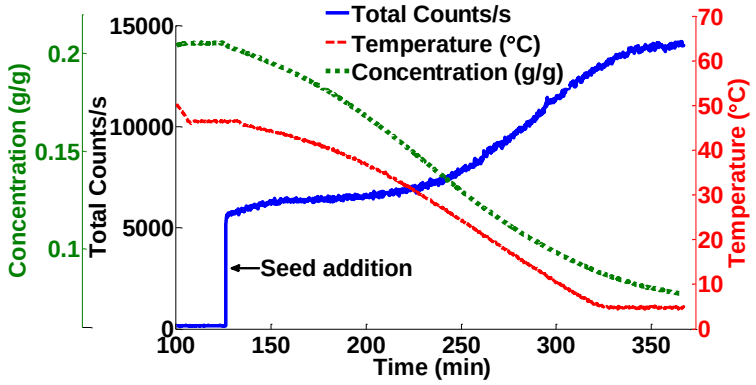



**Figure 4.15 SSC2 experiment with 5 % seed and 0.012 g/g as supersaturation setpoint**

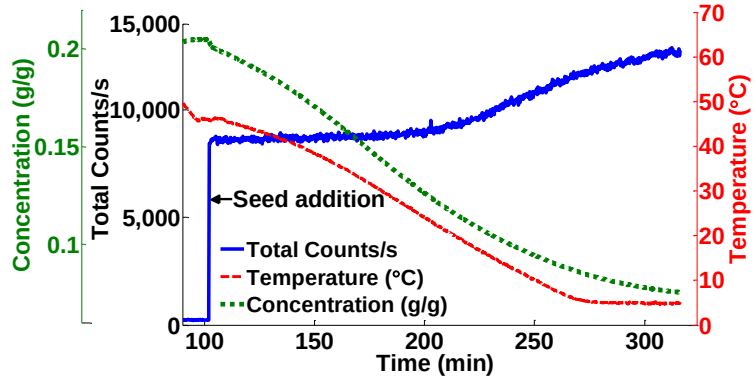



**Figure 4.16 SSC3 experiment with 10 % seed and 0.010 g/g as supersaturation setpoint**

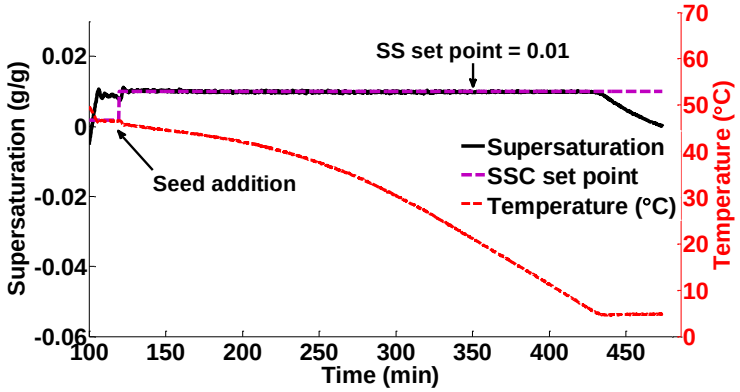



**Figure 4.17 Supersaturation profile for SSC1 experiment**

The temperature profiles are obtained automatically from the SSC, as the controller manipulates the temperature to maintain constant supersaturation. Compared to the linear cooling profile, the temperature decreases slowly for SSC1 and SSC2 experiments in the beginning. This slow

decrease in temperature can be related to slow consumption of supersaturation by the seed crystals. As the crystals grow and more surface area is available the temperature decreases faster to keep the supersaturation constant. However the slow growth of the particles ultimately resulted in significant secondary nucleation events for both SSC1 and SSC2 runs. In the SSC2 experiments higher supersaturation setpoint was used, which as expected, led to more significant nucleation, which started at an earlier stage of the batch than in the case of SSC1. When the concentration started to decrease due to the secondary nucleation event the SSC2 decreases the temperature even faster than SSC1, to try to keep a higher supersaturation, which in turn generates even more significant nucleation. The temperature was decreased rapidly after the nucleation event by the controller to maintain the supersaturation at the desired level.

To create more surface area to promote growth the amount of seed was doubled and another supersaturation control experiment was performed using the same, (lower) setpoint as for SSC1. This run (SSC3) resulted in a fast cooling profile since due to the larger number of particles the supersaturation generated was consumed rapidly. The amount of secondary nucleation was less in SSC3 compared to the other experiments. This is in correlation with other observations in the literature that indicate that the large number of crystals suppresses secondary nucleation (Doki *et al*., 2004), due to their higher surface area which promotes growth (Hojjati and Rohani, 2005).

Secondary nucleation affected the average particle size, as shown in Figure 4.18 (a), (b), (c) and (d). Only the data after nucleation is shown because of presence of noise when the solution was clear. In all the experiments the average particle size decreased after nucleation as more fines were generated in the system. As noted earlier SSC3 was less affected by nucleation events indicated by the smaller decrease in the SWMCL. The results suggest that the rate of secondary nucleation events dominated compared to the growth in this particular system. Paracetamol is a slow growing system, especially as the temperature is lowered while maintaining constant supersaturation. SWMCL plots also show that the average crystal size remained more or less between 100 - 110 μm for all the experiments, before nucleation took place, showing very little growth. This is in agreement with growth kinetic studies (Omar *et al*., 2008; Shekunov *et al*., 1996), which showed the growth velocity of crystal surface steps decreased as the temperature was lowered at constant supersaturation.

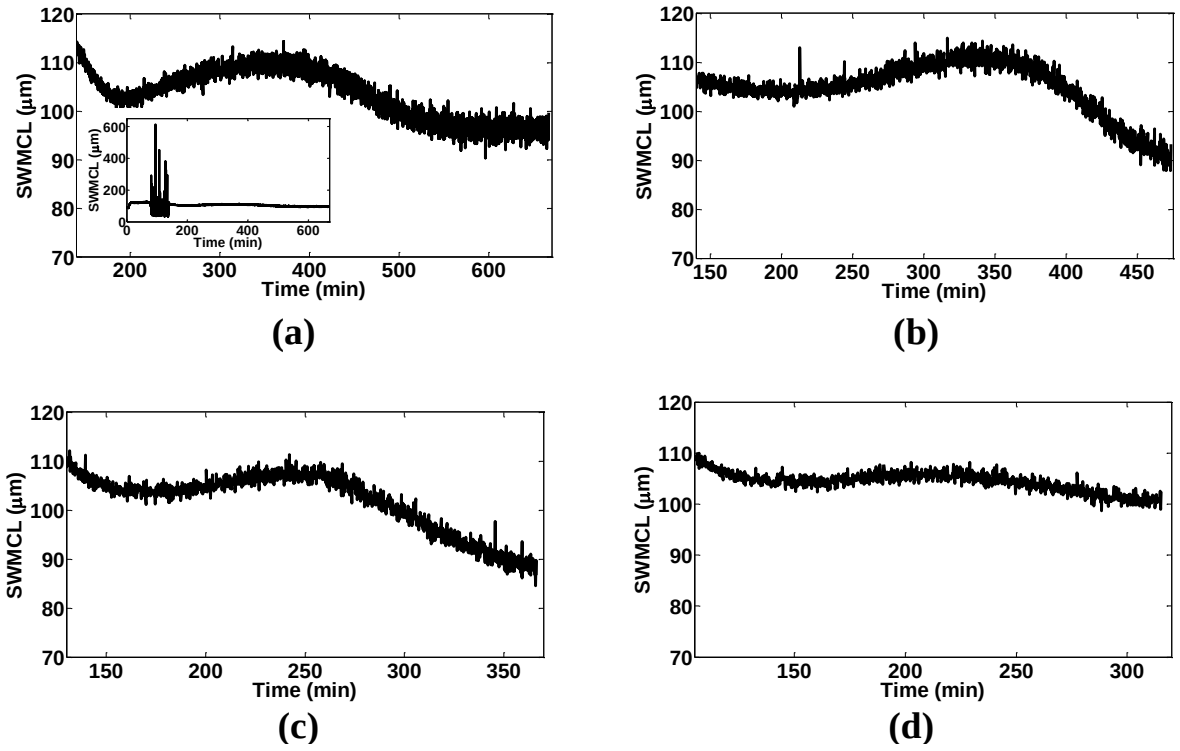



**Figure 4.18 SWMCL plots for seeded experiments (a) linear seeded crystallization (b) SSC1 (c) SSC2 (d) SSC3. The inset for linear seeded run shows high levels of noise in SWMCL when the solids are completely dissolved, hence only the SWMCL after nucleation is used for analysis.**

The comparison of the square weighted chord length distributions (SWCLD) indicate that a broader and bi-modal distribution was obtained (Figure 4.19) for linear cooling and the SSC experiments with the exception of SSC3, the uni-modal CSD for seeds is also shown. Bi-modality is obvious in case of linear cooling, SSC1 and SSC2, as in these cases significant nucleation occurred and hence large number of small particles was generated. In case of SSC3 although nucleation took place the number of new particles generated is less compared to the previously discussed profiles, hence bi-modality is not observed, except for a small shoulder on the CSD at smaller sizes. Similar results are indicated by Figure 4.18 (d), too, where the SWMCL for SSC3 run does not decrease significantly compared to the other profiles after nucleation. For ease of comparison the SWMCL will be referred as CSD from here onwards.

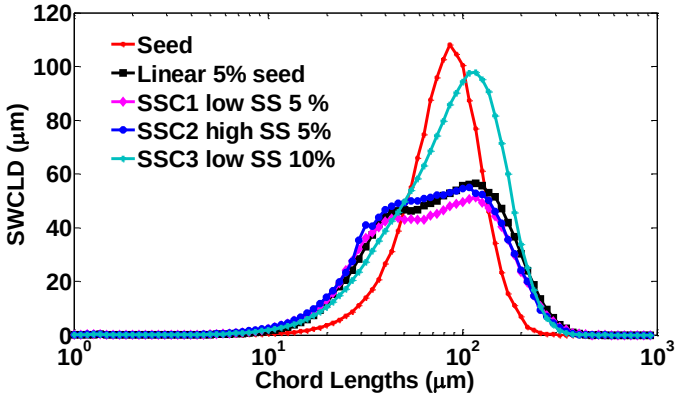



**Figure 4.19 Comparison of CSDs (at the end of the batches) for seeded cooling crystallization experiments. The CSD of the seed crystals used in all cases is also shown.**

### 4.4.3 Direct Nucleation Control Experiments

Six ADNC experiments were carried out with the aim to investigate the effects of different target counts/s, different upper and lower bounds and different heating/cooling rates on the control of the CSD. The details for these experiments are presented in Table 4.1.

In all ADNC experiments cooling was initiated after complete dissolution, resulting in significant primary nucleation; several heating and cooling cycles were required in each case before the counts stabilized around the target value.

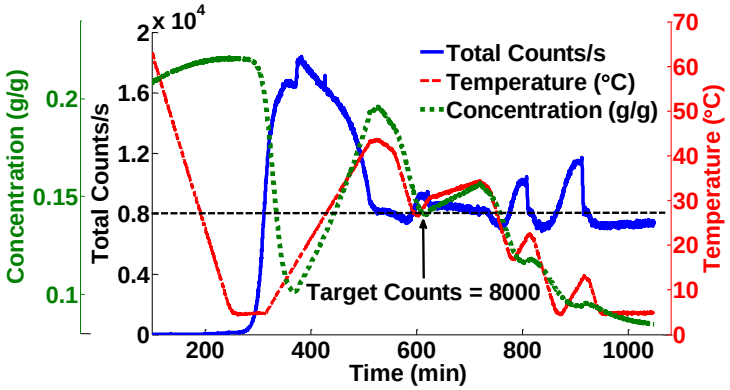



**Figure 4.20 ADNC1 with 8000 target counts and ±1000 limits**

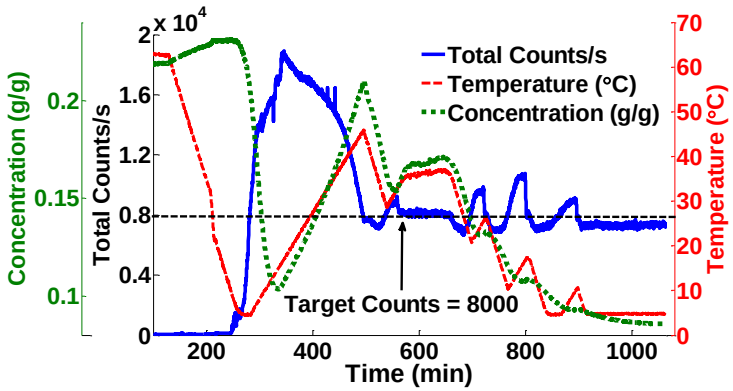



**Figure 4.21 ADNC2 with 8000 target counts and ±100 limits**

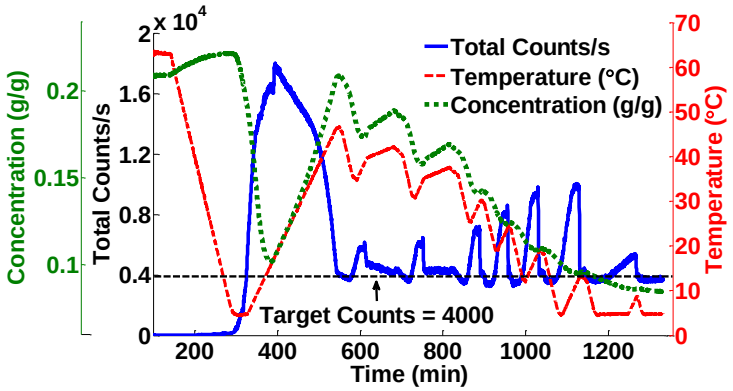



**Figure 4.22 ADNC3 with 4000 target counts and ±1000 limits**

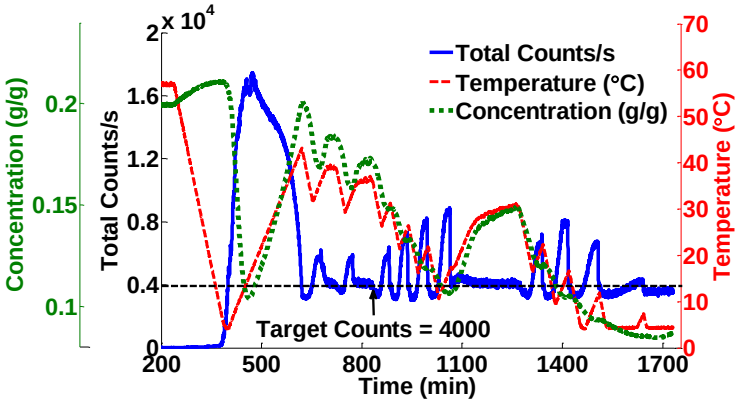



**Figure 4.23 ADNC4 with 4000 target counts and ±100 limits**

The difficulty in maintaining the counts at smaller target values can also be seen: the number of heating/cooling cycles doubled for the target of 4000 counts/s (Figure 4.22 and Figure 4.23) compared to 8000 counts/s (Figure 4.20 and Figure 4.21). This is understandable as the presence of a greater number of particles makes it more difficult for secondary nucleation to take place, as was observed in the case of SSC3. For both cases with narrow bounds, a greater number of heating/cooling cycles were required to maintain the system close to the target number of counts. Narrow bounds effectively produce on/off control where the heating and cooling phases switch between their maximum rates, producing overshoot in both the dissolution and nucleation events. The effect of narrow bounds is more pronounced in the case of 4000 target counts, where the largest number of heating/cooling cycles was required. The heating/cooling cycles for all ADNC experiments are shown in the phase diagrams on Figure 4.24 (a), (b), (c) and (d). Analysis of these figures helps in understanding the reduction of MSZW in the presence of particles and how ADNC adapts to this change in the MSZW.

In all four ADNC experiments the primary MSZW was approximately 45 °C and nucleation took place at about 5 °C. The very large primary nucleation zone generated very high initial supersaturation, leading to a very fast and significant nucleation. This has led to an overshoot of the target number of counts and the ADNC system switched to the heating stage. This first cooling and heating stage is indicated by the large cycles in the phase diagrams of all four experiments. Once the particles were generated, a significant reduction in MSZW was observed, as shown by the points joined together in Figure 4.24, which correspond to the all the secondary nucleation events representing the MSZW for secondary nucleation. In the second and subsequent cooling cycles particles were already present leading to nucleation much earlier and hence automatically switching to the heating stage. This leads to the smaller cycles in the phase diagram. These results demonstrate the main advantage of the ADNC approach, that it can detect any variations in MSZW and can change the operating conditions (heating or cooling rates) accordingly. This variation in the MSZW and ADNC's ability to adapt accordingly is evident in all the experiments. Additionally the ATR-UV/Vis spectroscopy ability to automatically determine the solubility curve is also shown. Starting from the slurry and slowly heating the system, the calibrated ATR-UV/Vis spectroscopy indicates the increase of the concentration with temperature in the suspension, which closely corresponds to the solubility curve of the system.

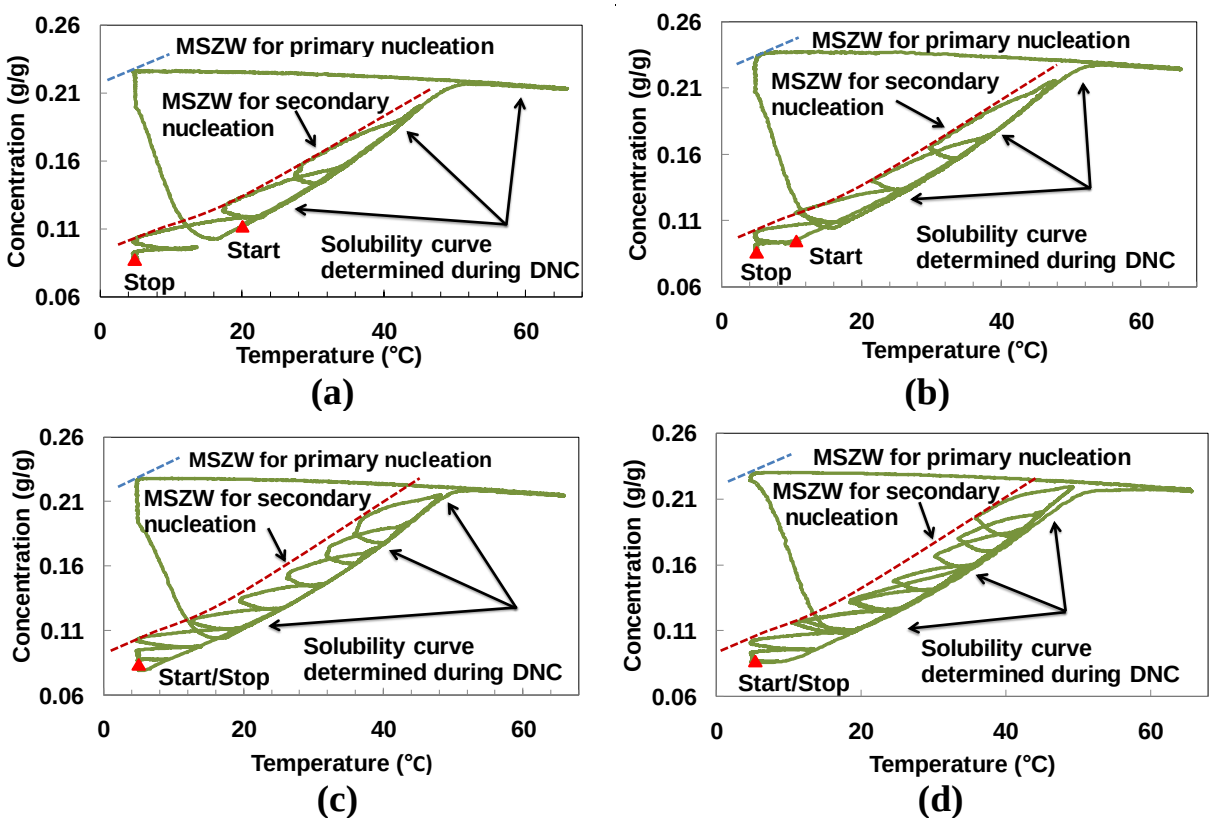



**Figure 4.24 Phase diagrams for direct nucleation control (ADNC) experiments (a) ADNC1 (b) ADNC2 (c) ADNC3 (d) ADNC4**

It has been seen in case of the seeded crystallizations and the SSC experiments that secondary nucleation events generated fines which adversely affected the final CSD. The evolutions of fine (<23 µm) and coarse particles (100-250 µm) in Figure 4.25 help in understanding the advantages of the ADNC approach. Fines are responsible for the broad CSD. ADNC works by dissolving fines and promoting growth of bigger particles. In Figure 4.25, for all ADNC runs, the first dissolution step after nucleation shows an increase in the number of coarse particles at the expense of fines. This increase in the number of coarse particles can be attributed to the size range used here i.e. 100-250 µm. As the temperature is increased the fines would dissolve while the bigger particles will reduce in size. The bigger particles undergoing dissolution were counted by the FBRM in the range used and the increase is coarse counts is thus the result of particles bigger than 250 µm undergoing dissolution. Heating/cooling cycles, which are used by the

ADNC approach, have been reported in literature as a method to improve the CSD by reducing the number of fines (Hojjati and Rohani, 2005; Bakar *et al*., 2009).

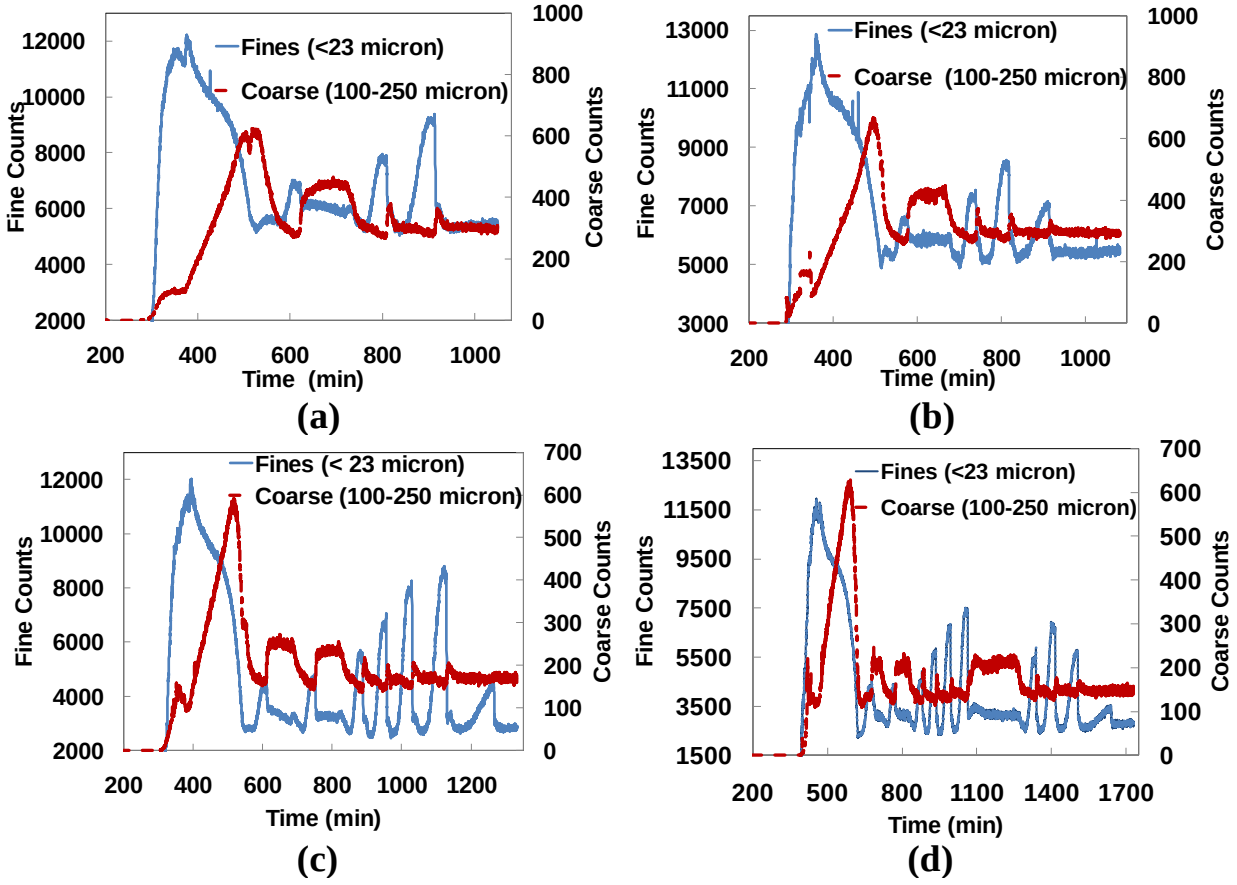



**Figure 4.25 Evolution of fine and course particles for ADNC experiments (a) ADNC1 (b) ADNC2 (c) ADNC3 (d) ADNC4**

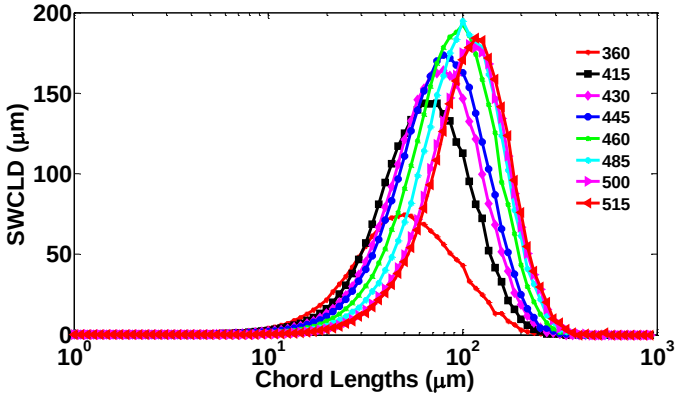



**Figure 4.26 Evolution of CSD during ADNC1. The time shown is in minutes.**

The CSD for ADNC1 at different times is shown in Figure 4.26. At approximately 360 minutes the CSD is shown just before the dissolution started as shown by the decreasing concentration in Figure 4.20. At 415 minutes the dissolution had started as shown by the increase in concentration. The subsequent CSDs apparently show growth of bigger crystals, which is in contrast to the dissolution of fines as both phenomenon cannot take place simultaneously as the temperature is increased. This shift in CSD towards the right side can be because of the "snowstorm effect" (Abu Bakar *et al*., 2010). This phenomenon takes place in the presence of large number of fine particles, which can hinder the FBRM ability to measure the large crystals. When the dissolution starts the number of fine particles is decreased and as a result more large particles are counted by the FBRM. In all ADNC experiments the number of fine particles was very large (always greater than 10000 counts/s), hence it is likely that the snowstorm effect is the cause of the shift in the CSD as the temperature was increased.

The same observation is illustrated by the SWMCL results for the ADNC experiments shown in Figure 4.27. The slight decrease in SWMCL at the time of dissolution events further supports the above argument, however, an overall increasing trend is seen in all cases. ADNC3 and ADNC4, which had the lowest target counts/s show the most growth. Continuous growth is observed throughout the process and as a result much larger crystals are obtained compared to the previously described approaches.

The SWMCL of 158 µm for the ADNC4 experiment is significantly more than the value of 77 µm obtained from the unseeded, slow linear cooling experiment. Furthermore, ADNC4 produced much larger crystals than were obtained in SSC3 (SWMCL of 101 µm). The SWMCL for the seeded SSC experiments started to decrease towards the end of the batch, because of late secondary nucleation event, the effect of which was seen as a bimodality in the CLD. Figure 4.28 shows a comparison of the CLD for the various ADNC and the SSC3 experiments. The ADNC results show mono-modal size distributions for all cases.

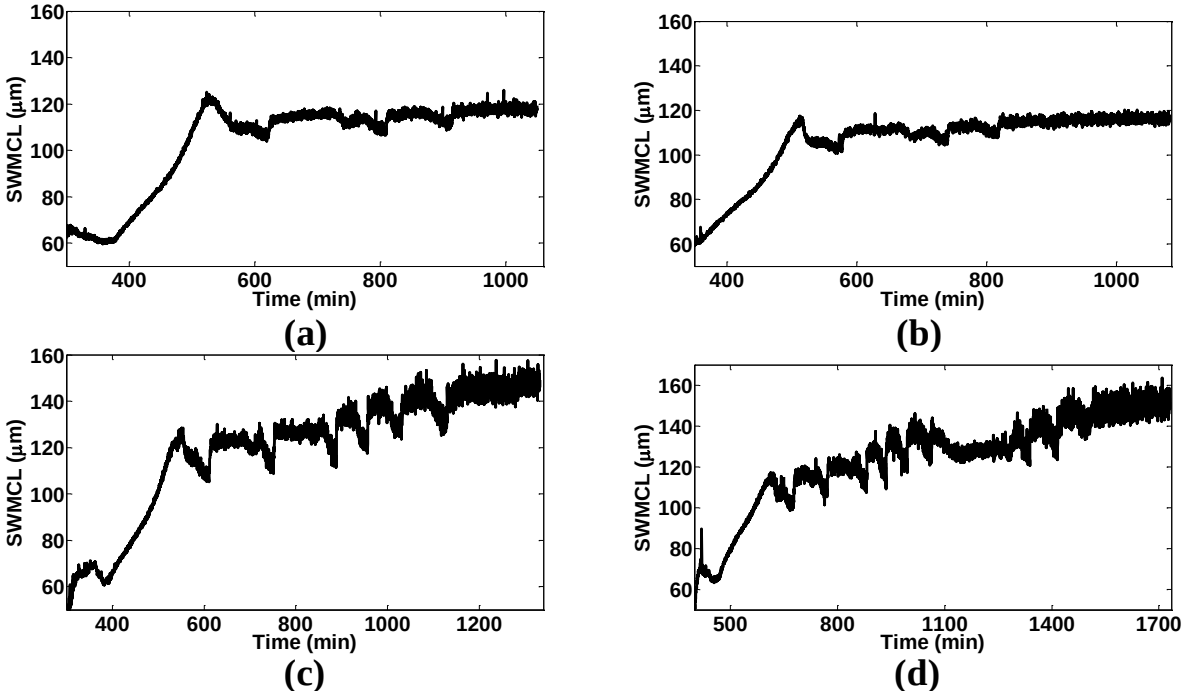



**Figure 4.27 SWMCL for ADNC experiments (a) ADNC1 (b) ADNC2 (c) ADNC3 (4) ADNC4**

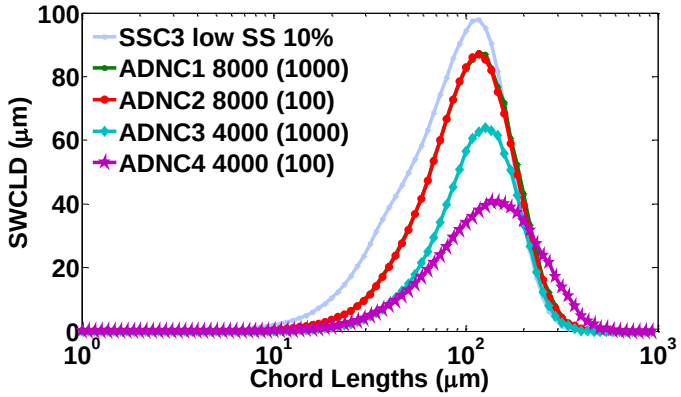



**Figure 4.28 CSD (at the end of the batches) comparison of ADNC experiments with SSC3, the setpoints for each ADNC run are shown in the bracket.**

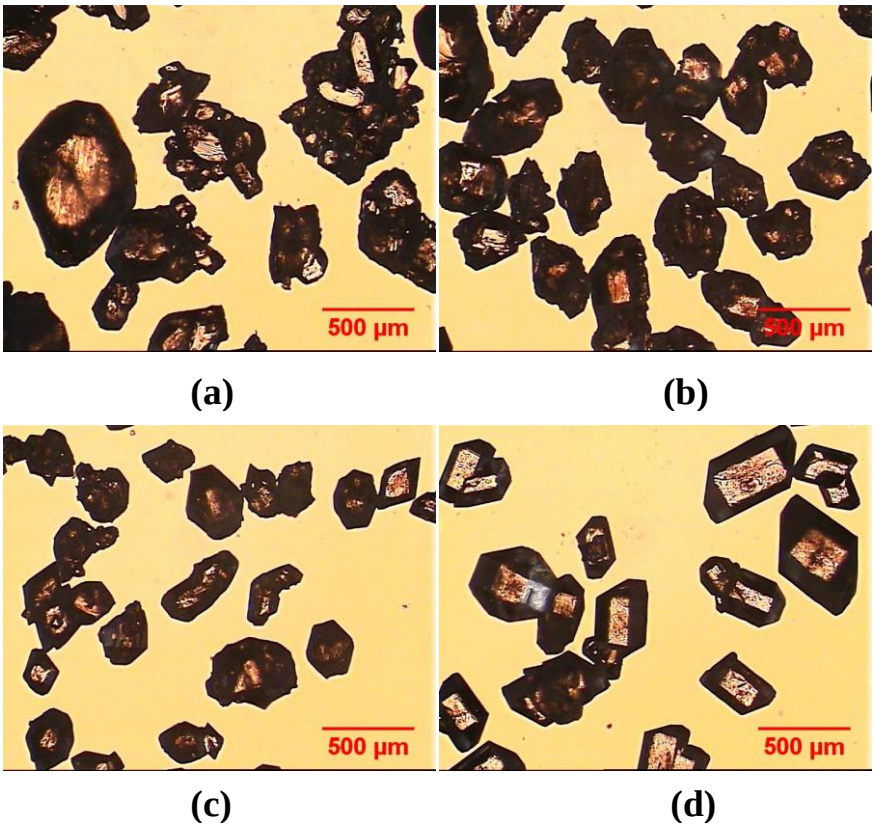



**Figure 4.29 Microscopic images of selected experiments for comparison (a) unseeded linear cooling experiment (b) seeded linear cooling experiment (c) SSC3 run (d) ADNC4**

The difference in the quality of crystals obtained is evident from the microscopic images of samples of the product obtained from each experiment, shown in Figure 4.29. The unseeded cooling crystallization produced a broad size distribution of agglomerated particles, as shown in Figure 4.29 (a). Some agglomeration is evident in Figure 4.29 (b) and (c) for the seeded linear cooling experiment, and SSC3. In contrast there is very little agglomeration seen for the ADNC4 experiment in Figure 4.29 (d) and the crystals are large with a narrow size distribution. In this last case, the continuous heating/cooling cycles in ADNC help in breaking any agglomerates that exist in the system, as well as preventing solvent inclusion between the crystals. Moreover, the crystals obtained from ADNC have well-defined shapes and sharp edges, indicating fewer defects on the crystal surfaces.

Two further ADNC experiments were carried out to evaluate the effect of different heating and cooling rates on the crystal product. In both cases the target counts were 4000 counts/s and the upper/lower limits were set at ±100 counts/s. The heating/cooling rates were 0.2 °C/min for

ADNC5 and 0.4 °C/min for the ADNC6 experiments. The results are shown in Figure 4.30 and Figure 4.31, respectively. Fewer heating/cooling cycles were required for ADNC5, which shows that this particular system is better controlled with slower heating/cooling rates, however, this may also depend on other factors such as the upper and lower bounds for the target counts/s. The greater number of cycles for ADNC6 also leads to longer batch times.

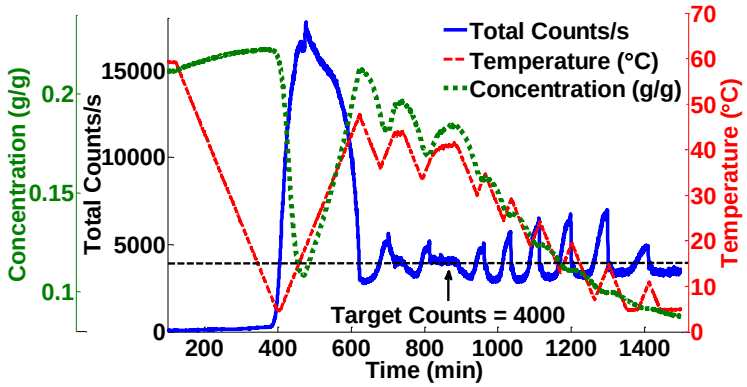



**Figure 4.30 ADNC5, heating/cooling rate 0.2 °C/min**

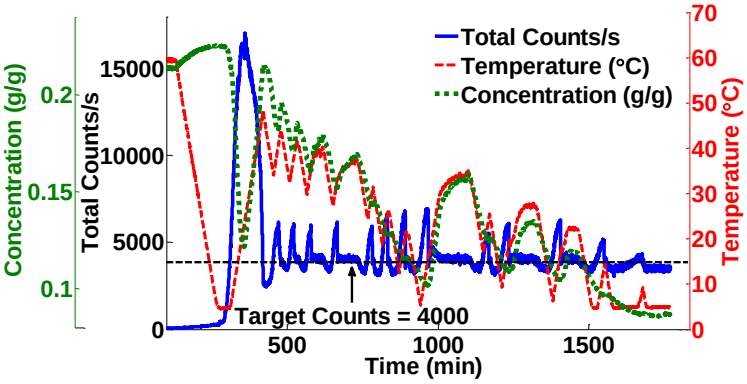



**Figure 4.31 ADNC6, heating/cooling rate 0.4 °C/min**

The phase diagrams for both runs in Figure 4.32 (a) and (b), show similar behaviour in terms of the MSZW variation and subsequent detection of secondary nucleation events by the ADNC approach. In both cases continuous growth of crystals was obtained, as was observed in the previous ADNC experiments (Figure 4.24). ADNC6 takes somewhat longer, but produces similar crystals, as expected since similar final counts were achieved. The yields in all experiments are similar and are fixed by using the same initial concentration and final temperature.

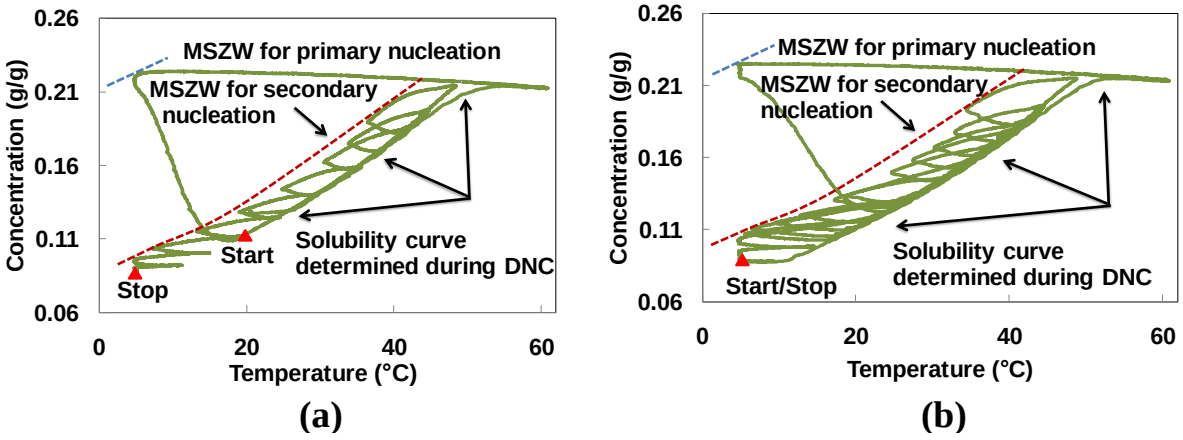



**Figure 4.32 Phase diagrams for (a) ADNC5 (b) ADNC6**

### 4.4.4 Combined ADNC and SSC Approach

So far the two control approaches, namely ADNC and SSC, have been applied independently. Both have their advantages and disadvantages. For example, the longer batch times and multiple heating/cooling cycles required in ADNC may not be feasible in some cases, especially at industrial or pilot plant scale, because of the slow dynamics of the heat transfer system. SSC on the other hand may result in secondary nucleation and smaller crystal sizes compared to ADNC as shown by the experimental results. For SSC, although a higher seed loading may partially or completely suppress the secondary nucleation, it is not always possible or feasible to seed the system. Furthermore variability in size distribution and quality of the seeds used can affect the final CSD (Aamir *et al*., 2010). To address these problems, in this section a combined ADNC and SSC approach is proposed which is based on the sequential application of the ADNC and SSC. ADNC is started first to create seed crystals by primary nucleation event (*in situ* seed generation), with the ADNC regulating the process to a desired number of counts/s, where it had been established that no further nucleation should occur. When the target number of counts/s has been achieved, the control is switched to the SSC to maintain the supersaturation constant throughout the remainder of batch time and hence to obtain crystals of the desired size and distribution. The approach is not limited to *in situ* seed generation and can be extended for external seed addition.

Two experiments with the combined approach were carried out, with the aim of obtaining larger crystals without any bimodality. For the first experiment (ADNC-SSC1), the target counts/s were 8000 (±1000), the heating rate was 0.2 °C/min, cooling rate was 0.4 °C/min and the supersaturation setpoint was at 0.01 g/g. For the second experiment (ADNC-SSC2), the target counts/s were 14000 (±1000), the heating rate was 0.2 °C/min, cooling rate was 0.4 °C/min and the supersaturation setpoint was 0.005 g/g. After initial dissolution, ADNC was turned on in both cases, and once the target counts were reached control was switched to SSC until the process reached the lower temperature limit of 5 °C. The operating profiles are shown in Figure 4.33 and Figure 4.34 for ADNC-SSC1 and ADNC-SSC2, respectively.

For ADNC-SSC1 a smaller number of particles were present, so the rate of generation of supersaturation was almost equal to the rate of consumption either by growth or secondary nucleation, resulting in almost a linear temperature profile. The presence of a smaller number of particles leads to secondary nucleation, similarly as it was shown in the previous experiments.

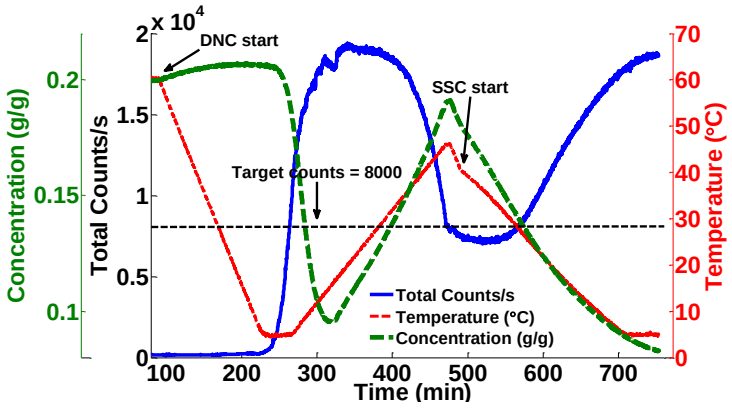



**Figure 4.33 ADNC-SSC1, target counts were 6000, supersaturation setpoint was 0.010 g/g**

The temperature profile resulted from the ADNC-SSC2 is significantly different. Although the supersaturation setpoint is smaller compared to the ADNC-SSC1 experiment, the presence of a large number of particles consume the supersaturation quickly, forcing the temperature to decrease at a higher rate. In both cases, the batch times are considerably shorter than for the ADNC runs.

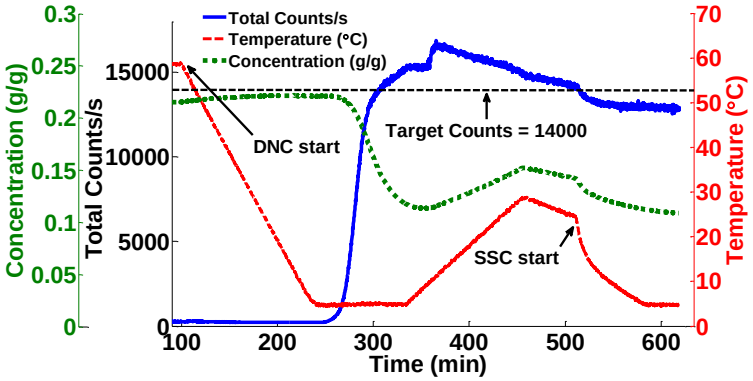



**Figure 4.34 ADNC-SSC2, target counts were 14000, supersaturation setpoint = 0.005 g/g**

Phase diagrams for both experiments are shown in Figure 4.35 (a) and (b) respectively. In both cases the primary nucleation happens at very high supersaturaion, leading to a fast decrease in concentration and steep increase in the number of counts/s. The target counts/s for the ADNC-SSC1 was 8000 counts/s, which is significantly lower than for the second experiment. This target was quickly exceeded by the increasing number of particles and hence the ADNC switched sooner to the heating stage. Furthermore, the temperature had to be raised significantly more than for ADNC-SSC2, to dissolve the excessive number of in situ generated particles, to achieve the low target count. This is indicated by the larger secondary loop in the phase diagram. After switching to SSC the controller was able to maintain the supersaturation at the required level throughout the process as shown in Figure 4.36, although significant nucleation took place.

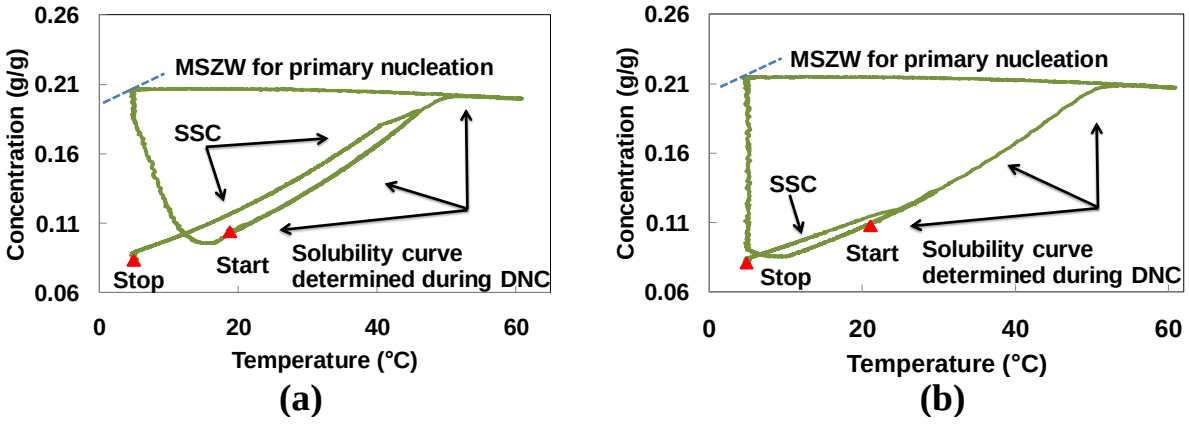



**Figure 4.35 Phase diagrams for (a) ADNC-SSC1 (b) ADNC-SSC2**

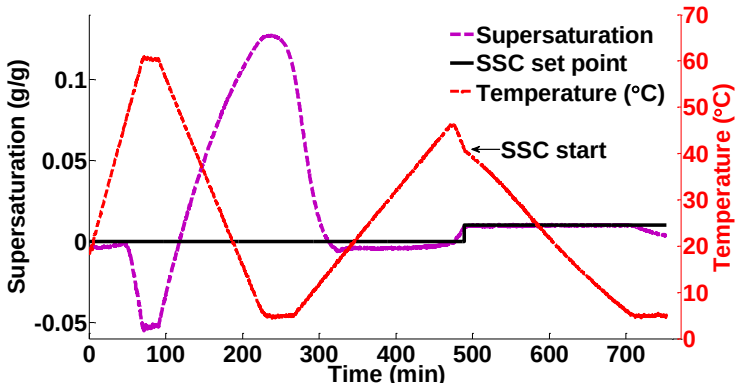



**Figure 4.36 Supersaturation profile for ADNC-SSC1 experiment, SS setpoint was 0.01 g/g**

For the ADNC-SSC2 nucleation took place at 5 °C and since the target counts/s was set at 14000, the decrease in concentration is significantly less than in the case of ADNC-SSC1 before the heating started, to generate the larger number of particles. To stabilize the system at the larger target number of counts, the heating phase stops at a lower temperature than for the ADNC-SSC1, and the approaches switches to the SSC. In this case also SSC is able to maintain supersaturation at the desired level throughout the process. Higher target counts and lower supersaturation setpoint were selected for the ADNC-SSC2 to suppress secondary nucleation event. Compared to the ADNC-SSC1 no nucleation took place in the case of ADNC-SSC2 because of presence of large number of particles and lower supersaturation setpoint during the SSC.

The SWCLDs for both experiments are shown in Figure 4.37. Bimodality is seen in the case of ADNC-SSC1, however, a uni-modal distribution is observed for ADNC-SSC2. For ADNC-SSC2 the distribution is shifted significantly more towards the right indicating the presence of larger crystals and less broader distribution than for ADNC-SSC1. This seem counterintuitive at first since the target counts/s for the initial seed generation was smaller for the ADNC-SSC1, suggesting that smaller number of seed particles were present in this case when the SSC started than in the case of the ADNC-SSC2. However, the subsequent significant secondary nucleation that occurred in the ADNC-SSC1 experiment increased the number of particles significantly above the particles present in the ADNC-SSC2 experiments, leading to the smaller SWCLD for the final product. During the ADNC-SSC2 experiment no secondary nucleation was observed resulting in more uniform crystals with larger mean size. Microscopic images of crystals obtained

from ADNC-SSC1 and ADNC-SSC2 are shown in Figure 4.38 (a) and Figure 4.38 (b). The crystals obtained from ADNC-SSC1 were smaller in size compared to that of ADNC-SSC2, the pictures are in correlation with the previous figures and show a better product quality using ADNC-SSC2. The batch time in both cases was significantly shorter than for the ADNC experiments but longer than the SSC experiments. There is a trade-off between batch time, crystal size and distribution, and any approach, or combination of approaches, will need to be tailored to the individual system and process requirements.

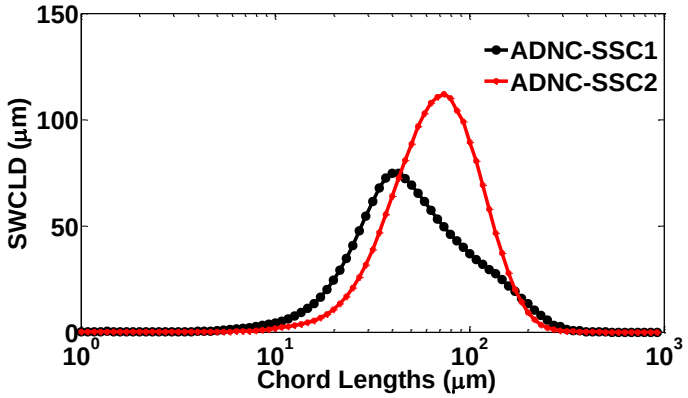
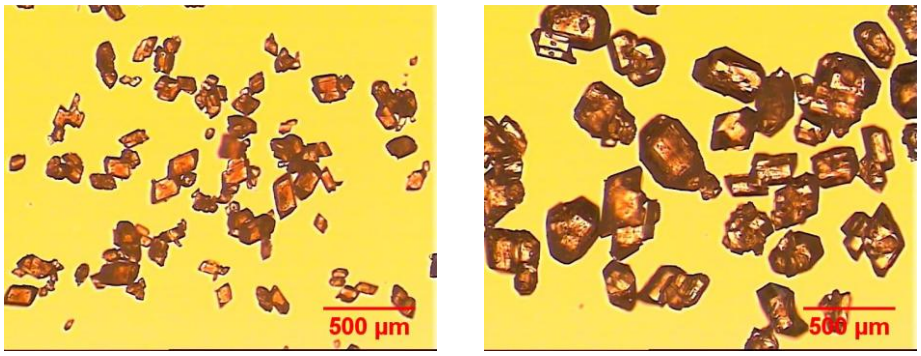



**Figure 4.37 CSD distributions for ADNC-SSC1 and ADNC-SSC2 experiments at the end of the batches**




**(a)** **(b)**

**Figure 4.38 Microscopic images of (a) ADNC-SSC1 (b) ADNC-SSC2**

## 4.5 Conclusions

Three control approaches, namely SSC, ADNC and ADNC-SSC using FBRM and ATR-UV/Vis spectroscopy were compared with each other and for the cases of seeded and unseeded cooling

crystallizations. Various statistics were used to assess the performance of each approach and it has been shown that the direct nucleation control approach, which requires no *a priori* information about the system, outperformed the other control strategies. For the paracetamol in isopropyl alcohol system, significant variations were found in the MSZW in the presence of crystals, which were responsible for the poor performance of control strategies other than the direct nucleation control approach.

The ADNC approach was able to detect any changes in the MSZW caused by the presence of particles or impurities. The phase diagrams automatically generated during these experiments helped in understanding why the ADNC approach is superior to the other approaches used. The main advantage of the ADNC is that continuous *in situ* removal of fines occurs during the heating stages, whereas the cooling stages help in the growth of bigger crystals. The largest crystals with uni-modal distribution were obtained with ADNC compared to other operating policies. The mean size of the crystals mainly depends on the target counts/s: a lower target counts/s resulted in larger crystals, but at the same time it was difficult to control the process and there was a need for more heating/cooling cycles, which resulted in longer batch times. The continuous heating/cooling cycles in ADNC also helped in de-agglomeration of the particles, resulting in reduced amounts of solvent inclusion. The crystals obtained had a well-defined shape, sharp edges and fewer surface defects.

Bimodal CSDs were observed for the SSC experiments and for the linear seeded experiments (the exception was SSC3 which used a higher seed loading). The SSC experiments showed how the seed loading can help in controlling or suppressing secondary nucleation events: runs with a higher seed loading gave the best results compared to the other seeded crystallization approaches. The ADNC approach has the disadvantage of longer batch times to accommodate the multiple heating/cooling cycles, whereas on the other hand the success of SSC largely depends on the seed loading and quality, any variation in the these two parameters can affect the final CSD. A hybrid approach of combining ADNC and SSC was used to address some of these issues. The batch times for ADNC-SSC were significantly shorter than for ADNC alone, but longer than simple SSC experiments. The mean crystal size obtained was smaller than with ADNC alone, but uni-modal CLD and larger crystals were obtained compared to when the SSC was used alone.

# Chapter 5 Assessment of Direct Nucleation Control Approach for Different Process Conditions during Cooling Crystallization

## 5.1 Introduction

During crystallization a variety of disturbances can take place. The majority of the typical control approaches in this case fail to bring the system back to the required state. Secondary nucleation is a frequently occurring phenomenon because of various reasons, including breakage and attrition, variations in MSZW and the presence of impurities. Other disturbances include formation of encrustation and its detachment (Briancon *et al*., 1997; Vendel and Rasmuson, 2000, Chianese *et al*., 1993). Encrustation is a naturally occurring undesirable process because of differences in the supersaturation at the wall and in the solution (Mersmann, 1988). There is a high probability of the crust detachment, causing secondary nucleation and leading to an undesired final CSD.

The current chapter is a continuation of the ADNC work presented in the previous chapter. Previously it was shown that ADNC gave superior results than SSC, programmed cooling or linear cooling. The main aim of this chapter is to test the robustness of ADNC approach when the system encounters different disturbances during the crystallization process. For comparison purposes, a disturbance free experiment from the previous chapter is selected. The results from several experiments running under ADNC in which different disturbances were introduced are then compared to assess the performance of this control approach. The experimental setup used was the same as described in chapter 3. The results obtained are as follows.

## 5.2 Results and Discussion

The performance of the ADNC approach was tested under various conditions, which included different seeding conditions to assess the effect of external seeding and *in situ* seed generation on the product quality. Details of all the experiments carried out are summarized in Table 5.1. The

solute (paracetamol in isopropanol) concentration in all experiments was 0.206 g/g. Details of the model used for concentration calculation have been previously described in chapter 3.

**Table 5.1 Summary of the experimental conditions**

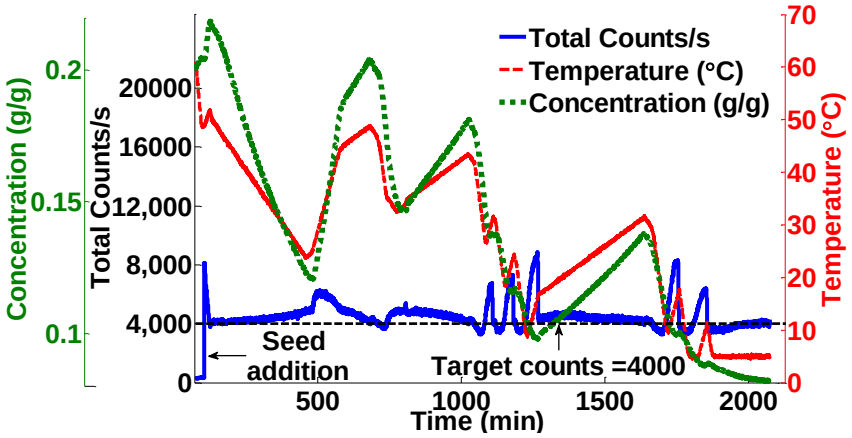
| No. | Experiment | Heating /cooling rate (°C/min) | Amount and type of seeds (mass %) | ADNC setpoint (Total counts/s) and bounds |
|---|---|---|---|---|
| 1 | Direct Nucleation Control run (ADNC4) | 0.2/0.4 | *In situ* seed generation | 4000 (±1000) |
| 2 | Seeded ADNC 1 (S-ADNC1) | 0.2/0.4 | 10 (crystalline) | 4000 (±1000) |
| 3 | Seeded ADNC 2 (S-ADNC2) | 0.2/0.4 | 5(crystalline) | 6000 (±1000) |
| 4 | Accidental seeding with ADNC 1 (AS-ADNC1) | 0.2/0.4 | 5 (crystalline) | 4000 (±1000) |
| 5 | Accidental seeding with ADNC 2 (AS-ADNC2) | 0.2/0.4 | 0.78 (powder) | 4000 (±1000) |

ADNC 4 was used as a bench mark to compare the performance of ADNC for different scenarios as mentioned in Table 5.1. Accidental seeding will be used to simulate the affects of breakage of crust and subsequent addition in the solution. For this purpose seeds of different sizes will be added to the system once the nucleation has taken place in the system. Two seeded ADNC experiments were also carried out to check the performance of ADNC for seeded systems.

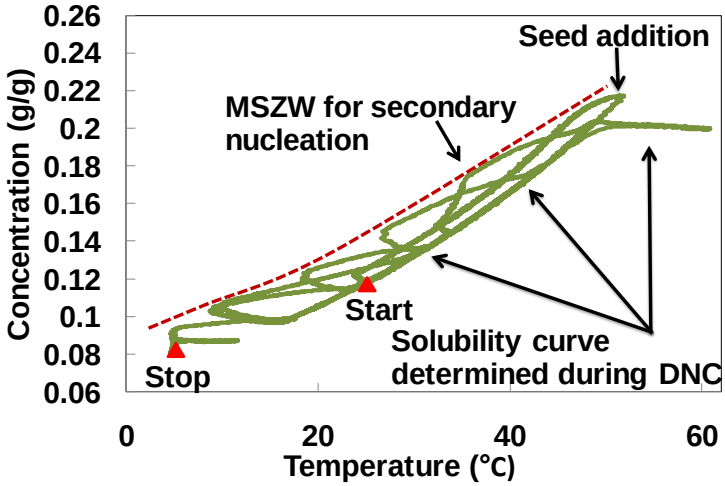
### 5.2.1 Seeded Direct Nucleation Control Experiments

A seeded experiment (S-ADNC1) was performed to check the performance of the ADNC in the case of external seeding. All the parameters such as target counts, upper and lower limits and heating/cooling rates were kept the same as in the ADNC4 experiment. After the initial dissolution the solution was cooled down to 48 °C i.e. just below the saturation temperature and 10 g of seeds were added. The seed addition is indicated by an increase in the FBRM counts to approximately 8000 in Figure 5.1 (a). The heating cycle was immediately started as the counts

crossed the upper limit. In this case, the control was able to bring the counts quickly to the setpoint. In the unseeded experiment ADNC4, nucleation occurred at a high supersaturation resulting in a rapid and significant increase in the number of counts/s, whereas in the case of experiment S-ADNC1, there is no nucleation occurring in the system as the seed is added at a low supersaturation and the number of particles is determined by the amount (and size) of seed particles added. During the S-ADNC1 experiment the counts for most of the time remained close to the target value, unlike in the case of the ADNC4 experiment where more oscillations in total counts were observed.




(a)




(b)

**Figure 5.1 (a) Total counts/s, concentration and temperature for S-ADNC1 (b) Phase diagram for S-ADNC1**

These results demonstrate that the most difficult part to control during crystallisation is the primary nucleation, when generally a very large number of small particles form suddenly. This sudden nucleation can induce more oscillations of the ADNC approach until stable counts are achieved, compared to the seeded operation when the system is never operated at a very high supersaturation. The phase diagram for the S-ADNC1 experiment (Figure 5.1 (b)) shows similar MSZW for the secondary nucleation as that of the ADNC4 experiment with the same target counts/s. This is expected since the secondary MSZW depends on the amount and properties of solids in the system. In both experiments similar number of seed particles with similar quality were used (both used crystalline seed, although for ADNC4 the seed was generated *in situ*). Figure 5.2 shows the variations in fine and coarse particles during the run, indicating that the number of larger particles were less susceptible to changes compared to the fines. The number of larger particles was affected more significantly only at higher temperature, while at lower temperatures no significant changes in their number took place.

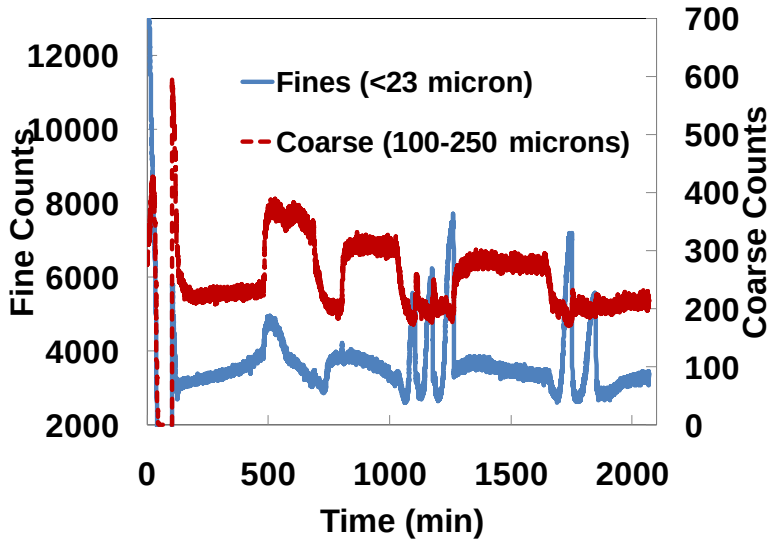



**Figure 5.2 Evolution of fine and coarse particles for S-ADNC1**

In the previous seeded experiment the main aim was to directly compare the performance of ADNC for internally generated and externally added seeds. Typically in seeded crystallization experiments it is expected that the added seeds will grow, suppress the secondary nucleation resulting in uni-modal CSD with minimum number of fines. Another seeded experiment was therefore performed in which the target counts were selected based on the total counts obtained

after the seed addition. The total counts, concentration and temperature profiles are shown in Figure 5.3 (a).

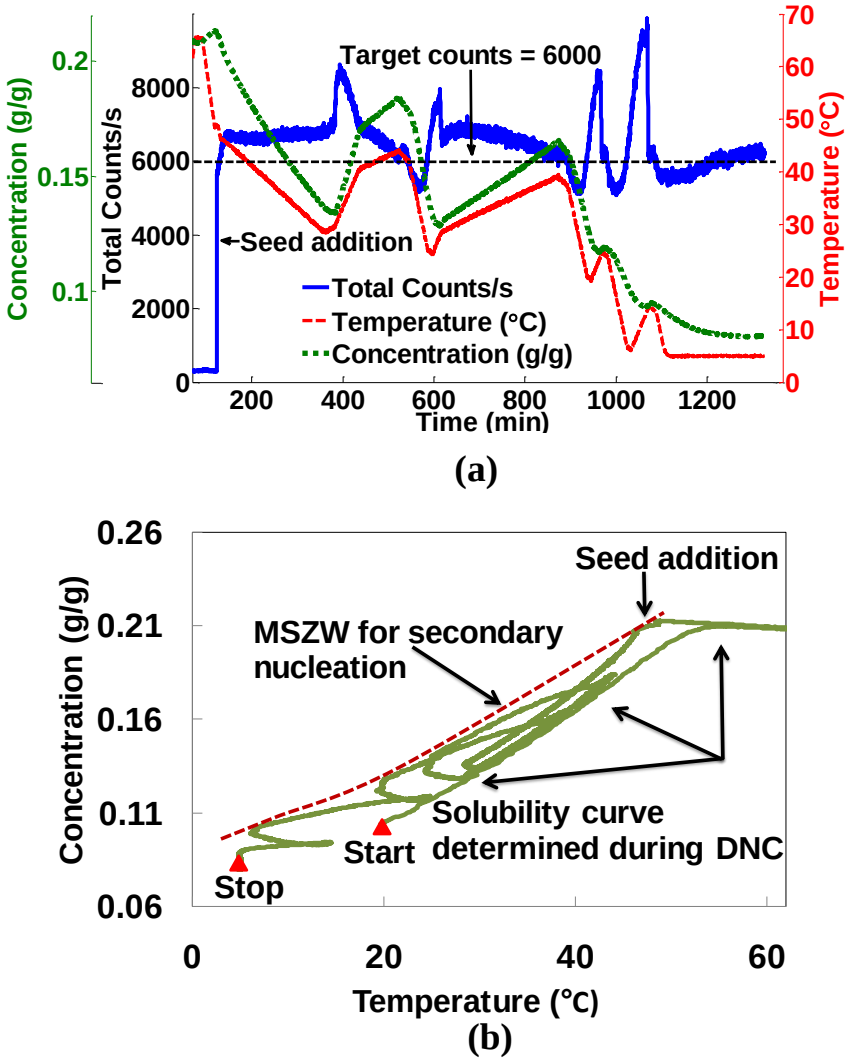



**Figure 5.3 (a) Total counts/s, concentration and temperature profile for S-ADNC2 (b) Phase diagram for S-ADNC2**

An amount of 5 g of crystalline seeds was added at 48 °C to the system. The maximum counts/s obtained were approximately 6500, based on which a setpoint of 6000 counts/s was selected. Since the upper and lower limits were ±1000 counts/s, therefore the controller switched to slow cooling mode after the addition of the seeds. The counts remained unchanged for a longer period of time during the beginning of the batch, however as the temperature was lowered, because of the slow growth of the system, nucleation took place when the supersaturation increased to a

critical limit. ADNC detected the secondary nucleation events and brought the counts back to the setpoint. Fewer heating/cooling cycles were required in this case as shown in Figure 5.3 (a). Figure 5.3 (b) shows similar reduction in MSZW as for the ADNC4 experiment. Smaller number of heating/cooling cycles can be explained as the presence of more particles suppresses secondary nucleation.

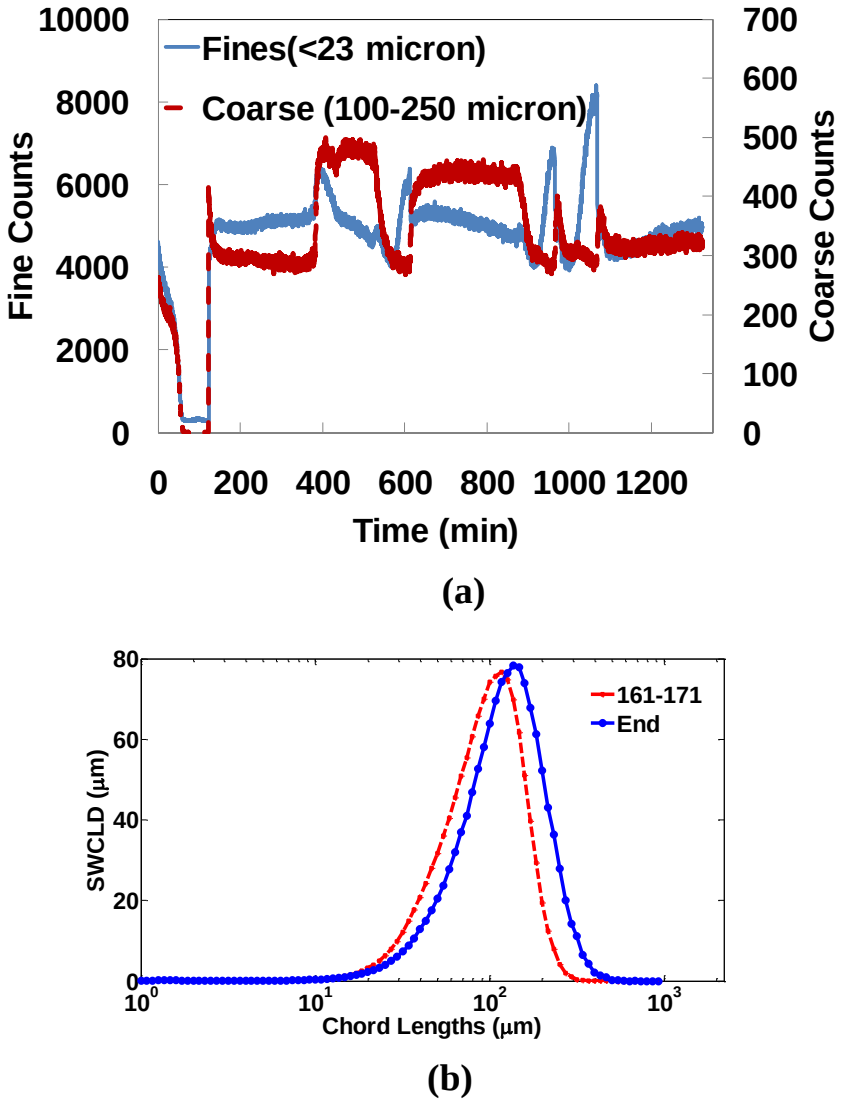


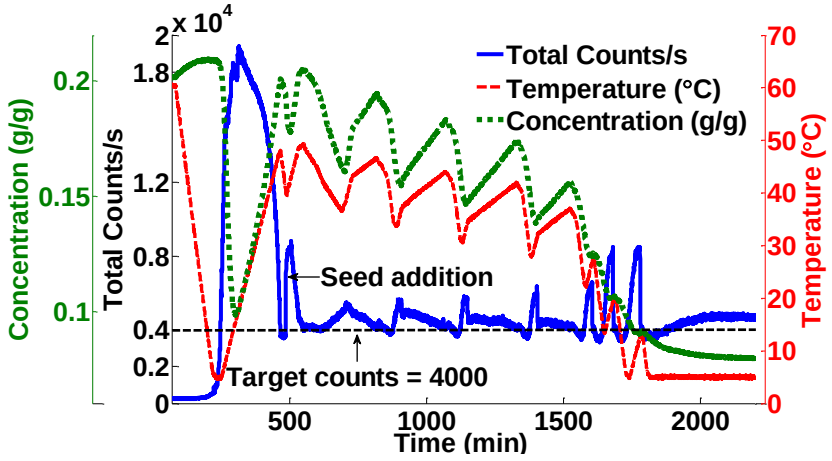

**Figure 5.4 (a) Evolution of fine and coarse particles for S-ADNC2 (b) Variation in CSD for S-ADNC2**

Fines and coarse counts plot in Figure 5.4 (a) shows similar behaviour as seen before. Very little change was seen in the coarse particles count, e.g. between 400-550 minutes the course count showed very little variations, whilst the fines were being dissolved; similar behaviour is seen during the subsequent heating/cooling cycles. CSD immediately after the seed addition and at the

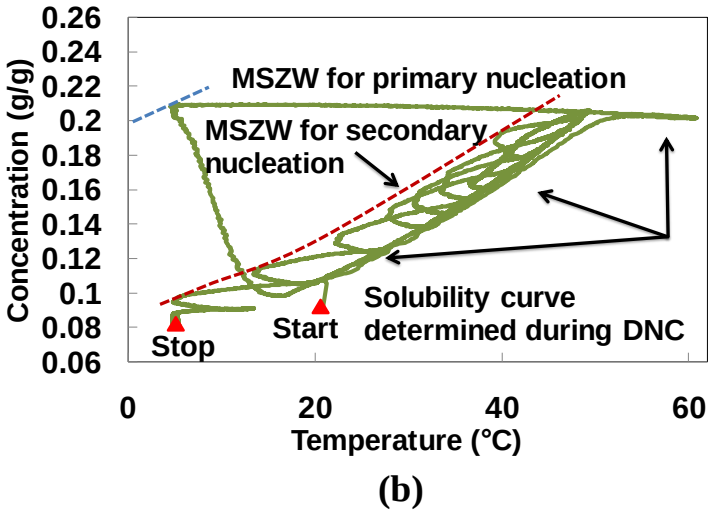
end of the run is shown in Figure 5.4 (b), despite the occurrence of several secondary nucleation events bigger crystals with unimodal distribution were obtained, showing that ADNC was able to eliminate the fines that were generated during the run.

### 5.2.2 Evaluation of Direct Nucleation Control in Case of Accidental Seeding

The main aim of these experiments was to test the ability of the ADNC approach, against accidental seeding, which is a common disturbance in industrial crystallisation systems generally caused by encrustation and subsequent detachment of solid particles.




(a)




(b)

**Figure 5.5 (a) Total counts/s, concentration and temperature profile for AS-ADNC1 (b) Phase diagram for AS-ADNC1**

Two experiments were performed with the conditions specified in Table 5.1. Target counts in both cases were set to 4000 so that a direct comparison of the performances with ADNC4 and seeded ADNC experiments is possible.

In the first run (AS-ADNC1) crystalline seeds were added as a disturbance. After the initial dissolution and nucleation (Figure 5.5 (a)), heating was started until the setpoint counts of 4000/s was reached, once the counts were stabilized 5 g of crystalline seeds were added as a disturbance.

The disturbance was corrected by the controller by increasing the temperature. The effect of correction can be seen as an increase in concentration because of the dissolution. Several heating/cooling cycles were needed as shown in Figure 5.5 (a) and (b) before the counts stabilized just above the setpoint at 5 °C. The phase diagram (Figure 5.5 (b)) is similar to the phase diagrams of the previous runs, indicating the adaptive dissolution cycles characteristic to the ADNC approach.

The variation in CSD before and after the moment of the simulated accidental seeding is shown in Figure 5.6 (b). The addition of seeds caused a significant change in the CSD, resulting in a much broader distribution. The first heating/cooling cycle after the seed addition started shifting the CSD towards the right, i.e. the added disturbance was being corrected accompanied by growth of the crystals. As a result of this, a CSD with bigger crystals was obtained in the end.

The plot of fines and coarse particles in Figure 5.6 (a) gives information about the nature of the disturbance in terms of the size range of particles. At the seed addition the number of course particles increased more significantly than for the fines, indicating that the particles were relatively large in size. This is expected since in this experiment crystalline seed was added. After the heating/cooling cycle which corrected the disturbance, the number of coarse particles stabilized at a value higher than the value before the disturbance also indicating that particles similar to the ones already present in the solution were added as part of the disturbance. After the correction a proportion of these particles was dissolved. The number of fine particles decreased to the same level, this is also evident from Figure 5.6 (b) where the shift in distribution indicates that particles contributing to the fines were gradually eliminated from the suspension.

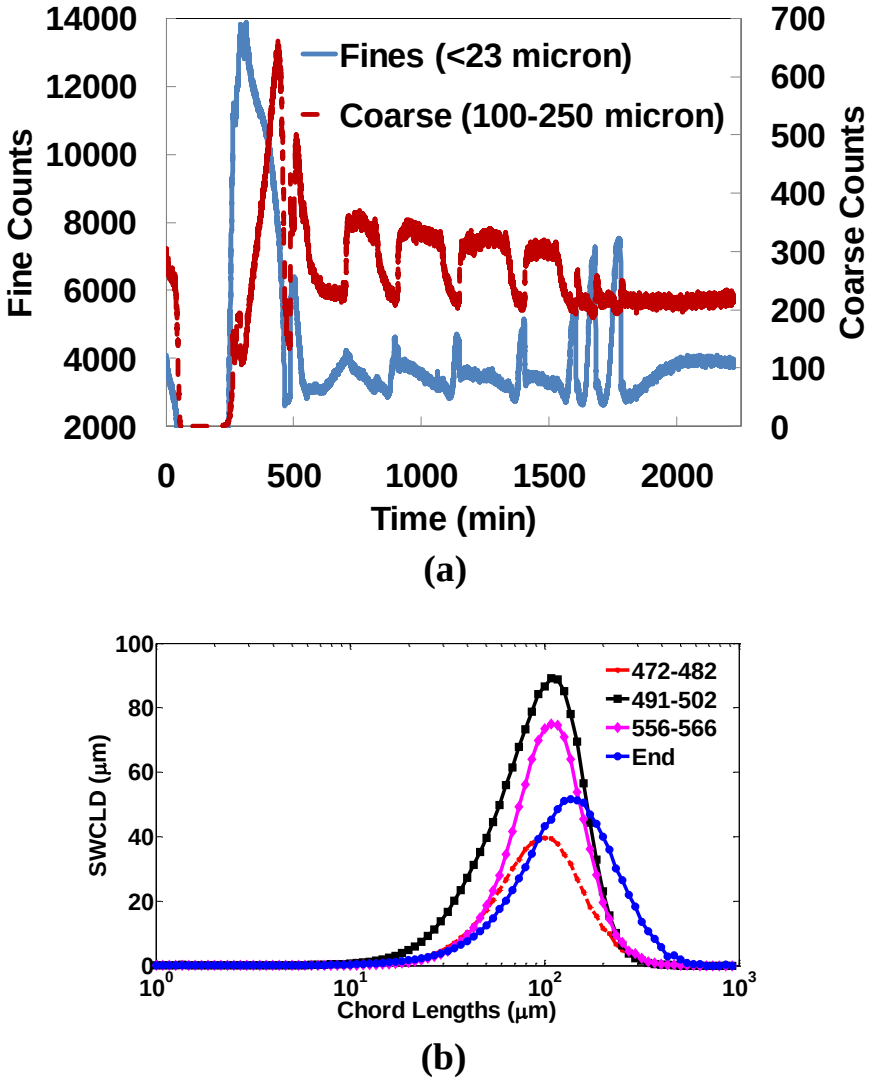
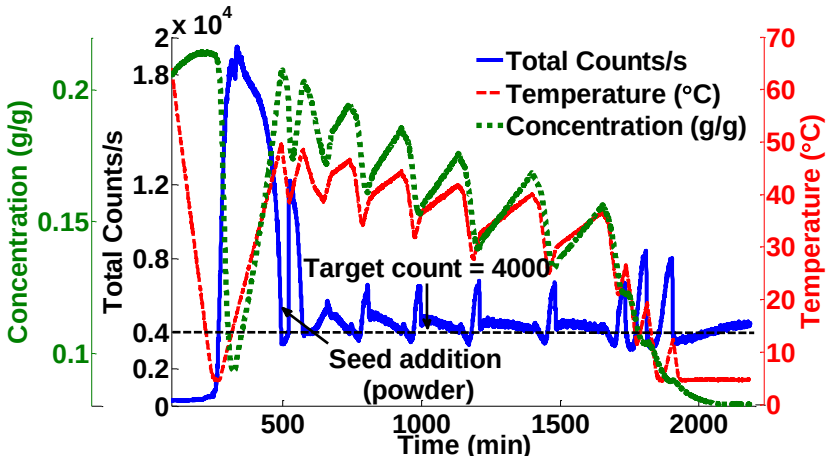
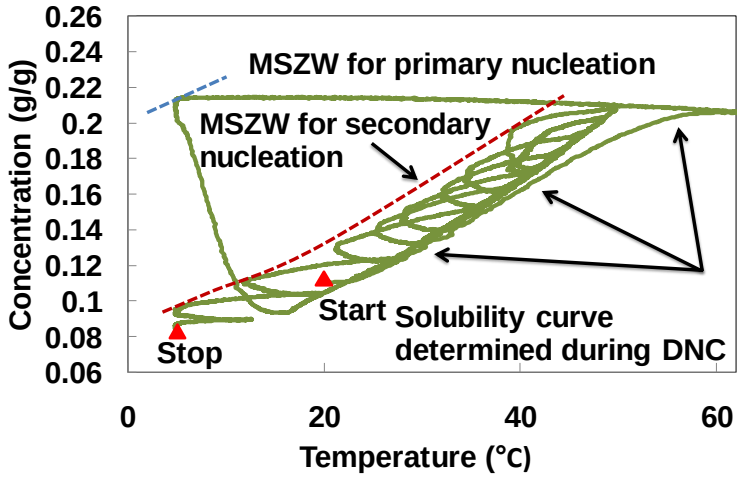



**Figure 5.6 (a) Evolution of fine and coarse particles for AS-ADNC1 (b) Variation in CSD for AS-ADNC1, 472-482 min CSD prior to seed addition, 491-502 min CSD immediately after seed addition, 556-566 min CSD after the correction, end of the experiment**

For the second accidental seeding experiment (AS-ADNC2) raw material in the form of powder was added as disturbance. The powder was added once the counts had reached the setpoint counts (4000 counts/s) after the first correction (Figure 5.7 (a)). Because of the very fine nature of the powder only 0.78 g was added which resulted in an increase in counts from 4000 to about 12000 counts/s.




(a)




(b)

**Figure 5.7 (a) Total counts/s, concentration and temperature profile for AS-ADNC2 (b) Phase diagram for AS-ADNC2**

The variation in CSD before and after the powder addition is shown in Figure 5.8 (b), which indicates that the majority of the particles were smaller than the already present crystals in the solution. After the ADNC correction the distribution became closer to the CSD from before the powder addition. Fine and coarse counts plot in Figure 5.8 (a) also show similar behaviour as the number of fines was brought closer to the previous counts. The evolution of larger crystals and the phase diagram (Figure 5.7 (b)) obtained were similar as seen before for the previous runs. The variation in CSD at different times is shown in Figure 5.8 (b), where gradually the disturbance is eliminated and final product with bigger crystals is obtained.

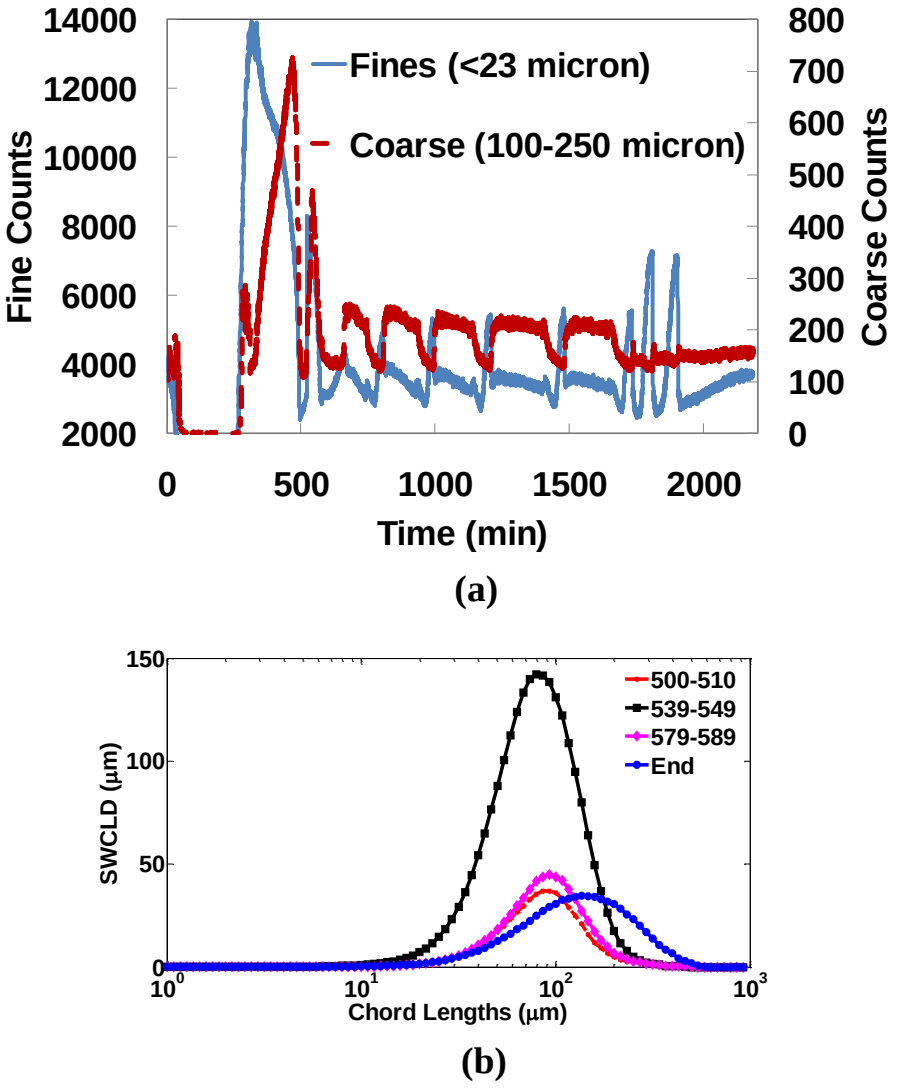



**Figure 5.8 (a) Evolution of fine and coarse particles for AS-ADNC2. (b) Variation in CSD for AS-ADNC2, 500-510 min CSD prior to seed addition, 539-549 min CSD immediately after seed addition, 579-589 min CSD after the correction, end of the experiment**

A comparison of the final CSDs of all the runs is shown in Figure 5.9. ADNC4 and AS-ADNC2 are very similar to each other as the disturbance in case of AS-ADNC2 consisted of very fine particles and was eliminated quickly from the solution, a very similar evolution of SWMCL can be seen for both cases as shown in Figure 5.10 (a) and Figure 5.10 (e). CSD for S-ADNC2 was expected to be different as the setpoint counts were different from the other runs. The SWMCL for this run, shown in Figure 5.10 (c) indicates that the presence of greater number of particles resulted in crystals relatively smaller than the other runs.

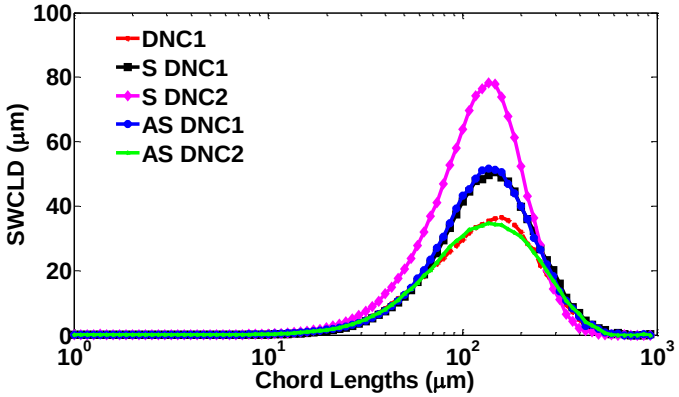



**Figure 5.9 Comparison of CSD (at the end of the batches) of all the experiments**

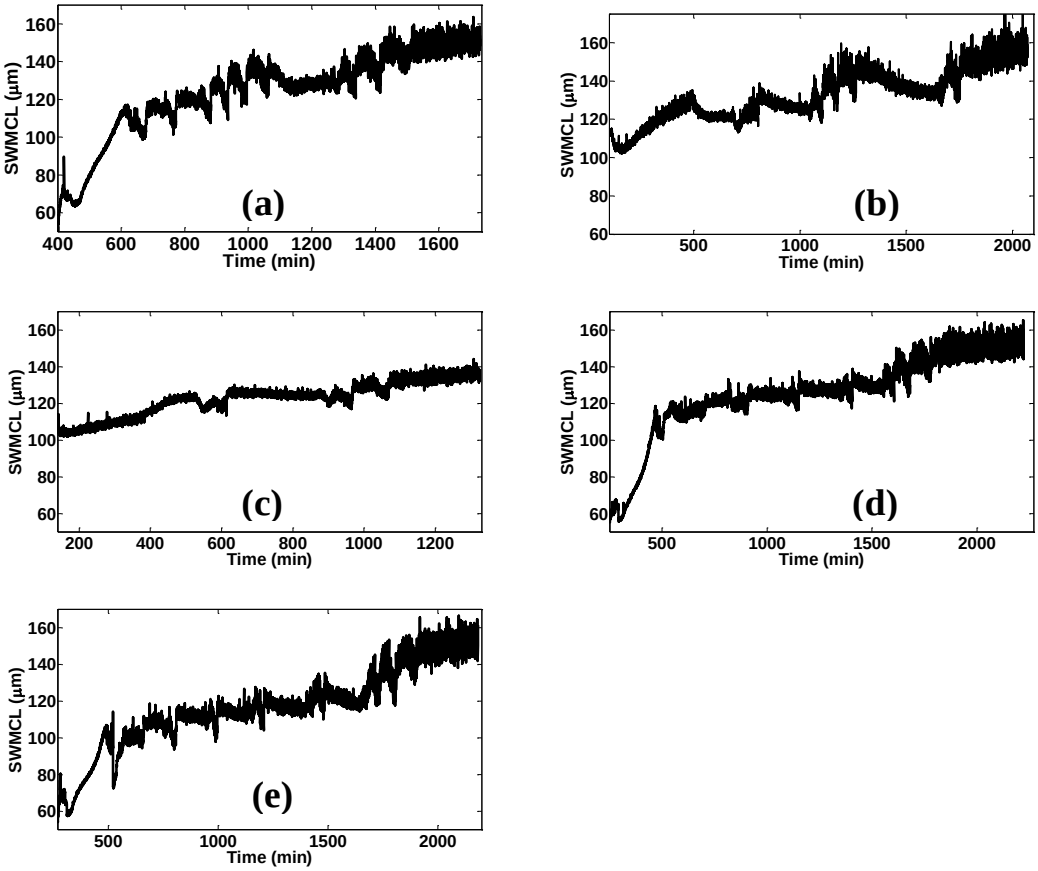



**Figure 5.10 SWMCL for (a) ADNC4 (b) S-ADNC1 (c) S-ADNC2 (d) AS-ADNC1 (e) AS-ADNC2**

The products resulted from the S-ADNC1 and AS-ADNC1 experiments showed very similar distributions. The seed addition and corrective actions were taken at similar time, hence the SWMCL plots also show similar behaviour. These runs can be used to judge the reproducibility

of the ADNC approach and its ability to produce consistently products of similar quality. No bimodality was observed in any of the experiments.

Micrographs of the products obtained from different runs are shown in Figure 5.11 (a)-(e). Large crystals without any agglomerations were obtained in all runs.

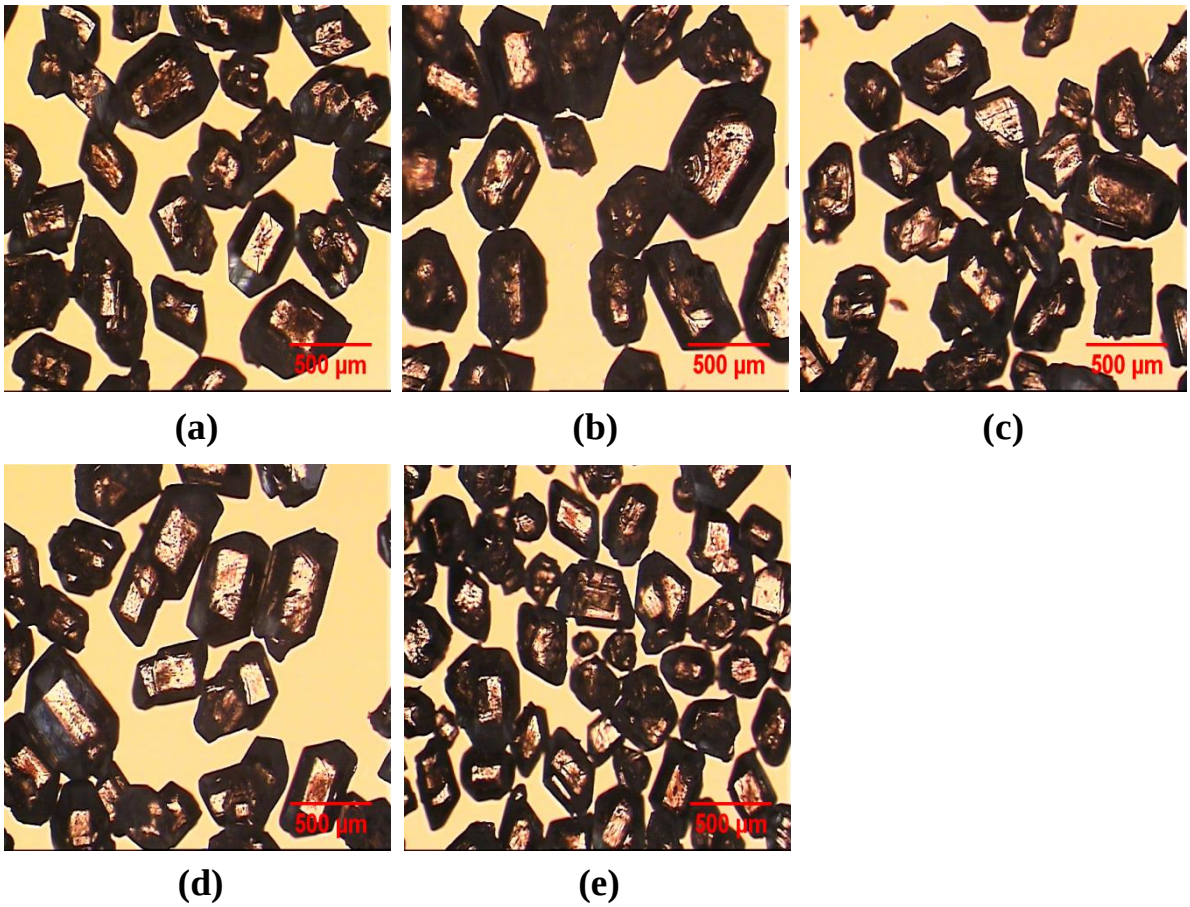



**Figure 5.11 Micrographs of the products (a) ADNC4 (b) AS-ADNC1 (c) AS-ADNC2 (d) S-ADNC1 (e) S-ADNC2**

## 5.3 Conclusions

An evaluation of the ADNC approach under different conditions has been presented for the first time in the case of cooling batch crystallisation using Paracetamol in IPA as the model system. The results of an experiment in which ADNC was used for *in situ* seed generation were used as a benchmark for the experiments with external seed additions and to study the effect of

disturbances, such as accidental seeding, that may occur during cooling crystallization process. The ADNC control was able to correct the disturbances and in all cases was able to bring the number of particles in the system close to the setpoint values. The different experimental conditions showed the robustness and effectiveness of the approach, especially its ability to detect any changes in the MSZW and number of particles. The final CSD obtained in all cases showed no bimodality, also no agglomeration was observed in any of the experiments.

The results provide evidence that FBRM can be used effectively as a process control tool in addition to its widespread application as a monitoring tool. The ADNC approach is simple and does not require model building, extensive modelling or experimentation.

# Chapter 6 Assessment of the Automated Direct Nucleation Control Approach as a Scale up Tool

## 6.1 Introduction

Crystallization is a widely used separation and purification technique in various industries. In the pharmaceutical industries it is mostly carried out as a batch process for both cooling and anti-solvent operating modes. Crystallization is a two phase process, i.e. liquid and solids exist in a suspension and considered as a difficult process to scale up. There are several reasons which make the scale up of crystallization process from laboratory to pilot and eventually to industrial scale a challenging task. It is reasonable to assume that perfectly mixed suspension can be obtained at laboratory scale (e.g. 1 L scale) (Rielly and Marquis, 2001). Also heating and cooling of the suspension can be easily controlled and the system can be made to follow desired temperature profiles because of sufficient heat transfer area. The same can be assumed for anti-solvent crystallization, where the anti-solvent is quickly dispersed in the bulk of the solution and therefore very little supersaturation gradients exist between the point of addition and the rest of the vessel (Myerson, 2002).

The situation on larger scale is quite different; it is almost impossible to achieve perfectly homogeneous conditions. Supersaturation gradients exist throughout the vessel because of differences in the temperatures near the heating surface or close to the point of anti-solvent addition. Variations in MSZW and secondary nucleation are some of the other problems that are encountered on large scale operations. It is a well know fact that crystals in larger vessels respond to changes in the microenvironments, which are in turn affected by changes in the macroenvironment (Myerson, 2002). These differences can have profound effect on the nucleation and crystal growth resulting in undesired CSD. To determine optimum set of operating conditions such as mixing and vessel geometry, computational fluid dynamics and population balance models are generally used. These models require accurate information about the vessel geometry, physical properties of the suspension such as viscosity, crystal size and other system and process related parameters. The output from these methods greatly facilitates

the design and scale up of crystallization processes, however, these methods are computationally very extensive and require considerable expertise for their development.

The ADNC approach, described previously, gave superior results compared to the open loop profiles. The main aim of this chapter is to evaluate the performance of this approach as a robust scale up tool. The approach as described previously requires no a priori information about the system. Another motivation of the work was to apply the control approach based on PAT tools on pilot plant scale. The topic of application of PAT tools for controlling crystallization process on larger scale is under-represented in the literature, only a handful of studies are available (Bakeev, 2010). One of the reasons that prevents the use of sophisticated control approaches on pilot or industrial scale is the difficulty in implementation of these strategies because of the very different process control environment, for example the connecting of an *in situ* spectroscopic tool to an industrial distributed control system (DCS) may require significant effort because of the different interfaces and connectivity issues. The later issue has been addressed in the CryPRINS software which enables quick and easy connectivity with different control environments using on OPC client/server architecture.

The work presented here aims to evaluate the potential application of the model-free ADNC approach on pilot plant scale crystallisation. Two case studies are presented here; in the first case, the ADNC approach for a new system, *ortho*-amino benzoic acid (OABA) and water, will be discussed. The new system was selected to demonstrate the applicability of the control approach for another system. A laboratory scale experiment was carried out initially as the basis for comparison. Based on this, the evaluation of the ADNC approach is carried out on the larger scale. A comparison with linear and natural cooling profiles is also performed at a pilot plant scale.

The second case is related to application of the same approach for paracetamol/isopropanol (PCM/IPA) system on a pilot plant scale. Based on the thorough evaluation of the ADNC approach presented in the earlier chapters, experimental conditions and operating protocol are recommended for experiments on a 100 L scale crystallisation system located at the AstraZeneca,

Charnwood site, and the results are briefly presented, which clearly indicate the potential of the ADNC approach to provide good product quality at industrial scale.

## 6.2 Experimental Procedure

### 6.2.1 Materials and Instrumentation

For the first case study, OABA, 98 % pure purchased from Sigma Aldrich was used with DI water as solvent. A 100 L stainless steel glass lined vessel fitted with glass coated anchor type impeller was used. PT 100 thermocouple was used for measurement of process temperature and an FBRM probe model A100 (Lasentec, USA) was used for monitoring the solid phase and implementation of the ADNC approach via the CryPRINS software. The jacketed crystallizer was connected to a heating/cooling unit (manufactured by Tool Temp, Switzerland, model TT-280). The temperature control unit was fitted with a digital controller (manufactured by CAL Controls, model CAL9400) capable of sending and receiving data via the MODBUS protocol. A software interface for the controller was developed in LabVIEW (National Instruments, U.K.), which allowed the communication with the digital controller using the MODBUS protocol and connection via the RS232 interface. At the same time the software allows communication with external systems (e.g. CryPRINS) via an OPC interface. The vessel was fitted with an overhead motor and the impeller speed used was 74 rpm. A picture of the experimental rig used is shown in Figure 6.1 and a schematic diagram is shown in Figure 6.2. The DSC analyses were carried out using a Q 10 model instrument (TA Instruments, Crawley, UK). In all the DSC runs the samples were kept at 40 °C for one minute in the beginning and after that heated up to 200 °C at a rate of 15 °C/min.

The experiments at AstraZeneca, Charnwood were conducted in a 100 L pilot scale crystallisation system using paracetamol (4-acetaminophenol 98 % purity, purchased from Aldrich) and analytical grade 2-propanol as solvent. The same methodology and software (CryPRINS) was used in the pilot plant as in the rest of the experiments presented in this chapter.

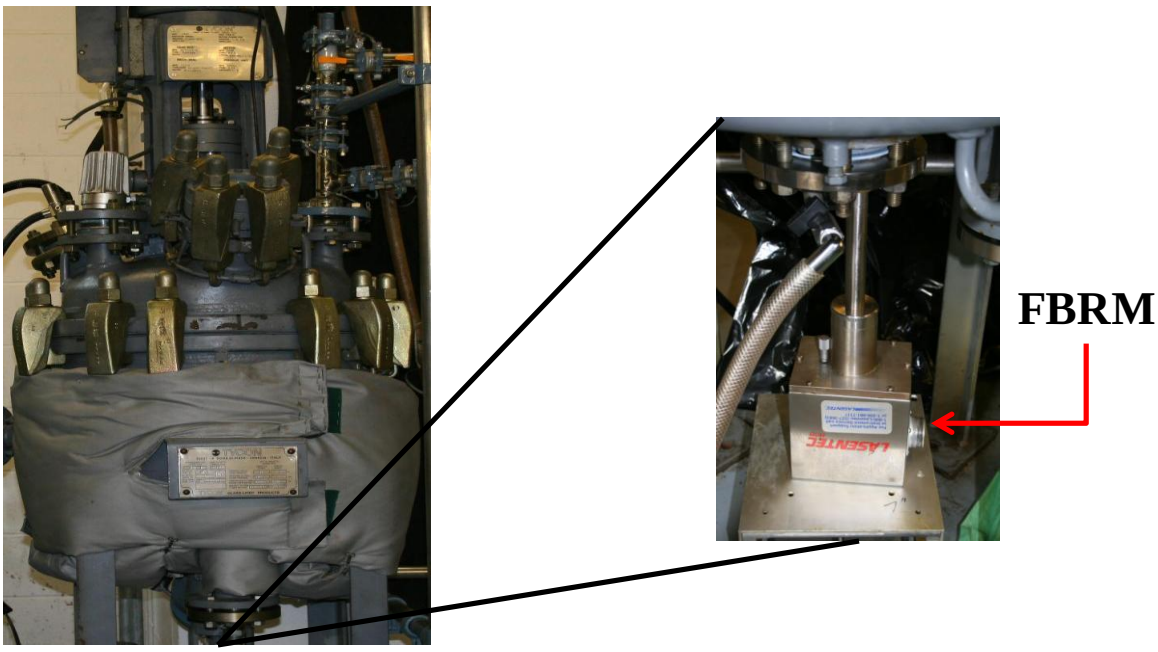



**Figure 6.1 Pilot plant crystallizer, 100 L capacity**

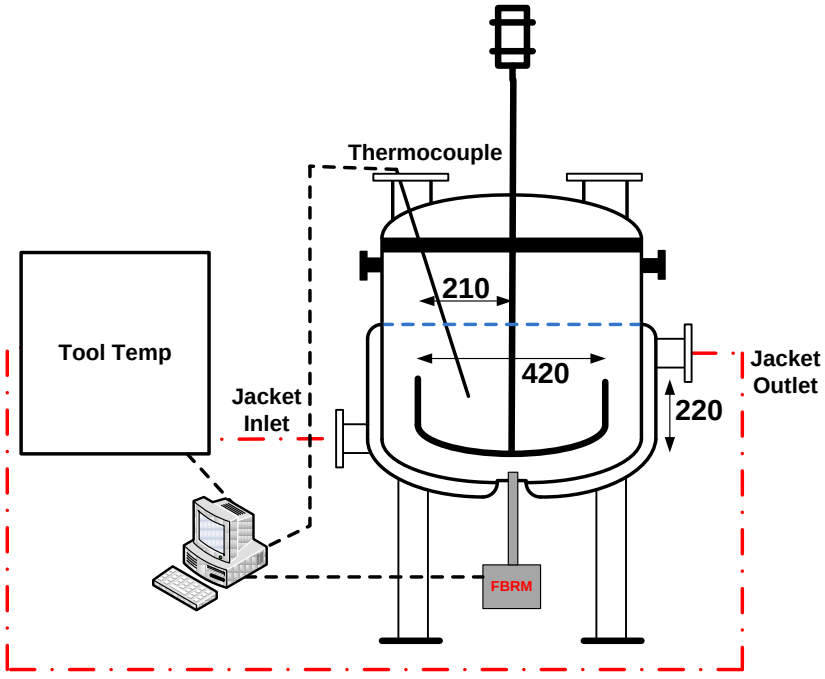



**Figure 6.2 Schematic representation of the rig used, dimensions shown are in cm**

## 6.3 Results and Discussion

### 6.3.1 Scale-up Experiments Using the OABA in Water System

***Laboratory Scale Experiments***

The main purpose of this case study was to analyze the performance of the ADNC for a different system used under different operating conditions. The pilot scale experimental setup used here had two hard constraints which limited the optimisation of the experimental conditions. Firstly the vessel was fitted with an anchor type impeller and could not be replaced. This type of impeller is used for highly viscous liquids and not recommended for suspensions. In the literature therefore the correlations are not available for optimizing impeller speed in correlation with the vessel geometry for suspending particles in the solution. The second hard constraint was related to the large delays in heat transfer between the jacket and the bulk of the solution resulting in slow changes in the temperature especially during the cooling phase. Because of the slow dynamics of the system it was decided to use jacket temperature directly as the manipulated input set by the ADNC.

Prior to the commencement of the experiments on the pilot plant scale, ADNC was used for OABA/water system on laboratory scale. The results obtained are shown in Figure 6.3.

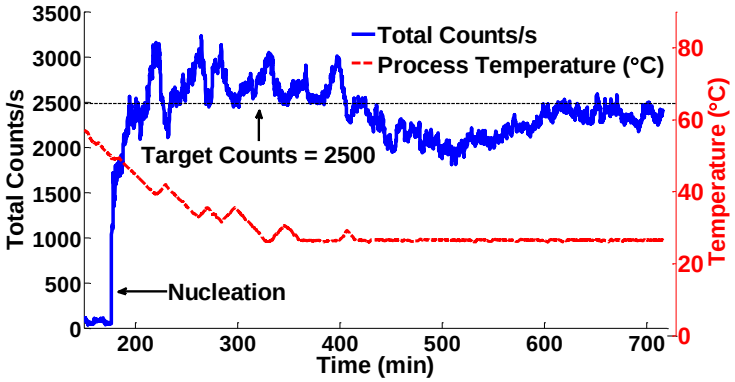



**Figure 6.3 Total counts/s and temperature profile for OABA/water laboratory scale experiment**

Since the counts/s measurement obtained from the FBRM, depends on the volume of the suspension, agitation speed and mixing conditions, a careful selections of the target counts/s on

different scales is important for consistent results. Selecting similar target counts/s in absolute value most likely would not be a feasible option. To address this issue it was decided to use "a certain percentage of the maximum counts" obtained by linear cooling, as obtained on each scale, as setpoint for the ADNC. For example a linear cooling experiment was carried out at laboratory scale and from its results a setpoint of 2500 counts was selected, which was approximately 60 % of the maximum counts from the linear cooling run. The upper and lower limits were selected as 2000 and 3000 respectively, $k_c$ and $k_h$ (proportional gain) values were kept at 1.

Figure 6.3 shows that nucleation event took place at about 50 °C, several small heating cooling cycles were required to keep the counts at the desired level until the process reached the lower temperature limit of 25 °C and the counts stabilized close to the target value of 2500. The evolution of coarse particles indicates steady growth in the system, as shown in Figure 6.4. These results show similar trend as seen previously for the PCM experiments, indicating dissolution of fines and growth of bigger crystals during heating cooling cycles. A micrograph of the product crystals obtained at the end of the batch is shown in Figure 6.5. These figures show that the ADNC approach was able to generate product with bigger crystals by continuous growth throughout the process by alternating heating/cooling cycles.

Having established that ADNC was applicable for the OABA/water system on the laboratory scale, pilot plant scale experiments were carried out, which are discussed in the next section.

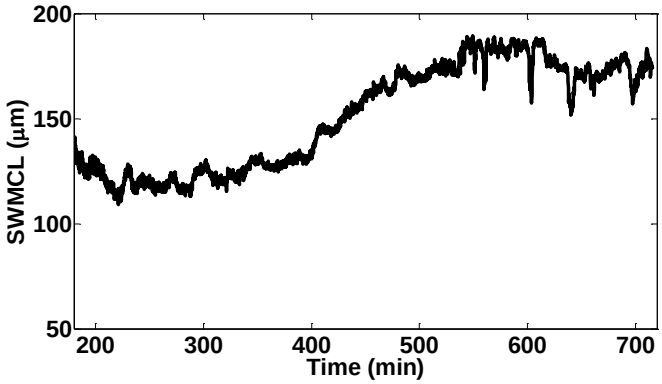



**Figure 6.4 Evolution of coarse particles for the laboratory scale OABA/water run using ADNC**

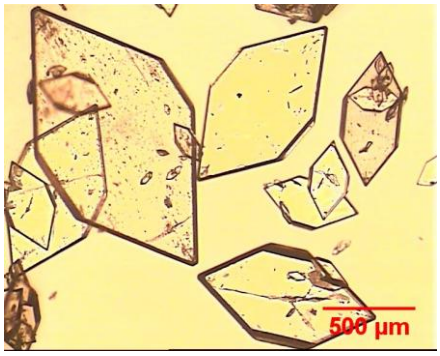



**Figure 6.5 Micrograph of OABA crystals (form 2) obtained by ADNC at laboratory scale (1 L)**

### *Pilot Scale Experiments*

The ADNC parameters used for ADNC at pilot plant scale are as follows: 4 °C/min was selected as the heating and cooling rate for the jacket temperature, $k_c$ and $k_h$ values were 1. These set of parameters were selected as they were able to change the process temperature at a rate of approximately 0.28 °C/min, very close to the heating/cooling rates on the laboratory scale. Same concentration of OABA was used and 25 °C was selected as the lower temperature limit.

Initially unseeded linear and natural cooling experiments were carried out for selection of a suitable setpoint for the ADNC, and for comparison of the product quality. Process and jacket temperature profiles are shown in Figure 6.6 and Figure 6.7 for both linear and natural cooling profiles, for understanding the heat transfer dynamics.

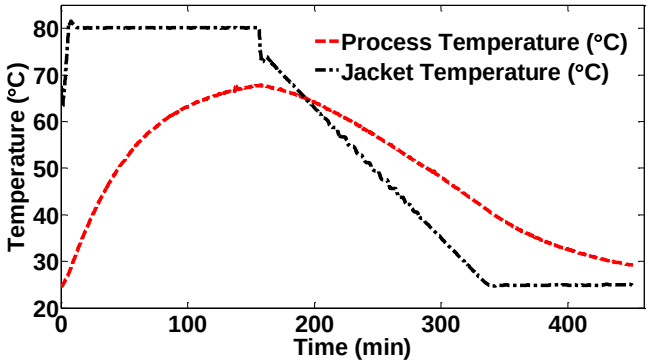



**Figure 6.6 Process and jacket temperature profiles for the linear cooling experiment at pilot plant scale**

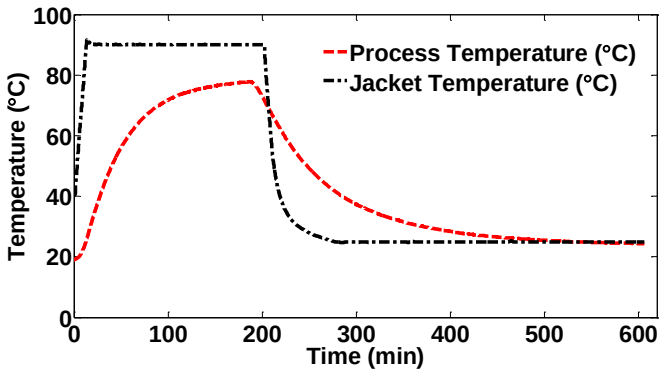



**Figure 6.7 Process and jacket temperature profiles for natural cooling experiment at pilot plant scale**

These profiles show that a considerable lag exists between the jacket and process temperatures. The lag is very noticeable once the jacket temperature falls below 45 °C. The process temperature obtained by using a linear jacket temperature approximately corresponds to a linear cooling (but of course with slower rate than that for the jacket temperature), whereas the steep natural cooling curve in the jacket temperature results in a much slower but natural cooling profile in the reactor. The crystallisation results obtained from these two profiles are shown in Figure 6.8 and Figure 6.9.

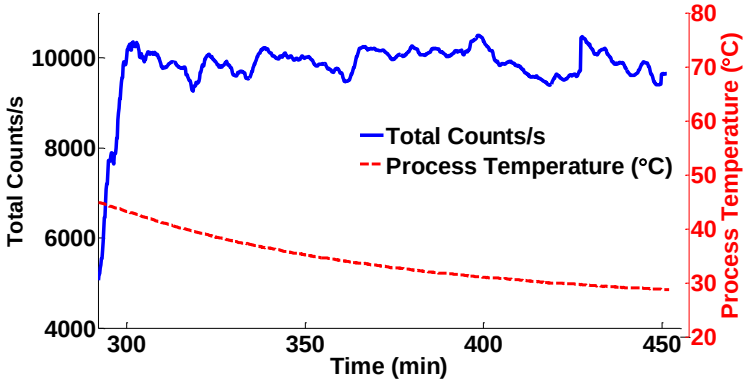



**Figure 6.8 Total counts/s and process temperature profile for linear cooling experiment at pilot plant scale**

In both cases the nucleation took place approximately at the same temperature between 45 °C and 50 °C, followed by cooling. The solution for natural cooling experiment was kept at this temperature for some time to observe if any secondary nucleation might take place. The total counts for linear cooling profile remained generally between 9500 and 10000, while counts in the case of natural cooling remained between 7500 and 8000.

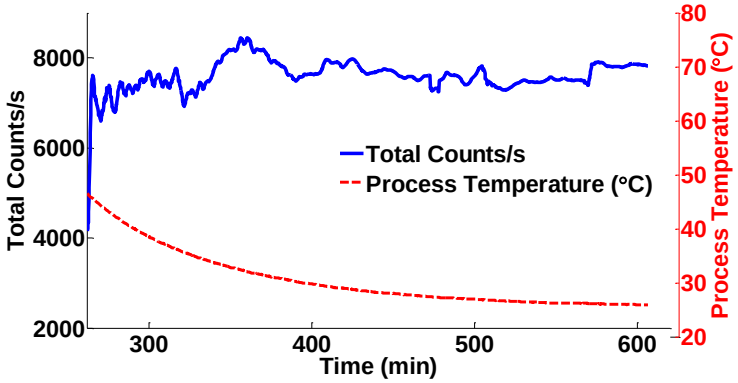



**Figure 6.9 Total counts/s and process temperature profile for natural cooling run**

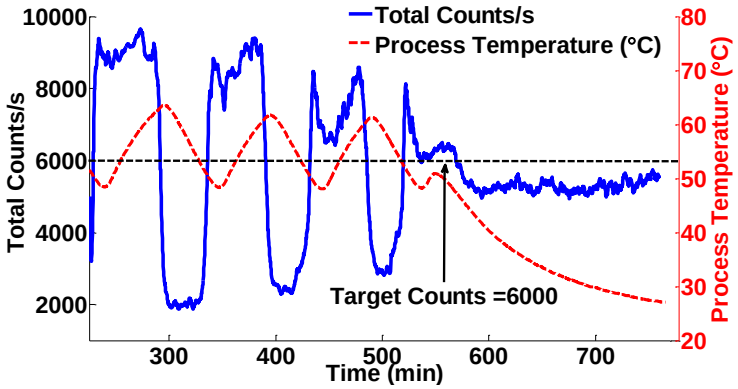
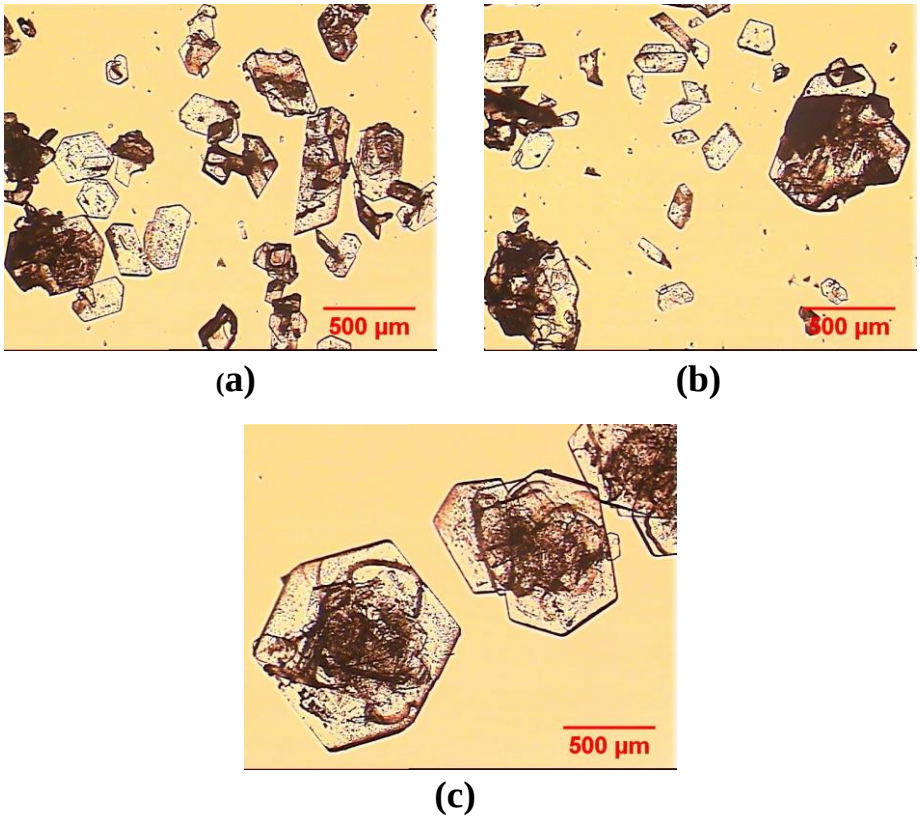



**Figure 6.10 Total counts/s and temperature profile for ADNC run**

Analysis of these figures shows that natural cooling resulted in small and agglomerated crystals. Less agglomeration was observed in the case of linear cooling, and the products in both cases had similar crystal sizes. Both products show the presence of a significant amount of fines, which is probably due to secondary nucleation and breakage of the crystals during the process. The ADNC approach in contrast with the two approaches produced significantly larger crystals without any agglomeration. The product crystals are with well-defined shapes and edges, with no fines present in the system. The results show that by maintaining the number of crystals at a lower level favours growth of larger crystals. The heating/cooling cycles prevent agglomeration of particles as shown in previous results and eliminate fines, which may form due to breakage or secondary nucleation.




(a) (b)

(c)

**Figure 6.11 Micrographs of crystals (a) linear cooling (b) natural cooling (c) ADNC approach**

These experiments also illustrated the excellent performance of the ADNC approach to remove the fines that form due to breakage, which is a common problem in the case of large-scale industrial crystallisation processes. Many pharmaceutical compounds crystallize as brittle needle or plate shaped particles prone to significant breakage due to impeller-crystal collisions, especially in larger crystallisers, causing bimodal product distributions and difficulties during the subsequent isolation of the product (e.g. long filtration times). Finding a suitable cooling rate for controlling the crystallisation of products prone to breakage is difficult, since a suitable compromise has to be found between potential nucleation and breakage. In order to avoid secondary nucleation, a slow cooling rate is preferred, which operates the system at low supersaturation. However this results in longer batch times, and hence can increase breakage due to longer period in which particles are exposed to collisions. A typical crystallisation operation that keeps the operating trajectory within the supersaturated region is unable to eliminate the formation of fines, whereas the ADNC is able to detect increase in number of particles, whether produced by secondary nucleation or breakage, and by automatically initiating heating cycles preferentially dissolve the unwanted fines.

A comparison of the ADNC approach on both scales show that smaller number of heating/cooling cycles was required on laboratory scale, on the other hand the temperature cycles in case of pilot plant were bigger in magnitude. This difference could be attributed to mixing and heat transfer differences at the two levels. This is also consistent with the earlier observations related to the more significant breakage observed at the large scale crystallisation process, which required a larger number of heating cooling cycles, to eliminate the fines. Additionally, the laboratory scale system swiftly follows any change in the temperature and as a result of this a better control over number of crystals is achievable. On the pilot scale the heat transfer dynamics especially for this particular experimental setup were significantly slower, resulting in a delayed response, and more significant overshoots. Even with these differences and limitations of the large scale crystallisation system, the ADNC approach gave better results than the natural and linear cooling profiles, and product crystals which were similar in size.

The difference in shape between the crystals resulting from the ADNC experiments is due to the different polymorphic forms of the products. OABA exists in three polymorphic forms. The transition temperature between form 1 and 2 was reported to be in the range of 45 °C (Jiang *et al.*, 2008). Form 1 is thermodynamically more stable at lower temperatures, whereas form 2 is more stable at higher temperatures.

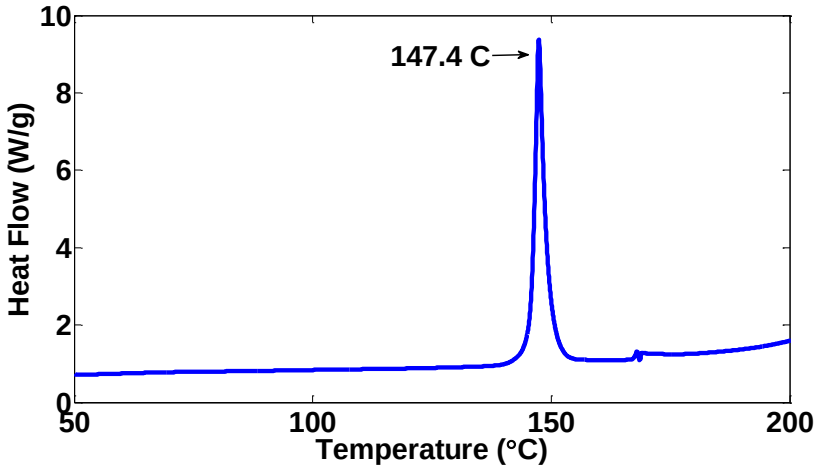



**Figure 6.12 DSC thermogram of OABA sample obtained at laboratory scale. Same results were obtained for samples from pilot scale experiments using the natural and linear cooling profiles.**

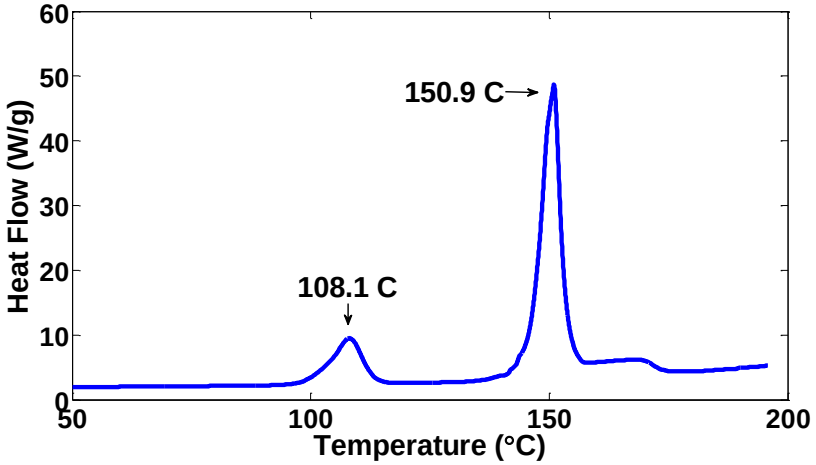



**Figure 6.13 DSC thermogram of OABA sample obtained at pilot plant using the ADNC approach**

The DSC analysis (shown in Figure 6.12 and Figure 6.13) confirmed that at large scale the more stable (at lower temperatures) form 1 crystals were produced in the DNC experiment, whereas in the linear and natural cooling experiments on the large scale and at the laboratory scale DNC experiment the metastable form 2 crystals were formed. The peak at 108.1 °C indicates transformation of form 1 to form 2 and the melting point of form 2 is 144 °C (Jiang *et al.*, 2008). Since all nucleation events occurred above the transition temperature (49 °C for the laboratory scale DNC, and 52 °C for the large scale DNC), most likely form 2 crystals were initially formed in all cases. The transformation of the metastable polymorph into the more stable form 1 is generally favoured by the increase in the temperature (Dang *et al*., 2009). Since during the large scale ADNC experiments the slurry was kept for long period of times at higher temperatures due to the more pronounced temperature cycles, than during the linear and natural cooling or the laboratory scale DNC experiments, which could increased the rate of transformation from form 2 to form 1. Furthermore, since the solubility of form 2 below 45 °C is higher than for form 1, the temperature cycles around the solubility curve can promote the dissolution of any form 2 potentially present in the system (Abu Bakar *et al*., 2009).

The MSZW is narrower on the large scale than on the laboratory scale; however the results indicate the ability of the ADNC to adapt the operating profile to variations in the MSZW. The DNC approach was able to produce similar CSD and mean crystal size on the large and laboratory scale however it was unable to detect the polymorphic transformation. For systems

with potential polymorphic transformations more careful design of the temperature cycling procedure is required based on the phase diagram of the polymorphic system (Abu Bakar *et al*., 2009).

To further evaluate the robustness of this approach on the pilot plant scale a second case study was performed, with the results described in the next section.

### 6.3.2 Industrial Scale-up Experiments Using the Paracetamol in IPA System

Experiments for PCM in IPA were performed at an industrial scale batch cooling crystallisation process located at AstraZeneca, Charnwood, following the procedure and recommendations obtained on the laboratory scale experiments. The objective was to evaluate the effectiveness of the approach on pilot scale for the PCM/IPA system. The same software system (CryPRINS) and methodology was used as in all the other experiments presented in the thesis. The ADNC obtained the measurements from industrial FBRM and ATR-UV/Vis spectroscopy probes. The calibration of the probe was performed following similar procedure as described in Chapters 3 and 4. The temperature profile was calculated by the ADNC controller and sent as a setpoint to the temperature control system via an industrial distributed control system (DCS), running an ABB Satellite Server. All communications were implemented via OPC protocol. Several experiments were performed, and sample results from one ADNC experiments are presented next. In this experiment a PCM concentration of 0.145 g/g was used, heating/cooling rates were 0.2 °C/min, DNC setpoint was 2000 (based on total counts/s), while 2040 and 1960 were used as upper and lower limits receptively. The results of the experiment carried out are shown in Figure 6.14.

The temperature was initially increased to 50 °C to ensure complete dissolution of the solids. At this point the DNC was started. The control approach successfully detected the increase in counts and managed to bring the system to the setpoint. After three heating and cooling cycles the counts were stabilized close to the setpoint and lower temperature limit was reached. The temperature profile obtained is similar to the temperature profiles obtained at the laboratory scale

(shown in chapters 4 and 5). The heating/cooling cycles removed fines and promoted growth of the crystals. This observation is evident from the phase diagram as shown in Figure 6.15, where control pushes the system to the undersaturated region for the dissolution of fines.

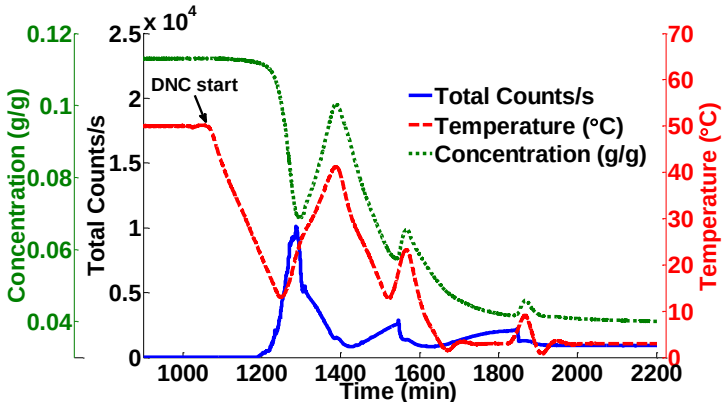



**Figure 6.14 Total counts/s, concentration and temperature profile for PCM/IPA run in the industrial pilot plant crystallizer**

The operating curve in the phase diagram Figure 6.15, indicates similar variations in MSZW as observed for the laboratory scale experiments presented in chapters 4 and 5; a much wider MSZW for primary nucleation and narrower MSZW for subsequent secondary nucleations. The primary nucleation occurred at a higher temperature (lower supersaturation) compared to the laboratory scale experiments. This is also in correlation with the observations in the case of the OABA experiments, which indicated a narrower MSZW for the larger scale. This again shows that dynamic changes take place in the crystallization vessels at different scales and the control approaches which do not take into account these variations can result in poor product quality. The heating/cooling cycles resulted in dissolution of fines and growth of crystals. The trend of the SWMCL (Figure 6.16.) shows a continuous growth of the particles at the expense of the dissolution of fines. Similarly to the laboratory scale experiments, large product crystals with uni-modal CSD were obtained in this case as shown in Figure 6.17.

These results shown here and in the previous chapters indicate that the ADNC approach for different systems and on both laboratory and large scales is able to successfully and consistently produce large crystals with a uni-modal distribution and without any agglomeration. The

approach works without any information about the process that might have been required for other control approaches.

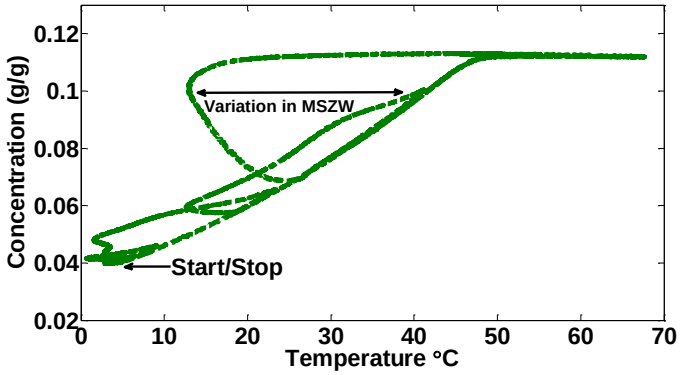



**Figure 6.15 Operating curve in the phase diagram during the ADNC of the industrial crystallisation reactor. The difference between the primary and secondary MSZW can be clearly seen.**

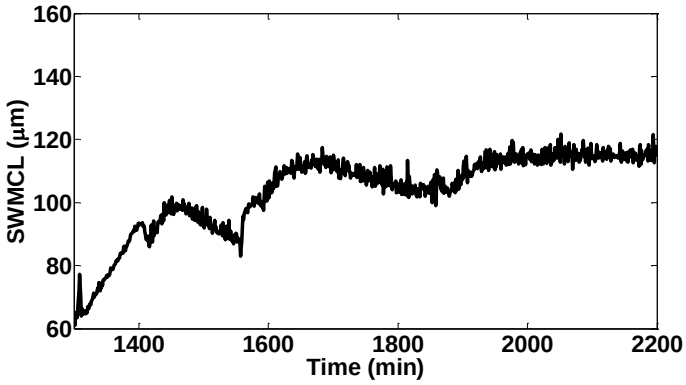



**Figure 6.16 Evolution of the SWMCL for the PCM/IPA run at the industrial scale crystallizer using the ADNC approach**

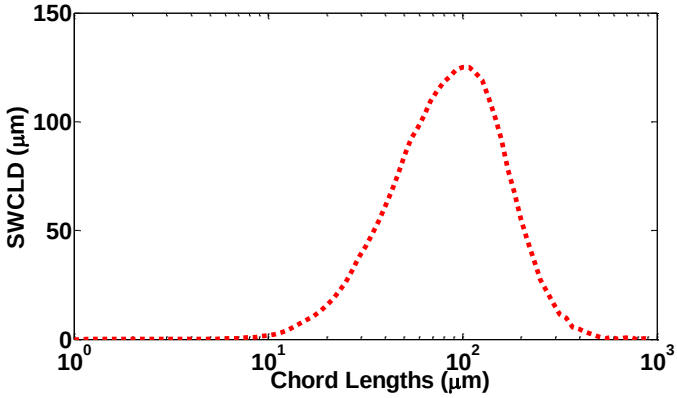



**Figure 6.17 CSD for PCM/IPA experiment at the end of the batch**

## 6.4 Conclusions

A thorough assessment of the ADNC approach on pilot plant scale was presented using two different systems. The main purpose was to test the ability of this approach to be used as a robust scale approach, and to analyze its performance on pilot scale in comparison with conventional linear and natural cooling profiles. Comparison of the results at laboratory and pilot scales validated that the ADNC approach can be used effectively to obtain non-agglomerated, large crystals with uni-modal size distribution on both scales without extensive experimentation and modelling. The approach also outperformed linear and natural cooling profiles in that it produced larger crystals with more uniform and uni-modal CSD, with minimal amount of fines. The results show that the ADNC approach can be used as a useful and robust tool for obtaining crystals with desired properties on both laboratory and pilot plant scales.

# Chapter 7 Separation and Monitoring of the crystallization of mixtures of Aminobenzoic Acid Isomers using ATR UV/Vis and FBRM

## 7.1 Introduction

This work focuses on the development of a calibration model for monitoring of a complex multi-component system using ATR-UV/Vis spectroscopy, covering both cooling and anti-solvent crystallizations, and on the development of an interconnected crystallisation system for the separation of the positional isomers of amino benzoic acid, via seeded cooling crystallization. Two cases are discussed, the separation of two and three isomers, when they are present together in the solution. The separation are to be achieved by using interconnected crystallizers system seeded with different isomers in each crystallizer (all at the same temperature) and ATR-UV/Vis spectroscopy and FBRM have been used to monitor the liquid and solid phases respectively.

Isomers are a class of compounds frequently encountered in the pharmaceutical, fine chemicals and agrochemical industries. They include geometrical and positional isomers, enantiomers and stereoisomers. Often these isomers exist as mixtures and since they have different physical and chemical properties their monitoring and isolation in the purest form is required. High performance liquid chromatography (HPLC) and capillary zone electrophoresis (CZE) are the most widely used techniques for the separation of the isomers. A significant literature deals with the application of these techniques, Hardy and Townsend (1988) separated positional isomers of oligosaccharides and glycopeptides by high performance ion exchange chromatography. Račaitytė *et al*. (2005) used CZE and reversed phase HPLC for the quantitative analysis of the monosaccharides**.**

Several applications of crystallization have been reported for the separation of isomers. Rousseau and O'Dell (1980) used seeded cooling crystallization for the separation of multiple solutes present together. Seeds for the desired solute were added causing secondary nucleation of that solute. Supersaturation was generated by reducing the temperature for growth of the added and generated seeds. The solution was filtered, heated up again and seeds for second solute were

added. The problems with this approach are multiple filtration steps, precise temperature control, the requirement of many small cooling steps as the undesired component can also nucleate in the vessel as the temperature is lowered, and possibly very low yield. A better approach for separation of enantiomers of mandelic acid using crystallization was proposed by Elsner *et al*. (2007), which involved two coupled crystallizers. In their theoretical approach only solids free liquid was to be interchanged between the two vessels and simulation studies suggested that this approach could increase the yield and purity of the product. Elsner *et al*. (2009) in another work demonstrated the use of a coupled crystallizer approach experimentally for the separation of dl-threonine. Svang-Ariyaskul *et al*. (2009) successfully used the coupled crystallizers concept for chiral separation of DL-glutamic acid. The solids free liquid was exchanged between the vessels using a 0.1 µm membrane. The product obtained using this system was 94 % pure and an increase in yield by 56.3 % compared to simple cooling crystallization.

In this contribution monitoring and separation of aminobenzoic acid (ABA) isomers has been carried out. ABA has three positional isomers namely ortho (OABA), meta (MABA) and para (PABA). These isomers are widely used, e.g. OABA is used in pharmaceuticals, in the manufacturing of perfumes, dyes, pigments and saccharin (Jiang *et al*., 2008), MABA is used in the manufacturing of analgesics and other chemicals (Svard *et al*., 2010), PABA is also used in pharmaceuticals, dyes and as additive (Gracin and Rasmuson, 2004). Apart from their clinical importance monitoring the concentrations of ABA isomers is also important in waste water when they are present together with other compounds. Schmidt *et al.* (1997) carried out analysis of ABA in waste water using HPLC. Zheng *et al*. (2006) used HPLC with four ionic liquids to separate the three ABA isomers, CZE was used by Fujiwara and Honda (1987) for the same separation.

In the current work the interconnected crystallizer approach is used for the separation of the positional isomers, *ortho*-, *meta*- and *para*-aminobenzoic acids for the first time. The work also demonstrates for the first time that a system with three interconnected crystallizers can be used successfully for the separation of three positional isomers. The methodology behind this approach is described as follows. The two or three isomers when dissolved together in the solution can be considered as separate compounds i.e. each component will have its own

supersaturation regardless of the other, assuming that there is no interaction between the different species. In coupled crystallizers setup the solution is continuously exchanged between the vessels through filters so as to maintain supersaturation at the same level. The isomers are seeded separately in their respective vessels. The supersaturation generated for each isomer now is used up by the respective seeds; a slow cooling rate will prevent any nucleation event. The supersaturations generated during the cooling for all components are continuously used up by the seeds which grow in their corresponding vessels, so there is less chance of any of the species nucleating in the vessels of the other species. Hence, pure isomers may be obtained from their respective vessels in the end.

## 7.2 Experimental Section

### 7.2.1 Materials and Equipment

Ortho-aminobenzoic acid (OABA), meta-aminobenzoic acid (MABA) and para-aminobenzoic acid (PABA), all 98 % pure from Sigma Aldrich were used in the experiments. Laboratory reagent grade iso-propanol (IPA), (Fisher Scientific) was used as solvent, while de-ionized water from a Milli-Q unit was used as anti-solvent. The experimental setup used was same as described in chapter 2.

For calibration experiments, reference measurements were made in clean IPA, water or IPA/water mixtures at 20 °C. Artificial neural network calculations for the development of the nonlinear calibration model were carried out using the Neural Network toolbox in MATLAB (The Mathworks), R2008b version, design of experiments was carried out using the statistical toolbox in R2008b version.

## 7.3 Calibration Model Development

### 7.3.1 Design of Experiments

A calibration model capable of determining the concentrations of OABA and PABA simultaneously was developed. Because of the presence of several variables design of experiments was used to minimize the number of experiments required. Four variables were considered for calibration model development, including the concentrations of OABA and PABA, solvent/anti-solvent ratio and temperature. In order to have a robust calibration model, it was decided to have 5 concentration levels. According to full factorial designs, $L^f$ experiments are needed to investigate the effect of $m$ variables at $L$ levels. In this case 1024 experiments would have been required, which is practically not feasible to carry out. As an alternative, the central composite design method was used for the design of experiments, as it gives a good coverage of the entire design space (Brereton, 2003), whilst providing a significantly smaller number of experiments than the full factorial design. Compared to the full factorial design, the number of experiments was reduced from 1024 to 36 experiments.

### 7.3.2 Monitoring and Calibration Model Development

Separately recorded sample spectra of OABA, PABA and MABA are shown in Figure 7.1 in IPA. The peak absorbance values for OABA, PABA and MABA are 339 nm, 293 nm and 311 nm respectively. The spectrum for the isomers when present together in the mixture is shown in Figure 7.2. From these figures it is evident that ATR-UV/Vis spectroscopy can be used to distinguish between the two isomers i.e. OABA and PABA even when they were present as mixture. MABA shows lower peak intensities in general; hence it is more difficult to detect the peak in the plot.

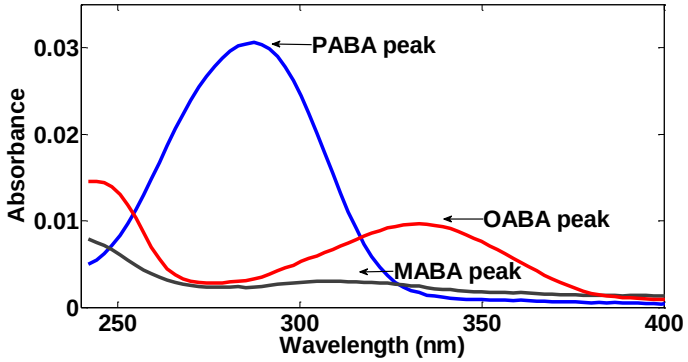



**Figure 7.1 Separately recorded spectra of OABA, PABA and MABA in IPA, all concentrations were 0.01 g/g**

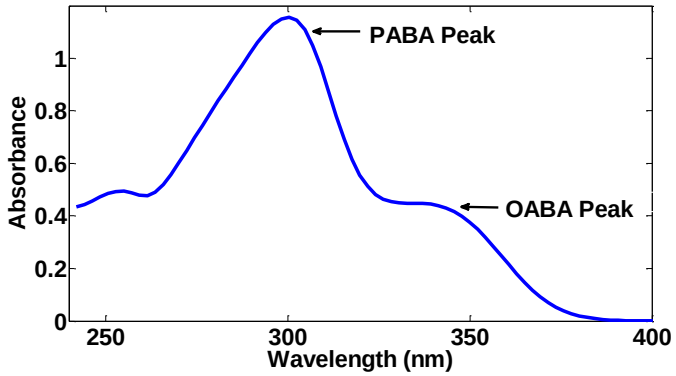



**Figure 7.2 Spectrum of OABA, PABA and MABA when present together. The spectrum was recorded with 100 % IPA, concentrations of OABA and PABA were 0.219 g/g.**

The calibration experiments were designed to cover several different solvent and anti-solvent ratios ranging from 100 % IPA to 80 % IPA along with several concentrations of OABA and PABA. For all calibration experiments the temperature was raised 10-15 °C above the saturation temperature for complete dissolution. The temperature was then decreased in steps at a rate of 0.6 °C/min and kept at certain temperatures for half an hour. The temperature was lowered in each case to 10 °C or until the nucleation took place. Only the spectral data obtained in the clear solution (i.e. when no solids were present) was used in the calibration model development. Typical experimental results from one of the experiments carried out during the calibration model development are shown in Figure 7.3. The robustness of the ATR-UV/Vis spectroscopy signal at various temperatures and its ability to detect dissolution and nucleation events can be seen. The decrease in the FBRM counts/s and increase in the UV signal in first part of the experiment indicate the dissolution of the compounds. Similarly the sudden decrease in the UV

signal and the sudden increase in the FBRM total counts/s show the nucleation event towards the end of the experiment. The variation of the absorbance during the temperature steps in the clear solution indicates the effect of the temperature on the absorbance. At the same concentration the absorbance increases with the decrease of the temperature. When the temperature was constant the UV absorbance showed very stable signal and negligible drift. The different concentrations used at several IPA/water ratios are shown in Table 7.1.

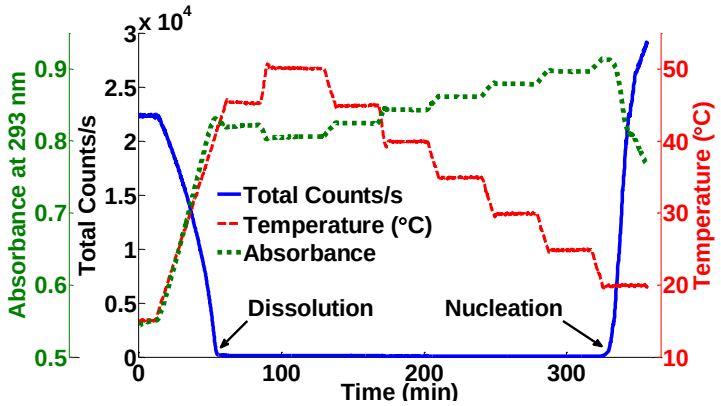



**Figure 7.3 Absorbance, total counts/s and temperature profiles for a calibration experiment**

**Table 7.1 Concentrations of OABA and PABA used at several IPA/water ratios for model building**

| 80 % IPA | | 85 % IPA | | 90 % IPA | | 95 % IPA | | 100 % IPA | |
|---|---|---|---|---|---|---|---|---|---|
| OABA (g/g) | PABA (g/g) | OABA (g/g) | PABA (g/g) | OABA (g/g) | PABA (g/g) | OABA (g/g) | PABA (g/g) | OABA (g/g) | PABA (g/g) |
| 0.145 | 0.097 | 0.136 | 0.136 | 0.108 | 0.108 | 0.152 | 0.152 | 0.18 | 0.12 |
| 0.145 | 0.145 | 0.187 | 0.136 | 0.145 | 0.145 | 0.209 | 0.152 | 0.18 | 0.179 |
| 0.178 | 0.145 | 0.187 | 0.186 | 0.161 | 0.145 | 0.209 | 0.209 | 0.18 | 0.219 |
| 0.194 | 0.145 | 0.204 | 0.203 | 0.161 | 0.163 | 0.2279 | 0.228 | 0.199 | 0.219 |
| 0.194 | 0.178 | | | 0.203 | 0.202 | | | 0.219 | 0.219 |
| 0.194 | 0.194 | | | | | | | | |

The data used for calibration consisted of 78 inputs, 76 wavelengths from 242 – 400 nm, temperature and solvent/anti-solvent ratio. The test data i.e. the data from the calibration experiments was pre-processed using SNV transformation. The data as mentioned in chapter 3 was checked for the presence of nonlinearity by plotting absorbance against the concentration as shown in Figure 7.4. A nonlinear relationship between absorbance at 339 nm and concentration can be seen here, suggesting that a nonlinear model would be required. Similar behaviour in the variation of absorbance values was observed at different wavelengths and temperatures as well.

Another source of nonlinearity is shown in Figure 7.5, absorbance values at constant temperature of 30 °C with same concentrations of OABA and PABA (0.145 g/g) are plotted but at different IPA ratios. The plot shows that even if both the solutes are present in the same amounts the absorbance values are affected by the percentage of IPA present. It was discussed in chapter 3 that presence of nonlinearity can result in poor performance of linear models and a simple nonlinear model was proposed for calibration model development. The application of nonlinear models in cases where single absorbance/derivative can be used is quite straightforward, however, in this case multiple species were present therefore making it difficult to select absorbance(s) which could be used for model development. Furthermore, the presence of multiple components and their overlapping spectra also suggested that absorbance/derivative at single wavelength would not be sufficient to model the whole system accurately. For comparison purpose models using PCR and ANN were developed, the results are discussed as follows.

Two calibration models (using the data from experiments shown in Table 7.1), one using PCR and one based on ANN were initially developed and tested for their predictive ability. The PCR model using 8 principal components (PCs) and the ANN model with one hidden layer with 22 neurons were selected as they gave better results during model testing.

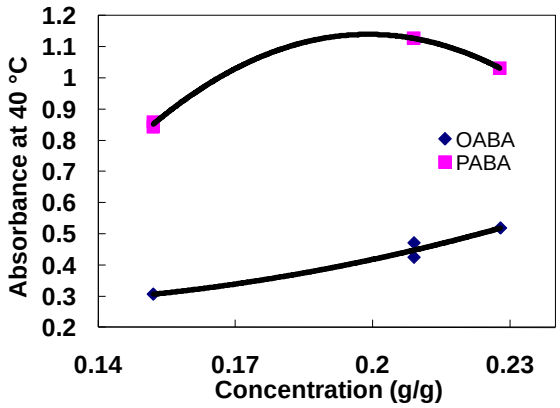



**Figure 7.4 Variation in absorbance at 339nm at constant temperature**

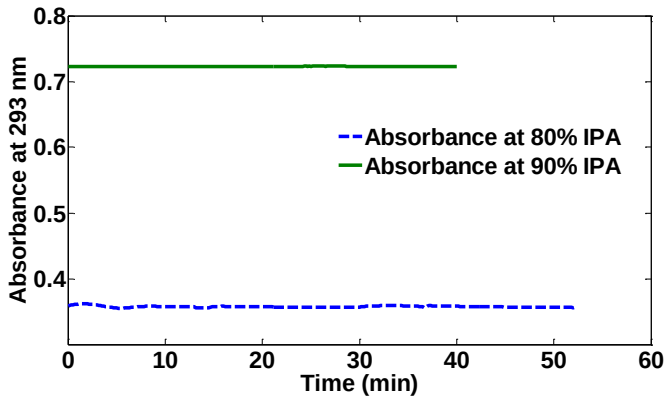



**Figure 7.5 Absorbance values at 30 °C. Concentrations of OABA and PABA were 0.145 g/g**

For validation of the calibration model developed two validation experiments were performed, a simple cooling crystallization experiment and a combined cooling and anti-solvent crystallization experiment. The models developed were initially validated using the cooling crystallization experiment.

The cooling crystallization experiment for validation of the developed models was carried out with 0.22 g/g of OABA and 0.15 g of PABA, the solvent used was 95 % IPA and 5 % water (by weight). The variation of peak absorbance values of OABA and PABA along with FBRM and temperature data are shown in Figure 7.6 and Figure 7.7. The temperature was raised to 60 °C to ensure complete dissolution of both isomers. The temperature was then decreased in steps until the nucleation took place. Both isomers nucleated approximately at the same time.

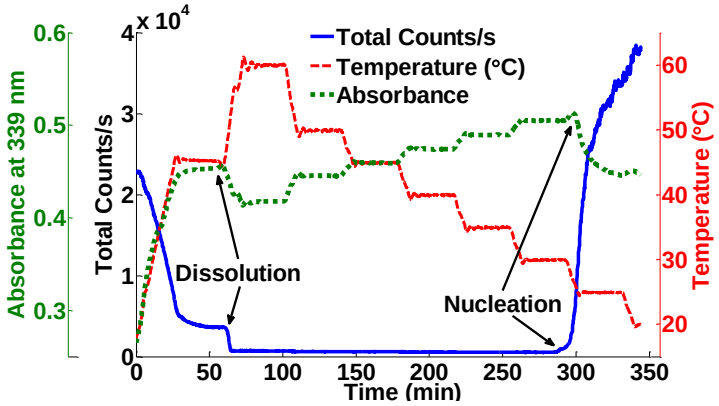



**Figure 7.6 Variation in peak OABA absorbance at 339 nm with temperature and total counts/s**

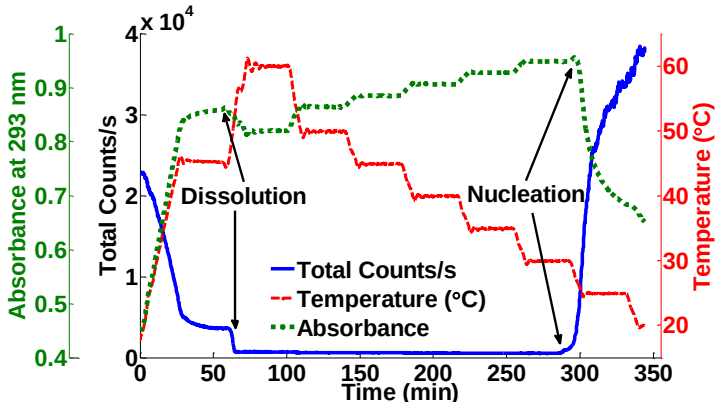



**Figure 7.7 Variation in peak PABA absorbance at 293 nm with temperature and total counts/s**

The predicted concentration of OABA by PCR is shown in Figure 7.8 and for PABA in Figure 7.10. ANN model predictions for OABA and PABA are shown in Figure 7.9 and Figure 7.11. For this cooling experiment both models were able to capture the temperature effect satisfactorily for both isomers as shown from the concentration profiles. The root mean square error of prediction was used for the selection of the model. The values obtained for OABA were 0.0012 g and 0.0113 g for the ANN and PCR models, respectively. For PABA these values were 0.0016 g and 0.0050 g for the ANN and PCR models, respectively. Based on these results the ANN model was selected, and a combined cooling and anti-solvent experiment was then conducted to further validate the accuracy and prediction of the selected model.

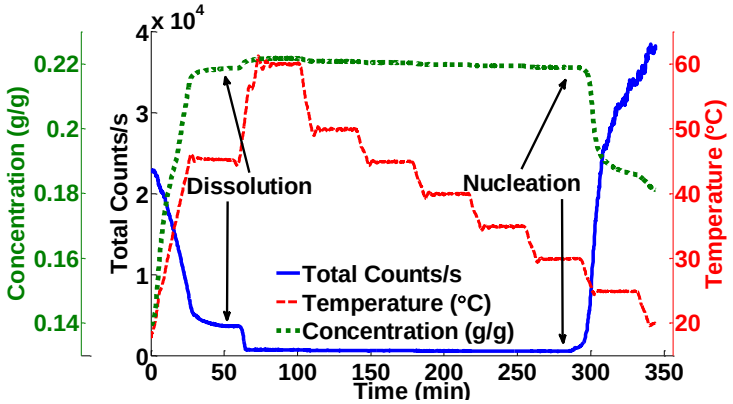



**Figure 7.8 Predicted concentration of OABA by the PCR model**

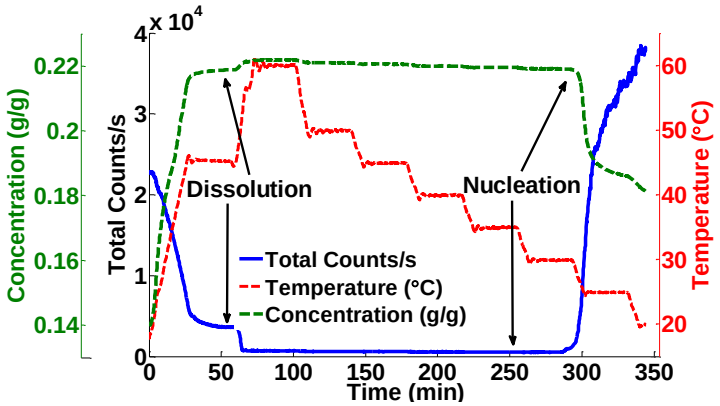



**Figure 7.9 Predicted concentration of OABA by the ANN model**

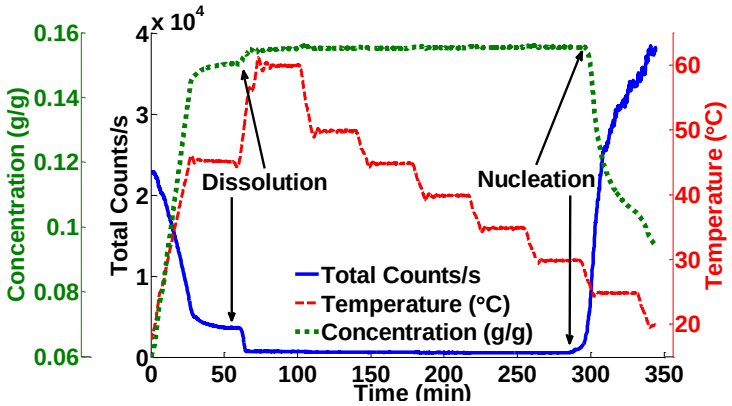



**Figure 7.10 Predicted concentration of PABA by the PCR model**

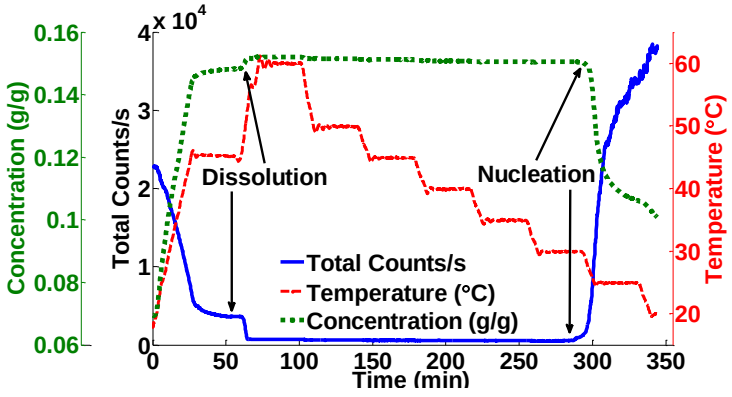



**Figure 7.11 Predicted concentration of PABA by the ANN model**

The second validation experiment using. combined cooling and anti-solvent crystallization is shown in Figure 7.12 and Figure 7.13. Quantities of 45 g of PABA and 66 g of OABA were added. The main purpose was to check the robustness of the model during combined anti-solvent

and cooling crystallization. The variation in the peak absorbances of OABA and PABA with changing temperature and concentration can be seen here. At approximately 200 minutes complete dissolution of OABA took place, while PABA dissolved at approximately 300 minutes. Between 300-500 minutes, there is a small decrease in FBRM counts which can be attributed to the presence of bubbles or impurities (which may have dissolved during the water addition). In both cases the absorbance values decrease after complete dissolution because of the increasing temperature. The complete dissolution of solids is also clearly indicated by a decrease in the total counts as detected by the FBRM. Water was used as an anti-solvent in this experiment. 40 g of water was added in four intervals. The dilution affect caused by water addition is visible by decreasing absorbance values at constant temperature. The system was cooled and held at 5 °C until it nucleated. The nucleation event was detected by both FBRM and ATR-UV/Vis spectroscopy by an increase in number of total counts/s and decrease in the absorbance values, respectively.

The ANN model in this case failed to predict the concentrations of both isomers accurately, especially during the anti-solvent addition part. Another disadvantage was the extremely long computational times which further hindered the usage and optimization of ANN based model. The PCR based model which was developed earlier also failed to predict the concentrations accurately and with significant differences in the actual and predicted values, especially during the anti-solvent addition part. In order to reduce the computational time and accuracy of the prediction for this validation experiment it was decided to test a combined PC-ANN based model. This approach applies a PCA in the first step to decrease the number of input parameters for the ANN model, and then uses an ANN model with the PCs as the input. This approach can significantly decrease the number of parameters in the ANN model.

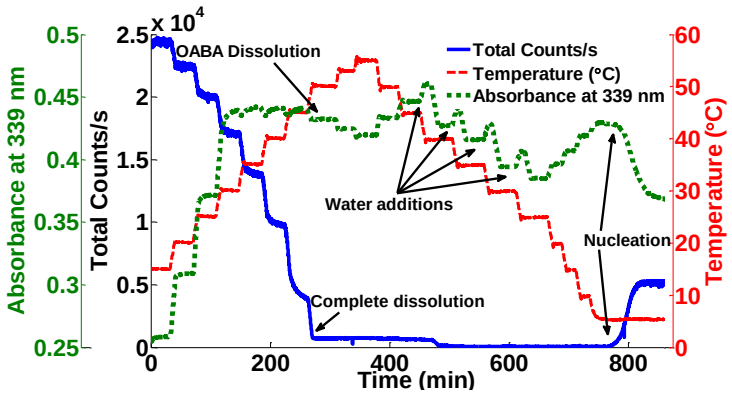



**Figure 7.12 Variation in total counts and absorbance at 339 nm for OABA**

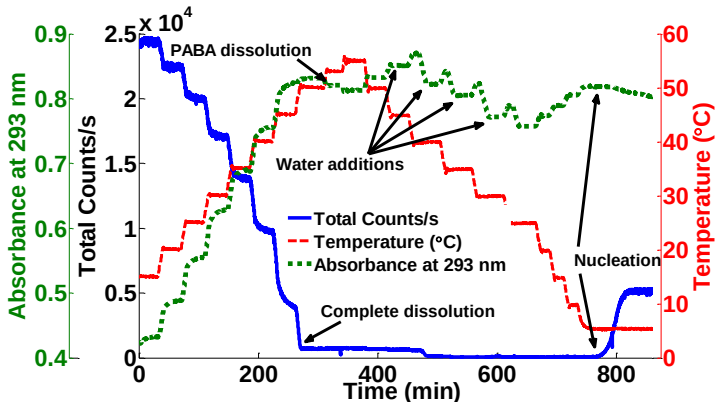



**Figure 7.13 Variation in total counts and absorbance at 293 nm for PABA**

The structure of the PC-ANN model developed is shown in Figure 7.14. The inputs to the ANN model were 8 principle components (PC1-PC8), which is a significant reduction in the number of inputs compared to the original test data, furthermore the computational time required to train the ANN model was substantially reduced, i.e. from several hours to less than 10 minutes. Several different network structures using Levenberg-Marquardt algorithm were tested with different number of neurons and iterations for the training. The network with 6 neurons and 400 iterations was selected as it gave the best results. The network consisted of 1 input layer, 1 hidden layer and an output layer. The transfer functions for the hidden layer were tansigmoid, while purelin (both of these are standard transfer functions available in the artificial neural networks toolbox) was used as the transfer function in the output layer. Tansigmoid was used because of its ability to handle nonlinear data.

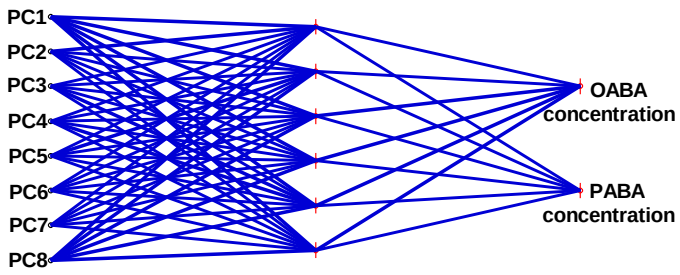



**Figure 7.14 Structure of PC-ANN model used with 8 inputs and 2 outputs**

The performance and robustness of the model developed is shown in Figure 7.15 and Figure 7.16. The RMSEP values obtained were 0.2916 g and 0.3561 g for OABA and PABA respectively. Since concentration is influenced by the dilution effect when anti-solvent is added to the system, instead of concentrations, dissolved mass is plotted here to show the prediction capability of the model for cooling and anti-solvent crystallization. The initial dissolution phase is indicated by an increase in the dissolved mass in steps with regards to variations in the temperature. After this no significant change is seen for both OABA and PABA dissolved masses, even during the water additions until the nucleation took place towards the end as indicated by a decrease in masses. The model developed was thus able to capture temperature and anti-solvent effects satisfactorily.

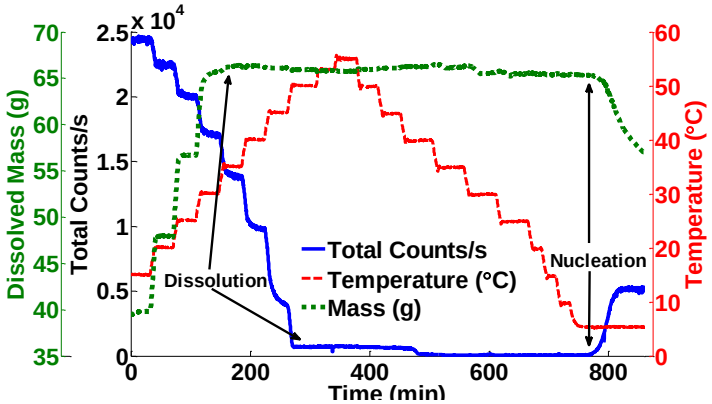



**Figure 7.15 Predicted dissolved mass of OABA**

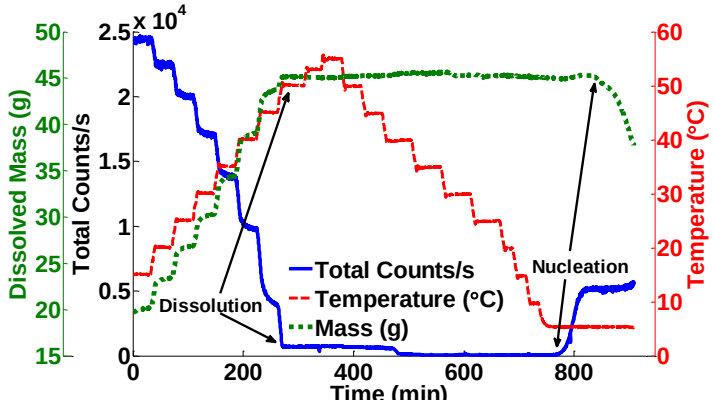



**Figure 7.16 Predicted dissolved mass of PABA**

As a next step separation of the two and three isomers was carried out using water as solvent. Water was used as solvent for separation experiments to simplify the setup and minimize material usage as solubilities of OABA and PABA are significantly higher in IPA or the IPA/water mixtures used during the calibration model development.

## 7.4 Separation of the two Isomers

Initially separation of OABA and PABA using water as solvent was carried out. The experimental setup for separation of two isomers is shown in Figure 7.17. The jackets of both vessels were connected to each other to maintain the same temperature in both vessels. In vessel 1, FBRM and ATR-UV/Vis spectroscopy probes were present, while the second FBRM along with the thermocouple were present in vessel 2. The solution prepared was saturated with respect to OABA at 35 °C and at 30 °C with respect to PABA. Approximately equal amounts of OABA and PABA were added in both vessels. The temperature was then raised to 55 °C for complete dissolution. The system was cooled down to 40 °C before the inter vessel circulation of solution started through sintered disk filters at a rate of 60 mL/min using peristaltic pumps. The solution was cooled down to 22 °C at a rate of 0.1 °C/min, maintaining the same temperature in each vessel.

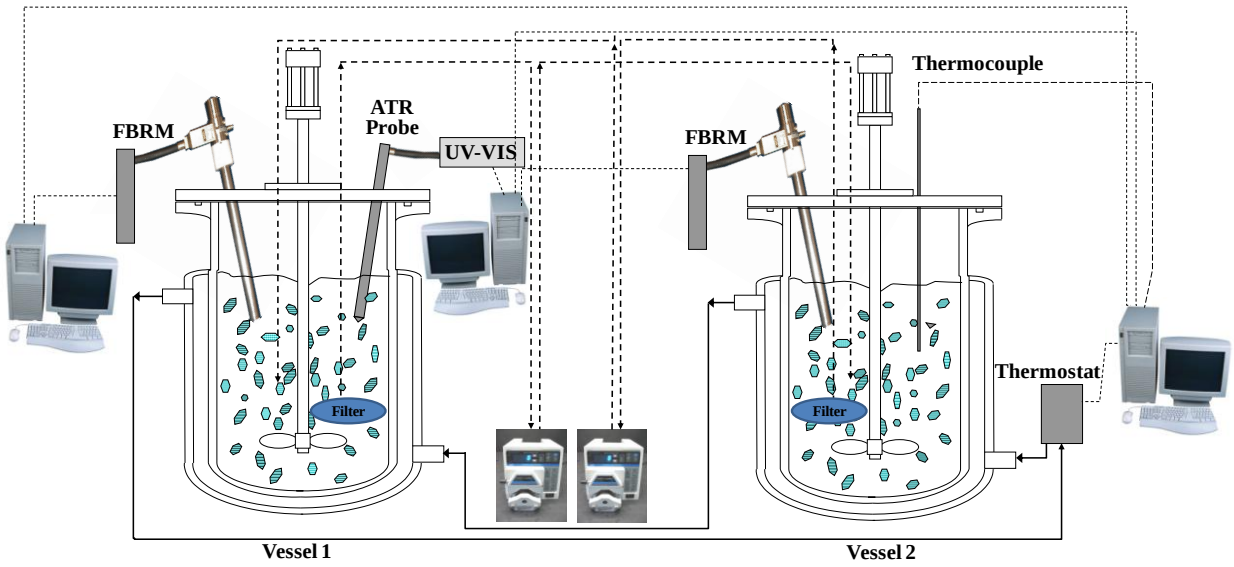



**Figure 7.17 Experimental setup used for the separation of the two isomers**

The results for vessels 1 and 2 are shown in Figure 7.18and Figure 7.19 respectively. Inter vessel mixing was started earlier to make sure homogeneous solutions were present in both vessels. The small decreases in absorbance values at approximately 90 minutes indicate the start of the inter vessel mixing. An amount of 15 % of OABA seeds based on the initial amount of solute, and size range of 125-185 µm (according to sieve analysis), were added in vessel 1 at 34 °C, as indicated by the increase in total counts. The absorbance values at 339 nm show an increasing trend, which was probably as a result of dissolution and temperature decrease, also indicated by a slight decrease in the FBRM counts/s. However, after about 135 minutes the absorbance remains relatively unchanged indicating that the temperature effect has been countered by the decrease in OABA concentration (and hence absorbance) because of growth of the seed crystals. The increase in the FBRM counts/s at 180 minutes gave a false indication of nucleation. These increases in the counts were caused by the presence of the bubbles on the probe window. This is further supported by the absorbance values, which should have shown a sharp decrease in case of nucleation. The phenomenon of bubbles affecting the FBRM readings has been reported by Simon *et al*. (2009). Saarimaa *et al*. (2006) showed results for FBRM measuring bubbles and materials together and FBRM also showed counts even for a blank sample, purely because of the presence of the bubbles. The other factors, which favoured the formation of bubbles on the probe were probe orientation with respect to the impeller and low solid concentration, as the solids were expected to wash away any bubbles, which may form on the probe window.

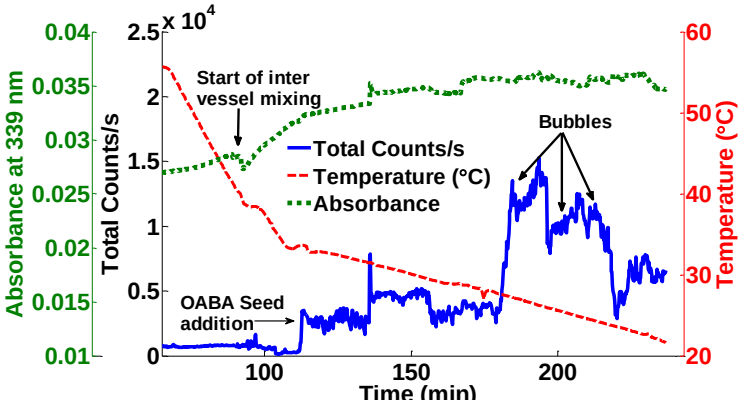



**Figure 7.18 Absorbance and total counts profile for vessel 1 (OABA)**

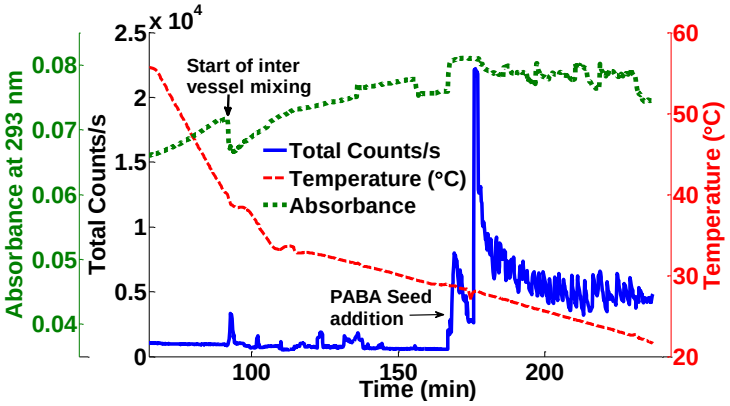



**Figure 7.19 Absorbance and total counts profile for vessel 2 (PABA)**

In vessel 2, 14.9 % PABA seeds were added at 29 °C, based on the initial amount, with size range 125-185 µm according to the sieve analysis. The slight decrease in counts/s at 167 minutes indicates a dissolution event as supported by the increase in absorbance values at 293 nm. The sharp peak at 173 minutes indicates an artefact in FBRM readings as no changes are seen in the absorbance values. The counts after this peak fluctuate between 3000-6000 counts/s. These fluctuations were caused by sticking of crystals on the filter and their cleaning by reversing the flow in the pipe by the peristaltic pump. The inter vessel flow was periodically reversed for cleaning the filters. Only the liquid present in the pipe was used during this cleaning, this was made sure by keeping the pipes above the liquid level in both vessels.

The purpose of this experiment was to separate the two isomers. The purity of the recovered product is therefore of primary importance. For this purpose DSC analyses were performed on the solids recovered from each vessel. The melting points of OABA and PABA are 147 °C and 187 °C, respectively. In Figure 7.20 DSC analysis of the products recovered from vessel 1 along with the DSC analysis of the seeds used are shown. The results of the DSC analysis of the product from vessel 2, along with the seeds used are shown in Figure 7.21.

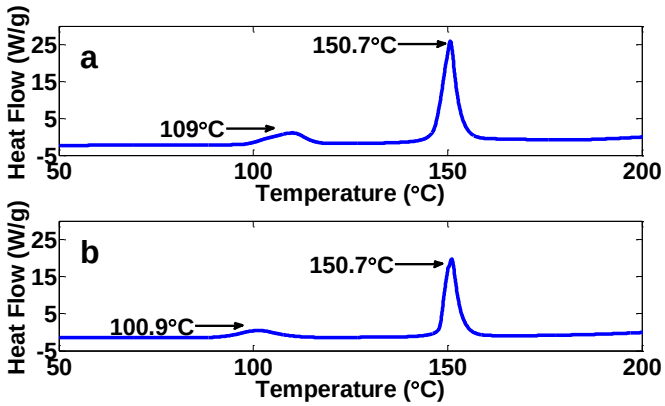



**Figure 7.20 DSC thermogram of OABA (a) seeds (b) recovered product from the 2 isomers separation experiment. Heating rate was 15 °C/min.**

The plots show no cross contamination of the two isomers in either of the vessels. The small peaks close to 100 °C for the OABA samples indicate polymorphic transformation of form 1 to form 2. Figure 7.22 and Figure 7.23 show microscopic images of seeds and recovered product from both vessels. In both cases larger crystals were obtained compared to the seed crystals.

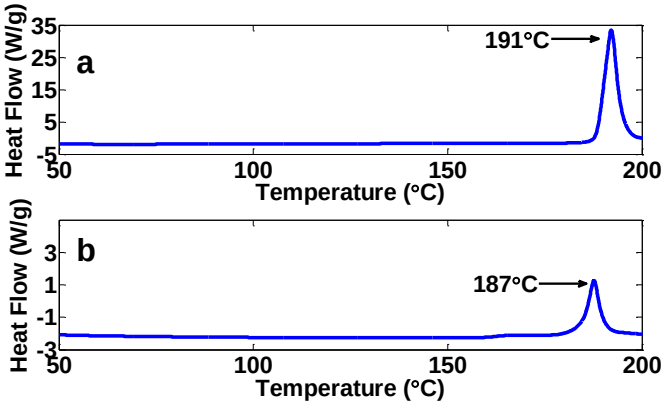



**Figure 7.21 DSC thermogram of PABA (a) seeds (b) recovered product from the 2 isomers separation experiment. Heating rate was 15 °C/min.**

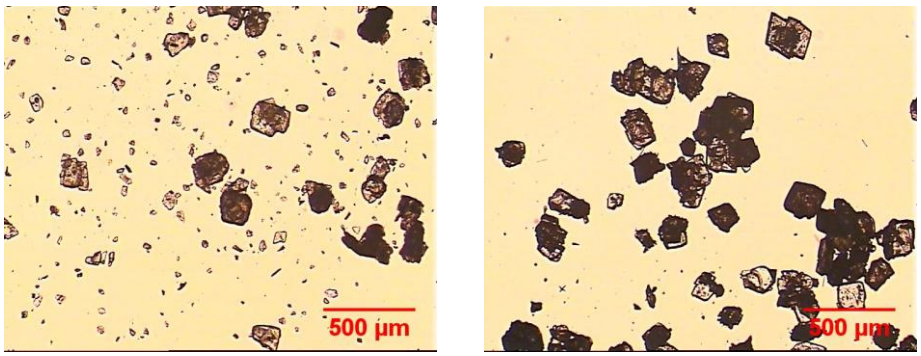



**Figure 7.22 Microscopic images of OABA (a) seed (b) recovered product from the 2 isomers separation experiment**

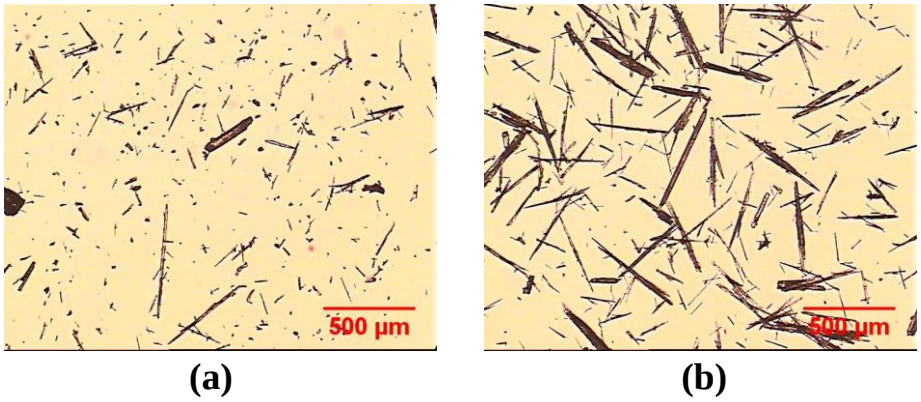



**Figure 7.23 Microscopic images of PABA (a) seed (b) recovered product from the 2 isomers separation experiment**

A positive yield with respect to both isomers was obtained. An amount of 1.203 g of OABA seeds was added and 2.5478 g were recovered. In case of PABA, 1.0629 g seeds were added and 1.3134 g solids were recovered. The recovered products correspond to 36.33 % and 13.439 % of the theoretical yield based on solubility data for OABA and PABA respectively. Low yield here can be attributed to a number of factors. Presence of multiple organic solutes can enhance the aqueous solubility of the solutes as compared to when they are present in water in the absence of other cosolutes (Chiou *et al*., 1986). This increase in solubility explains the dissolution of some seed crystals, although they were added below the saturation temperatures in case of both isomers. Another factor was the loss of product during recovery at the end as the solids had a

tendency to stick on the filters. After the successful separation of the two isomers, separation of the three isomers was also carried out, this is discussed in the next section.

## 7.5 Separation of the three Isomers

For separation of the three isomers, OABA, PABA and MABA were used as solutes, while water was used as solvent. The experimental setup used for separation of the three isomers is shown in Figure 7.24, indicating the third vessel which was added for MABA. The vessel configurations in terms of equipment were same as for the two vessels setup, no data were recorded in the second vessel (used for MABA seeding).

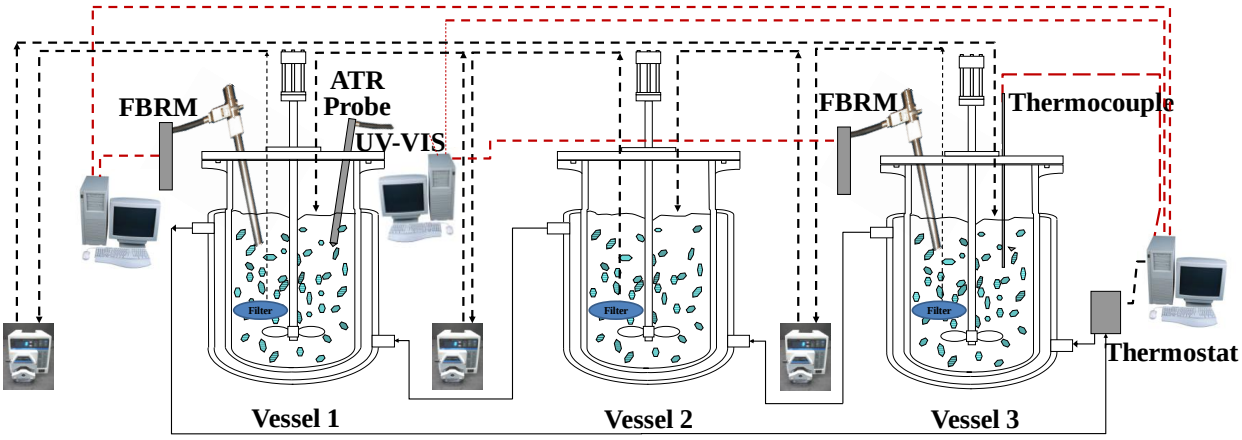



**Figure 7.24 Experimental setup used for the separation of the three isomers**

Solution prepared was saturated with respect to OABA at 35 °C, MABA at 33 °C and at 30 °C with respect to PABA. Approximately equal amounts of OABA, MABA and PABA were added in all three vessels, the temperature was then raised to 55 °C for complete dissolution. The system was cooled down to 40 °C before the inter vessel circulation of solution was started through sintered disk filters at a rate of 60 mL/min using three peristaltic pumps. The solution was cooled down to 20 °C at a rate of 0.1 °C/min.

Inter vessel mixing was started at 125 minutes as indicated by the change in absorbance values as shown in Figure 7.25 and Figure 7.26. 15 % OABA seeds based on the initial amount of solute, within the size range of 125-185 µm, according to the sieve analysis, were added in vessel 1 at 34 °C, as indicated by an increase in the total counts/s.

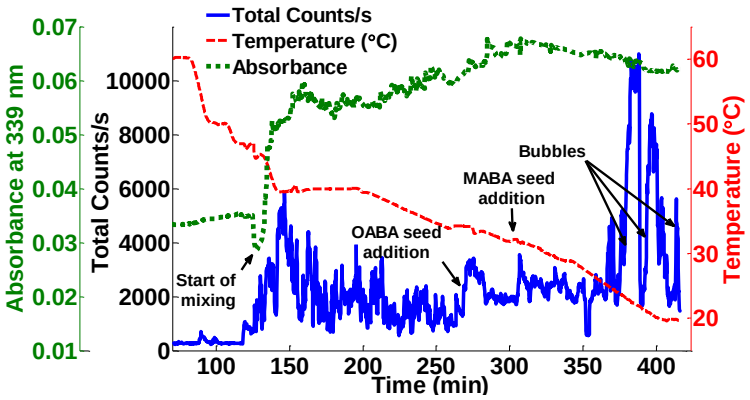



**Figure 7.25 Absorbance and total counts profile for vessel 1 (OABA)**

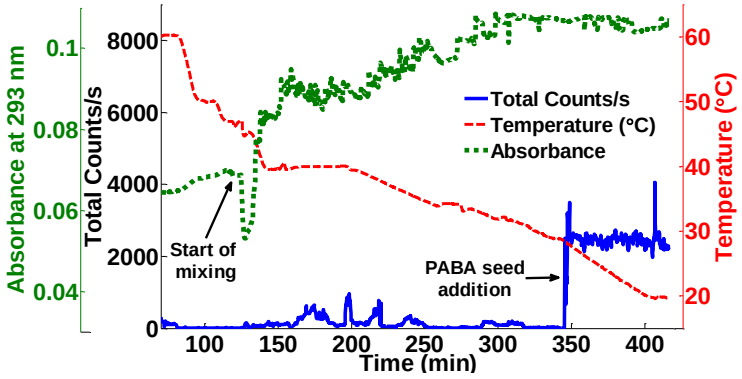



**Figure 7.26 Absorbance and total counts profile for vessel 3 (PABA)**

Absorbance values at 339 nm show an increasing trend, after the dissolution event, as seen in the case of the 2 isomer separation experiment previously. The noisy FBRM data, prior to seed addition and from 350 minutes onwards is the result of bubbles sticking on the probe window. MABA seeds, again 15 % of the initial amount of solute, with size range 125-185 µm, according to sieve analysis, were added in the second vessel at 32 °C. Decrease in absorbance values in Figure 7.25 can be seen, indicating decrease in concentration of both isomers.

In vessel 3, 14.9 % PABA seeds based on the initial solute content, with size range of 125-185 µm, according to sieve analysis, were added at 29 °C. The absorbance data at 293 nm (Figure 7.26) is rather flat even after addition suggesting that temperature and growth effects were countered in case of PABA. Flow directions were also reversed in this experiment as well to eliminate filter clogging. DSC analyses were carried out to check the purity of the products recovered from all three vessels. The results are shown in Figure 7.27, Figure 7.28 and Figure 7.29 respectively. Again no cross contamination of isomers in either of the vessels was observed. Melting point of MABA is 178 °C. The peak at 160 °C in the MABA thermogram indicates the polymorphic transformation of form 1 to form 2 (Svard *et al.*, 2010).

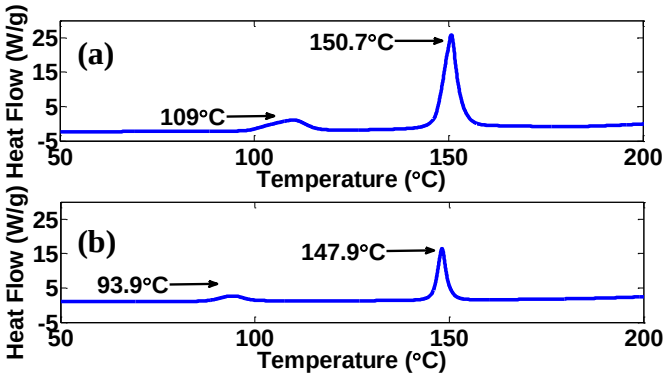



**Figure 7.27 DSC thermogram of OABA (a) seed (b) recovered product from the 3 isomers separation experiment. Heating rate was 15 °C/min.**

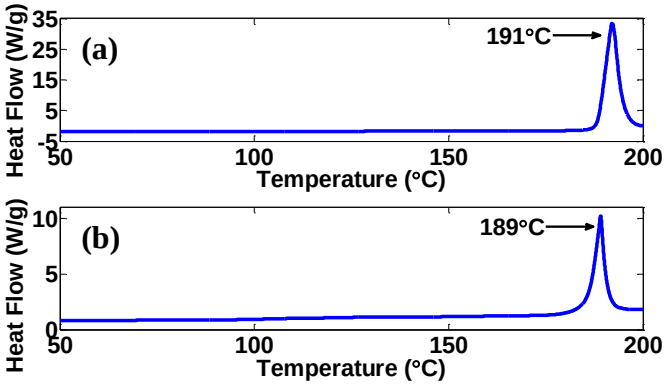



**Figure 7.28 DSC thermogram of PABA (a) seed (b) recovered product from the 3 isomers separation experiment. Heating rate was 15 °C/min.**

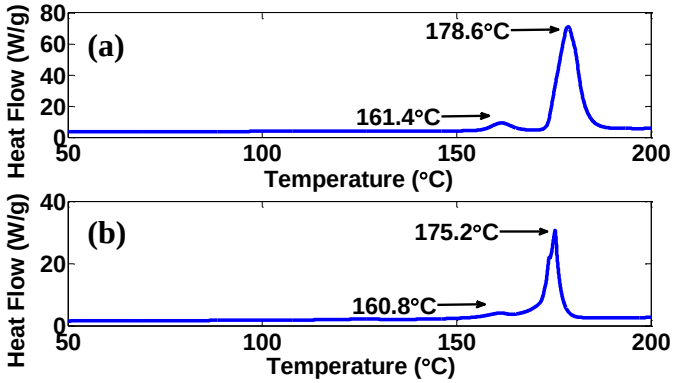



**Figure 7.29 DSC thermogram of MABA (a) seed (b) recovered product from the 3 isomers separation experiment. Heating rate was 15 °C/min.**

The amount of solids added in this case were 1.7283 g OABA, 1.5801 g PABA and 1.6972 g MABA, while the recovered products were 2.4166 g OABA, 2.1572 g PABA and 1.8884 g MABA. The recovered products correspond to yields of 12 %, 17.05 % and 4.98 % with respect to the theoretical yield. The reasons for low yield have been discussed previously. MABA had the lowest yield in this case which was as a result of solids sticking and forming lumps which were difficult to break, hence resulting in little growth of the crystals, due to decreased surface area.

Figure 7.30 shows the microscopic images of recovered OABA and PABA crystals, showing growth when compared with the seed crystals. MABA images were not taken as solids were recovered in the form of lumps.

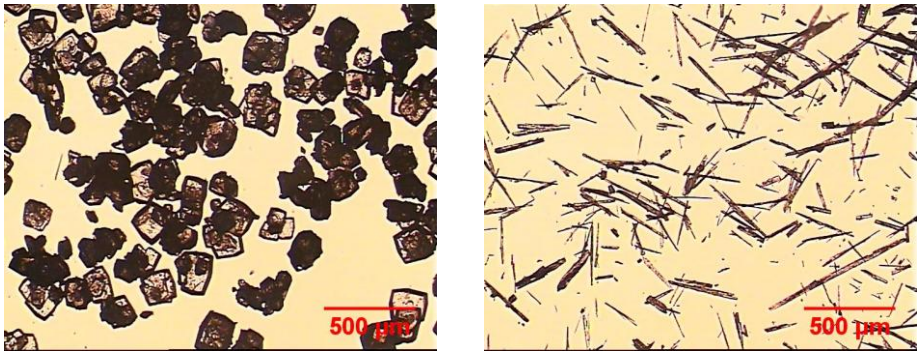



**Figure 7.30 Microscopic image of recovered products from the 3 isomers separation experiment (a) OABA (b) PABA**

## 7.6 Conclusions

A calibration model using PC-ANN was developed for a complex multi component solution covering both cooling and anti-solvent crystallization processes. The PC-ANN based calibration proved to be a useful chemometric tool for nonlinear and complex systems. ATR-UV/Vis spectroscopy has been shown as a potentially powerful PAT tool with potential applications in monitoring multi-component crystallization processes. FBRM and ATR-UV/Vis spectroscopy complement each other and provide useful information about the system. Separations of the two and three isomers were carried out successfully, using two and three interconnected crystallization vessels. Despite the low yield, pure products were obtained. The process can be optimized further by using a better filter design, however the designed methodology has the potential to be used on a larger scale as a system for isomer separation.

# Chapter 8 Conclusions and Future Work

## 8.1 Conclusions

The main aim of the work presented was to use PAT and chemometrics for process monitoring and control and hence improve the quality of the product in a consistent way. For this purpose control approaches using ATR-UV/Vis spectroscopy and FBRM were developed and successfully implemented. The second aim was to use chemometrics combined with PAT for monitoring complex multi-component systems. In the following section the main conclusions are summarized:

A systematic methodology for calibration model development for ATR-UV/Vis spectroscopy was presented, different linear and nonlinear model were compared for their predictive ability. It was shown that the selection of the variables and choice of calibration method must be carried out by analyzing the data for nonlinearities, as the predictive ability of model strongly depends on these factors. A simple nonlinear model was developed and subsequently used in SSC implementation.

A SSC approach using ATR-UV/Vis spectroscopy was developed and implemented for PCM/IPA system. This was the first time that an experimental study of feedback supersaturation control using ATR-UV/Vis spectroscopy had been carried out. The system controlled by this approach was able to follow particular profiles in the phase diagram yielding better quality product. This approach offers a quick direct design approach for crystallization processes.

An automated DNC approach using FBRM was successfully implemented and evaluated for the PCM/IPA system. The ADNC approach outperformed the traditionally used linear and natural cooling profiles and crystals with bigger mean size and uni-modal distributions were obtained for all cases. A combined ADNC-SSC using innovative internal seeding methodology was also developed. The approach combined the information provided by FBRM and ATR-UV/Vis

spectroscopy. Results show that the crystalline product obtained using this approach was better than the crystals obtained from linear cooling profiles.

The performance of ADNC was analyzed under different disturbances that are frequently encountered in the industrial environment and for external seeding as well. The results indicate that ADNC responded well to these disturbances and big uniform crystals and CSD without any bi-modality were obtained. The approach performed equally well in the case of external seeding also A robust scale-up approach using ADNC was then implemented successfully on 100 L scale for the OABA and water system and again performed better than the natural and linear cooling profiles.

A complex nonlinear calibration model using PC-ANN was developed for simultaneous concentration monitoring of multicomponent system using ATR-UV/Vis spectroscopy absorbances. A novel multiple crystallizer setup was developed and successfully used for the separation of the isomers of ABA. ATR-UV/Vis spectroscopy and two FBRM's were used for monitoring the process. The isomers with higher degree of purity were successfully separated. This approach offers an alternative to expensive HPLC for separation of multiple compounds. The approach is simple to implement and gave satisfactory results.

A number of useful and easy to implement control approaches were developed, implemented and evaluated for their performance. The use of ATR-UV/Vis spectroscopy and FBRM for control approaches can be a valuable addition in the QBD framework. The robust scale-up approach has huge potential for application on industrial scale. The key feature of these approaches has been to obtain desired crystalline product consistently, commercially these can lead to minimize operation costs by minimizing the batch to batch variability and hence improved product quality. A simple but effective approach based on seeded cooling crystallization can be implemented on industrial scale as well for the separation of the compounds. All these factors are in line with the FDA's PAT initiative of improving product quality, reduction in development and manufacturing costs and time.

## 8.2 Future Work

The following section includes several recommendations for future work based on the results presented in this thesis:

The efficiency of the ADNC approach has been demonstrated for two model pharmaceutical systems. Considering the much broader scope of crystallization there is great potential for the ADNC approach to be applied in other sectors at different scales, e.g. crystallization of food related compounds, other fine and bulk chemical compounds etc.

The SSC control approach also has similar potential and should be evaluated further for its application for other compounds especially for fast growing systems. In the present work supersaturation was controlled at a constant level. Production of a particular polymorph by following mode complex supersaturation profiles in the phase diagram using the SSC can be another application with significant potential. Similarly the combined ADNC-SSC approach has not been fully explored and can be a beneficial tool in the crystallization processes. Anti-solvent crystallization is also frequently used for many crystallisation processes and the automated ADNC approach based on solvent/antisolvent addition can be developed.

The separation of isomers can be optimized further especially the yield can be increased by using a more efficient setup, and solvent in which the isomers have higher solubility. Also the proposed approach should be extended for other frequently occurring mixtures as well, e.g. a smaller but similar setup, consisting of crystallisation cells separated by membranes (which allow the mixing of liquid but not the solid) could be developed and applied for protein separation.

The model compound OABA showed some interesting polymorphic behaviour, during the large scale trials of the ADNC approach. Work is currently underway to quantify the productions and presence of different polymorphs under different conditions using the PAT tools used in the work.

Finally the current trends in continuous manufacturing and crystallisation call for the development of new control approaches for continuous processes. The approaches developed and evaluated in this thesis can be tailored and applied for continuous crystallisation, with significant potential benefits and impact in the pharmaceutical industries.

# References

AALTONEN, J., RANTANEN, J., SIIRIA, S., KARJALAINEN, M., JORGENSEN, A., LAITINEN, N., SAVOLAINEN, M., SEITAVUOPIO, P., LOUHI-KULTANEN, M. and YLIRUUSI, J., 2003. Polymorph Screening Using Near-Infrared Spectroscopy. *Analytical Chemistry,* **75**(19), pp. 5267-5273.

AAMIR, E., NAGY, Z.K. and RIELLY, C.D., 2010. Optimal seed recipe design for crystal size distribution control for batch cooling crystallisation processes. *Chemical Engineering Science,* **65**(11), pp. 3602-3614.

ABU BAKAR, M.R., NAGY, Z.K., SALEEMI, A.N. and RIELLY, C.D., 2009. The Impact of Direct Nucleation Control on Crystal Size Distribution in Pharmaceutical Crystallization Processes. *Crystal Growth & Design,* **9**(3), pp. 1378-1384.

ABU BAKAR, M.R., NAGY, Z.K. and RIELLY, C.D., 2010. Investigation of the Effect of Temperature Cycling on Surface Features of Sulfathiazole Crystals during Seeded Batch Cooling Crystallization. *Crystal Growth & Design,* **10**(9), pp. 3892-3900.

ADAMS, C.P. and BRANTNER, V.V., 2010. Spending on new drug development1. *Health Economics,* **19**(2), pp. 130-141.

ADAMS, C.P. and BRANTNER, V.V., 2006. Estimating The Cost Of New Drug Development: Is It Really $802 Million? *Health Affairs,* **25**(2), pp. 420-428.

ADAMS, M.J., 2004. Chemometrics in Analytical Spectroscopy, 2nd edition, Royal Society of Chemistry.

ADHIYAMAN, R. and BASU, S.K., 2006. Crystal modification of dipyridamole using different solvents and crystallization conditions. *International Journal of Pharmaceutics,* **321**(1-2), pp. 27-34.

AGATONOVIC-KUSTRIN, S. and BERESFORD, R., 2000. Basic concepts of artificial neural network (ANN) modeling and its application in pharmaceutical research. *Journal of Pharmaceutical and Biomedical Analysis,* **22**(5), pp. 717-727.

ANDERSON, J.E., MOORE, S., TARCZYNSKI, F. and WALKER, D., 2001. Determination of the onset of crystallization of N1-2-(thiazolyl)sulfanilamide (sulfathiazole) by UV-Vis and calorimetry using an automated reaction platform; subsequent characterization of polymorphic forms using dispersive Raman spectroscopy. *Spectrochimica Acta Part A: Molecular and Biomolecular Spectroscopy,* **57**(9), pp. 1793-1808.

BAKAR, M.R.A., NAGY, Z.K. and RIELLY, C.D., 2009; 2009. Seeded Batch Cooling Crystallization with Temperature Cycling for the Control of Size Uniformity and Polymorphic Purity of Sulfathiazole Crystals. *Organic Process Research & Development,* **13**(6), pp. 1343-1356.

BAKEEV, K.A., 2010. Process Analytical Technology, Blackwell.

BARRETT, P. and GLENNON, B., 2002. Characterizing the Metastable Zone Width and Solubility Curve Using Lasentec FBRM and PVM. *Chemical Engineering Research and Design,* **80**(7), pp. 799-805.

BARTHE, S. and ROUSSEAU, R.W., 2006. Utilization of Focused Beam Reflectance Measurement in the Control of Crystal Size Distribution in a Batch Cooled Crystallizer. *Chemical Engineering & Technology,* **29**(2), pp. 206-211.

BARTHE, S.C., GROVER, M.A. and ROUSSEAU, R.W., 2008. Observation of Polymorphic Change through Analysis of FBRM Data: Transformation of Paracetamol from Form II to Form I. *Crystal Growth & Design,* **8**(9), pp. 3316-3322.

BAUER, J., SPANTON, S., HENRY, R., QUICK, J., DZIKI, W., PORTER, W. and MORRIS, J., 2001. *Ritonavir: An Extraordinary Example of Conformational Polymorphism.* Springer Netherlands.

BERGLUND, A. and WOLD, S., 1997. INLR, implicit non-linear latent variable regression. *Journal of Chemometrics,* **11**(2), pp. 141-156.

BRERETON, R.G., 2003. Chemometrics Data Analysis for the Laboratory and Chemical Plant, Wiley.

BILLOT, P., COUTY, M. and HOSEK, P., 2010. Application of ATR-UV Spectroscopy for Monitoring the Crystallisation of UV Absorbing and Nonabsorbing Molecules. *Organic Process Research & Development,* **14**(3), pp. 511-523.

BLAGDEN, N., DE MATAS, M., GAVAN, P.T. and YORK, P., 2007. Crystal engineering of active pharmaceutical ingredients to improve solubility and dissolution rates. *Advanced Drug Delivery Reviews,***59**(7), pp. 617-630.

BLEICHER, K.H., BOHM, H., MULLER, K. and ALANINE, A.I., 2003. Hit and lead generation: beyond high-throughput screening. *Nat Rev Drug Discov,* **2**(5), pp. 369-378.

BOERSMA C FAU - KLOK, ROGIER M, FAU, K.R., FAU, B.J., NAUNTON M FAU - VAN DEN BERG, PAUL B, VAN DEN BERG PB FAU - DE JONG-VAN DEN BERG, LOLKJE T W, DE JONG-VAN DEN BERG LT FAU - POSTMA, MAARTEN J and MJ, P., *Drug costs developments after patent expiry of enalapril, fluoxetine and ranitidine: a study conducted for the Netherlands.*

BORISSOVA, A., KHAN, S., MAHMUD, T., ROBERTS, K.J., ANDREWS, J., DALLIN, P., CHEN, Z. and MORRIS, J., 2008; 2009. *In Situ* Measurement of Solution Concentration during the Batch Cooling Crystallization of l-Glutamic Acid using ATR-FTIR Spectroscopy Coupled with Chemometrics. *Crystal Growth & Design,* **9**(2), pp. 692-706.

BOURQUIN, J., SCHMIDLI, H., VAN HOOGEVEST, P. and LEUENBERGER, H., 1997. Application of Artificial Neural Networks (ANN) in the Development of Solid Dosage Forms. *Pharmaceutical Development and Technology,* **2**(2), pp. 111-121.

BRAATZ, R.D., 2002. Advanced control of crystallization processes. *Annual Reviews in Control,* **26**(1), pp. 87-99.

BRIANÇON, S., COLSON, D. and KLEIN, J.P., 1997. Experimental Study and Theoretical Approach of Cooling Surfaces Fouling in Industrial Crystallizers. *Chemical Engineering Research and Design,***75**(2), pp. 147-151.

BRITTAIN, H.G., 2009 Polymorphism is Pharmaceutical Solids, Informa Healthcare USA, Inc.

CAILLET, A., PUEL, F. and FEVOTTE, G., 2006. In-line monitoring of partial and overall solid concentration during solvent-mediated phase transition using Raman spectroscopy. *International Journal of Pharmaceutics,* **307**(2), pp. 201-208.

CAZES, J., 2005. Ewing's Analytical Instrumentation Handbook, 3rd edition, Marcel Dekker

CHEN, C. and CRAFTS, P.A., 2006. Correlation and prediction of drug molecule solubility with the NRTL-SAC model. In: W. MARQUARDT AND C. PANTELIDES, ed, *Computer Aided Chemical Engineering.*Elsevier, pp. 859-864.

CHEW, J.W., BLACK, S.N., CHOW, P.S. and TAN, R.B.H., 2007. Comparison between Open-Loop Temperature Control and Closed-Loop Supersaturation Control for Cooling Crystallization of Glycine.*Industrial & Engineering Chemistry Research,* **46**(3), pp. 830-838.

CHEW, J.W., CHOW, P.S. and TAN, R.B.H., 2007. Automated In-line Technique Using FBRM to Achieve Consistent Product Quality in Cooling Crystallization. *Crystal Growth & Design,* **7**(8), pp. 1416-1422.

CHIANESE, A., DI BERARDINO, F. and JONES, A.G., 1993. On the effect of secondary nucleation on the crystal size distribution from a seeded batch crystallizer. *Chemical Engineering Science,* **48**(3), pp. 551-560.

CHIOU, C.T., MALCOLM, R.L., BRINTON, T.I. and KILE, D.E., 1986. Water solubility enhancement of some organic pollutants and pesticides by dissolved humic and fulvic acids. *Environmental Science & Technology,* **20**(5), pp. 502-508.

COSTA, C.B.B., MACIEL, M.R.W. and FILHO, R.M., 2005. Factorial design technique applied to genetic algorithm parameters in a batch cooling crystallization optimisation. *Computers & Chemical Engineering,* **29**(10), pp. 2229-2241.

DANG, L., YANG, H., BLACK, S. and WEI, H., 2009. The Effect of Temperature and Solvent Composition on Transformation of β to α Glycine As Monitored *in Situ* by FBRM and PVM. *Organic Process Research & Development,* **13**(6), pp. 1301-1306.

DE BEER, T.R.M., VERGOTE, G.J., BAEYENS, W.R.G., REMON, J.P., VERVAET, C. and VERPOORT, F., 2004. Development and validation of a direct, non-destructive quantitative method for medroxyprogesterone acetate in a pharmaceutical suspension using FT-Raman spectroscopy. *European Journal of Pharmaceutical Sciences,* **23**(4-5), pp. 355-362.

DENEAU, E. and STEELE, G., 2005. An In-Line Study of Oiling Out and Crystallization. *Organic Process Research & Development,* **9**(6), pp. 943-950.

DIMASI, J.A., HANSEN, R.W. and GRABOWSKI, H.G., 2003. The price of innovation: new estimates of drug development costs. *Journal of Health Economics,* **22**(2), pp. 151-185.

DOKI, N., SEKI, H., TAKANO, K., ASATANI, H., YOKOTA, M. and KUBOTA, N., 2004. Process Control of Seeded Batch Cooling Crystallization of the Metastable β Form Glycine Using an In-Situ ATR-FTIR Spectrometer and an In-Situ FBRM Particle Counter. *Crystal Growth & Design,* **4**(5), pp. 949-953.

DOU, Y., QU, N., WANG, B., CHI, Y.Z. and REN, Y.L., 2007. Simultaneous determination of two active components in compound aspirin tablets using principal component artificial neural networks (PC-ANNs) on NIR spectroscopy. *European Journal of Pharmaceutical Sciences,* **32**(3), pp. 193-199.

DOU, Y., MI, H., ZHAO, L., REN, Y. and REN, Y., 2006. Determination of compound aminopyrine phenacetin tablets by using artificial neural networks combined with principal components analysis. *Analytical Biochemistry,* **351**(2), pp. 174-180.

DUNUWILA, D.D. and BERGLUND, K.A., 1997. ATR FTIR spectroscopy for *in situ* measurement of supersaturation. *Journal of Crystal Growth,* **179**(1-2), pp. 185-193.

DUNUWILA, D.D., CARROLL, L.B. and BERGLUND, K.A., 1994. An investigation of the applicability of attenuated total reflection infrared spectroscopy for measurement of solubility and supersaturation of aqueous citric acid solutions. *Journal of Crystal Growth,* **137**(3-4), pp. 561-568.

ELSNER, M.P., ZIOMEK, G. and SEIDEL-MORGENSTERN, A., 2007. Simultaneous preferential crystallization in a coupled, batch operation mode—Part I: Theoretical analysis and optimization. *Chemical Engineering Science,* **62**(17), pp. 4760-4769.

ELSNER, M.P., ZIOMEK, G. and SEIDEL-MORGENSTERN, A., 2009. Efficient separation of enantiomers by preferential crystallization in two coupled vessels. *AICHE Journal,* **55**(3), pp. 640-649.

ERDEMIR, D., LEE, A.Y. and MYERSON, A.S., 2009. Nucleation of Crystals from Solution: Classical and Two-Step Models. *Accounts of Chemical Research,* **42**(5), pp. 621-629.

FALCON, J.A. and BERGLUND, K.A., 2004. *In Situ* Monitoring of Antisolvent Addition Crystallization with Principal Components Analysis of Raman Spectra. *Crystal Growth & Design,* **4**(3), pp. 457-463.

FENG, L. and BERGLUND, K.A., 2002. ATR-FTIR for Determining Optimal Cooling Curves for Batch Crystallization of Succinic Acid. *Crystal Growth & Design,* **2**(5), pp. 449-452.

FÉVOTTE, G., CALAS, J., PUEL, F. and HOFF, C., 2004. Applications of NIR spectroscopy to monitoring and analyzing the solid state during industrial crystallization processes. *International Journal of Pharmaceutics,* **273**(1-2), pp. 159-169.

FÉVOTTE, G., 2002. New perspectives for the on-line monitoring of pharmaceutical crystallization processes using *in situ* infrared spectroscopy. *International Journal of Pharmaceutics,* **241**(2), pp. 263-278.

FUJIWARA, M., CHOW, P.S., MA, D.L. and BRAATZ, R.D., 2002. Paracetamol Crystallization Using Laser Backscattering and ATR-FTIR Spectroscopy: Metastability, Agglomeration, and Control. *Crystal Growth & Design,* **2**(5), pp. 363-370.

FUJIWARA, M., NAGY, Z.K., CHEW, J.W. and BRAATZ, R.D., 2005. First-principles and direct design approaches for the control of pharmaceutical crystallization. *Journal of Process Control,* **15**(5), pp. 493-504.

FUJIWARA, S. and HONDA, S., 1987; 1987. Effect of addition of organic solvent on the separation of positional isomers in high-voltage capillary zone electrophoresis. *Analytical Chemistry,* **59**(3), pp. 487-490.

GEMPERLINE, P., 2006. Practical Guide to Chemometrics, 2nd edition, CRC Press

GELADI, P., 2003. Chemometrics in spectroscopy. Part 1. Classical chemometrics. *Spectrochimica Acta Part B: Atomic Spectroscopy,* **58**(5), pp. 767-782.

GONZALEZ-DIAZ, H., VILAR, S., SANTANA, L. and URIARTE, E., 2007. Medicinal Chemistry and Bioinformatics - Current Trends in Drugs Discovery with Networks Topological Indices. *Current Topics in Medicinal Chemistry,* **7**, pp. 1015-1029.

GOOD, D.J. and RODRIÌGUEZ-HORNEDO, N., 2009. Solubility Advantage of Pharmaceutical Cocrystals. *Crystal Growth & Design,* **9**(5), pp. 2252-2264.

GRÃIN, H., BORISSOVA, A. and ROBERTS, K.J., 2003. In-Process ATR-FTIR Spectroscopy for Closed-Loop Supersaturation Control of a Batch Crystallizer Producing Monosodium Glutamate Crystals of Defined Size. *Industrial & Engineering Chemistry Research,* **42**(1), pp. 198-206.

GRABOWSKI H., VERNON J. and DIMASI J.A., 2002. Returns on Research and Development for 1990s New Drug Introductions. *PharmacoEconomics,* **20**, pp. 11-29.

GRACIN, S. and RASMUSON, Ã.C., 2004; 2004. Polymorphism and Crystallization of p-Aminobenzoic Acid. *Crystal Growth & Design,* **4**(5), pp. 1013-1023.

GUO, Z., ZHANG, M., LI, H., WANG, J. and KOUGOULOS, E., 2005. Effect of ultrasound on anti-solvent crystallization process. *Journal of Crystal Growth,* **273**(3-4), pp. 555-563.

HARDY, M.R. and TOWNSEND, R.R., 1988. Separation of positional isomers of oligosaccharides and glycopeptides by high-performance anion-exchange chromatography with pulsed amperometric detection. *Proceedings of the National Academy of Sciences of the United States of America,* **85**(10), pp. 3289-3293.

HARPER, P.M. and GANI, R., 2000. A multi-step and multi-level approach for computer aided molecular design. *Computers & Chemical Engineering,* **24**(2-7), pp. 677-683.

HAUSMAN, D.S., CAMBRON, R.T. and SAKR, A., 2005. Application of on-line Raman spectroscopy for characterizing relationships between drug hydration state and tablet physical stability. *International Journal of Pharmaceutics,* **299**(1-2), pp. 19-33.

HEATH, A., FAWELL, P., BAHRI, P. and SWIFT, J., 2002. Estimating Average Particle Size by Focused Beam Reflectance Measurement (FBRM). *Particle & Particle Systems Characterization,* **19**(2), pp. 84-95.

HERMANTO, M.W., CHOW, P.S. and TAN, R.B.H., 2010. Implementation of Focused Beam Reflectance Measurement (FBRM) in Antisolvent Crystallization to Achieve Consistent Product Quality. *Crystal Growth & Design,* **10**(8), pp. 3668-3674.

HINZ, D., 2006. *Process analytical technologies in the pharmaceutical industry: the FDA's PAT initiative.* Springer Berlin / Heidelberg.

HOJJATI, H. and ROHANI, S., 2006. Measurement and Prediction of Solubility of Paracetamol in Water−Isopropanol Solution. Part 1. Measurement and Data Analysis. *Organic Process Research & Development,* **10**(6), pp. 1101-1109.

HOJJATI, H. and ROHANI, S., 2005. Cooling and seeding effect on supersaturation and final crystal size distribution (CSD) of ammonium sulphate in a batch crystallizer. *Chemical Engineering and Processing,* **44**(9), pp. 949-957.

HOWARD, K.S., NAGY, Z.K., SAHA, B., ROBERTSON, A.L. and STEELE, G., 2009. Combined PAT-Solid State Analytical Approach for the Detection and Study of Sodium Benzoate Hydrate. *Organic Process Research & Development,* **13**(3), pp. 590-597.

HU, Y., LIANG, J.K., MYERSON, A.S. and TAYLOR, L.S., 2005. Crystallization Monitoring by Raman Spectroscopy: Simultaneous Measurement of Desupersaturation Profile and Polymorphic Form in Flufenamic Acid Systems. *Industrial & Engineering Chemistry Research,* **44**(5), pp. 1233-1240.

HUKKANEN, E.J. and BRAATZ, R.D., 2003. Measurement of particle size distribution in suspension polymerization using *in situ* laser backscattering. *Sensors and Actuators B: Chemical,* **96**(1-2), pp. 451-459.

JIA, C., YIN, Q., ZHANG, M., WANG, J. and SHEN, Z., 2008. Polymorphic Transformation of Pravastatin Sodium Monitored Using Combined Online FBRM and PVM. *Organic Process Research & Development,* **12**(6), pp. 1223-1228.

JIANG, S., TER HORST, J.H. and JANSENS, P.J., 2008. Concomitant Polymorphism of o-Aminobenzoic Acid in Antisolvent Crystallization. *Crystal Growth & Design,* **8**(1), pp. 37-43.

JONES, A.G., 1974. Optimal operation of a batch cooling crystallizer. *Chemical Engineering Science,* **29**(5), pp. 1075-1087.

KAITIN, K.I., 2010. Deconstructing the Drug Development Process: The New Face of Innovation. *Clinical pharmacology and therapeutics,* **87**(3), pp. 356-361.

KARUNANITHI, A.T., ACQUAH, C., ACHENIE, L.E.K., SITHAMBARAM, S., SUIB, S.L. and GANI, R., 2007. An experimental verification of morphology of ibuprofen crystals from CAMD designed solvent.*Chemical Engineering Science,* **62**(12), pp. 3276-3281.

KEE, N.C.S., TAN, R.B.H. and BRAATZ, R.D., 2009. Selective Crystallization of the Metastable α-Form of L-Glutamic Acid using Concentration Feedback Control. *Crystal Growth & Design,* **9**(7), pp. 3044-3051.

KEYHANI, S., DIENER-WEST, M. and POWE, N., 2006. Are Development Times For Pharmaceuticals Increasing Or Decreasing? *Health Affairs,* **25**(2), pp. 461-468.

KITAMURA, M. and SUGIMOTO, M., 2003. Anti-solvent crystallization and transformation of thiazole-derivative polymorphs—I: effect of addition rate and initial concentrations. *Journal of Crystal Growth,***257**(1-2), pp. 177-184.

KOUGOULOS, E., JONES, A.G., JENNINGS, K.H. and WOOD-KACZMAR, M.W., 2005. Use of focused beam reflectance measurement (FBRM) and process video imaging (PVI) in a modified mixed suspension mixed product removal (MSMPR) cooling crystallizer. *Journal of Crystal Growth,* **273**(3-4), pp. 529-534.

LEUNER, C. and DRESSMAN, J., 2000. Improving drug solubility for oral delivery using solid dispersions. *European Journal of Pharmaceutics and Biopharmaceutics,* **50**(1), pp. 47-60.

LEWINER, F., FÉVOTTE, G., KLEIN, J.P. and PUEL, F., 2001. Improving batch cooling seeded crystallization of an organic weed-killer using on-line ATR FTIR measurement of supersaturation. *Journal of Crystal Growth,* **226**(2-3), pp. 348-362.

LI, M. and WILKINSON, D., 2005. Determination of non-spherical particle size distribution from chord length measurements. Part 1: Theoretical analysis. *Chemical Engineering Science,* **60**(12), pp. 3251-3265.

LINDENBERG, C., KRAÌˆTTLI, M., CORNEL, J., MAZZOTTI, M. and BROZIO, J., 2009. Design and Optimization of a Combined Cooling/Antisolvent Crystallization Process. *Crystal Growth & Design,* **9**(2), pp. 1124-1136.

LIOTTA, V. and SABESAN, V., 2004. Monitoring and Feedback Control of Supersaturation Using ATR-FTIR to Produce an Active Pharmaceutical Ingredient of a Desired Crystal Size. *Organic Process Research & Development,* **8**(3), pp. 488-494.

LIU, X., SUN, D., WANG, F., WU, Y., CHEN, Y. and WANG, L., 2011. Monitoring of antisolvent crystallization of sodium scutellarein by combined FBRM?PVM?NIR. *Journal of pharmaceutical sciences,* , pp. n/a-n/a.

LOAN, M., PARKINSON, G., NEWMAN, M. and FARROW, J., 2002. Iron oxy-hydroxide crystallization in a hydrometallurgical residue. *Journal of Crystal Growth,* **235**(1-4), pp. 482-488.

LORENZ, H., PERLBERG, A., SAPOUNDJIEV, D., ELSNER, M.P. and SEIDEL-MORGENSTERN, A., 2006. Crystallization of enantiomers. *Chemical Engineering and Processing,* **45**(10), pp. 863-873.

MA, D.L., TAFTI, D.K. and BRAATZ, R.D., 2002. Optimal control and simulation of multidimensional crystallization processes. *Computers & Chemical Engineering,* **26**(7-8), pp. 1103-1116.

MANGIN, D., PUEL, F. and VEESLER, S., 2009. Polymorphism in Processes of Crystallization in Solution: A Practical Review. *Organic Process Research & Development,* **13**(6), pp. 1241-1253.

MASSART,D.L., 1997. Handbook of Chemometrics and Qualimetrics, Elsevier

MERSMANN, A., 2001. Crystallization Technology Handbook. Marcel Dekker Inc.

MERSMANN, A., 1988. Design of Crystallizers. *Chemical Engineering and Processing,* **23**(4), pp. 213-228.

MODARRESI, H., CONTE, E., ABILDSKOV, J., GANI, R. and CRAFTS, P., 2008. Model-Based Calculation of Solid Solubility for Solvent Selection—¸A Review. *Industrial & Engineering Chemistry Research,***47**(15), pp. 5234-5242.

MOHAN, R., BOATENG, K.A. and MYERSON, A.S., 2000. Estimation of crystal growth kinetics using differential scanning calorimetry. *Journal of Crystal Growth,* **212**(3-4), pp. 489-499.

MONNIER, O., FEVOTTE, G., HOFF, C. and KLEIN, J.P., 1997. Model identification of batch cooling crystallizations through calorimetry and image analysis. *Chemical Engineering Science,* **52**(7), pp. 1125-1139.

MONNIER, O., FÉVOTTE, G., HOFF, C. and KLEIN, J.P., 1996. An advanced calorimetric approach for population balance modelling in batch crystallization processes. *Thermochimica Acta,* **289**(2), pp. 327-341.

MÜLLER, B.W., 2001. Good Manufacturing Practices for Pharmaceuticals Sidney H. Willing (Editor), 5th ed., Marcel Dekker, New York-Basel; 2001-02-07. *European Journal of Pharmaceutics and Biopharmaceutics,* **51**(3), pp. 274-274.

MULLIN, J.W., 2001. Crystallization. Butterworth-Heinemann.

MYERSON, A.S., 2002. Handbook of industrial crystallization. Butterworth-Heinemann.

NAES, T., 2002. A user-friendly guide to multivariate calibration and classification. NIR Publications.

NAGY, Z.K., FUJIWARA, M. and BRAATZ, R.D., 2008. Modelling and control of combined cooling and antisolvent crystallization processes. *Journal of Process Control,* **18**(9), pp. 856-864.

NAGY, Z.K. and BRAATZ, R.D., 2004. Open-loop and closed-loop robust optimal control of batch processes using distributional and worst-case analysis. *Journal of Process Control,* **14**(4), pp. 411-422.

NAGY, Z.K., CHEW, J.W., FUJIWARA, M. and BRAATZ, R.D., 2008. Comparative performance of concentration and temperature controlled batch crystallizations. *Journal of Process Control,* **18**(3-4), pp. 399-407.

NAGY, Z.K., FUJIWARA, M., WOO, X.Y. and BRAATZ, R.D., 2008; 2008. Determination of the Kinetic Parameters for the Crystallization of Paracetamol from Water Using Metastable Zone Width Experiments. *Industrial & Engineering Chemistry Research,* **47**(4), pp. 1245-1252.

NAGY, Z.K., FUJIWARA, M., WOO, X.Y. and BRAATZ, R.D., 2008. Determination of the Kinetic Parameters for the Crystallization of Paracetamol from Water Using Metastable Zone Width Experiments. *Industrial & Engineering Chemistry Research,* **47**(4), pp. 1245-1252.

NAGY, Z.K., 2007. Model based control of a yeast fermentation bioreactor using optimally designed artificial neural networks. *Chemical Engineering Journal,* **127**(1-3), pp. 95-109.

O'BRIEN, L.E., TIMMINS, P., WILLIAMS, A.C. and YORK, P., 2004. Use of *in situ* FT-Raman spectroscopy to study the kinetics of the transformation of carbamazepine polymorphs. *Journal of Pharmaceutical and Biomedical Analysis,* **36**(2), pp. 335-340.

OMAR, W., AL-SAYED, S., SULTAN, A. and ULRICH, J., 2008. Growth rate of single acetaminophen crystals in supersaturated aqueous solution under different operating conditions. *Crystal Research and Technology,* **43**(1), pp. 22-27.

OMAR, W. and ULRICH, J., 1999. Application of Ultrasonics in the On-line Determination of Supersaturation. *Crystal Research and Technology,* **34**(3), pp. 379-389.

OSÉS, J., FERNÁNDEZ-PAN, I., MENDOZA, M. and MATÉ, J.I., 2009. Stability of the mechanical properties of edible films based on whey protein isolate during storage at different relative humidity. *Food Hydrocolloids,* **23**(1), pp. 125-131.

O'SULLIVAN, B., BARRETT, P., HSIAO, G., CARR, A. and GLENNON, B., 2003. *In Situ* Monitoring of Polymorphic Transitions. *Organic Process Research & Development,* **7**(6), pp. 977-982.

O'SULLIVAN, B. and GLENNON, B., 2005. Application of *in Situ* FBRM and ATR-FTIR to the Monitoring of the Polymorphic Transformation of d-Mannitol. *Organic Process Research & Development,* **9**(6), pp. 884-889.

Ostwald, W. Zeitschrift fuer Physikalische Chemie, Stoechiometrie und Verwandtschaftslehre (1897), 22, 289-330 From: J. Chem. Soc., Abstr. 72, II, 308-9 1897 CODEN: ZEPCAC

PAUL, E.L., TUNG, H. and MIDLER, M., 2005. Organic crystallization processes. *Powder Technology,* **150**(2), pp. 133-143.

PAVIA,D.L. LAMPMAN.G.M. KRIZ.G.S. Vvyan.J.R., 2009. Introduction to Spectroscopy. 4th edition, Brooks/Cole, USA.

PÖLLÄNEN, K., HÄKKINEN, A., REINIKAINEN, S., LOUHI-KULTANEN, M. and NYSTRÖM, L., 2005. ATR-FTIR in monitoring of crystallization processes: comparison of indirect and direct OSC methods. *Chemometrics and Intelligent Laboratory Systems,* **76**(1), pp. 25-35.

PÖLLÄNEN, K., HÄKKINEN, A., REINIKAINEN, S., RANTANEN, J., KARJALAINEN, M., LOUHI-KULTANEN, M. and NYSTRÖM, L., 2005. IR spectroscopy together with multivariate data analysis as a process analytical tool for in-line monitoring of crystallization process and solid-state analysis of crystalline product. *Journal of Pharmaceutical and Biomedical Analysis,* **38**(2), pp. 275-284.

PÖLLÄNEN, K., HÄKKINEN, A., REINIKAINEN, S., RANTANEN, J. and MINKKINEN, P., 2006. Dynamic PCA-based MSPC charts for nucleation prediction in batch cooling crystallization processes. *Chemometrics and Intelligent Laboratory Systems,* **84**(1-2), pp. 126-133.

PONS, M., MILFERSTEDT, K. and MORGENROTH, E., 2006. Modeling of chord length distributions. *Chemical Engineering Science,* **61**(12), pp. 3962-3973.

QU, H., LOUHI-KULTANEN, M., RANTANEN, J. and KALLAS, J., 2006. Solvent-Mediated Phase Transformation Kinetics of an Anhydrate/Hydrate System. *Crystal Growth & Design,* **6**(9), pp. 2053-2060.

RAČAITYTĖ, K., KIESSIG, S. and KÁLMÁN, F., 2005. Application of capillary zone electrophoresis and reversed-phase high-performance liquid chromatography in the biopharmaceutical industry for the quantitative analysis of the monosaccharides released from a highly glycosylated therapeutic protein. *Journal of Chromatography A,* **1079**(1-2), pp. 354-365.

RAJEWSKI, R.A. and STELLA, V.J., 1996. Pharmaceutical applications of cyclodextrins. 2. in vivo drug delivery. *Journal of Pharmaceutical Sciences,* **85**(11), pp. 1142-1169.

RANDOLPH, A.D., WHITE, E.T. and LOW, C.D., 1981. On-line measurement of fine-crystal response to crystallizer disturbances. *Industrial & Engineering Chemistry Process Design and Development,* **20**(3), pp. 496-503.

RAW, A.S., FURNESS, M.S., GILL, D.S., ADAMS, R.C., HOLCOMBE, F.O. and YU, L.X., 2004. Regulatory considerations of pharmaceutical solid polymorphism in Abbreviated New Drug Applications (ANDAs). *Advanced Drug Delivery Reviews,* **56**(3), pp. 397-414.

RAWLINS, M.D., 2004. Cutting the cost of drug development? *Nat Rev Drug Discov,* **3**(4), pp. 360-364.

RIELLY, C.D. and MARQUIS, A.J., 2001. A particle's eye view of crystallizer fluid mechanics. *Chemical Engineering Science,* **56**(7), pp. 2475-2493.

RODRÃGUEZ-HORNEDO, N. and MURPHY, D., 1999. Significance of controlling crystallization mechanisms and kinetics in pharmaceutical systems. *Journal of pharmaceutical sciences,* **88**(7), pp. 651-660.

RODRIGUEZ-HORNEDO, N., NEHM, S.J., SEEFELDT, K.F., PAGAN-TORRES, Y. and FALKIEWICZ, C.J., 2006. Reaction Crystallization of Pharmaceutical Molecular Complexes. *Molecular Pharmaceutics,* **3**(3), pp. 362-367.

ROUSSEAU, R.W. and O'DELL, F.P., 1980; 1980. Separation of Multiple Solutes by Selective Nucleation. *Industrial & Engineering Chemistry Process Design and Development,* **19**(4), pp. 603-608.

RUF, A., WORLITSCHEK, J. and MAZZOTTI, M., 2000. Modeling and Experimental Analysis of PSD Measurements through FBRM. *Particle & Particle Systems Characterization,* **17**(4), pp. 167-179.

SAARIMAA, V., SUNDBERG, A., HOLMBOM, B., BLANCO, A., FUENTE, E. and NEGRO, C., 2006. Monitoring of Dissolved Air Flotation by Focused Beam Reflectance Measurement. *Industrial & Engineering Chemistry Research,* **45**(21), pp. 7256-7263.

SALES, F., CALLAO, M.P. and RIUS, F.X., 1997. Multivariate standardization techniques using UV-Vis data. *Chemometrics and Intelligent Laboratory Systems,* **38**(1), pp. 63-73.

SARKAR, D., ROHANI, S. and JUTAN, A., 2006. Multi-objective optimization of seeded batch crystallization processes. *Chemical Engineering Science,* **61**(16), pp. 5282-5295.

SATHE, D., SAWANT, K., MONDKAR, H., NAIK, T. and DESHPANDE, M., 2010. Monitoring Temperature Effect on the Polymorphic Transformation of Acitretin Using FBRM Lasentec. *Organic Process Research & Development,* **14**(6), pp. 1373-1378.

SEADER, J.D. & Henley, E.J. 2005, "Separation Process Principles", Wiley.

SCHMIDT, T.C., PETERSMANN, M., KAMINSKI, L., VON LÃW, E. and STORK, G., 1997. *Analysis of aminobenzoic acids in waste water from a former ammunition plant with HPLC and combined diode array and fluorescence detection.* Springer Berlin / Heidelberg.

SCHOLL, J., BONALUMI, D., VICUM, L., MAZZOTTI, M. and MULLER, M., 2006. *In Situ* Monitoring and Modeling of the Solvent-Mediated Polymorphic Transformation of L-Glutamic Acid. *Crystal Growth & Design,* **6**(4), pp. 881-891.

SHAIKH, A.A., SALMAN, A.D., MCNAMARA, S., LITTLEWOOD, G., RAMSAY, F. and HOUNSLOW, M.J., 2005. *In Situ* Observation of the Conversion of Sodium Carbonate to Sodium Carbonate Monohydrate in Aqueous Suspension. *Industrial & Engineering Chemistry Research,* **44**(26), pp. 9921-9930.

SHAN, G., IGARASHI, K., NODA, H. and OOSHIMA, H., 2002. Production of large crystals with a narrow crystal size distribution by a novel WWDJ batch crystallizer. *Chemical Engineering Journal,* **85**(2-3), pp. 161-167.

SHEIKHZADEH, M., TRIFKOVIC, M. and ROHANI, S., 2008. Adaptive MIMO neuro-fuzzy logic control of a seeded and an unseeded anti-solvent semi-batch crystallizer. *Chemical Engineering Science,* **63**(5), pp. 1261-1272.

SHEIKHZADEH, M., TRIFKOVIC, M. and ROHANI, S., 2008. Fuzzy logic and rigid control of a seeded semi-batch, anti-solvent, isothermal crystallizer. *Chemical Engineering Science,* **63**(4), pp. 991-1002.

SHEKUNOV, B.Y. and YORK, P., 2000. Crystallization processes in pharmaceutical technology and drug delivery design. *Journal of Crystal Growth,* **211**(1-4), pp. 122-136.

SHEKUNOV, B.Y., AULTON, M.E., ADAMA-ACQUAH, R.W. and GRANT, D.J.W., 1996. Effect of temperature on crystal growth and crystal properties of paracetamol. *Journal of the Chemical Society, Faraday Transactions,* **92**(3), pp. 439-444.

SIMON, L.L., NAGY, Z.K. and HUNGERBUHLER, K., 2009. Comparison of external bulk video imaging with focused beam reflectance measurement and ultra-violet visible spectroscopy for metastable zone identification in food and pharmaceutical crystallization processes. *Chemical Engineering Science,* **64**(14), pp. 3344-3351.

SINGHAL, D. and CURATOLO, W., 2004. Drug polymorphism and dosage form design: a practical perspective. *Advanced Drug Delivery Reviews,* **56**(3), pp. 335-347.

STARBUCK, C., SPARTALIS, A., WAI, L., WANG, J., FERNANDEZ, P., LINDEMANN, C.M., ZHOU, G.X. and GE, Z., 2002. Process Optimization of a Complex Pharmaceutical Polymorphic System via *In Situ* Raman Spectroscopy. *Crystal Growth & Design,* **2**(6), pp. 515-522.

SVAÌˆRD, M., NORDSTROÌˆM, F.L., JASNOBULKA, T. and RASMUSON, Ã.C., 2010. Thermodynamics and Nucleation Kinetics of m-Aminobenzoic Acid Polymorphs. *Crystal Growth & Design,* **10**(1), pp. 195-204.

SVANG-ARIYASKUL, A., KOROS, W.J. and ROUSSEAU, R.W., 2009. Chiral separation using a novel combination of cooling crystallization and a membrane barrier: Resolution of DL-glutamic acid. *Chemical Engineering Science,* **64**(9), pp. 1980-1984.

TAVARE, N.S. 1995, "Industrial Crystallization: Process Simulation analysis and Design, Plenum Press

TADAYYON, A. and ROHANI, S., 1998. Determination of Particle Size Distribution by Par-Tech® 100: Modeling and Experimental Results. *Particle & Particle Systems Characterization,* **15**(3), pp. 127-135.

THOMPSON, D.R., KOUGOULOS, E., JONES, A.G. and WOOD-KACZMAR, M.W., 2005. Solute concentration measurement of an important organic compound using ATR-UV spectroscopy. *Journal of Crystal Growth,* **276**(1-2), pp. 230-236.

THURSTON, T.J., BRERETON, R.G., FOORD, D.J. and ESCOTT, R.E.A., 2004. Principal Components plots for exploratory investigation of reactions using ultraviolet-visible spectroscopy: application to the formation of benzophenone phenylhydrazone. *Talanta,* **63**(3), pp. 757-769.

TOGKALIDOU, T., FUJIWARA, M., PATEL, S. and BRAATZ, R.D., 2001. Solute concentration prediction using chemometrics and ATR-FTIR spectroscopy. *Journal of Crystal Growth,* **231**(4), pp. 534-543.

TOGKALIDOU, T., TUNG, H., SUN, Y., ANDREWS, A. and BRAATZ, R.D., 2002; 2002. Solution Concentration Prediction for Pharmaceutical Crystallization Processes Using Robust Chemometrics and ATR FTIR Spectroscopy. *Organic Process Research & Development,* **6**(3), pp. 317-322.

TUNG, H.H., 2009. Crystallization of organic compounds: an industrial perspective. Wiley.

VEKILOV, P.G., 2010. Nucleation. *Crystal Growth & Design,* **10**(12), pp. 5007-5019.

VAN DER HAM, F., SECKLER, M.M. and WITKAMP, G.J., 2004. Eutectic freeze crystallization in a new apparatus: the cooled disk column crystallizer. *Chemical Engineering and Processing,* **43**(2), pp. 161-167.

VARESIO, E., GAUVRIT, J., LONGERAY, R., LANTÉRI, P. and VEUTHEY, J., 1997. Central composite design in the chiral analysis of amphetamines by capillary electrophoresis. *Electrophoresis,* **18**(6), pp. 931-937.

VENDEL, M. and RASMUSON, Å.C., 2000. Initiation of Incrustation by Crystal Collision. *Chemical Engineering Research and Design,* **78**(5), pp. 749-755.

VERGOTE, G.J., DE BEER, T.R.M., VERVAET, C., REMON, J.P., BAEYENS, W.R.G., DIERICX, N. and VERPOORT, F., 2004. In-line monitoring of a pharmaceutical blending process using FT-Raman spectroscopy. *European Journal of Pharmaceutical Sciences,* **21**(4), pp. 479-485.

WANG, F. and BERGLUND, K.A., 2000. Monitoring pH Swing Crystallization of Nicotinic Acid by the Use of Attenuated Total Reflection Fourier Transform Infrared Spectrometry. *Industrial & Engineering Chemistry Research,* **39**(6), pp. 2101-2104.

WIBOWO, C., CHANG, W.-. and NG, K.M., 2001. Design of integrated crystallization systems. *AICHE Journal,* **47**(11), pp. 2474-2492.

WOO, X.Y., NAGY, Z.K., TAN, R.B.H. and BRAATZ, R.D., 2009. Adaptive Concentration Control of Cooling and Antisolvent Crystallization with Laser Backscattering Measurement. *Crystal Growth & Design,* **9**(1), pp. 182-191.

WORLITSCHEK, J. and MAZZOTTI, M., 2004. Model-Based Optimization of Particle Size Distribution in Batch-Cooling Crystallization of Paracetamol. *Crystal Growth & Design,* **4**(5), pp. 891-903.

WORLITSCHEK, J., HOCKER, T. and MAZZOTTI, M., 2005. Restoration of PSD from Chord Length Distribution Data using the Method of Projections onto Convex Sets. *Particle & Particle Systems Characterization,* **22**(2), pp. 81-98.

YI, Y.J. and MYERSON, A.S., 2006. Laboratory Scale Batch Crystallization and the Role of Vessel Size. *Chemical Engineering Research and Design,* **84**(8), pp. 721-728.

YU, L.X., LIONBERGER, R.A., RAW, A.S., D'COSTA, R., WU, H. and HUSSAIN, A.S., 2004. Applications of process analytical technology to crystallization processes. *Advanced Drug Delivery Reviews,* **56**(3), pp. 349-369.

YU, Z.Q., CHOW, P.S. and TAN, R.B.H., 2006. Application of Attenuated Total Reflectance Fourier Transform Infrared (ATR-FTIR) Technique in the Monitoring and Control of Anti-solvent Crystallization. *Industrial & Engineering Chemistry Research,* **45**(1), pp. 438-444.

YU, Z.Q., CHOW, P.S. and TAN, R.B.H., 2006. Seeding and Constant-Supersaturation Control by ATR-FTIR in Anti-Solvent Crystallization. *Organic Process Research & Development,* **10**(4), pp. 717-722.

ZHAO, L., DOU, Y., MI, H., REN, M. and REN, Y., 2007. Non-destructive determination of metronidazole powder by using artificial neural networks on short-wavelength NIR spectroscopy.*Spectrochimica Acta Part A: Molecular and Biomolecular Spectroscopy,* **66**(4-5), pp. 1327-1332.

ZHOU, G.X., FUJIWARA, M., WOO, X.Y., RUSLI, E., TUNG, H., STARBUCK, C., DAVIDSON, O., GE, Z. and BRAATZ, R.D., 2006. Direct Design of Pharmaceutical Antisolvent Crystallization through Concentration Control. *Crystal Growth & Design,* **6**(4), pp. 892-898.

E. Ref [1] Boston Consulting Group

http://www.bcg.com/expertise_impact/publications/default.aspx

(Accessed 15th Jan, 2011)

E. Ref [2] International Conference of Harmonisation

www.ich.org

(Accessed 1 February 2009)

E. Ref [3] Strategic Directions International

http://www.strategic-directions.com/pdf/PAT-ProcessAnalyticalTechnology.pdf

(Accessed 15th Jan, 2011)

E. Ref [4] Business Cooperation Company

http://www.bccresearch.com/

(Accessed 15th Jan, 2011)

E. Ref [5] Pike Tech.

http://www.piketech.com/technical/application-pdfs/AN_0601_CrystalPlates_MIRacle.pdf

(Accessed 15th Jan, 2011)

# Appendix A

| Process monitoring | | | |
|---|---|---|---|
| Zhou *et al*., 2006 | Anti-solvent crystallization of a proprietary drug compound using toluene as solvent, n-heptane as antisolvent | Supersaturation control, dissolution and nucleation detection | ATR-FTIR |
| Liotta and Sabesan, 2004 | Cooling crystallization of a proprietary drug compound using toluene as solvent | Solubility and MSZW determination, supersaturation control | ATR-FTIR |
| Barrett and Glennon, 2002 | Potash alum in water | Solubility and MSZW determination | PVM |
| Fujiwara *et al*., 2002 | Cooling crystallization of paracetamol in water | MSZW determination, size, monitoring, supersaturation control, monitoring | ATR-FTIR |
| Yu *et al*., 2005 | Anti-solvent crystallization of paracetamol in acetone-water mixtures, water as anti-solvent | Agglomeration, effects of stirring and anti-solvent addition rate | |
| Yu *et al*., 2006 | Anti-solvent crystallization of paracetamol in acetone-water mixtures, water as anti-solvent | Growth monitoring, seeding policy and supersaturation control | ATR-FTIR |
| Yi and Myerson, 2006 | Cooling and anti-solvent crystallization of glycine in water, water-methanol mixtures, methanol as anti-solvent | Effects of seeding, mixing, vessel size, nucleation detection, size monitoring | |
| Lindenberg *et al*., 2009 | Combined cooling and anti-solvent crystallization crystallization of acetylsalicylic acid in ethanol water mixtures | Population balance modelling, estimation of growth and nucleation parameters, growth monitoring | ATR-FTIR |
| Deneaue and Steele, 2005 | Proprietary drug compound in ethanol-water mixture | Monitoring of oiling out and crystallization | ATR-UV/Vis spectroscopy, PVM |
| Nagy *et al.*, 2008 | Paracetamol in water | Estimation of kinetic parameters, MSZW | ATR-FTIR |

| | | | |
|---|---|---|---|
| | | determination | |
| Howard *et al*., 2009 | Sodium benzoate in water | Monitoring of hydrate formation | |
| Kougoulos *et al*., 2004 | unknown | Nucleation detection and growth monitoring | PVM |
| De Beer et al., 2004 | Medroxyprogesterone acetate | Calibration model development for raman spectroscopy | |
| Falcon and Berglund, 2004 | Progestrone and acetone, water as anti-solvent | PCA of raman spectra | |
| Liu et al., 2011 | Sodium scutellarien and water, acetone as anti-solvent | Monitoring of liquid and solid phases | NIR, Raman |
| **Polymorphism** | | | |
| O'Sullivan *et al.*, 2003 | D-manitol and sucrose in ethanol-water and toluene | Monitoring of polymorphic transformation and comparison with other *in situ* techniques | PVM, Raman |
| O'Sullivan and Glennon, 2005 | Cooling crystallization of D-manitol in water | Monitoring of polymorphic transformation | ATR-FTIR |
| Shaikh *et al*., 2005 | Sodium carbonate in water | Monitoring of polymorphic transformation | PVM |
| Barthe *et al*., 2008 | Paracetamol in water | Monitoring of polymorphic transformation | |
| Sathe *et al*., 2010 | Acitretin in IPA | Solubility measurements, monitoring of polymorphic transformation | NIR, Raman |
| Jia *et al*., 2008 | Pravastatin Sodium in IPA-water | Monitoring of polymorphic transformation and effects of temperature, solvent ratio and mixing speed | PVM |
| **CLD to CSD** | | | |
| Barthe and Rousseau, 2006 | Cooling crystallization of paracetamol in ethanol | Conversion of CLD to CSD, growth monitoring, fines removal | |
| Worlitschek and Mazzotti, 2004 | Cooling crystallization of paracetamol in ethanol | Conversion of CLD to CSD, estimation of kinetic parameters and optimal temperature trajectory | |
| Worlitschek *et al*., 2005 | Cermic beads and titanium dioxide particles | Conversion of CLD to CSD | |

| | | | |
|---|---|---|---|
| Ruf *et al.*, 2000 | Glass, ceramic, potassium sulphate, toluene and water | Conversion of CLD to CSD | |
| Hukkanen and Braatz, 2003 | Polyvinylchloride | Conversion of CLD to CSD | |
| Li and Wilkinson, | Unknown | Conversion of CLD to CSD | |
| **Instrument analysis and performance** | | | |
| Barrett and Glennon, 1999 | Alkaline frit in water | Effects of probe position and orientation | |
| Bontha *et al*., 2000 | Graphite, silica, kaolin, gibbsite, bentonite, mica flakes and plastic beads in water | Effect of slurry concentration, flowrate, solution colour, scan time, comparison with sieve analysis, effect of air bubbles | |
| Heath *et al*. 2002 | Aluminium and alcite particles | Comparison with other measuring techniques, focal position, mixing, effect of solids concentration | |

# Appendix B

**List of Publications**

## Journal Papers

1. **A. N. Saleemi**, Z. K. Nagy, C. D. Rielly, Comparison of Supersaturation Control and Direct Nucleation Control of Crystal Size Distributions using ATR-UV/Vis and FBRM, *Crystal Growth and Design*. In review

2. **A.N. Saleemi**, Z. K. Nagy, C. Rielly, Separation and monitoring of the crystallization of mixture of aminobenzoic acid isomers using ATR-UV/Vis and FBRM, *Chemical Engineering Science.* In review

3. **A.N. Saleemi**, Z. K. Nagy, C. Rielly, Assessment of Automated Direct Nucleation Control Approach for Different Process Conditions during Cooling Crystallization, *Organic Process Research and Development*. In review

4. **A.N. Saleemi**, Z. K. Nagy, C. Rielly, Application of the Automated Direct Nucleation Control Approach as a Scale up Tool in Cooling Crystallization, *Organic Process Research and Development*. In review

5. **A.N. Saleemi**, Z. K. Nagy, C. Rielly, Calibration Model Development for ATR-UV/Vis Spectroscopy for Organic and Inorganic Crystallization Monitoring, *Organic Process Research and Development*. In review

6. M. R. Abu Bakar, Z. K. Nagy, **A. N. Saleemi**, C. D. Rielly, The impact of direct nucleation control on crystal size distribution in pharmaceutical crystallization processes, *Crystal Growth and Design*, 9 (3), 1378-1384, 2009. (**19 citations**)

## Proceeding Papers (Peer Reviewed)

7. **A.N. Saleemi**, Z. K. Nagy, C. Rielly, Separation and monitoring of the crystallization of mixture of aminobenzoic acid isomers using ATR-UV/Vis and FBRM, in *Proc. of the 18th International Symposium on Industrial Crystallization (ISIC 18*), Zurich, Switzerland, September 13-16, 2011, accepted.

8. Z. K. Nagy, **A.N. Saleemi**, C. Rielly, Supersaturation and Direct Nucleation Control with in situ Seed Generation of an Industrial Pharmaceutical Crystallization Process Using a Crystallization Process Informatics System (CryPRINS), in *Proc. of the 18th International*

*Workshop on Industrial Crystallization (BIWIC 2011)*, Delft, The Netherlands, September 7-9, 2011, accepted.

9. **A.N. Saleemi**, Z. K. Nagy, C. Rielly, Investigation of the Polymorphism and Morphology Variations of Ortho-Aminobenzoic Acid in Cooling Crystallization, in *Proc. of the 18th International Workshop on Industrial Crystallization (BIWIC 2011)*, Delft, The Netherlands, September 7-9, 2011, accepted.

10. **A.N. Saleemi**, Z. K. Nagy, C. Rielly, An Innovative tri-crystallizer set-up for the separation of the three positional isomers of aminobenzoic acid using cooling crystallization, in *Proc. of the 18th International Workshop on Industrial Crystallization (BIWIC 2011)*, Delft, The Netherlands, September 7-9, 2011, accepted.

11. Z. K. Nagy, M. R. Abu Bakar, **A.N. Saleemi**, PAT Based In Situ Monitoring and Control of the Polymorphic Purity of Pharmaceuticals In Batch Cooling Crystallization, in *Proc. of the AIChE 2011 Annual Meeting*, Minneapolis, USA, October 17-21, 2011, accepted.

12. Z. K. Nagy, **A.N. Saleemi**, G. Steele, Quality-by-Design of the Crystal Size Distribution of An Anti-Arrhythmic Drug Using a Crystallisation Process Informatics System (CryPRINS), in *Proc. of the AIChE 2011 Annual Meeting*, Minneapolis, USA, October 17-21, 2011, accepted.

13. **A.N. Saleemi**, Z. K. Nagy, C. Rielly, Separation and monitoring of the crystallization of mixture of aminobenzoic acid isomers using ATR-UV/Vis and FBRM, in *Proc. of the UK-PharmSci 2011 Conference*, Nottingham, U.K., August 31- September 2, 2011, accepted.

14. **A.N. Saleemi**, Z. K. Nagy, G. Steele, Quality-by-Design of the crystal size distribution of an anti-arrhythmic drug using a Crystallisation Process Informatics System (CryPRINS), in *Proc. of the UK-PharmSci 2011 Conference*, Nottingham, U.K., August 31- September 2, 2011, accepted.

15. **A.N. Saleemi**, Z. K. Nagy, M. R. Abu Bakar, PAT Based In Situ Monitoring and Control of the Polymorphic Purity of Pharmaceuticals In Batch Cooling Crystallization, in *Proc. of the UK-PharmSci 2011 Conference*, , Nottingham, U.K., August 31- September 2, 2011, accepted.

16. **A.N. Saleemi**, Z. K. Nagy, C. Rielly, Separation and monitoring of the crystallization of mixture of aminobenzoic acid isomers using ATR-UV/Vis and FBRM, in *Proc. of the 17th International Workshop on Industrial Crystallization (BIWIC 2010)*, Halle, Wittenberg, Germany, 88-95, September 8-10, 2010.

17. **A.N. Saleemi**, Z. K. Nagy, C. Rielly, Application of direct nucleation control approach on laboratory and pilot scale crystallisation using FBRM, in *Proc. of the 17th International Workshop on Industrial Crystallization (BIWIC 2010)*, Halle, Wittenberg, Germany, 426-433, September 8-10, 2010.

18. M. R. Abu Bakar, **A. N. Saleemi**, C. D. Rielly, Z. K. Nagy, Direct nucleation control of crystal size distribution in pharmaceutical crystallization, in *Proc. of the 17th International Symposium on Industrial Crystallization (ISIC 17*), Maastricht, The Netherlands, ISBN 9789076019277, Vol. 1, 67-82, September 14-17, 2008.

**Presentations**

**Oral Presentations**

19. **A.N. Saleemi**, Z. K. Nagy, C. Rielly, Robust Supersaturation Control and Scale up in Pharmaceutical Crystallization using ATR UV/Vis and FBRM, at *UK-China Particle Technology forum III*, Birmingham, U.K., July 3-6, 2011, accepted.

20. **A.N. Saleemi**, Z. K. Nagy, C. Rielly, Application of direct nucleation control approach on laboratory and pilot scale crystallisation using FBRM, at *the 17th International Workshop on Industrial Crystallization (BIWIC 2010)*, Halle, Wittenberg, Germany, September 8-10, 2010.

21. **A.N. Saleemi**, Z. K. Nagy, C. Rielly, Separation and monitoring of the crystallization of mixture of aminobenzoic acid isomers using ATR-UV/Vis and FBRM, at "*What's New in Fluid Separations" organised by the Institution of Chemical Engineers (IChemE) Fluid Separations Subject Group (FSSG)*, Sunbury-on-Thames, U.K., June 4, 2010.

**Poster Presentations**

22. **A.N. Saleemi**, Z. K. Nagy, C. Rielly, Separation and monitoring of the crystallization of mixture of aminobenzoic acid isomers using ATR-UV/Vis and FBRM, in *Proc. of the UK-PharmSci 2011 Conference*, Nottingham, U.K., August 31- September 2, 2011, accepted.

23. **A.N. Saleemi**, Z. K. Nagy, G. Steele, Quality-by-Design of the crystal size distribution of an anti-arrhythmic drug using a Crystallisation Process Informatics System (CryPRINS), in *Proc. of the UK-PharmSci 2011 Conference*, Nottingham, U.K., August 31- September 2, 2011, accepted.

24. **A.N. Saleemi**, Z. K. Nagy, C. Rielly, Separation and monitoring of the crystallization of mixture of aminobenzoic acid isomers using ATR-UV/Vis and FBRM, in *Proc. of the 18th International Symposium on Industrial Crystallization (ISIC 18*), Zurich, Switzerland, September 13-16, 2011, accepted.

25. **A.N. Saleemi**, Z. K. Nagy, C. Rielly, Investigation of the Polymorphism and Morphology Variations of Ortho-Aminobenzoic Acid in Cooling Crystallization, in *Proc. of the 18th International Workshop on Industrial Crystallization (BIWIC 2011)*, Delft, The Netherlands, September 7-9, 2011, accepted.

26. **A.N. Saleemi**, Z. K. Nagy, C. Rielly, An Innovative tri-crystallizer set-up for the separation of the three positional isomers of aminobenzoic acid using cooling crystallization, in *Proc. of the 18th International Workshop on Industrial Crystallization (BIWIC 2011)*, Delft, The Netherlands, September 7-9, 2011, accepted.

27. **A.N. Saleemi**, Z. K. Nagy, C. Rielly, Investigation of the Polymorphism and Morphology Variations of Ortho-Aminobenzoic Acid in Cooling Crystallization, *Proc. of the 2011 Conference of the British Association for Crystal Growth*, London, U.K., July 10-12, 2011, accepted.

28. **A.N. Saleemi**, Z. K. Nagy, C. Rielly, An Innovative tri-crystallizer set-up for the separation of the positional isomers of aminobenzoic acid using cooling crystallization, *Proc. of the 2011 Conference of the British Association for Crystal Growth*, London, U.K., July 10-12, 2011, accepted.

29. **A.N. Saleemi**, Z. K. Nagy, C. Rielly, Separation and monitoring of the crystallization of mixture of aminobenzoic acid isomers using ATR-UV/Vis and FBRM, in *Proc. of the 17th International Workshop on Industrial Crystallization (BIWIC 2010)*, Halle, Wittenberg, Germany, 88-95, September 8-10, 2010,

30. **A.N. Saleemi**, Z. K. Nagy, C. Rielly, Application of direct nucleation control approach on laboratory and pilot scale crystallisation using FBRM, in *Proc. of the 17th International Workshop on Industrial Crystallization (BIWIC 2010)*, Halle, Wittenberg, Germany, 426-433, September 8-10, 2010,.

31. **A.N. Saleemi**, Z. K. Nagy, C. Rielly, Monitoring of the crystallization of mixture of amino benzoic acid isomers using ATR UV/Vis and FBRM, in *Proc. of the 2009 Conference of the British Association for Crystal Growth*, Bristol, U.K., 113, September 6-8, 2009.

32. **A.N. Saleemi**, Z. K. Nagy, C. Rielly, A Tale of Pharmaceutical Crystallization, *Loughborough University Graduate School Poster Competition*, April, 2009. The poster won runner up prize.

33. **A.N. Saleemi**, Z. K. Nagy, C. Rielly, Monitoring of the crystallization of mixture of amino benzoic acid isomers using ATR UV/Vis and FBRM, in *Proc. of the 2008 Conference of the British Association for Crystal Growth*, Loughborough, U.K., 71, September 7-9, 2008.

34. **A.N. Saleemi**, Z. K. Nagy, C. Rielly, Supersaturation control based robust scale-up of pharmaceutical crystallization using ATR UV/Vis and FBRM, in *Proc. of the 2008 Conference of the British Association for Crystal Growth*, Loughborough, U.K., 72, September 7-9, 2008.

## Abstracts

35. **A.N. Saleemi**, Z. K. Nagy, C. Rielly, Investigation of the Polymorphism and Morphology Variations of Ortho-Aminobenzoic Acid in Cooling Crystallization, *Proc. of the 2011 Conference of the British Association for Crystal Growth*, London, U.K., July 10-12, 2011, accepted.

36. **A.N. Saleemi**, Z. K. Nagy, C. Rielly, An Innovative tri-crystallizer set-up for the separation of the positional isomers of aminobenzoic acid using cooling crystallization, *Proc. of the 2011 Conference of the British Association for Crystal Growth*, London, U.K., July 10-12, 2011, accepted.

37. **A.N. Saleemi**, Z. K. Nagy, C. Rielly, Robust supersaturation control and scale up in pharmaceutical crystallization using ATR UV/Vis and FBRM, in *Proc. of the 2010 Conference of the British Association for Crystal Growth*, Manchester, U.K., 85-86, September 5-7, 2010.

38. **A.N. Saleemi**, Z. K. Nagy, C. Rielly, Monitoring of the crystallization of mixture of amino benzoic acid isomers using ATR UV/Vis and FBRM, in *Proc. of the 2009 Conference of the British Association for Crystal Growth*, Bristol, U.K., 113, September 6-8, 2009.

39. **A.N. Saleemi**, Z. K. Nagy, C. Rielly, Monitoring of the crystallization of mixture of amino benzoic acid isomers using ATR UV/Vis and FBRM, in M. Louhi-Kultanen, H. Hatakka, (Eds.) *Proc. of the 16$^{th}$ International Workshop on Industrial Crystallization (BIWIC 2009)*, Lappeenranta, Finland, ISBN 978-952-214-806-3, 397, September 9-11, 2009.

40. **A.N. Saleemi**, Z. K. Nagy, C. Rielly, Monitoring of the crystallization of mixture of amino benzoic acid isomers using ATR UV/Vis and FBRM, in *Proc. of the 2008 Conference of the British Association for Crystal Growth*, Loughborough, U.K., 71, September 7-9, 2008.

41. **A.N. Saleemi**, Z. K. Nagy, C. Rielly, Supersaturation control based robust scale-up of pharmaceutical crystallization using ATR UV/Vis and FBRM, in *Proc. of the 2008 Conference of the British Association for Crystal Growth*, Loughborough, U.K., 72, September 7-9, 2008.

42. Z. K. Nagy, **A.N. Saleemi**, M. R. Haji-Abu-Bakar, C. D. Rielly, Direct nucleation control of crystallization processes using focused bean reflectance measurement, in *Proc. of the 2007 Conference of the British Association for Crystal Growth*, Dublin, Ireland, 31-32, September 4-5, 2007.